CIVIL ENGINEERING DEPARTMENT

A SENSITIVITY STUDY OF THE GROUND HYDROLOGIC MODEL

USING DATA GENERATED

BY AN ATMOSPHERIC GENERAL CIRCULATION MODEL

Shu Fen Sun

M.S., University of Connecticut, 1982

SCHOOL OF ENGINEERING
THE UNIVERSITY OF CONNECTICUT
STORRS, CONNECTICUT

A SENSITIVITY STUDY OF THE GROUND HYDROLOGIC MODEL

USING DATA GENERATED

BY AN ATMOSPHERIC GENERAL CIRCULATION MODEL

Shu Fen Sun

M.S., University of Connecticut, 1982

A Dissertation

Submitted in Partial Fulfillment of the

Requirements for the Degree of

Doctor of Philosophy

at

The University of Connecticut

1985

A SENSITIVITY STUDY OF THE GROUND HYDROLOGIC MODEL

USING DATA GENERATED

BY AN ATMOSPHERIC GENERAL CIRCULATION MODEL

Shu Fen Sun

M.S., University of Connecticut, 1982

A Dissertation

Submitted in Partial Fulfillment of the

Requirements for the Degree of

Doctor of Philosophy

at

The University of Connecticut

1985

A SENSITIVITY STUDY OF THE GROUND HYDROLOGIC MODEL
USING DATA GENERATED
BY AN ATMOSPHERIC GENERAL CIRCULATION MODEL

Shu Fen Sun, Ph.D.

The University of Connecticut, 1985

In this study, the Ground Hydrologic Model (GHM) developed by Lin, Alfano and Bock (1978) for use in an atmospheric general circulation model (GCM) has been refined. A series of sensitivity studies of the new version of the GHM were conducted for the purpose of understanding the role played by various physical parameters in the GHM.

This version of the GHM has made the following refinements:

1) The GHM is coupled directly with the planetary boundary layer (PBL), using Deardorff's (1972) parameterization.

2) A bulk vegetation layer is added with a more realistic large-scale parameterization.

3) The infiltration rate is modified using Green-Ampt's (1911) formula.

Shu Fen Sun -- The University of Connecticut, 1985

The GHM has been tested using input data derived from a GCM simulation run for eight North America regions for 45 days. The results are compared with those of the resident GHM in the GCM. The daily average of grid surface temperatures from both models agree reasonably well in phase and magnitude. However, large difference exists in one or two regions on some days. The daily average evaportranspiration is in general 10-30% less than the corresponding value given by the resident GHM.

Sensitivity studies have been Conducted for:

1) Initial conditions and lower boundary conditions. The effect of different initial soil moisture conditions in the surface layer persists approximately one week, while in the lower layer at least as long as the operational period. Different lower boundary conditions only produce minor effects.

2) Vegetation density. For extreme cases of desertification and afforestation, the effects of the vegetation density on surface temperature, evaporation, sensible heat and soil moisture are most significant.

3) Canopy resistance. Mainly the daily averaged grid evapotranspiration and the soil moisture content are effected.

4) Surface albedo. Albedo exerts a large effect on the energy balance and thus temperature variation.

5) Depth of root zone and root density distribution. The effects from these two parameters on the grid evaporation, sensible heat, moisture content and temperature are small.

APPROVAL PAGE

Doctor of Philosophy Dissertation
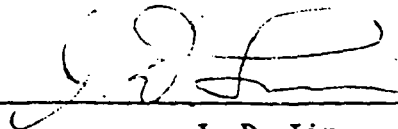
A SENSITIVITY STUDY OF THE GROUND HYDROLOGIC MODEL

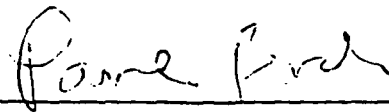USING DATA GENERATED

BY AN ATMOSPHERIC GENERAL CIRCULATION MODEL
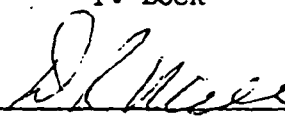
Presented by

Shu Fen Sun, M.S.

Major Adviser _____
J. D. Lin

Associate Adviser _____
P. Bock

Associate Adviser _____
D. R. Miller

The University of Connecticut

1985

ACKNOWLEDGEMENTS

I want to acknowledge the contribution to this research work provided by my major advisor Professor J. D. Lin. Dr. Lin suggested the topic of this dissertation, and constantly guided and helped me through the planning, programming and results analysis of the research work.

I also want to express my thanks to my associate advisor, Professors P. Bock and D. R. Miller, for their help, guidance and encouragement during the course of this investigation, and review of this thesis.

Thanks should also be given to Mr. Focazio and Mr. Thistle for their friendship and help.

The people in the Civil Engineering Department are owed a debt of gratitude for their help and support while I pursued my graduate study at the University of Connecticut.

Finally, I am grateful to the staff in the University Computer Center for their assistance.

TABLE OF CONTENT

LIST OF TABLE

LIST OF FIGURE

NOTATIONS

A,B,C	coefficients in Equation (3.5.11b)
$A(\theta_i)$	$D(\theta_i)$ or $K(\theta_i)$ in (3.3.4) (cm^2/s or cm/s)
A_{ij}	D_{ij} or K_{ij} (cm^2/s or cm/s)
a_l	albedo
a_{lb}	albedo of bare soil
a_{lc}	albedo of canopy
a_r	coefficient in Equation (2.4.2a) ($cm^{2.4}/s$)
a_1	coefficient in Equation (2.4.4a) (cm/s)
a_2	coefficient in Equation (2.4.4a)
a_3	coefficient in Equation (2.4.4a)
b	variable in Equation (3.5.5c) ($^oK)^{-1}$
b_1	coefficient in Equation (2.4.4b) (cm^2/s)
b_2	coefficient in Equation (2.4.4b)
b_3	coefficient in Equation (2.4.4b)
C	volumetric heat capacity of soil ($cal/cm^3/^oK$)
C_c	volumetric heat capacity of canopy ($cal/cm^3/^oK$)
C_D	drag coefficient inside canopy
C_p	specific heat of air ($cal/g/^oK$)
C_{TN}	heat transfer coefficient in the neutral case
C_{uN}	friction coefficient in the neutral case
C_T	heat transfer coefficient ($-F/(u_*(T_{vm}-T_{vs}))$)
C_u	friction coefficient (u_*/u_m)

c_t	a constant in equation (3.3.21) (=2520 s/cm)
c_1	ratio of evaporation from the vegetated ground surface to total evapotranspiration from canopy in equation (3.4.3)
c_6	coefficient in Equation (3.3.17)
c_7	coefficient in Equation (3.3.17)
c_9	coefficient in Equation (3.3.21)
D	diffusivity of soil (cm^2/s)
Dt	time interval (=1800 sec.)
d	displacement (cm)
d_i	depth of the ith layer in root zone (cm)
d_{ij}	average transport distance between soil layer i and j in Equation (3.3.5) (cm)
d_1	depth of the surface layer in root zone (cm)
d_2	depth of the lower layer in root zone (cm)
$\bar{d}_1$	penetrating depth of diurnal temperature wave in Equation (3.2.1) (cm)
E	evaporation ($g/cm^2/s$)
E_b	evaporation from bare soil ($g/cm^2/s$)
E_c	evapotranspiriion from canopy layer ($g/cm^2/s$)
E_p	potential evapotranspiration ($g/cm^2/s$)
E_{pb}	potential evaporation from bare soil ($g/cm^2/s$)
E_{pc}	potential evapotranspiriion from canopy layer ($g/cm^2/s$)
E_{sd}	daily averaged grid evaporation predicted by GCM ($g/cm^2/s$)

E_t grid evapotranspiratiion from GHM $(g/cm^2/s)$

E_{td} daily averaged grid evapotranspiration predicted by GHM $(g/cm^2/s)$

E_u maximum unstressed transpiration or unstressed transpiration from canopy $(g/cm^2/s)$

F kinematic vertical flux in equation (3.4.7) $(cm/s*^oK)$

F_{av} grid kinematic vertical flux $(cm/s*^oK)$

F_b kinematic vertical flux from bare soil $(cm/s*^oK)$

F_c kinematic vertical flux from canopy layer $(cm/s*^oK)$

F_T kinematic sensible heat flux $H/(\rho_a*Cp)$ $(cm/s*^oK)$

F_{Tav} grid kinematic sensible heat flux $(cm/s*^oK)$

F_{Tb} kinematic sensible heat flux from bare soil $(cm/s*^oK)$

F_{Tc} kinematic sensible heat flux from canopy $(cm/s*^oK)$

F_w kinematic moisture flux (E/ρ_a) (cm/s)

F_{wav} grid kinematic moisture flux (cm/s)

F_{wb} kinematic moisture flux from bare soil (cm/s)

F_{wc} kinematic moisture flux from canopy layer (cm/s)

G grid heat flux into soil surface or heat flux inside soil in equation (2.4.5) (ly/s)

G_b heat flux into bare soil surface (ly/s)

G_c heat flux into vegetated ground surface (ly/s)

g	gravitational acceleration (cm/s^2)
H	sensible heat flux (ly/s) or total water potential in section 2.4.1 (cm)
H_b	sensible heat flux from bare soil (ly/s)
H_c	sensible heat flux from canopy (ly/s)
H_{cb}	sensible heat flux from ground surface to canopy layer (ly/s)
H_{sd}	daily averaged grid sensible heat predicted by GCM (ly/s)
H_t	grid sensible heat (ly/s)
H_{td}	daily averaged grid sensible heat predicted by GHM (ly/s)
H_o	depth of ponding water (cm)
h	thickness of planetary boundary layer (cm)
h_c	height of canopy (cm)
I_b	infiltration at bare soil (cm/s)
I_c	infiltration at vegetated ground surface (cm/s)
I_o	I_b or I_c (cm/s)
I_{si}	infiltration of snow melt (cm/s)
K	soil hydraulic conductivity (cm/s) or temperature in Kelvin
k	Von Karman constant (=0.35)
K_r	constant in Equation (2.4.2b) (cm/s)
K_s	saturated soil hydraulic conductivity (cm/s)
L	latent heat constant (cal/g)
LAI	leaf area index
L_f	distance from soil surface to wetting front (cm)
L_m	Moning-Obukhov length (cm)
ly	Langley (cal/cm^2)
P	air pressure (mbar)

P_r precipitation rate (cm/s)

q moisture flux in soil (cm/s) or specific humidity

q_b specific humidity at lower boundary of PBL over bare soil surface

q_c specific humidity at lower boundary of PBL over canopy layer surface

$q_*^*(T_c)$ or q_c^* saturated specific humidity at T_c

$q_*^*(T_{gb})$ or q_b^* saturated specific humidity at T_{gb}

q_m mean specific humidity within the planetary boundary layer

q_s q_b or q_c

q_{ij} moisture flux between soil layer i and j (cm/s)

R 0.74 in Equation (3.4.9b)

R_{di} plant root density in layer i (i=1, 2)

RI_b Richardson Number

RI_c critical Richardson number (=3.05)

R_{LN} net long wave radiation(amount absorbed minus amount emitted) in equation (2.6.1) (ly/s)

R_n net radiation (ly/s)

R_{nb} net radiation over bare soil (ly/s)

R_{nc} net radiation over canopy layer (ly/s)

R_o runoff in equation (3.3.13) (cm/s)

R_{off} surface and subsurface runoff (cm/s)

R_{si} subsurface runoff in layer i (i=1,2) (cm/s)

R_s short wave radiation (ly/s)

r_c canopy resistance to transpiration (=r_{cm}) (s/cm)

r_{cb} air resistance inside canopy in equation (4.2.22) (s/cm)

r_{cm} minimum unstressed canopy resistance (s/cm)

r_{cr}	canopy resistance to actual transpiration (s/cm)
r_v	air resistance to evaporation or transpiration (s/cm)
S	potential temperature (^{O}K)
S_{av}	grid surface potential temperature (^{O}K)
S_b	potential temperature of the bare soil surface (^{O}K)
S_c	potential temperature of the canopy layer (^{O}K)
S_f	suction head (cm)
S_L	long wave radiation (ly/s)
S_m	mean potential temperature within PBL (^{O}K)
S_s	S_b or S_c (^{O}K)
S_w	short wave radiation (ly/s)
T	temperature (^{O}K)
T_{ad}	daily averaged air temperature (^{O}K)
T_a	air temperature at the anemometer height (^{O}K)
T_g	grid surface temperature defined in section 3.5 or ground surface temperature in equation (1.2.1) (^{O}K)
T_c	temperature of canopy layer (^{O}K)
T_{cd}	daily averaged temperature of canopy layer (^{O}K)
T_{gb}	surface temperature of bare soil (^{O}K)
T_{gbd}	daily averaged surface temperature of bare soil (^{O}K)
T_{gc}	temperature of vegetated ground surface (^{O}K)
T_{gd}	daily averaged grid surface temperature from GHM defined in section 3.5 (^{O}K)
T_{gab}	aver($|T_{gd}-T_{ad}|$) over 45 days (^{O}K)
T_{gamax}	max($|T_{gd}-T_{ad}|$) in 45 days (^{O}K)
T_{gsb}	aver($|T_{gd}-T_{gsd}|$) over 45 days (^{O}K)

T_{gsd}	daily averaged grid surface temperature from GCM (^{O}K)
T_{gsmax}	$\max(|T_{gd}-T_{gsd}|)$ in 45 days (^{O}K)
T_m	mean temperature in planetary boundary layer (^{O}K)
T_{samax}	$\max(|T_{gsd}-T_{ad}|)$ in 45 days (^{O}K)
T_{sab}	$\mathrm{aver}(|T_{gsd}-T_{ad}|)$ over 45 days (^{O}K)
T_v	virtual potential temperature (^{O}K)
T_{vav}	virtual grid surface potential temperature (^{O}K)
T_{vb}	virtual potential temperature of bare soil surface (^{O}K)
T_{vm}	average virtual potential temperature within planetary boundary layer (^{O}K)
T_{vc}	virtual potential temperature of canopy layer (^{O}K)
T_{vs}	virtual potential temperature of bare soil surface or canopy layer (^{O}K)
$\bar{T}$	layer-average temperature of soil layer (^{O}K)
$\bar{T}_d$	daily averaged layer-average temperature (^{O}K)
U_i	water uptake rate by the root in ith layer (i=1,2) (cm/s)
u_*	friction velocity (cm/s)
u_a	wind velocity at the anemometer height (cm/s)
u_{*av}	grid friction velocity (cm/s)
u_{*b}	friction velocity over bare soil surface (cm/s)
u_{*c}	friction velocity over canopy layer (cm/s)
u_{cb}	mean wind velocity inside canopy in equation (4.2.23) (cm/s)
U_m or u_m^m	mean wind velocity within planetary boundary layer (cm/s)
VMC	volumetric moisture content
V_1	volume fraction of sand and silt

V_2	volume fraction of clay
V_3	volume fraction of organic matter
X_c	extinction coefficient in equation (2.5.1)
X_M	heat storage increment rate of biomass in canopy (ly/s)
z_o	surface roughness parameter (cm)
z_{ob}	bare soil surface roughness parameter (cm)
z_{oc}	canopy surface roughness parameter (cm)
z_{oav}	grid surface roughness (cm)
z	distance below the soil surface (cm)

Greek

α	E_u/E_{pc} or $(1+2\delta/d_1)$
α_r	parameter in Equation (2.4.2) (cm^{-1})
β_b	scaling factor in equation (3.6.1)
β_c	scaling factor in equation (3.6.4)
δ	1 cm (thin surface layer thickness) in Equation (3.2.1)
θ	volumetric moisture content
θ_{av}	$\theta - \theta_{pwp}$ from GHM
θ_{avf}	θ_{av}/θ_{avm} or $(\theta_{bard} - \theta_{pwp})/\theta_{avm}$ for GHM (daily averaged available moisture fraction)
θ_{avsf}	$\theta_{avsd}/\theta_{avms}$ (daily average moisture content fraction for GCM)
θ_{avm}	$\theta_{fc} - \theta_{pwp}$ from GHM
θ_{avms}	maximum available water = $(\theta_{fcs} - \theta_{pwps})$ in GCM
θ_{avsd}	daily averaged available moisture content in GCM
θ_{bard}	daily average of $(\theta_1 * d_1 + \theta_2 * d_2)/(d_1 + d_2)$ from GHM
θ_{fc}	volumetric moisture content at field capacity in GHM

θ_{fcs}	volumetric moisture content at field capacity in GCM
θ_i	volumetric moisture content in layer i
θ_{in}	initial moisture content
θ_{ini}	initial moisture content in ith layer
θ_{pwp}	volumetric moisture content at wilting point
θ_{pwps}	volumetric moisture content at wilting point in GCM
θ_s	volumetric moisture content at saturation
θ_t	threshold value of moisture content
θ_{1d}	daily averaged moisture content in upper layer
θ_{2d}	daily averaged moisture content in lower layer
λ_1	heat conductivity of sand and silt (cal/cm/s/$^{\circ}$K)
λ_2	heat conductivity of clay (cal/cm/s/$^{\circ}$K)
λ_3	heat conductivity of organic matter (cal/cm/s/$^{\circ}$K)
ρ_a	air density (g/cm^3)
ρ_w	water density (g/cm^3)
σ_b	bare soil fraction in grid
ΔT	variable in Equation (3.5.19b) ($^{\circ}$K)
σ_c	vegetation fraction in grid
ψ	soil matrix potential (cm)
ψ_r	soil matrix potential in Table 2.4.1 (cm)
τ	86400 (sec)

Note: All variables preceded by 'grid' indicate these variables are grid averaged. All variable preceded by 'daily' indicate these variables are daily averaged.

Chapter I

INTRODUCTION

1.1 SIGNIFICANCE OF LAND SURFACE PROCESSES

In the earth environment, there are two basic transfer processes, the transfer of water and heat between land surfaces and the atmosphere. The hydrologic cycle deals with the transport of water in the gas, liquid and solid states. Precipitation as one of the main components in the cycle is the predominant source of water supply to the earth. It contributes to soil moisture and groundwater through infiltration and deep percolation, or remains as surface water through surface or subsurface runoff. However, approximately 60 to 70% of precipitated water on land surfaces returns to the atmosphere through evapotranspiration. The part of the hydrologic cycle near the atmosphere-land interface can be isolated and described by the principles of conservation of water mass. For a one-dimensional soil column of finite depth below the ground surface, the equation for the water balance is

$$dM/dt = P_r - E - R_o - R_b \qquad (1.1.1)$$

where M is the water stored in the column, P_r the precipitation including snow and ice melt on the land surface, E

the evapotranspiration, R_o the surface and subsurface runoff, and R_b the deep percolation. All variables in Eq. (1.1.1) except P_r are closely related to the soil moisture content in the column.

The other important process on land surfaces is the heat exchange between land surfaces and the atmosphere. Short-wave solar irradiation and long wave irradiation from the atmosphere are the main supplies of the thermal energy for the hydrologic system. The latent heat plays an important role in linking the thermal energy exchange with the water cycle.

If the heat transfer of snow and ice melt and plant photosynthesis are neglected, the net heat flux to the ground G can be determined by the energy balance on the ground surface,

$$G = R_n - L*E - H \qquad (1.1.2)$$

where R_n is the net radiation, L the latent heat of vaporization of water, E the evapotranspiration upward from the surface and H the sensible heat flux. The terms in the right-hand-side of Eq. (1.1.2) are greatly affected by ground surface temperature and in turn the surface temperature is determined by the heat transport process.

The total evaporation in a year averaged over the land is 0.45 m (Brutsaert, 1981) per unit surface area. It is much more than the fresh water stored in a soil column

(0.161 m) or in an atmospheric column (0.0274 m) of the same cross-sectional area. In other words, the hydrological process at the land surface is quite capable of renewing the moisture in soil and in the air.

In recent years, it has been shown in the course of atmospheric general circulation modeling that land surface processes exert a great influence on atmospheric movements and climatic changes (Eagleson, 1981; Mintz, 1981; Shukla and Mintz, 1982). Numerical experiments have been carried out under different land surface conditions and parameterizations. The results show large differences in the calculated precipitation, temperature and motion of the atmosphere. These studies have indicated that a physically realistic land surface hydrology model is essential to provide a GCM with a better estimate of exchange of pertinent properties on the atmosphere-land surface.

Mathematically, a GCM needs to be supplied with lower boundary conditions at the land surface. An interactive ground hydrology model should be designed to simulate the soil moisture content and ground temperature as well as estimate the moisture and heat fluxes across the atmosphere-land interface for the purpose of providing the source terms in the governing equations of GCM.

GCMs have been developed through several generations (Carson, 1981) and have now reached a relatively advanced

stage. The most current GCMs are complex and make increasingly large demands on the most advanced computers. However, their representation of land surface processes is still crude and simplistic. This situation urges researchers to engage a more active and concerted effort on the land surface process study in order to provide a physically realistic GHM for use in GCMs.

1.2   PREVIOUS STUDY

Reviewing the previous work, one finds that the study of land surface processes interactive with a GCM has gone through a number of developmental stages. In the earlier stage, GCMs use only fixed boundary conditions, for example, completely saturated soil with zero heat capacity. In fact, there was no ground hydrology involved. The concept of zero soil heat capacity was used by Manabe et al. (1965) and later employed in a GCM by Gates and Schlesinger (1977). The consequence of this assumption is an enlargement of the amplitude of diurnal surface temperature variation. A 'bucket' hydrologic model was developed by Manabe (1969) and used by Washington and Willimson (1977). This model was designed to incorporate the most critical feature of soil moisture without resorting to a more rigorous approach such as Philip and deVries (1957). The depth of water contained in the bucket represents the soil moisture per unit surface area in the plant root zone available for

evapotranspiration. The bucket has a capacity equivalent to the maximum available soil moisture in the root zone or the field capacity of soil. By following Budyko (1961), actual evaporation is scaled from the potential evaporation through a proportionality factor which depends on the available soil moisture content. Runoff occurs only if water contained in the bucket exceeds the depth of the bucket. In the model, the effects of different land surface cover, different soil type, and their spatial and temporal variation are not considered. Thus, the bucket model appears to be oversimplified. Deardorff (1978) proposed a hydrologic model with inclusion of a canopy layer. In his model, the force-restore method was used to describe soil temperature, which is distinguished by a ground surface temperature with diurnal variation and a layer-average temperature with seasonal change. Vegetation canopy were modeled as a single layer with no heat capacity. Soil moisture was calculated in a way similar to the ground temperature. The soil is divided into two layers: a upper surface layer of 10 cm thick and deep layer of 50 cm thick. The equations describing moistures in these two layers are similar to those describing the temperatures but with different physical parameters.

The model developed by Lin, Alfano and Bock (1978) is one of the more advanced models for use in a GCM, which includes physically-based hydrological phenomena. Since this

study is developed from this model, it will be discussed in some detail.

It is a two-layer ground hydrology model, which was designed to dynamically interact with the atmospheric general circulation model developed at the NASA Goddard Laboratory for Atmospheric Science (GLAS) as described in Halem et al. (1979), Somerville et al. (1974) and Tsang and Karn (1973). Figure 1.2.1 (from Alfano, 1981) demonstrates schematically the main physical features of the model.

In order to be compatible with the GLAS GCM, the land surface grid formation and the grid corresponding code in this model are exactly the same as the GCM (see Tsang and Karn, 1973). Each grid is a rectangular cell of 4° longitude by 5° latitude. The grid code for the latitude and longitude is shown in Table 1.2.1.

A global characterization of soil and vegetation was incorporated into the model. Five types of soil texture from fine sand to clay loam based on the work of Ritjema (1970) and twelve categories of vegetation from tropical rain forest to desert (Strahler, 1971) were used. A soil texture and a vegetation type were specified for each grid with further subgrid parameterization of vegetation density by fractional portions of bare soil and vegetative cover. Their relative fraction changes with grids and is also adjusted for seasonal variation and for latitude. In this

model, the ground temperature was calculated by the modified force-restore method (Lin, 1980). Even though the root zone was layered similar to Deardorff's, the rate equations for soil moisture in the two layers were based on the Richards law, in which all coefficients are derived from physical principles.

The prognostic variables for describing the soil moisture in this model are volumetric moisture contents in the surface layer and in the lower layer and for evaluating the heat budget are grid surface temperature and layer average temperature. The specification of the two layers for soil moisture movement is not necessarily the same as those for heat transport. The outputs from the model also include latent heat and sensible heat fluxes.

Recently, a multi-layer canopy model was proposed by Mintz et al. (1983) for the NASA GCM, which refines to some extent the Lin et al. model to account for the effect of rainfall interception.

Longitude, $1 \leq I \leq 72$

Longitude:	175	165	155	145	135	125	115	105	95	85	75	65	55	45	35	25	15	5
Index: I	E 72	70	68	66	64	62	60	58	56	54	52	50	48	46	44	42	40	38
	W 2	4	6	8	10	12	14	16	18	20	22	24	26	28	30	32	34	36

Latitude, $1 \leq J \leq 46$

Latitude:	90	82	74	66	58	50	42	34	26	18	10	2
Index: J	N 46	44	42	40	38	36	34	32	30	28	26	24
	S 1	3	5	7	9	11	13	15	17	19	21	23

Table 1.2.1 Relating between (I,J) and (Longitude, Latitude) coordinate systems.
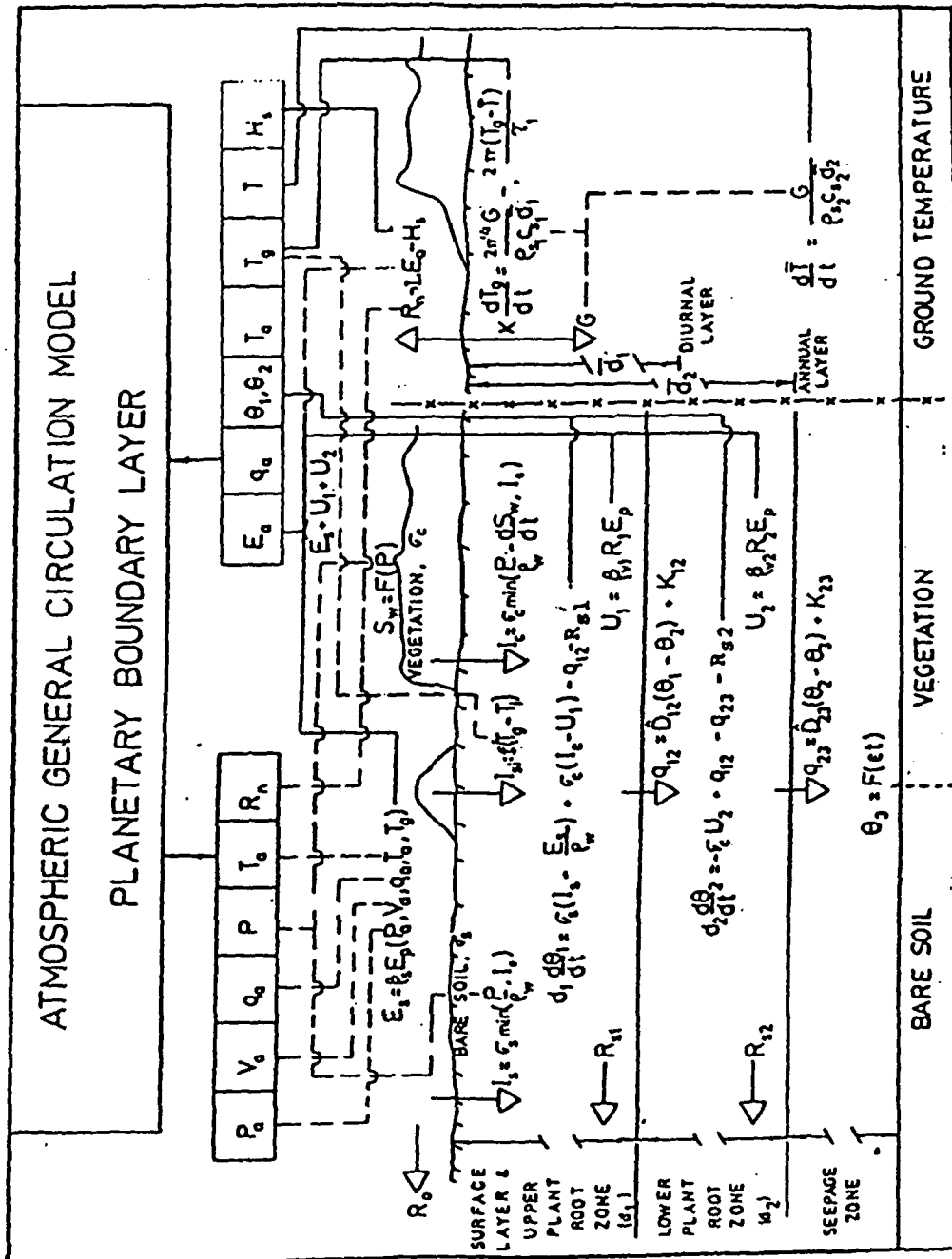
Figure 1.2.1 The ground hydrology model formulation - GHM.

1.3 SCOPE OF THE STUDY

In this study, several improvements on the Lin et al. model were implemented and a series of sensitivity studies of the GHM for a number of the pertinent physical parameters has been conducted.

This new version of the model is designed to couple with atmospheric variables in the PBL in stead of the surface values which are derived by extrapolation from the results in the lower layers of the GCM (Alfano, 1981). This approach will eliminate the crude approximation by the extrapolation. Moreover, in view of the large horizontal scale used by the GCM and GHM, it is inconceivable that the atmospheric conditions can be uniform over a grid near the land surface, say, at the 'anemometer height'. The actual physical system has the PBL between the free atmospheric field described by the GCM and the land surface (Brutsart, 1981). It is this layer that plays a dominant role in the transfer of momentum, moisture and sensible heat through turbulent transport and free convection.

Although many schemes for evaluating the turbulent transport in PBL have been proposed, one can classify them into two categories. Mellor and Yamada (1974) proposed a method using several layers within the lowest 2-3 km above the land surface to resolve the vertical structure of the PBL explicitly. This method is clear and direct but it re-

quires several finite-difference levels in the PBL to achieve tolerable computational accuracy.

Another approach is to parameterize all aspects of the PBL for a GCM. The drag coefficient and the bulk heat transfer coefficient are linked with a bulk Richardson Number defined for the entire PBL. The accuracy of this approach depends on the information available to describe the PBL. This knowledge has been accumulated recently. The parameterization suggested by Deardorff (1972) has been tested numerically and appears to be adequate for use in existing GCMs. The parameterization scheme will be adapted in this study.

A bulk canopy layer over the vegetated ground surface is added to the model. Vegetation canopy plays an important role in the heat balance and water cycle and exerts significant physiological and morphological effects on land surface processes (Deardorff, 1978; Mintz et al., 1983). Figure 1.3.1 (Mintz et al., 1983) describes the mean annual water and energy balance of a short and a tall vegetation, as derived from the measurements in two adjacent catchments having nearly the same atmospheric conditions. The total evapotranspiration loss from the forest catchment is more than twice as large as that from the grass covered catchment. With the grass cover, 58% of the net radiation energy on the surface is used for evapotranspiration and 42% for

the sensible heating of the atmospheric boundary layer. But
with the forest cover, the energy used for evapotranspira-
tion exceeds the radiational heating by 15%, and this re-
sults in a removal of sensible heat from the boundary lay-
er, i.e. a negative Bowen ratio. Although the atmospheric
conditions are about the same for the two catchments, the
net radiation R_n is 10% larger with the forest cover than
with the grass cover. This is not only because the forest
is darker and absorbs more of the incident solar beam, but
also because the lower forest temperature will cause the
forest to emit less infrared radiation. This example dem-
onstrates that a canopy either modeled as a bulk layer or
multi-layers between the atmosphere and ground surface are
critical for describing land surface processes.

The role played by infiltration in the partition of pre-
cipitation is very important. Its rate can affect the mag-
nitude of surface and subsurface runoff as well as the
amount of water stored in the soil. The infiltration rate
is determined by many factors such as vegetation type, soil
texture, rain intensity and so on. Its accurate evaluation
requires sophisticate numerical methods.

There are several methods being used currently to esti-
mate infiltration rate. The most known are the empirical
equation of Kostiakov (Childs, 1969) and Horton (1940)
which have been popular because of their simplicity and ap-

plicability to most situations. However, both equations contain parameters that are difficult to predict because they have no physical basis. A more recent empirical equation was given by Holtan (1961). It expresses the infiltration rate as a function of unoccupied pore space in soil. The model is convenient to use but its parameters including the characteristic depth are difficult to determine.

A simple equation proposed by Green-Ampt (1911) has recently attracted new attention because it has clear physical meaning and can be expressed by a simple formula derived from the Richards law. In this study, this method will be adopted.

Finally, the atmospheric stability effects will be included. When the atmosphere is stable, turbulent mixing is suppressed and exchanges between the air and the land surface will be reduced. Conversely, if the unstable condition occurs, the turbulent mixing is intensified and exchanges between the air and the land surface will increase. The true neutral case is rare. Thus, inclusion of the stability effects provides a better estimation of heat and moisture fluxes.

Verification of a large-scale hydrologic model such as this is extremely difficult because data are not generally available. Some of them are even not well understood. In

order to understand the effects of the parameters on the GHM, a wide range of sensitivity study is justified. The sensitivity studies that were performed are described as follows.

1) Different initial and boundary conditions.

Natural hydrologic conditions vary temporally and spatially. This is also true for initial and boundary conditions in the GHM. For example, the moisture conditions in the rainy season are totally different from those in dry months. Also, the moisture content in a high rainfall region is different from that in a desert. This situation requires a great deal of data to prescribe the initial and boundary conditions everywhere at a given time. Since these data sets are not likely to be available in the near future, the problem of how long and to what extent the effect introduced by approximate or arbitrary initial and boundary conditions will persist should be studied. Two extreme moisture initial conditions (wet and dry) and two currently used lower boundary conditions are studied.

2) Selected physical parameters. There exists a wide latitude of variation in the parameters that are used in the GHM. Many of them can not be prescribed precisely for the large-scale parameterization. For example, transpiration is influenced by canopy resistance and the distribution of the root system, but there are not sufficient data available

for the global characterization used in the model. The sensitivity study can show us to what extent the effects from the variation of each parameter are and then can provide some insight for improving GHMs in the future.

The ground hydrologic model is designed to interact with a GCM, but for the purpose of model development and testing it is much more practical and efficient to conduct the study non-interactively. This means the GHM is driven directly by prescribed atmospheric variables in the PBL that are derived from the GCM output data. For this study, the input data is available globally for 45 days from July 10 to August 25 in 1975 from the NASA GLAS GCM. Only eight regions with different climate and different land surface characteristics across the North America continent are selected for the model evaluation and the sensitivity studies. The eight regions, following the code index (I,J) in Alfano (1981) and Tsang and Karn (1973) are listed in Table 1.3.1 with * mark. The relation between (I,J) and (longitude, latitude) is shown in Table 1.3.2 where the number in the parenthesis on the upper left indicates the longitude and the number on the lower right indicates the latitude.
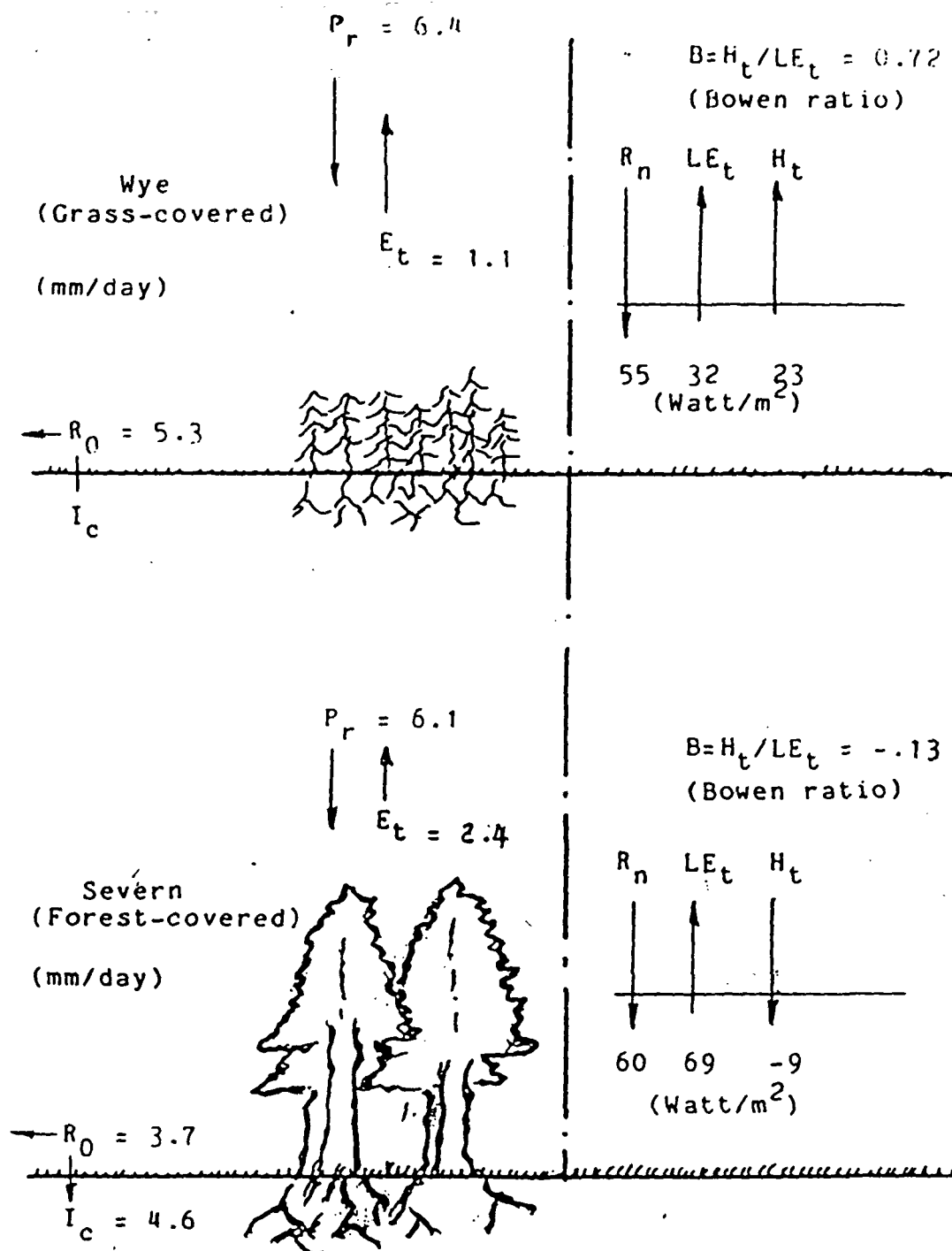
Figure 1.3.1 Measured mean-annual water and energy balances of adjacent grass-covered and forest-covered catchments, in central Wales, U.K., (Mintz, Sellers and Willmont, 1983)

17

J \ I	13	15	17	19	21	22
35			*			
34						*
33	*	*	*	*	*	
32				*		

Table 1.3.1   Index for eight regions

J \ I	13	15	17	19	21	22
35			100 46			
34						75 42
33	120 38	110 38	100 38	90 38	80 38	
32				90 34		

Table 1.3.2   Latitude (north) and longitude (west) for eight regions

Chapter II

SPECIFICATION OF LAND SURFACE CHARACTERISTICS

Land surface hydrological processes are strongly influenced by the properties of land surface cover and the soil underneath. Although land represents only around 29.2% of the earth's surface $(146*10^6 \text{ km}^2)$, its effects on the atmospheric general circulation and climate become significant when air moves over the continents. The land surface cover is never uniform. It varies spatially from complete bare soil to fully covered vegetation. It varies dynamically according to seasonal variation of vegetal surface cover due to climatic adjustment and biological evolution of plants. So, an important, prerequisite step to the development of the GHM is the characterization of soil and vegetation from grid to grid and with seasonal changes.

Despite the fact that a one-dimensional transport of momentum, heat and moisture is applied to each grid, the horizontal variability of the GHM is accomplished by varying the land surface character from grid to grid. In this chapter, this necessary information about the global land surface will be provided, much of which has been described in Lin et al. (1978) and Alfano (1981). In order to realistically model land surface processes spatially and tempo-

rally, the following characterization should be provided to every grid in the GHM:

1) specification of soil types and their relevant properties.

2) specification of vegetation types and their relevant properties

3) specification of vegetation fraction and its seasonal variation

2.1   SOIL TYPE AND ITS DISTRIBUTION

In this subsection, the available global soil data will be evaluated in order to supply the GHM with appropriate information.

Soil consists of solid phase (organic matter and mineral), liquid phase (water) and gas phase (air, water vapor and other gases). The size of mineral particles ranges from very fine clay particles of less than 0.002 mm in diameter to coarse sandy particles of up to 2 mm in diameter. The U.S. Department of Agriculture, based on the fraction of sand, silt and clay contained in the mineral matter of soil, has presented a classification of 12 soil textures (Bridges, 1978) which is shown in a textural triangle in Figure 2.1.1. The classification is critical because the water movement inside the soil is dependent upon the textural composition. In the GHM, following Alfano's work,

the soil is characterized by its texture into 5 types that
are consistent with the 12 soil textures in Figure 2.1.1.
The five types of soil labeled as A to E are listed below :

Soil type label with letter	Class by textural specification
A	Sand
B	Sandy loam
C	Loamy sand
D	Loam
E	Silt clay loam

The percentage of sand, silt and clay in the mineral for the 5 types of soil was obtained by Buckman and Brady (1960) and is shown in Table 2.1.1.

Soil type	% of sand and silt in mineral	% of clay in mineral
Sand (A)	95	5
Sandy loam (B)	90	10
Loamy sand (C)	95	5
Loam (D)	65	15
Silt clay loam (E)	70	30

Table 2.1.1   Percentage of soil, silt and clay
in the GHM soil type

Soil Types in GHM   Soil Types Not in GHM

A-1 Sand, A-2 Silt   S-1   Clay

B   Sandy loam   S-2   Sandy Clay

C   Loamy sand   S-3   Silty Clay

D-1 Loam, D-2 Silt loam

E-1 Clay loam, E-2 Sandy clay loam

E-3 Silty clay loam
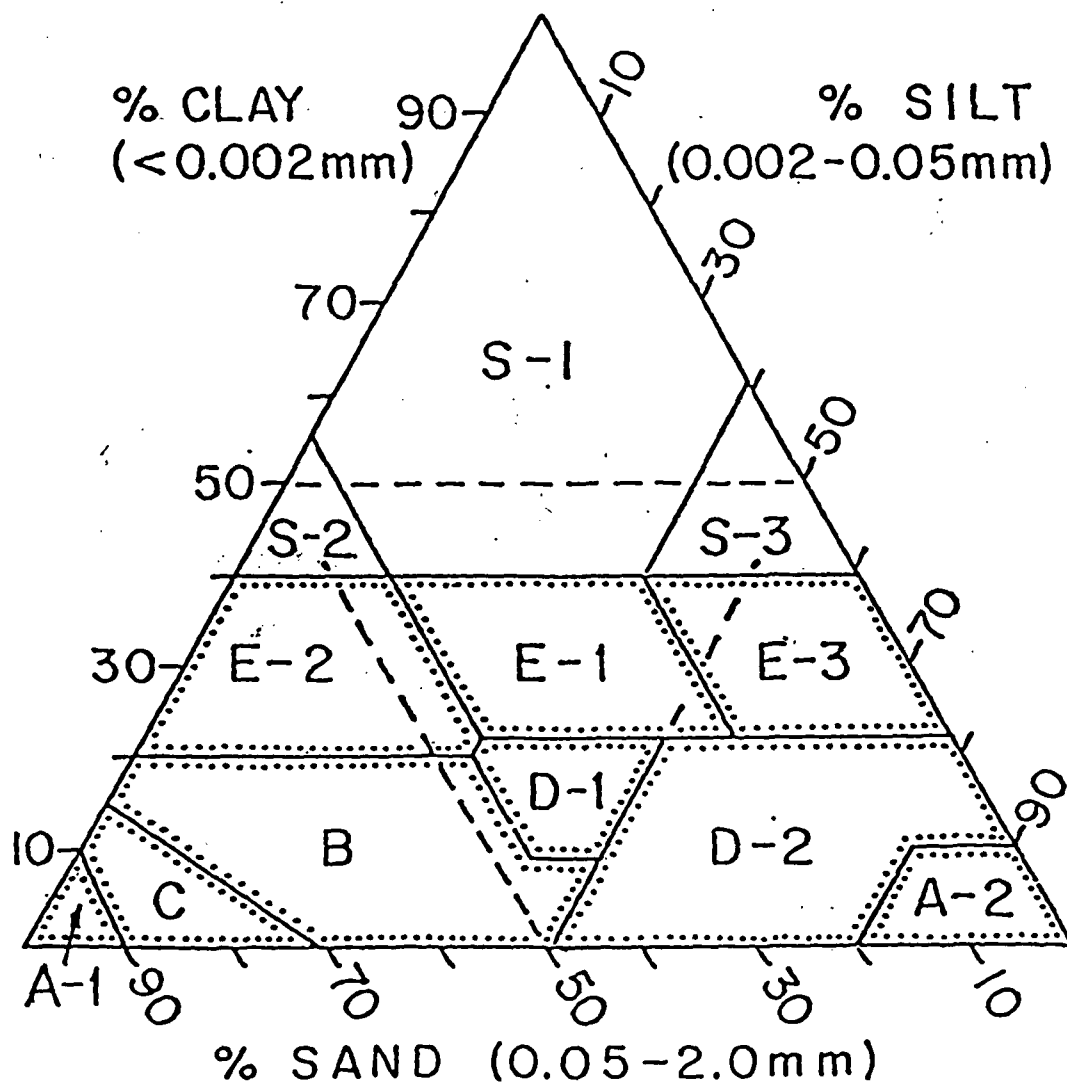
Figure 2.1.1   Model textural soil representation of
the U.S. Department of Agriculture
textural class triangle.

The water content in the soil is an important variable for determining matrix potential, hydraulic and thermal properties. Different types of soil have different water holding capacity.

Ritjema (1970) grouped the soil into 20 types and presented the relationships between soil moisture and the soil properties for each type of soil. Ritjema's classification was related to the classification with 5 soil types (Alfano, 1981) for use in the GHM. Table 2.1.2 shows the relation and gives the water holding properties for different types of soil. In the table (Alfano, 1981), θ_{fc} is defined as the value when the matrix potential $\psi = -350$ H_2O-cm and θ_{pwp} is defined as the value when $\psi = -16,000$ H_2O-cm.

The five types of soil in the GHM should be related to the soil distribution (Eyre, 1968) in the world to specify the soil type in every grid. Figure 2.1.2 (Strahler, 1963) shows the map of the world soil group distribution. The linkage between the soil type in the GHM and the zonal soil categories (Mitchell, 1976; Chow, 1964) which then can be related to the world soil groups (Strahler, 1971) was schemed by Alfano (1981) and is used in this study. (see Table 2.1.3)

The previously defined relationship between zonal soil categories and the 5 textural soil types permits a global distribution of soil to be specified on the basis of the

zonal soil categories. Alfano has presented the distribution in a map form as given in Fig. 2.1-3a and b.

Soil Type	θ_{fc}	θ_{pwp}	θ_{avm}	θ_s
Coarse Sand	.020	.012	.008	.395
A Medium Fine Sand	.066	.023	.043	.35
Find Sand	.14	.04	.10	.36
Humors Loamy Medium Coarse Sand	.33	.11	.22	.47
C Light Loamy Medium Coarse sand	.22	.10	.12	.40
Loamy medium Coarse sand	.16	.02	.14	.30
Loamy fine sand	.13	.06	.07	.44
B Sandy loam	.16	.06	.10	.47
Loose loam	.26	.11	.15	.46
Fine sandy loam	.25	.09	.16	.50
Silt loam	.31	.09	.22	.51
D Loam	.27	.10	.17	.50
Sandy clay loam	.30	.18	.12	.43
E Silty clay loam	.32	.19	.13	.48
Clay loam	.38	.26	.12	.45
Light clay	.33	.21	.11	.45
Silty clay	.44	.26	.18	.51
Basin clay	.48	.32	.16	.54
peat	.68	.27	.41	.86

Note: The first one in every type is used in the GHM

Table 2.1.2 Characteristic soil moisture values, θ_{fc} θ_{pwp} and θ_s from Rijtema's (1970) soil types.

World Groups (Strahler,1971)	Zonal Category (NO) (Michell,1976)	Textural soil Type (letter)
podzolized soils	Podzol (2)	Sandy loam (B)
	Gray brown (3)	Loamy sand (C)
	Mtn Valleys (9)	Sandy loam (B)
Lateritic soils	Lateritic (5)	Silty clay Loam (E)
Grassland soils	Prairie (4)	Loamy sand (C)
	Chestnut brown (7)	Loam (D)
	Chernozems (6)	Loam (D)
Soils of Arid region	Sierozgems (8)	Sand (A)
Soils of cold region	Tundra (1)	Sandy (B)

Table 2.1.3 Linkage among soil type, zonal soil categories and world soil groups (Alfano, 1981)

World distribution of the
principal zonal soil groups
after U.S. Dept. Agriculture

1 Tundra   2 Podzols
3 Gray-brown podzolic soils
   (with brown forest soils)
4 Prairie soils (with degraded
   chernozems)
5 Latosols and red-yellow soils
6 Chernozems and red-chestnut soils
7 Chestnut, brown, and
   reddish-brown soils
8 Sierozems, desert, and red desert soils
9 Azonal (mountain) soils

Figure 2.1.2 World map of principal zonal soil groups (Strahler, 1963)

No.	Description
4	Prairie soils and degraded chernozem
5	Lateritic soils terra rosa
6	Chernozems and reddish chestnut soils

No.	Description
1	Tundra
2	Podzols (w/much bog)
3	Gray brown podozolic soils (with brown forest soils)
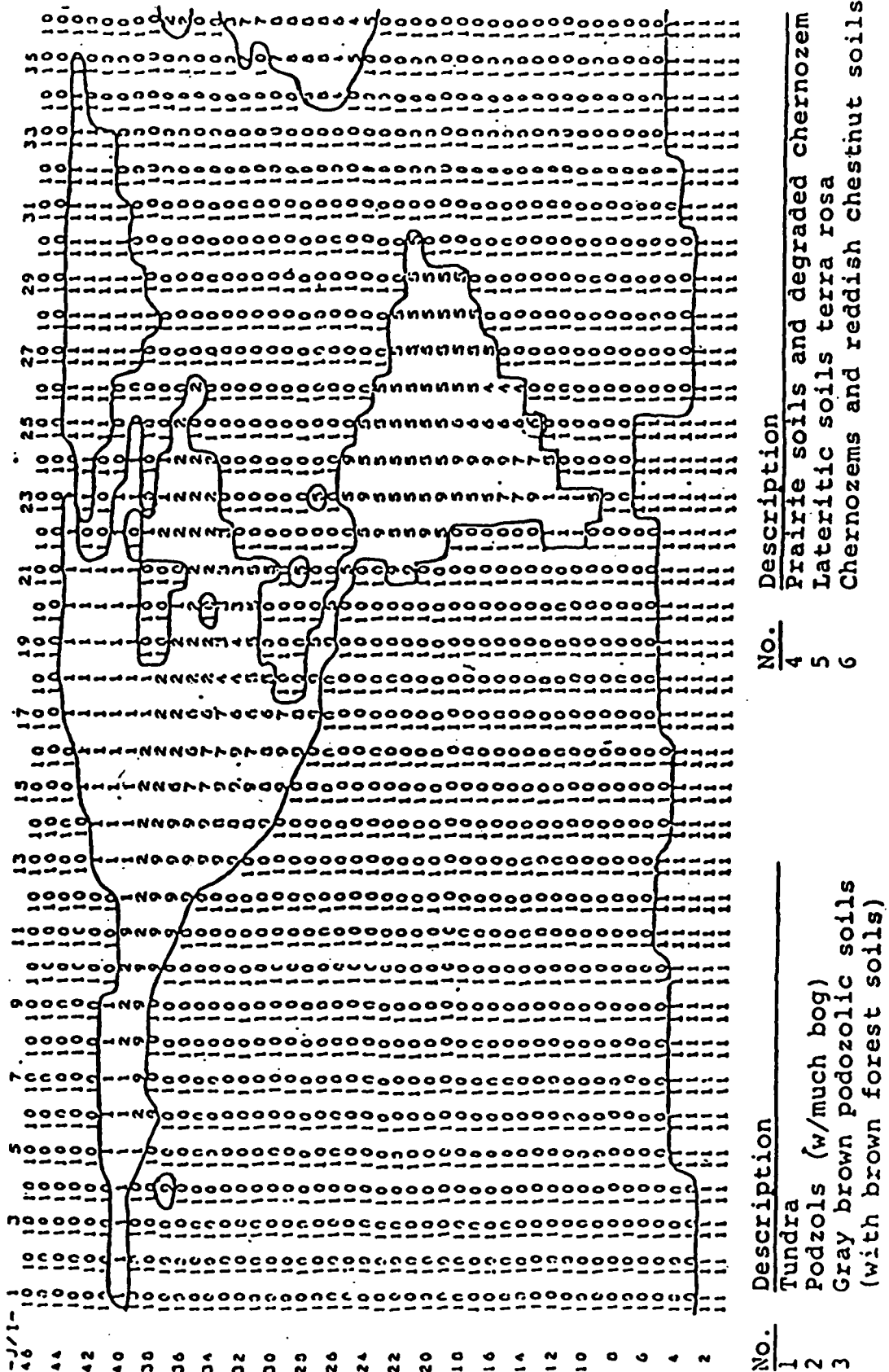
Figure 2.1-3a World zonal soil categories (Kellogg, 1941; Mitchell, 1976), western half of the world.

No.   Description
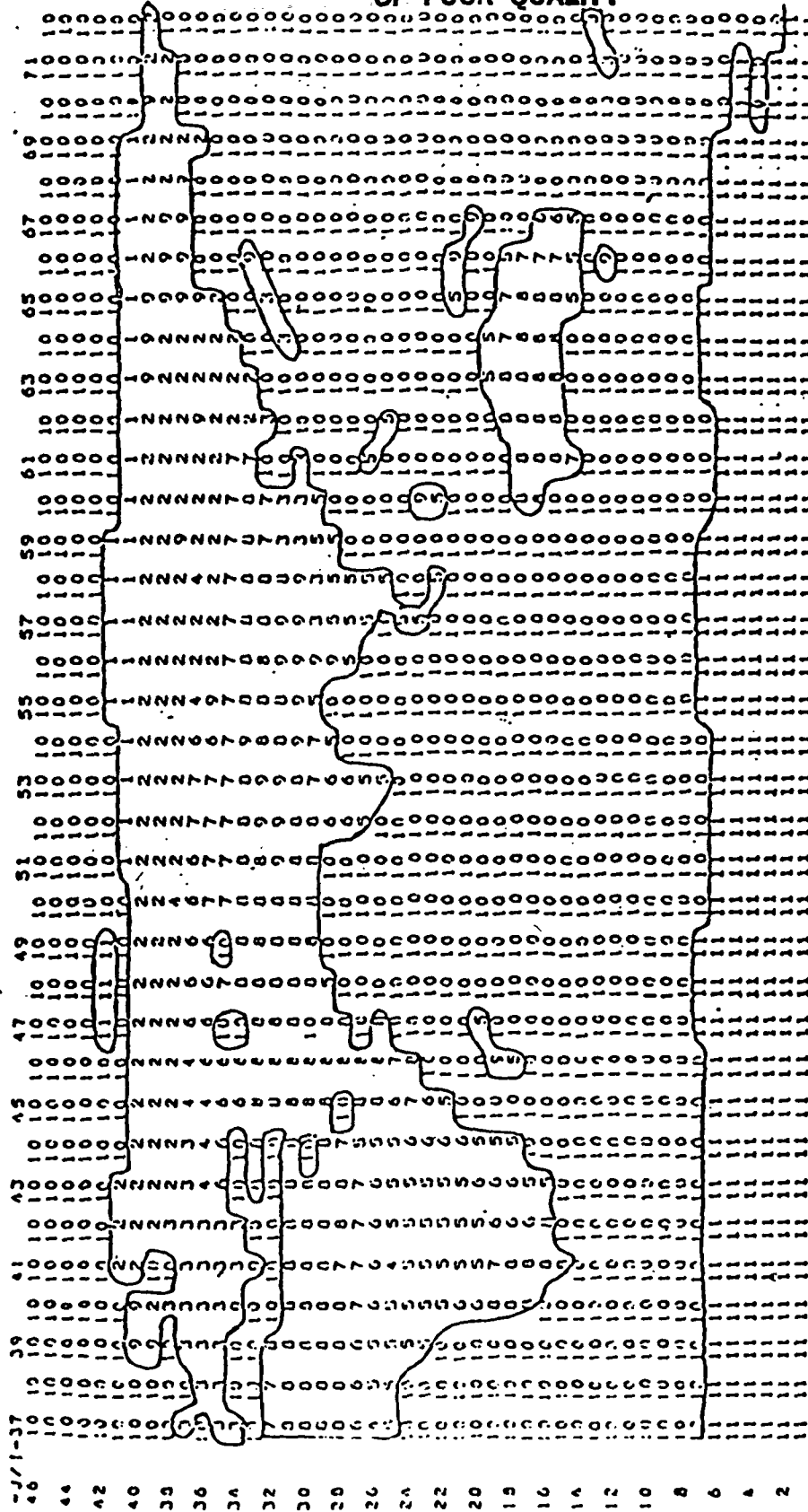
10   Ocean or lake
11   Ice

No.   Description

7   Chestnut, brown and reddish brown
8   Sierozems desert and red desert soils
9   Mountian and valley areas

Figure 2.1-3b World zonal soil categories (Kellogg, 1941; Mitchell, 1976),
eastern half of the world.

2.2 VEGETATION TYPE AND ITS DISTRIBUTION.

Attention should be paid to the vegetation cover when studying land surface processes. A canopy acting as an intermediate interface between the air and soil is more active than a bare soil surface not only because its structure can stimulate turbulence to intensify exchange between the air and land surface, but also because its root system can take up more water from the deep soil layer to maintain a high evapotranspiration rate. Also, vegetation can adjust the atmospheric demand by its own biological reaction such as opening and closing stomatal pores to control transpiration. The behavior of canopy makes modeling the vegetation functions more important and also more difficult.

The spatial vegetation distribution strongly depends on the climate which forms vegetation zones called zonobiomass. This zonobiomass are more or less modified by the soil properties, orography and other factors. The classification with eleven types for the world vegetation was used by Alfano (1981), based on Strahler's paper. They are:

1) Equatorial and tropical rainforest

2). Temperate rainforest

3) Evergreen hardwood rainforest

4) Raingreen forest, wood land, scrab and savanna

5) Steppe and prairie grasslands

6) Dry desert and semidesert

7) Summergreen deciduous forest

8) Needleleaf forest

9) Arctic tundra

10) Icecaps

11) Highland areas

The detailed description of the 11 types of vegetation can be found in Alfano (1981). The distribution of vegetation was described by Eyre (1968) and Strahler (1971). The distribution of the different kinds of vegetation was derived from the best available detailed map for parameterization of the global land surface, and is typical of other distributions (Collinson, 1977). Figure 2.2-1 shows the distribution of vegetation for all the land grids in the world (Alfano, 1980)

The volumetric organic matter fraction in a soil for vegetation types is given in the table below.

Type (Strahler, 1971)	Volumetric organic matter fraction (Buckman, 1960)
Rainforest	15.
Temperate rainforest	10.
Evergreen hardwood forest	7.5
Raingreen forest	10.
Steppe and prairie grasslands	5.0
Dry desert and semidesert	2.5
Summergreen deciduous forest	10.
Needleleaf forest	7.5
Arctic tundra	5.0
Highland areas	5.0
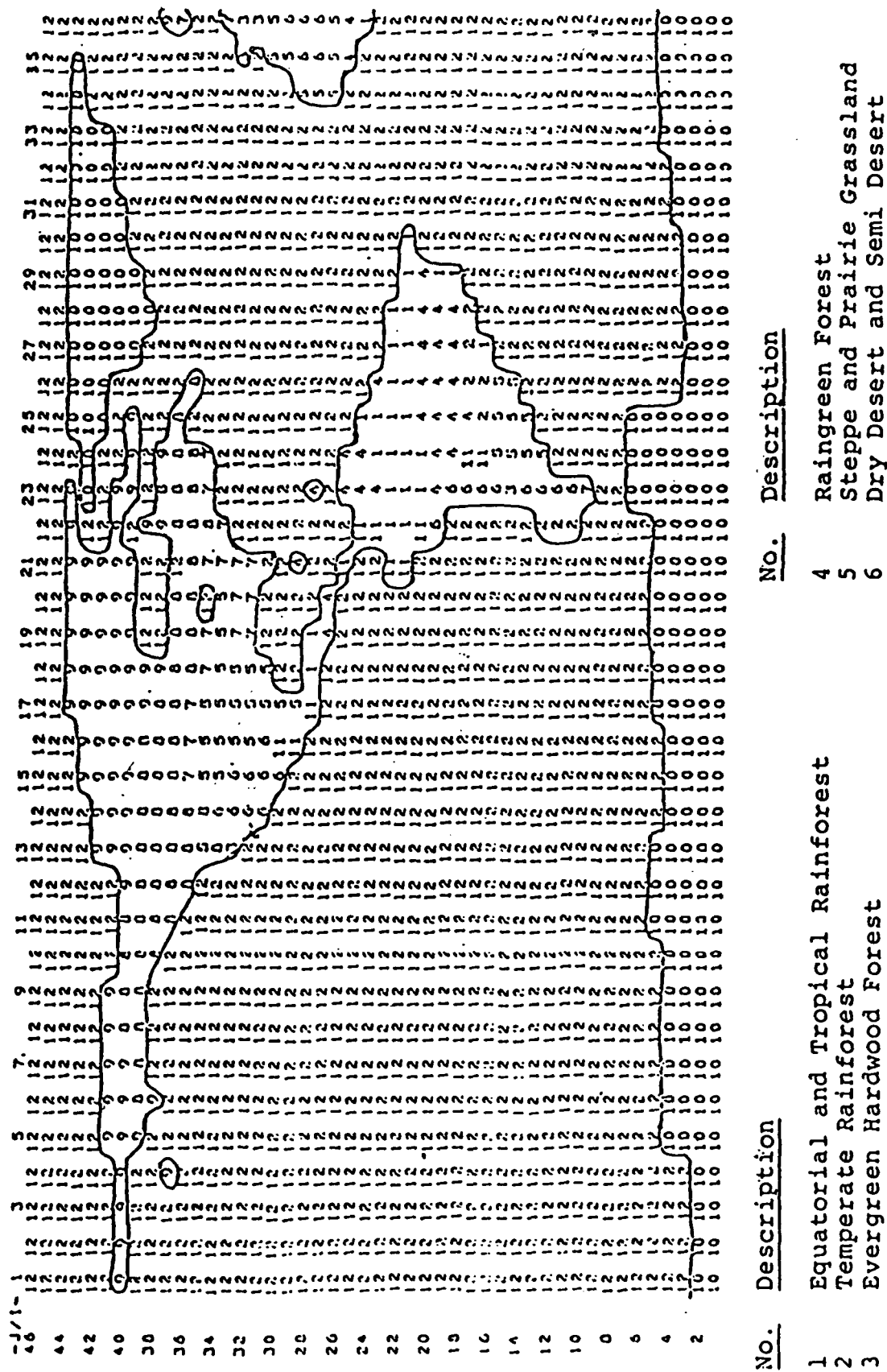
Figure 2.2-1a World vegetation types (Strahler, 1971), western half of the world.

No.   Description

1   Equatorial and Tropical Rainforest
2   Temperate Rainforest
3   Evergreen Hardwood Forest

No.   Description

4   Raingreen Forest
5   Steppe and Prairie Grassland
6   Dry Desert and Semi Desert

34
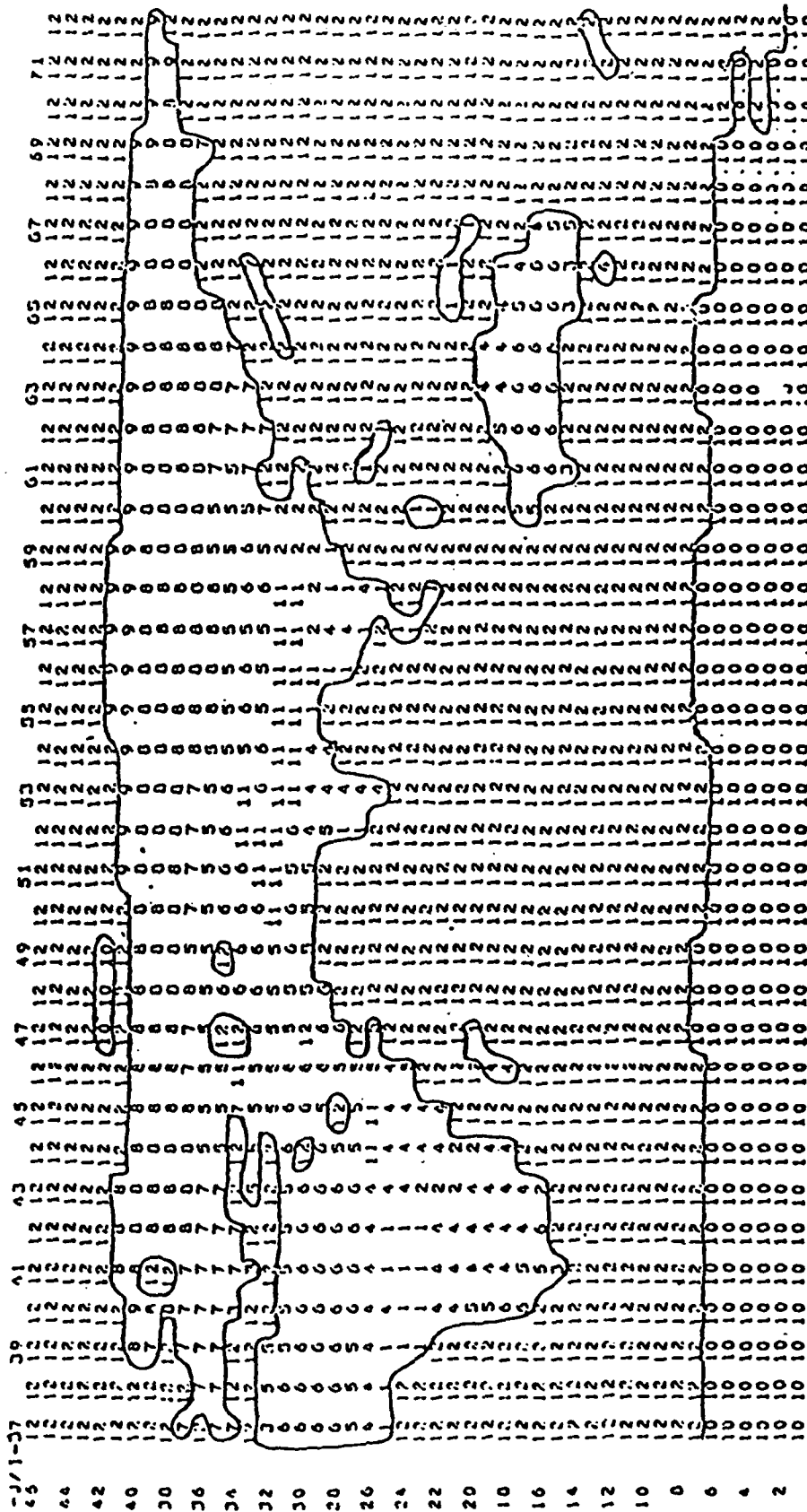
No.	Description
7	Summer Green Deciduous Forest
8	Needleaf Forest
9	Arctic Tundra

No.	Description
10	Ice
11	Highland Areas
12	Ocean or Lakes

Figure 2.2-1b World vegetation types (Strahler, 1971), eastern half of the world.

2.3 SUBGRID VEGETATION PARAMETERIZATION -- DISTRIBUTION AND VARIATION

The vegetation density is represented by the vegetation fraction σ_c in a grid and differs from grid to grid and varies with season. The definition of vegetation fraction is the fractional portion of vegetated cover in a grid. Then, the bare soil fraction is $\sigma_b = 1 - \sigma_c$. So, if $\sigma_c = 0.6$, it means that a grid is covered with 60% of vegetation and 40% of bare soil. Based on the pictorial difference in color and tone from the map (Strahler, 1971; Peele, 1975; Lee, 1977), Alfano (1981) assumed that the density corresponds to the full growing season and derived the global distribution map by the minimum bare soil fraction σ_b as shown in Figures 2.3-1a and 2.3-1b.

Figure 2.3-1 specifies the minimum bare soil fraction distribution for all land grids. However, the vegetation fraction changes with seasons. Actual vegetation fraction should be modified on the basis of the minimum σ_b and the annual percentage of the period in foliage.

To consider the seasonal change of σ_c (Figure 2.3.2), Alfano makes the following suggestions:

1) The period of vegetation in foliage, in days, which is correlated to the seasonal change in solar energy, consists of a 17.5 % (Rosenberg, 1974, Money, 1976) portion for growth (spring), a 65 % for full foliage (summer) and a 17.5 % for senescent (fall) shown in Figure 2.3-2

2) The foliage development is always centered on the summer with the following key Julian dates:

a) the start of vegetation development (JGSS)

b) the beginning of the full summer foliage (JGSSP)

c) the end of vegetation development (JGSFP)

d) the end of the foliage period returning to winter conditions (JGSF)

e) the number of days in the foliage or green season (JDGS)

3) The annual percentage of the period in foliage (JDGS/365) is specified as a linear function of latitude determined from the typical foliage pattern (Money, 1976) with continual full foliage below 22° latitude and no foliage change above 66.5° latitude (Lee, 1980) as shown in Figure 2.3.3.
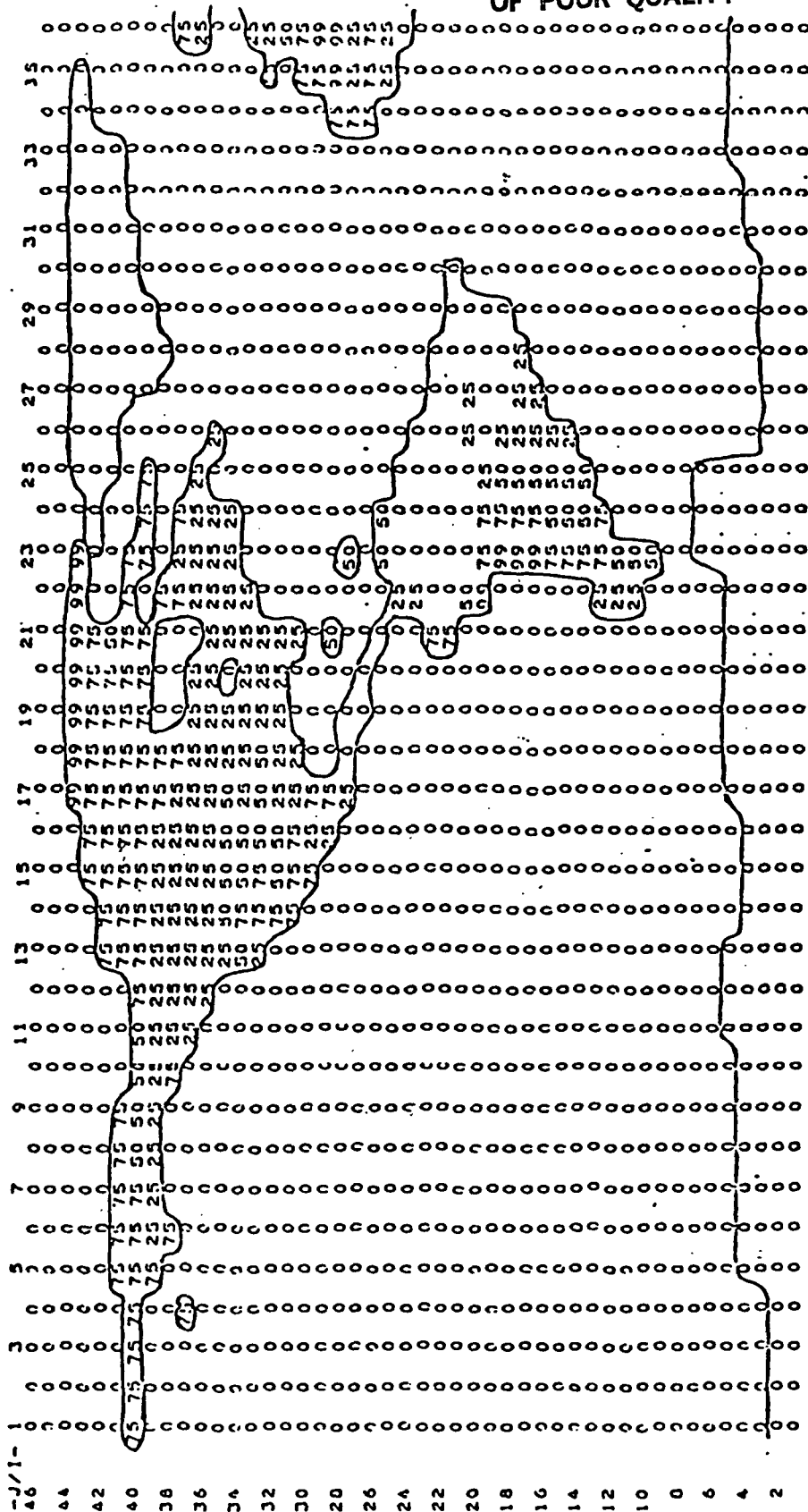
Figure 2.3-1a Annual percentage of bare soil 100 σ_b, western half of the
world (Strahler, 1971; Peele, 1975; Lee 1977).

Figure 2.3-1b Annual percentage of bare soil 100 σ_b, eastern half of the world (Strahler, 1971; Peele, 1975; Lee 1977).
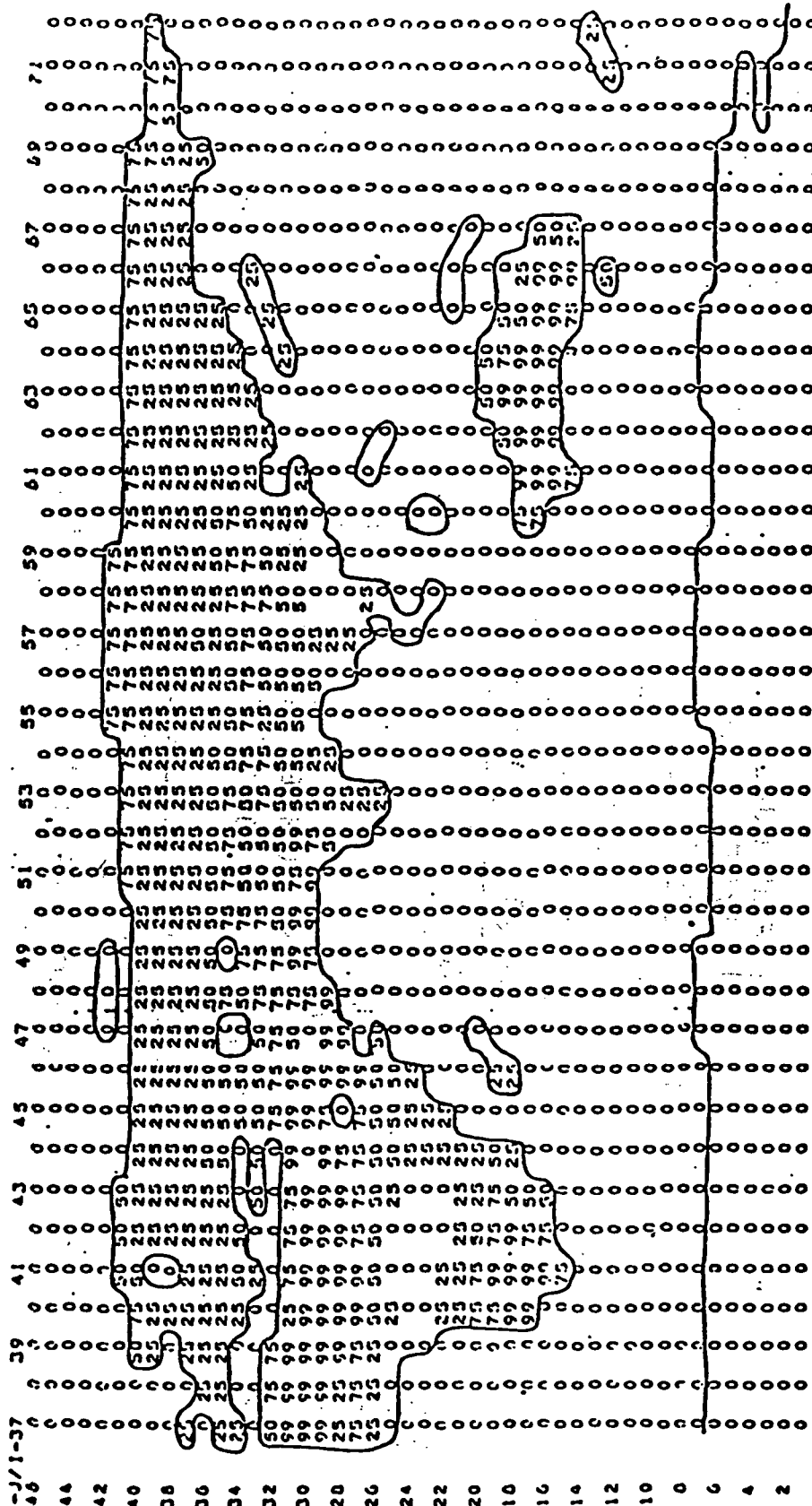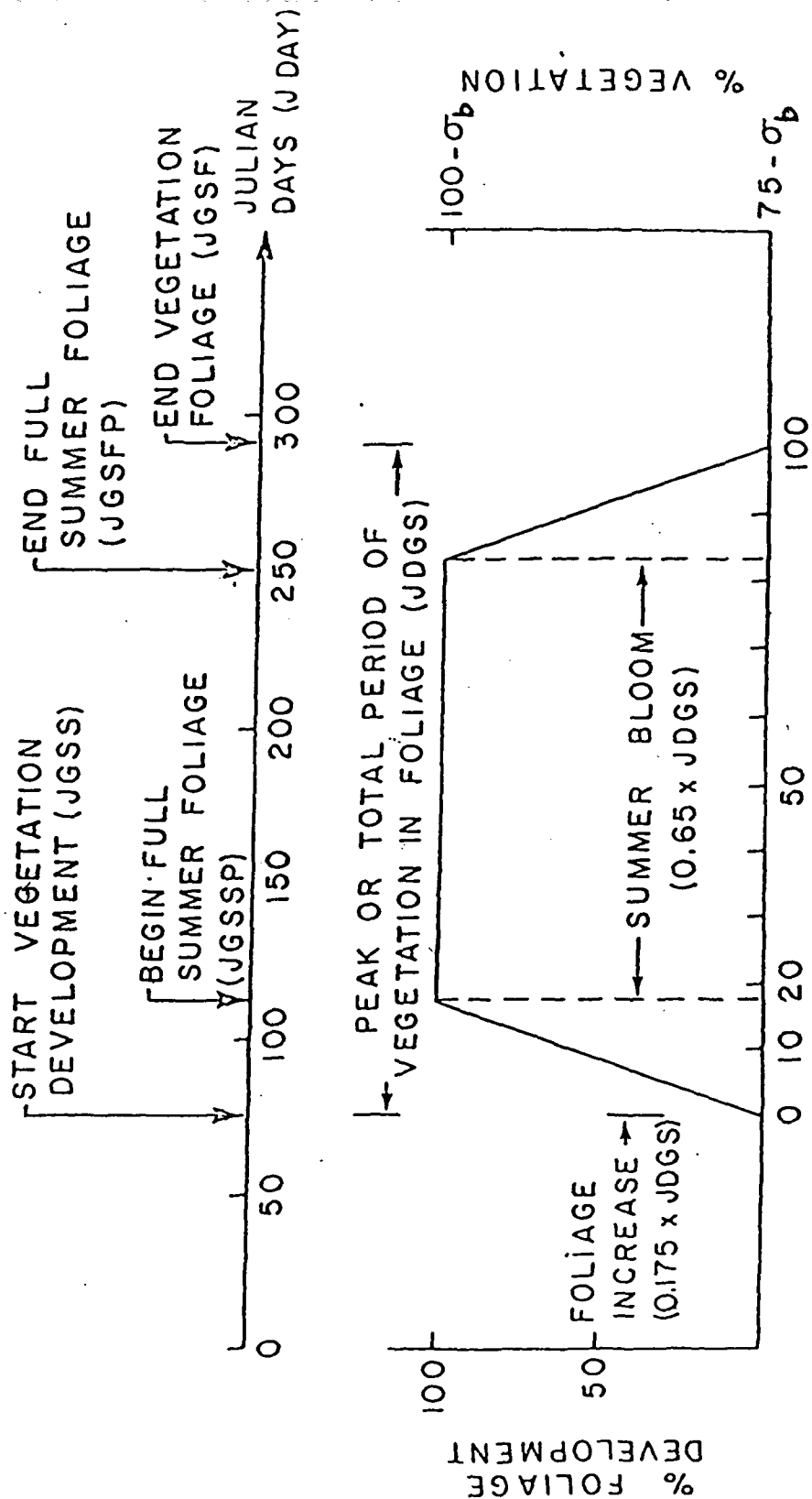
Figure 2.3.2 An example of seasonal variation for New Jersey.
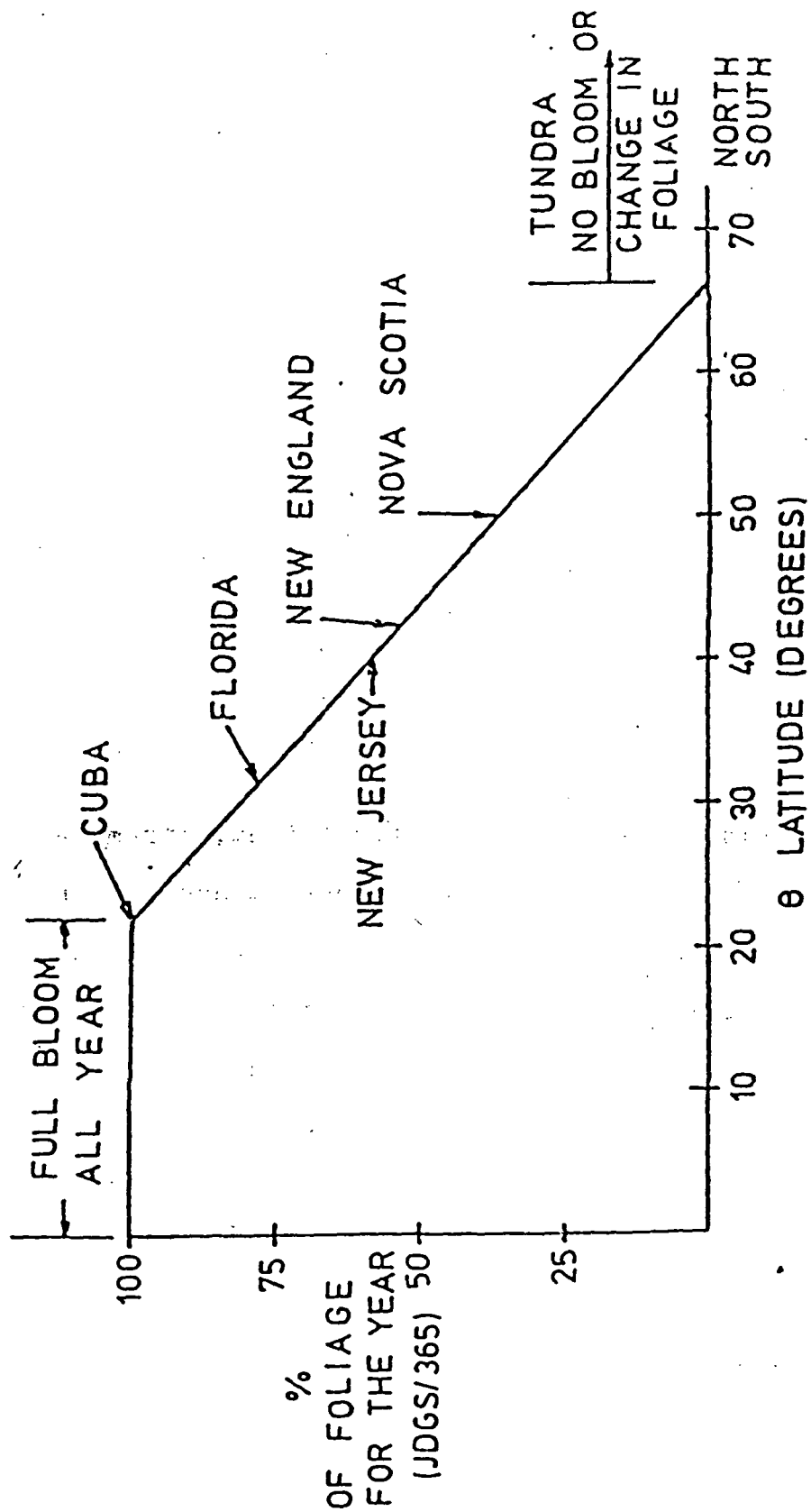
Figure 2.3.3 Percentage of vegetation foliage for the year
as a function of latitude (Alfano, 1981)

2.4   SOIL PROPERTIES

Two kinds of soil properties, the hydraulic property and the thermal property, must be considered in the GHM. These properties are related to the soil moisture content.

When one deals with the water movement in soil, the basic principle for moisture flux q in the soil is Richards' law (Richards, 1931) which is expressed by (for one-dimensional)

$$q = -K * \partial\psi/\partial z + K \qquad (2.4.1.a)$$

$$\text{or} \qquad = -D * \partial\theta/\partial z + K \qquad (2.4.1.b)$$

$$D = K * d\psi/d\theta \qquad (2.4.1.c)$$

where ψ is the soil matrix potential, K is the hydraulic conductivity and D is the diffusivity.

It should be pointed out first that, from a physical view point, the Eq. (2.4.1b,c) doesn't add any information to Eq. (2.4.1a). On the other hand, the expression in Eq. (2.4.1b) will be difficult to treat at the interface of heterogeneous soil because there is normally a sharp discontinuity in the soil moisture contents across the interface of layered soil and only the potential remains continuous across the interface (Hanks and Ashcroft, 1980). However, the expression is more acceptable in the general case because of its explicity and simplicity.

2.4.1 Total water potential and matrix potential

The total water potential H is formally defined as the amount of work that a unit quantity of water in an equilibrium soil water system requires when it moves to a pool of water in the reference state at the same temperature (Hanks and Ashcroft, 1980). Disregarding the osmotic potential and pressure potential, H consists of matrix potential and gravitational potential:

$$H = \psi + z$$

The gravitational potential is independent of soil nature and equal to the vertical distance z between a reference point and the point in question.

The matrix potential ψ is related to the adsorptive force of the soil matrix (hence, "matrix potential") and equal to the vertical distance between that point in the soil and the water surface of a manometer filled with water and connected to the soil point in question via a ceramic cup. It is a function of soil moisture, soil type and so on.

For a given soil, the matrix potential of moisture in the soil is not a unique function of the soil moisture content. This phenomenon is known as hysteresis (Hanks nd Ashcroft, 1980). In Figure 2.4.1, the wetting and drying processes produce an envelope that gives the extreme ranges of

possible water content that can be associated with any particular matrix potential.

The moisture matrix potential curves used in this GHM for five types of soil has been given by Ritjema (1970), which are obtained from measurements taken during the soil drying process. They are shown in Figure 2.4.2 (Alfano, 1981)
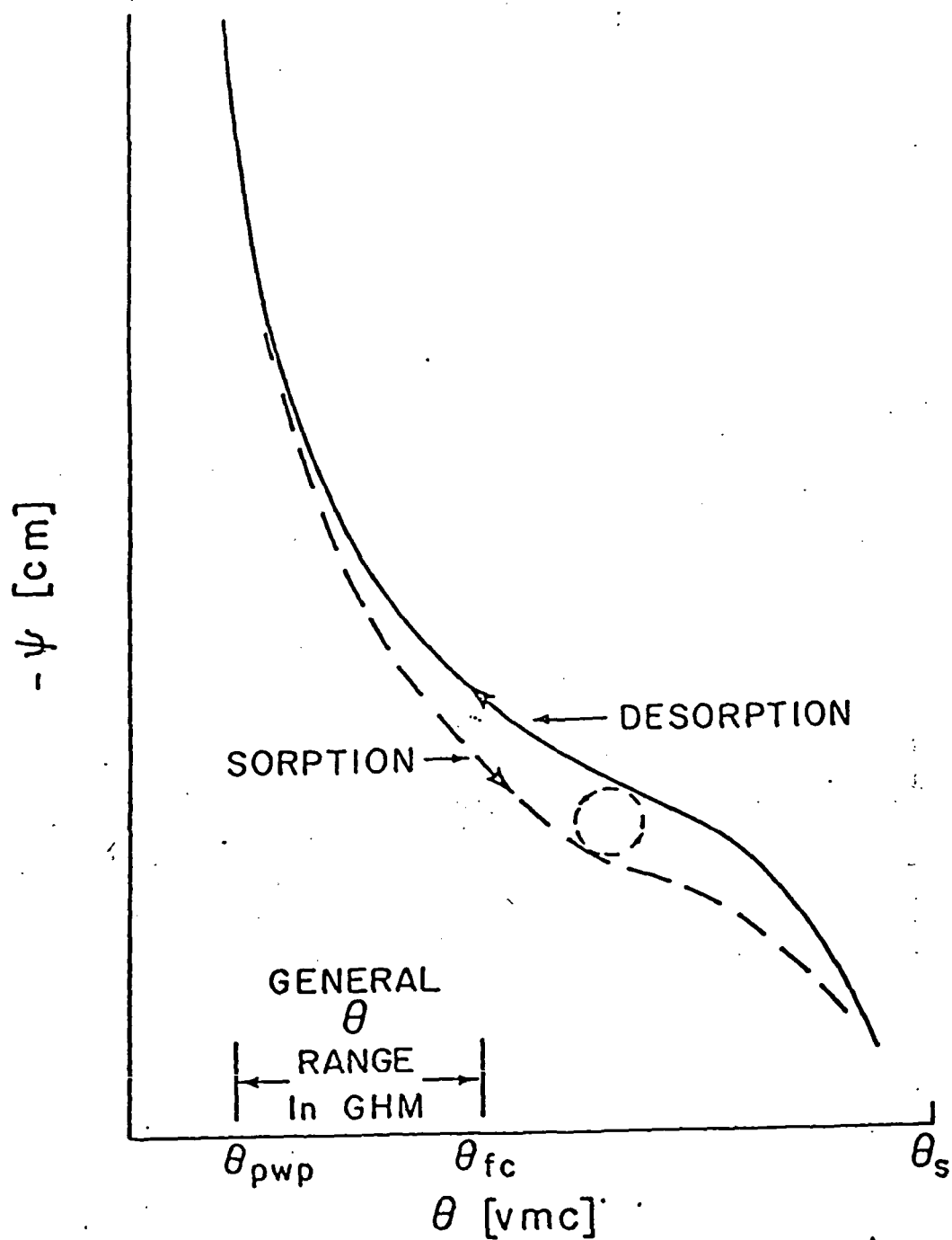
Figure 2.4.1   Soil suction curves for desorption and
sorption as a function of moisture content
(Hillel, 1977;   Slayter, 1977).
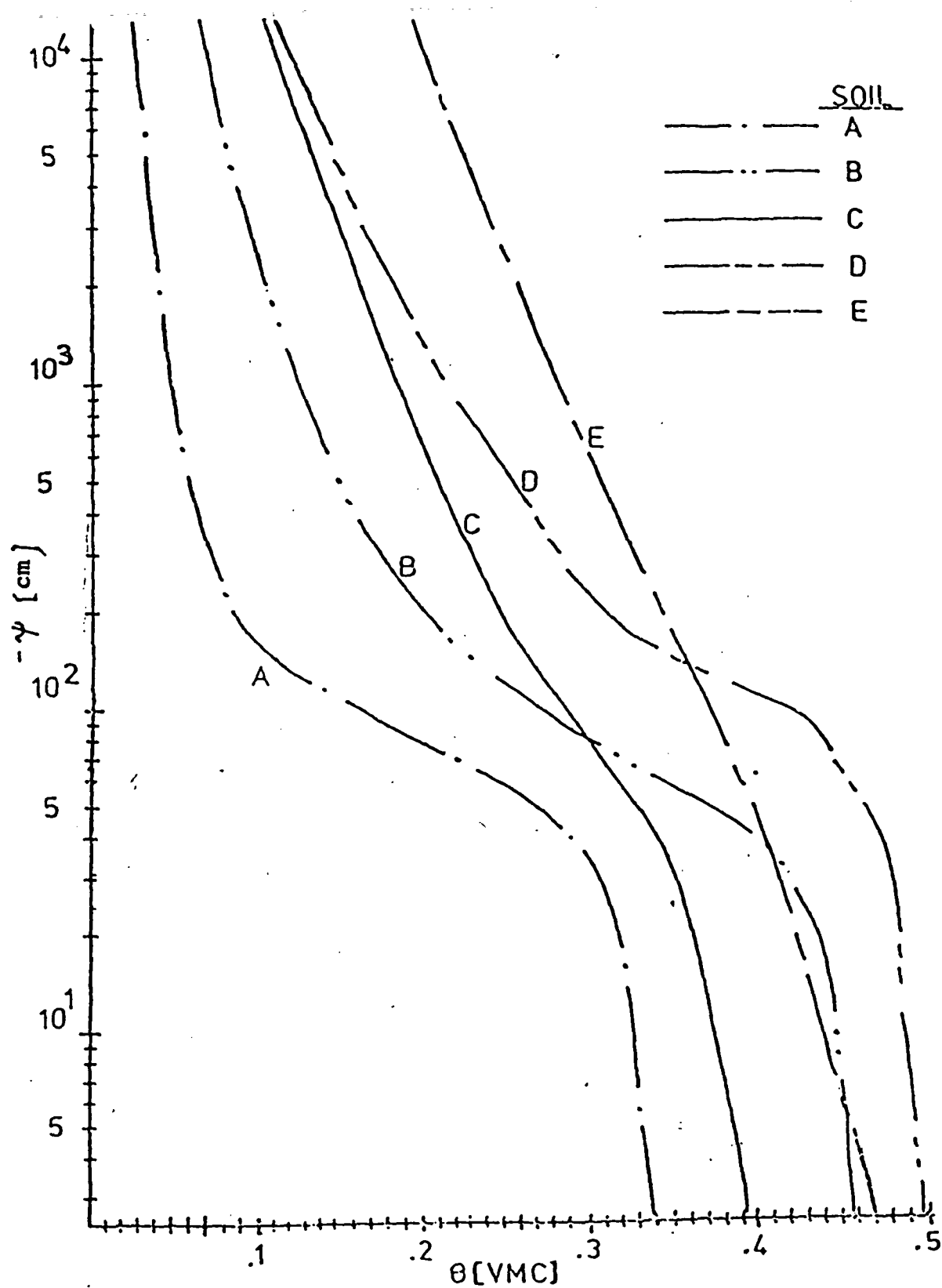
Figure 2.4.2   Soil matrix potential versus soil
moisture content (Alfano, 1981)

2.4.2 Hydraulic conductivity

The hydraulic conductivity is related to the moisture content. The hydraulic conductivity is very difficult to determine in the field and can only be measured (Nielsen et al., 1964; 1973) in the field under very favorable conditions. Even in the laboratory, the experimental measurement is also difficult (Nilsen and Biggar, 1961). The empirical formulas suggested by Ritjema (1970) are

$$K(\theta) = a_r * (-\psi(\theta))^{-1.4} \qquad \psi < \psi_r \qquad (2.4.2a)$$

$$K(\theta) = K_r * \exp(\alpha_r * \psi) \qquad \psi > \psi_r \qquad (2.4.2b)$$

where a_r, α_r, K_r, ψ_r was given by Ritjema (1970) and shown in Table (2.4.1)

Alfano, based on Eq. (2.4.2), has plotted the curves of $K(\theta)$ versus volumetric moisture content for five types of soil which are shown in Figure 2.4-3.

Soil Type ( )	a_r [cm$^{2.4}$ s^{-1}]	$-\psi_r$ [cm]	K_r [cm s^{-1}]	α_r [cm^{-1}]
Medium Fine Sand (A)	3.8×10^{-5}	125	1.27×10^{-3}	.0822
Sandy Loam (B)	2.8×10^{-6}	150	1.9×10^{-4}	.0737
Loamy Medium Sand (C)	6.1×10^{-5}	100	2.7×10^{-5}	.0562
Loam (D)	1.7×10^{-4}	300	5.78×10^{-5}	.0231
Silty Clay Loam (E)	4.2×10^{-4}	300	1.74×10^{-5}	.0237

Table 2.4.1 Constants for soil conductivity formulas of Rijtema (1970), for five soil types.

Figure 2.4-3a Hydraulic conductivity versus soil
moisture content (Alfano, 1981)
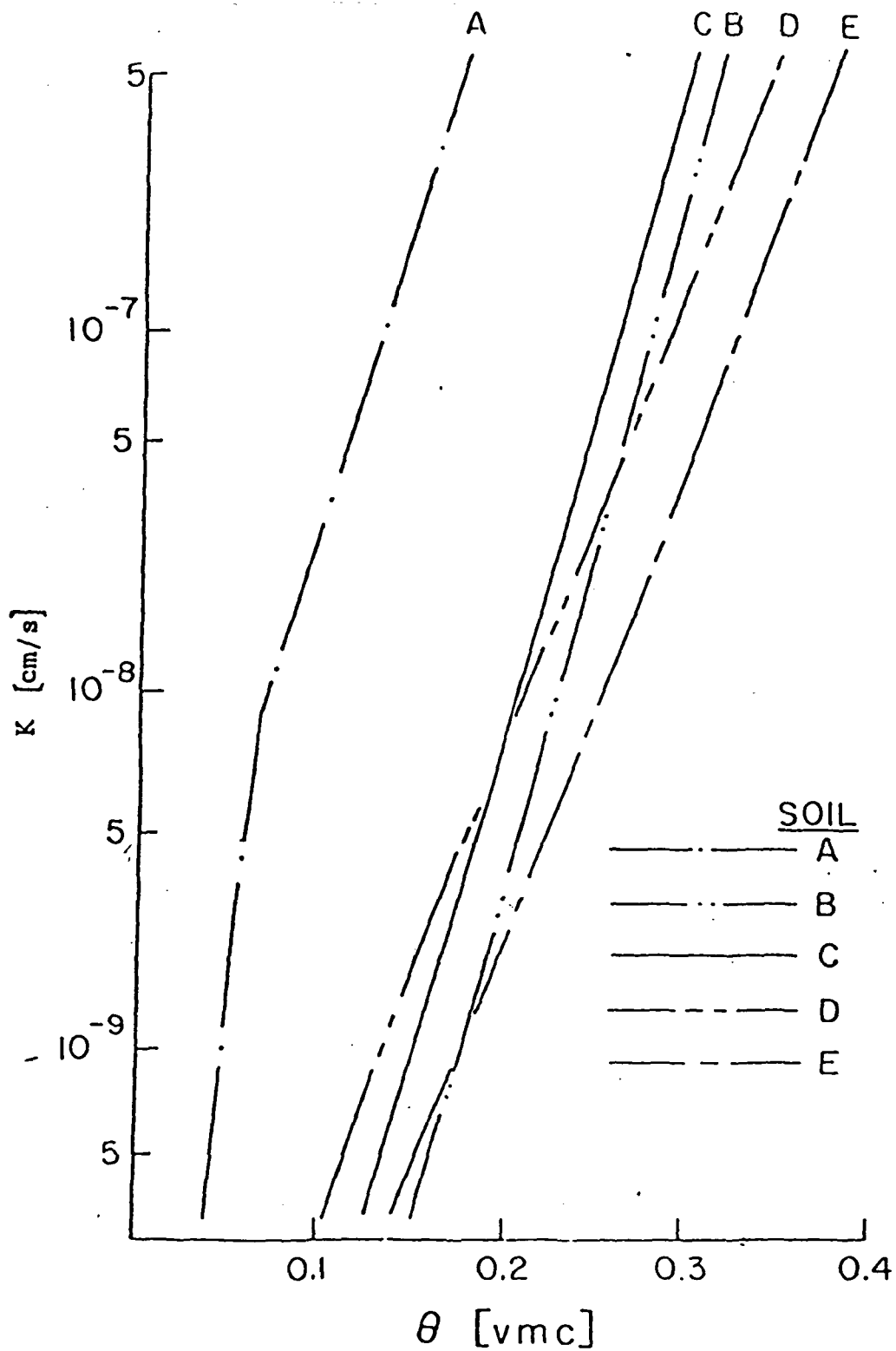
Figure 2.4-3b   Hydraulic conductivity versus soil
moisture content (Alfano, 1981)
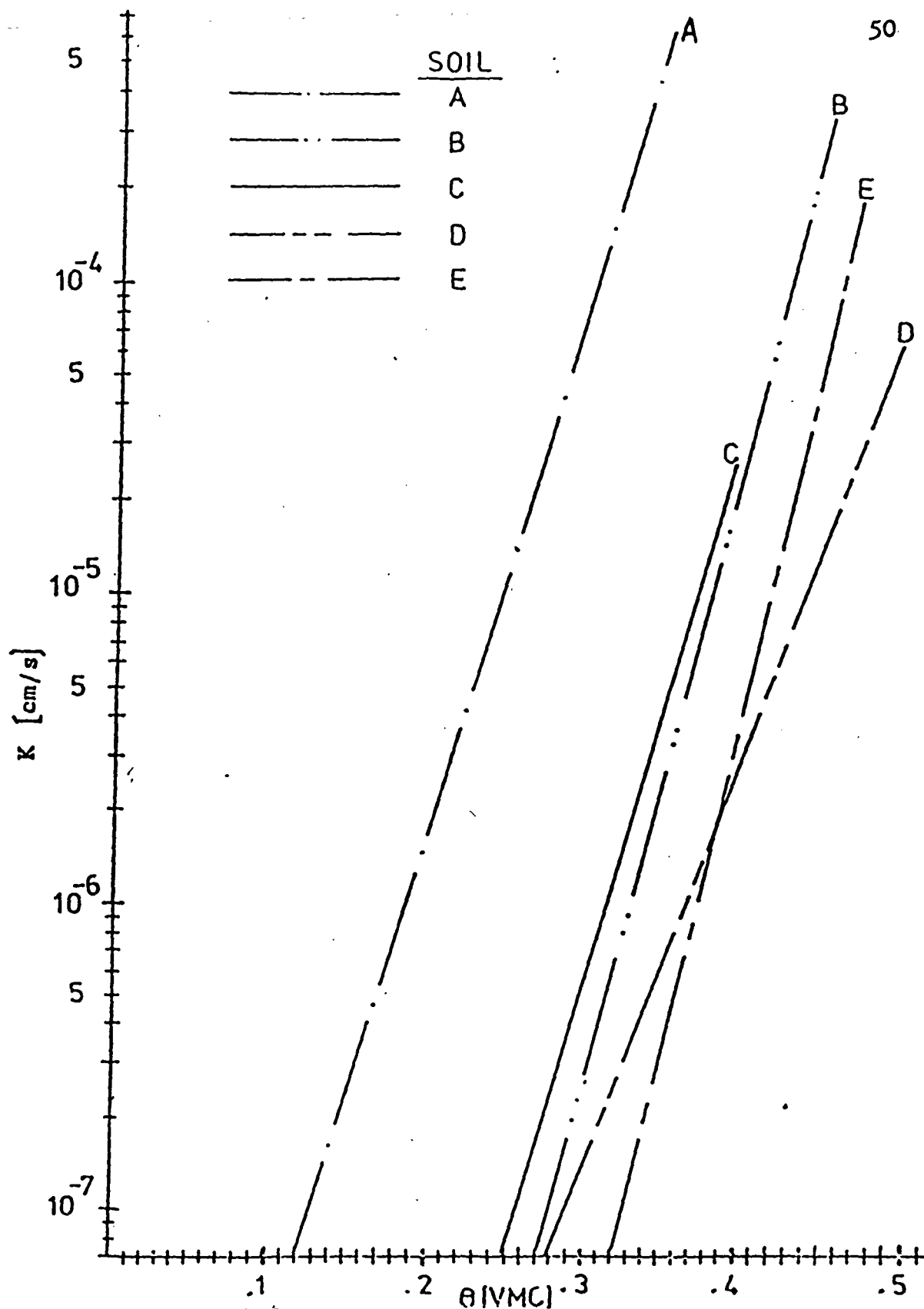
Figure 2.4-3c   Hydraulic conductivity versus soil
moisture content (Alfano, 1981)

2.4.3 Diffusivity

Alfano calculated diffusivity with Eq. (2.4.1c) using the values of K and ψ given by Ritjema (1970) which are plotted in Figure 2.4-4 for five types of soil.

In order to make the integration of K and D more convenient, the relation of K and D with the soil moisture content was approximated in several segments by the following equations (Alfano, 1981):

$$K(\Theta) = a_1 \exp(a_2(\Theta - a_3)) \qquad (2.4.4a)$$

$$D(\Theta) = b_1 \exp(b_2(\Theta - b_3)) \qquad (2.4.4b)$$

where a_1, a_2, a_3, b_1, b_2, and b_3 are constants which will only change the magnitude from one segment to another. The constants are listed in Table 2.4.2.
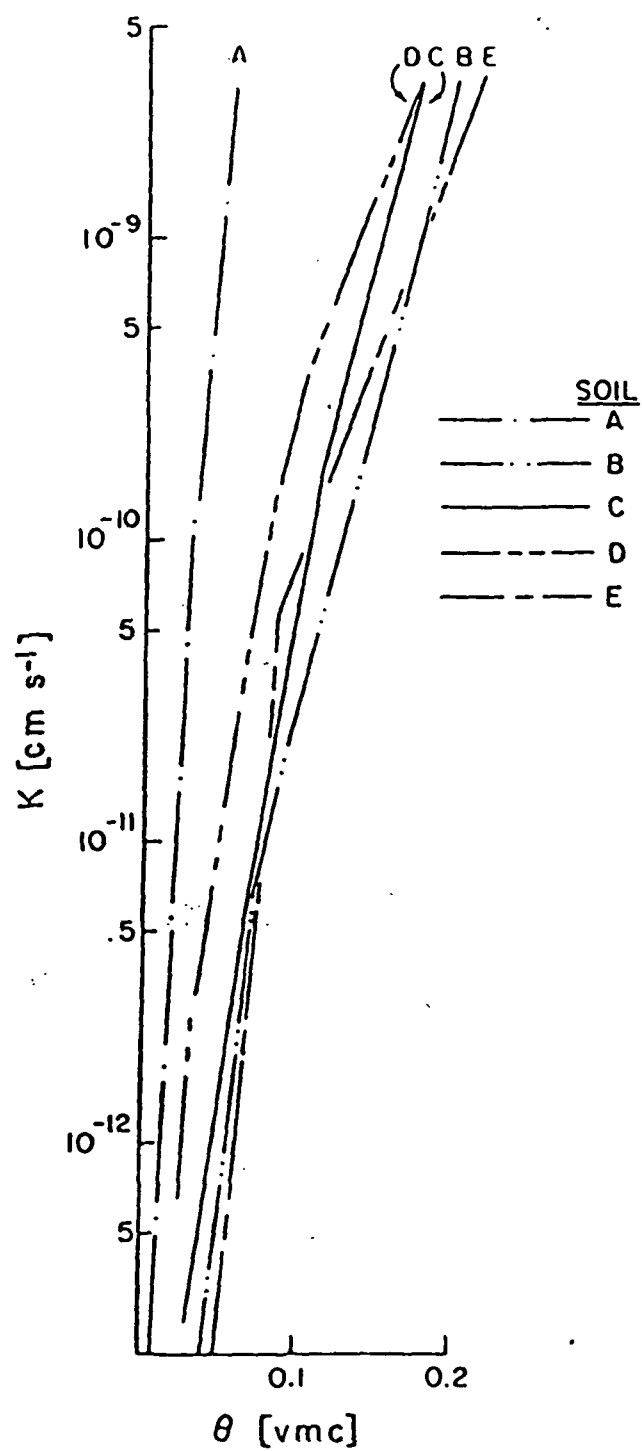
Figure 2.4-4a Diffusivity versus soil moisture
content (Alfano, 1981)
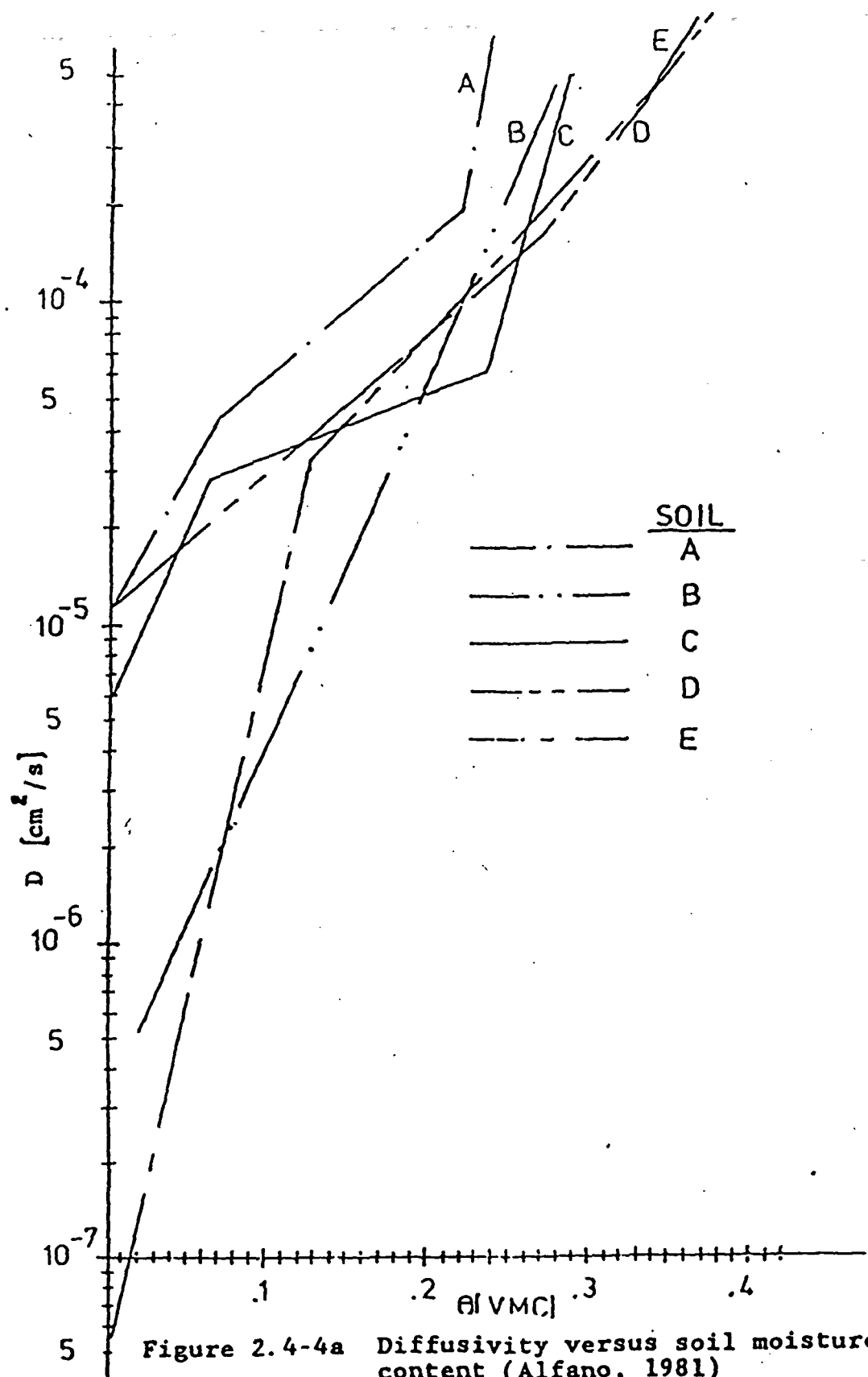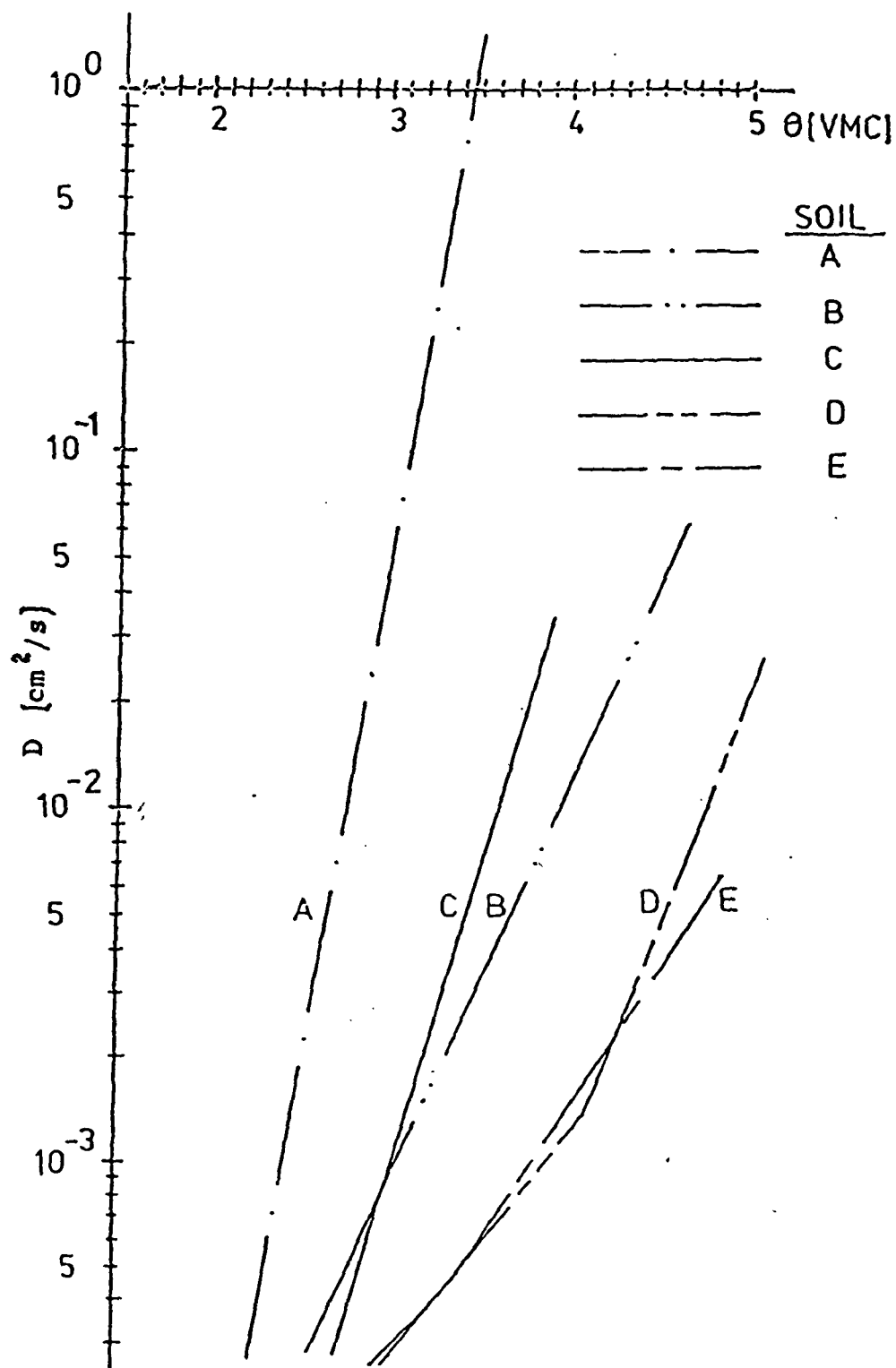
Figure 2.4-4b   Diffusivity versus soil moisture
content (Alfano, 1981)

Soil type	θ (vmc)	a1 (cm/s)	a2	a3 (vmc)	θ (vmc)	b1 (cm²/s)	b2	b3 (vmc)
Medium fine Sand (A)	0<.058 0>.058	6.2E-9 5.5E-4	143.864 38.70	.058 .35	0.<0<.066 .066<0<.22 .22<0<.35	4.E-5 1.85E-4 1.3E-0	19.53 9 .93 68.02	.066 .22 .35
Sandy loam (B)	0.<0<.465	5.E-10	44.383	.162	0.<0<.465	6.E-2	26.35	.465
Loamy medium Sand (C)	0.<0<.12 .12<0<.22 .22<0<.394	3E-10 1.7E-8 2E-5	78.65 40.31 40.57	.12 .22 .394	0<0<.065 .065<0<.24 .24<0<.394	2.8E-5 6.E-5 3.5E-2	25.28 4.348 41.29	.065 .24 .394
Loam (D)	0.<0<.125 .125<0<.503	7.5E-10 5.E-5	64.0 29.57	.125 .503	0<0<.27 .27<0<.41 .41<0<.503	1.6E-4 1.4E-3 2.0E-2	6.27 17.17 29.5	.27 .41 .503
Silty clay	0<0<.09	7.0E-11	110.64	.09	0<0<.13	3.3E-5	51.6	.13
Loam (E)	.09<0<.33 .33<0<.475	1E-7 1.7E-4	30.22 51.2	.33 .475	.13<0<.34 .34<0<.475	4.5E-5 5.0E-3	12.42 17.81	.34 .475

Table 2.4.2 Constants for parameterizing conductivity and diffusivity into straight line segments for five soil types of Rijtema (1970).

2.4.4 Thermal property -- heat conductivity and heat capacity

Heat exchange in a soil is primarily caused by conduction. The heat flux in the soil can be described by Fourier's law. For vertical heat flux in a one-dimensional column, it can be expressed by

$$G = -\lambda dT/dz \qquad (2.4.5)$$

where G is heat flux positive downward and λ is conductivity (cal $cm^{-1}s^{-1}deg^{-1}$). The conductivity λ is expressed as a linear function of the volumetric fraction of the components such as sand and silt, clay and organic matter and given by

$$\lambda = \sum_{i=1}^{3} \lambda_i V_i \qquad (2.4.6)$$

where V_i is the volumetric fraction for sand and silt, clay and organic matter, and λ_i is the corresponding conductivity. In the GHM, The heat conductivity λ_i was obtained by fitting linear segments to the curves given by Sellers (1961) as follows while considering moisture effect (Alfano, 1981):

For sand and silt,

$$\lambda_1 = 0.001(61\theta + 0.5) \qquad \theta < 0.05 \qquad (2.4.7a)$$
$$= 0.001(14.2\theta + 2.85) \qquad 0.05 < \theta < 0.18 \qquad (2.4.7b)$$
$$= 0.001(1.86\theta + 5.1) \qquad \theta > 0.18 \qquad (2.4.7c)$$

For clay,

$$\lambda_2 = 0.001(21\theta + 0.4) \qquad \theta < 0.14 \qquad (2.4.7d)$$
$$= 0.001(3.13\theta + 3.0) \qquad \theta > 0.14 \qquad (2.4.7e)$$

For organic matter,

$$\lambda_3 = 0.001(0.42\theta + 0.1) \qquad \theta < 0.24 \qquad (2.4.7f)$$
$$= 0.001(1.7\theta - 0.17) \qquad \theta > 0.24 \qquad (2.4.7g)$$

Another important property for soil is the heat capacity of the soil. Sellers (1965) suggested that the soil volumetric heat capacity C can be estimated by averaging the heat capacities for the components in the soil:

$$C = 0.46(V_1 + V_2) + 0.6V_3 + \theta_i \quad (cal/cm^3/{}^\circ K) \qquad (2.4.8)$$

where $(V_1 + V_2)$ is the volumetric fraction of mineral, V_3 is the volumetric fraction of organic matter and θ_i is the volumetric moisture content in layer i.

2.5   VEGETATION MORPHOLOGY AND PHYSIOLOGY

With regard to heat and moisture transfer in a soil-plant-atmosphere continuum, the canopy morphology and physiology play a very important role. For the canopy morphology, there are four important parameters: canopy height h_c, zero displacement thickness d and roughness height z_o relating to the turbulence flow in the atmosphere, leaf area index LAI relating to light penetration from the canopy top down to the vegetated ground surface, and the root system in soil which relates to the water uptake.

For the canopy physiology, the most important factor for hydrologic modeling is the canopy resistance which adjusts the transpiration rate from leaves.

2.5.1 Vegetation morphology

In the GHM, the whole canopy is treated as a bulk layer. Only the integral effect of the localized parameters is considered in the bulk layer model.

1) Leaf area index LAI:

Leaf area index is defined as the total area of leaves over unit area of the ground surface. Its magnitude influences heat and water transport processes.

First, when the light penetrates from the canopy top down through the canopy, most of it is intercepted and absorbed by the leaves. The residual, which can arrive at the ground surface, may be approximately expressed by an exponential decay law:

$$R_n(bot) = R_n(top)exp(-X_c*LAI) \qquad (2.5.1)$$

where $R_n(top)$ is the net radiation at the top of the canopy, $R_n(bot)$ is the portion of the net radiation reaching the ground surface, X_c is the extinction coefficient which depends on the type of canopy, the leaf surface orientation and the solar elevation angle. LAI is the leaf area index.

Second, the absorbed net radiation by the canopy will be partitioned into latent heat, sensible heat and heat storage inside the bulk canopy layer. The heat storage capacity depends on the heat capacity of the bulk layer which is primarily determined by biomass and moisture contained in the canopy.

Third, the actual transpiration is dependent on the can-
opy resistance and is expressed by

$$E_c = \mathcal{P}_a*(q^*(T_c)-q_a)/(r_v+r_{cr}) \qquad (2.5.2)$$

where $q^*(T_c)$ is the saturated specific humidity, q_a the
specific humidity in air, r_v the air resistance to the ac-
tual transpiration and r_{cr} the canopy resistance to the ac-
tual transpiration. The canopy resistance is approximately
related to the leaf resistance by (Landsberg, 1975)

$$r_c = r_1/LAI \qquad (2.5.3)$$

where r_1 is the leaf resistance for the canopy which is
approximately equal to the stomatal resistance r_s.

There are many articles reporting leaf area index val-
ues for different kinds of plants (Landsberg and Cutting,
1975; Montheis, 1975; Perrier, 1981). From the available
data it was found that the value of leaf area index depends
on the species. Table 2.5.1 exemplifies the values of LAI
for different plants (Perrier, 1981). In the GHM, an aver-
age value LAI = 3 is taken for a short canopy such as
grassland and crop, and LAI = 6 or 7 for a tall forest.

Plant	Leaf area index (LAI)
Evergreen forest	7-10
Bereal coniferous zone	2-10
Mediteranean semipervirent forest	4-5
Mozon forest and mixed dry forest	6-10 (even to 15)
Decidous temperate forest (total vegetation)	4-6 (6-8)
Woody savanna	1-1.5 (dense) .2-.4 (dry weather) 2-4 (rain season)
Temperate grassland Douglas fir	3-6 -6 (projected area base) (Landsberg, P71, 75)
Grassland	4.4 (Landsberg, P44, 75)

Table 2.5.1   Leaf area index for different canopies
(Perrier, 1981)

2) Root density distribution

The transpiration from leaves to the air depends in part on the ability of the root system to absorb water from the soil. The uptake capacity is dependent on the root distribution and development. Available data for the root distribution in soil is not sufficient to give a systematic summary or quantitative description of root. Its field measurement is very difficult. There are some scattered data for the crop root system but only a few are related to the forest root system. (Miller, 1938; Ritjema, 1970; Huttel, 1975; Hillel, 1977; Wood, 1980; Perrier, 1981; Waggoner and Turner, 1971).

The root density should be properly defined as the density of root surface because the root weight may not be correlated with the mechanism of the water uptake in forest. The root density in the first layer is defined as R_{d1} equal to the surface area of roots in layer 1 divided by total surface area of roots in the whole root zone.

Table 2.5.2 lists some of the available data for evaluation in the GHM. Figure 2.5-1 shows the distributions of some root systems.

In the GHM, the distribution used is the same as the shallow and deep root systems suggested by Hillel (1977).

Canopy	Root density R_{d1} in top 10 cm	Root density from 10 cm to around 1 m	Reference
Ivory forest	0.21- 0.47	0.79-0.53	Huttel (75)
Hardwood woody	0.50	0.50	Wood (80)
Savanna	0.50	0.50	Perrier(81)
Grass land	0.50	0.50	Perrier(81)
Shallow root system	0.50	0.50	Hillel (77)
Deep root system	0.25	0.75	Hillel (77)

Table 2.5.2   Root density distribution
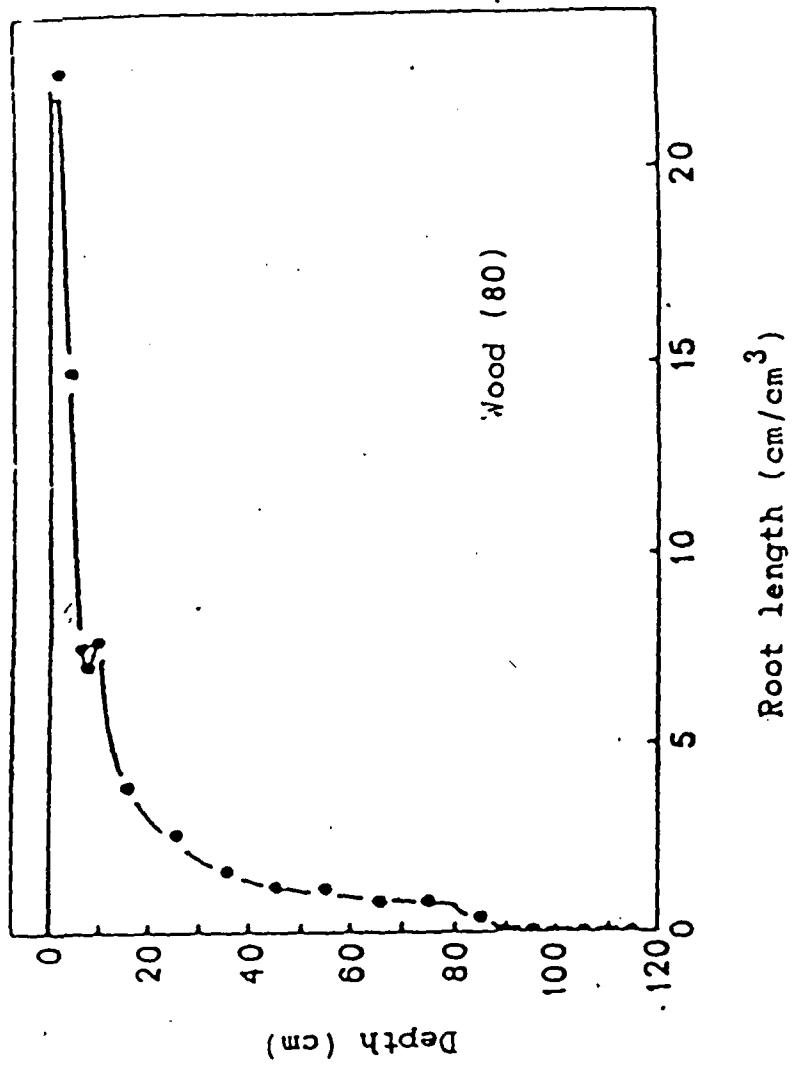
Figure 2.5-1a Hardwood forest at Hubbard Brook

Cumulative root biomass versus
depth for grassland

Perrier (81)

(a) grassland savanna "Loudetia simplex"
(b) grassland savanna "Andropogoneen"
(c) bush savanna "Andropogonees"
(d) woody savanna "Andropogonees"
(e) never burnt bush savanna

Root density RD
as a function of depth
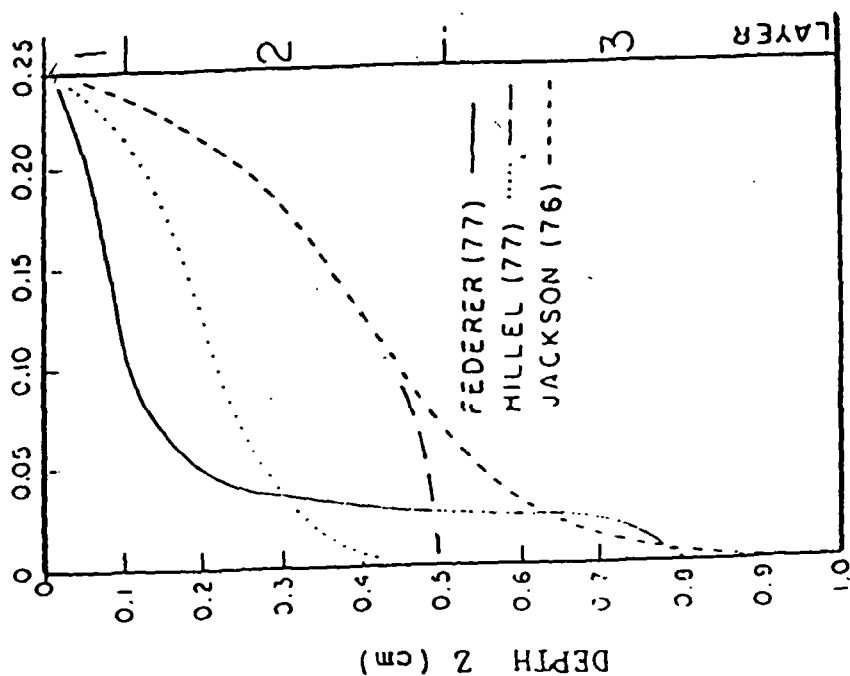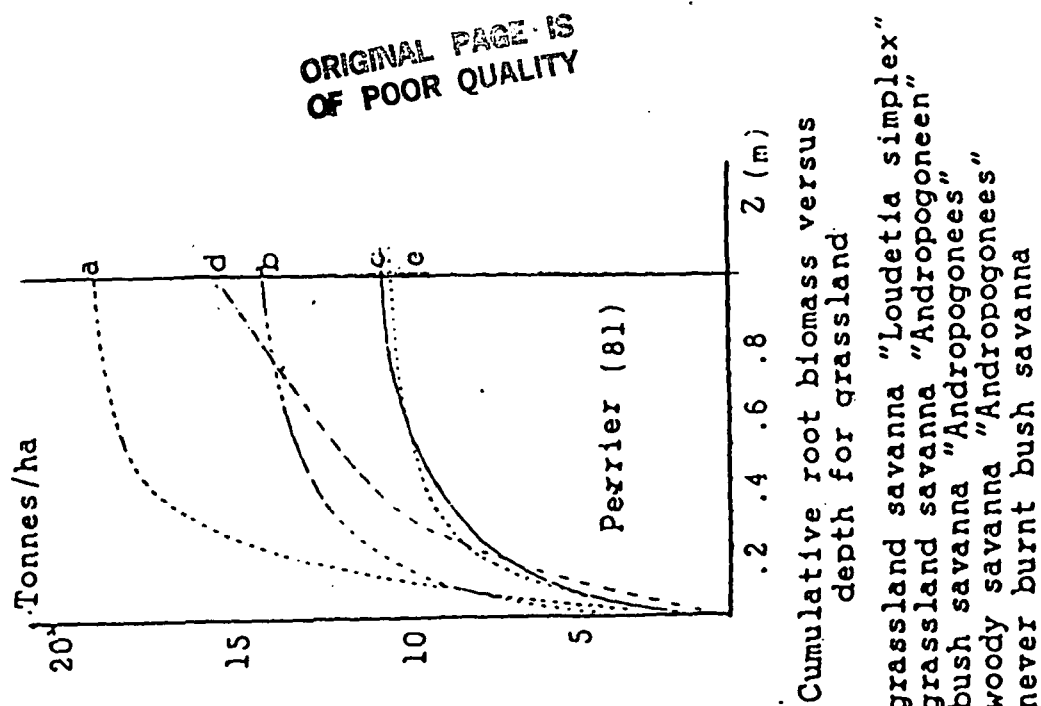
Figure 2.5-1b Root density as a function of depth

2.5.2 Canopy physiology -- canopy resistance

Canopy resistance r_c, in general, may be considered as the impedance to water transport from the vegetal surface to the air. r_c is approximately equal to leaf resistance r_l divided by leaf area index (LAI). The leaf resistance r_l is almost equal to the stomatal resistance r_s provided the stomata are not closed entirely (Monteith, 1975)

Canopy resistance (or leaf resistance or stomatal resistance) is affected by many factors such as light, wind velocity, air temperature, air humidity and leaf water potential (Landsberg and Cutting, 1975) (see Figure 2.5-2).

In this study, Eq. (2.5.2) is not used for calculating actual transpiration because of uncertainty of the canopy resistance r_{cr}. The actual transpiration is calculated by scaling from the potential (or maximum) unstressed transpiration E_u which is defined as follows:

$$E_u = \rho_a * [q^*(T_c) - q_a] / (r_v + r_{cm}) \qquad (2.5.4)$$

where r_{cm} is the minimum unstressed canopy resistance. In all succeeding sections, r_c is used to denote this minimum resistance r_{cm}. The minimum canopy resistance is assumed to be a constant which depends on the vegetation type. r_c = 75 s/m for tall canopy and r_c = 100 s/m for short canopy are used in this study.

Variation of canopy resistance

for three days during the growing

season of Matador grassland, 1971

Variation, with leaf water potential,

of the leaf resistance to evaporation

Figure 2.5-2a Variation of leaf resistance and canopy resistance

Figure 2.5-2b   Relationship between stomatal resistance r_s and vapor pressure deficit δe for three ranges of soil matrix potential Ψ_M for Douglas Fir (Landsberg and Cutting, 1975)
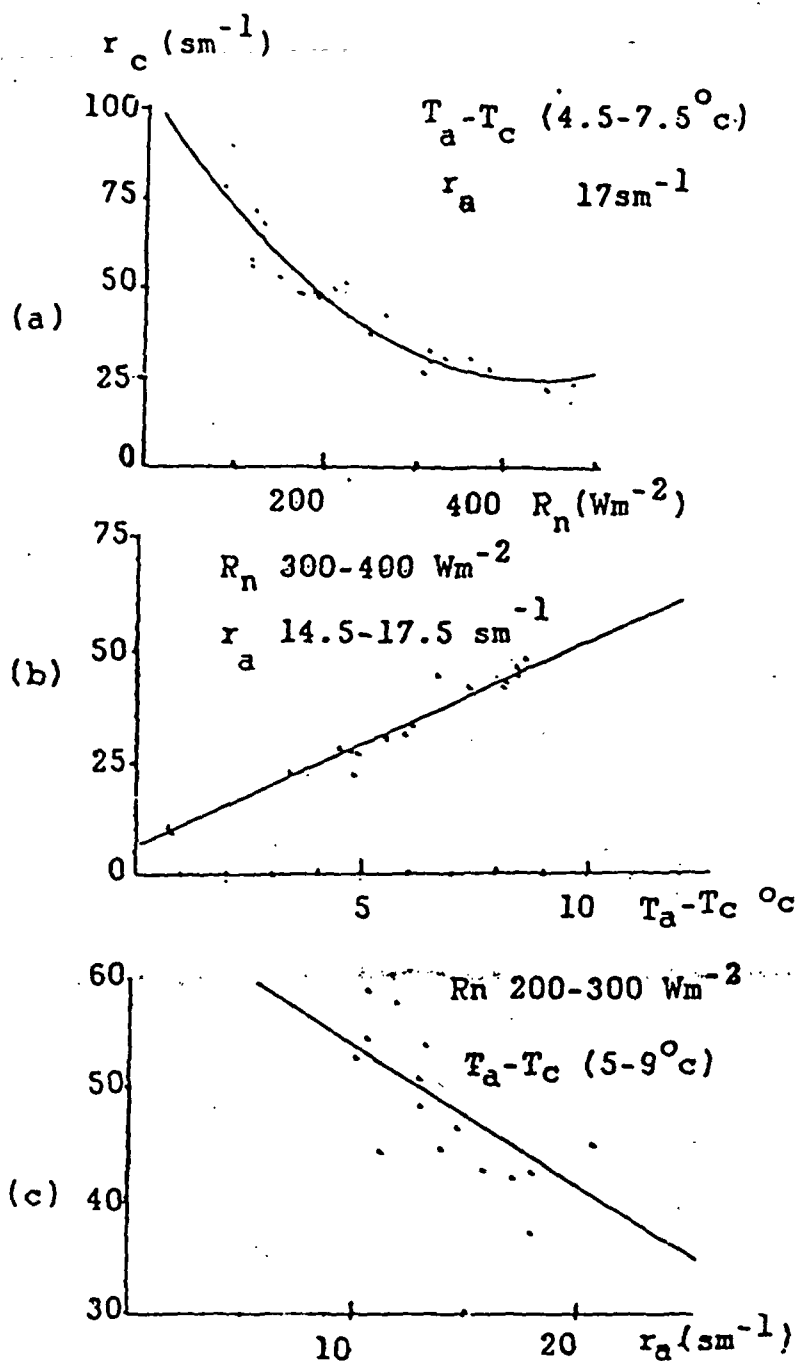
Figure 2.5-2c Wheat crop resistance versus net radiation
(a), air deficit (b) and wind speed plotted
as a function of the crop aerodynamic
resistance (c) (Perrier, 1981).

2.6 ALBEDO

Albedo is defined as the fraction of shortwave radiation reflected by the land surface cover. According to this definition, the net radiation R_n absorbed by a surface is

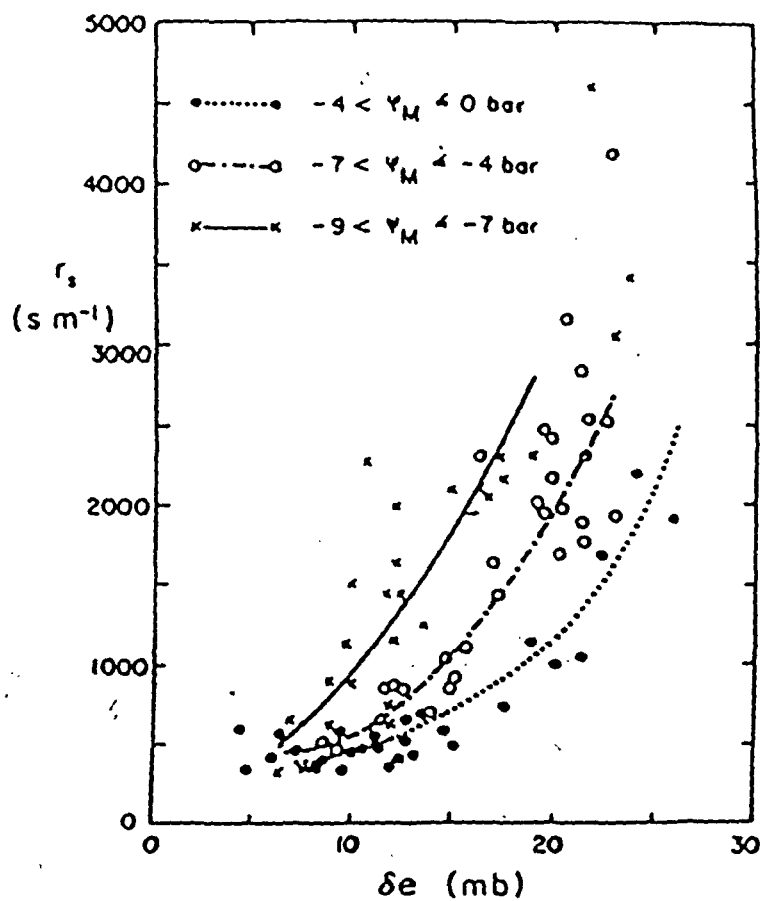$$R_n = R_s*(1.-a_1)+ R_{LN} \qquad (2.6.1)$$

where R_s --- the shortwave radiation

R_{LN} -- the net long wave radiation (amount absorbed minus the amount emitted by a surface).

a_1 --- albedo (in percentage)

Albedo depends on several factors such as sun elevation, direct solar to scattered radiation ratio, land surface cover and surface conditions (moisture, roughness and so on). Kondratyev (1981) and Carson (1981) have discussed the available information in detail and presented the parameterization of albedo for use in numerical climate models.

In the GHM, Alfano's scheme is followed, which was based on the work done by Idso et al. (1975), Strahler (1971), Monteith (1975) and Federer (1968). The albedo of soil is a function of soil moisture. It can be expressed as a segmental linear function and given by

$$a_{1b}=30.-2.*\theta_{avf}/0.6 \qquad 0<\theta_{avf}<0.6$$
$$=28.-16.*(\theta_{avf}-0.6)/0.4 \qquad 0.6<\theta_{avf}<1.$$

where $\theta_{avf} = (\theta_1-\theta_{pwp})/(\theta_{fc}-\theta_{pwp})$ and θ_1 is the volumetric moisture content in the surface layer.

The canopy albedo a_{lc} is determined by the canopy type and the water stress condition (or soil moisture) as well as the location where the canopy grows (Posey and Clapp, 1964). Corby et al. (1977) gave the albedo distribution along the latitude for use in a 5-level atmospheric model. In the GHM, the albedo for the different canopies is shown in Table 2.5.3 (Alfano, 1981), which accounts for canopy type and soil moisture content.

f

NO.	Vegetation type	Albedo
1,2	Tropical & Temperate Rainforest	14
3	Evergreen hardwood Forest	12
4	Raingreen forest	$20 - 8*(\bar{\theta}-\theta_{pwp})/(\theta_{fc}-\theta_{pwp})$
5	Grasslannd	20
6	Desert	$30 - 15*(\bar{\theta}-\theta_{pwp})/(\theta_{fc}-\theta_{pwp})$
7	Deciduous forest	18
8	Needleaf forest	18
9	Arctic tundra 1 JDAY 125 126 JDAY 125	Spring (NH):39-19(JDAY/125) Fall (NH):20-19(JDAY/125)
10	Ice	40-80 (Tsang & Karn, 1972)
11	Highland Areas	$25 - 10*(\bar{\theta}-\theta_{pwp})/(\theta_{fc}-\theta_{pwp})$
12	OCEAN	7-9 (Tsang & Karn, 1972)

$\bar{\theta} = 0.2\theta_1 + 0.8\theta_2$

JDAY: Julian day
NH: Northern Hemisphere

Table 2.5.3 Vegetation albedo parameterization

Chapter III

DESCRIPTION OF MOISTURE MOVEMENT AND HEAT
TRANSFER

Only the one-dimensional vertical transports of the moisture and heat are considered. The exchanges of water and heat are between the air and soil, the air and canopy, the canopy and vegetated ground surface, and the soil in the root zone. Figures 3.1-1a,b show the schematic of the processes. In the figures, the subgrid parameterization is accomplished by dividing a grid into two parts : canopy and bare soil. The bare soil fraction is σ_b and the rest of the grid, $\sigma_c = (1.- \sigma_b)$, is the canopy fraction. For moisture movement, the root zone is divided into two layers : a thin surface layer over a lower deep layer extending to the bottom of the root zone. For heat transport, a surface layer has a thickness of 1 cm and the whole layer thickness (see Figure 3.1-1b) equals the depth of penetration of the annual temperature wave. The thicknesses of the layers used for the soil moisture movement do not coincide with those used for the heat transport. Over the vegetated ground surface, one more canopy layer is added.

Figure 3.1-1a   Moisture movement

$$\alpha \cdot \frac{dT_{gb}}{dt} = \frac{2 \cdot G_b}{C \cdot \overline{d}_1} - \frac{2\pi}{\tau} \cdot (T_{gb} - \overline{T})$$

$$\frac{dT_{gc}}{dt} = \frac{2 \cdot G_c}{C \cdot \overline{d}_1} - \frac{2\pi}{\tau} (T_{gc} - \overline{T})$$

(Diurnal layer)

$$\frac{d\overline{T}}{dt} = \frac{\sigma_c G_c + \sigma_b G_b}{C \cdot \sqrt{365\pi \cdot \overline{d}_1}}$$

(Annual layer)
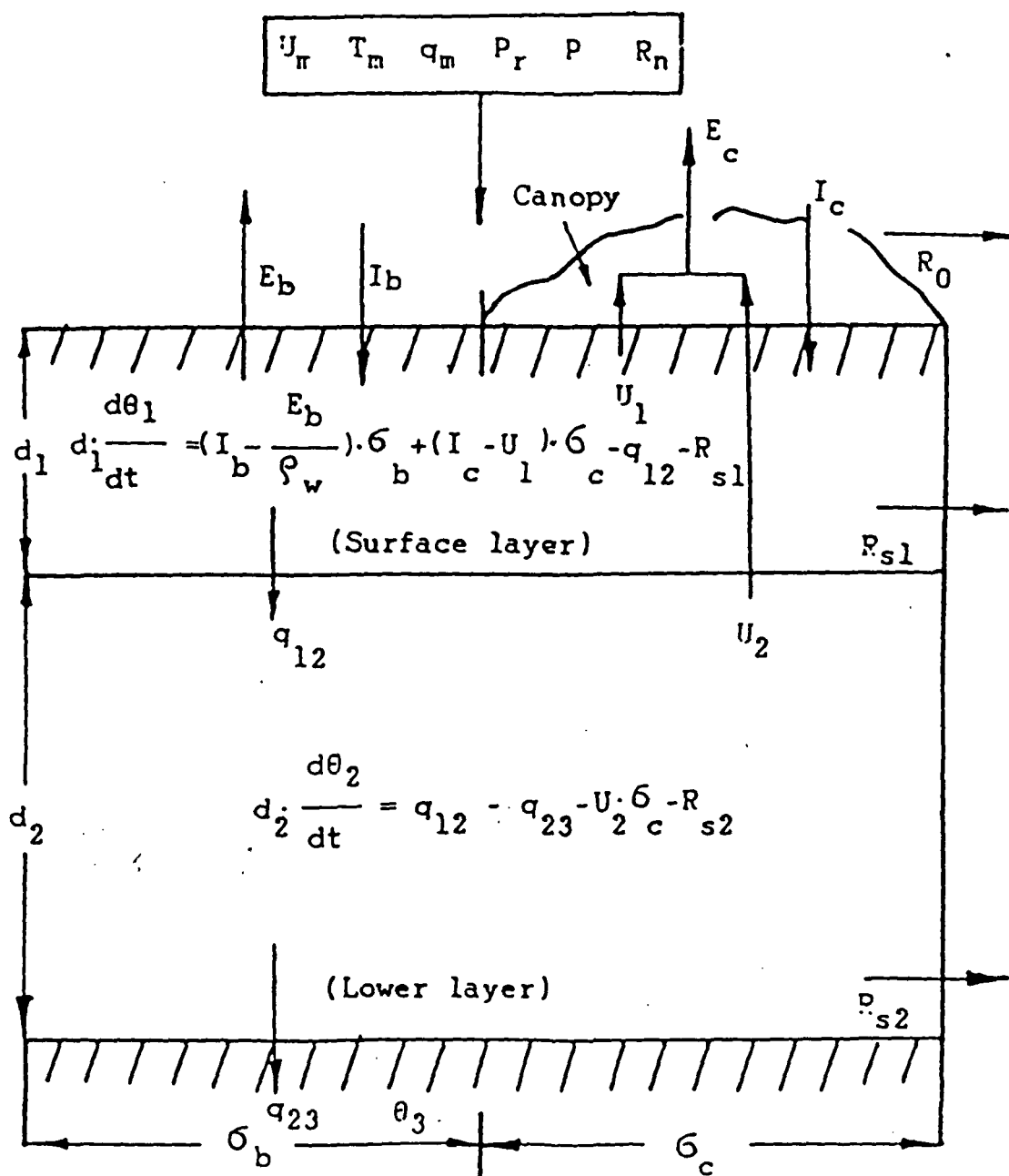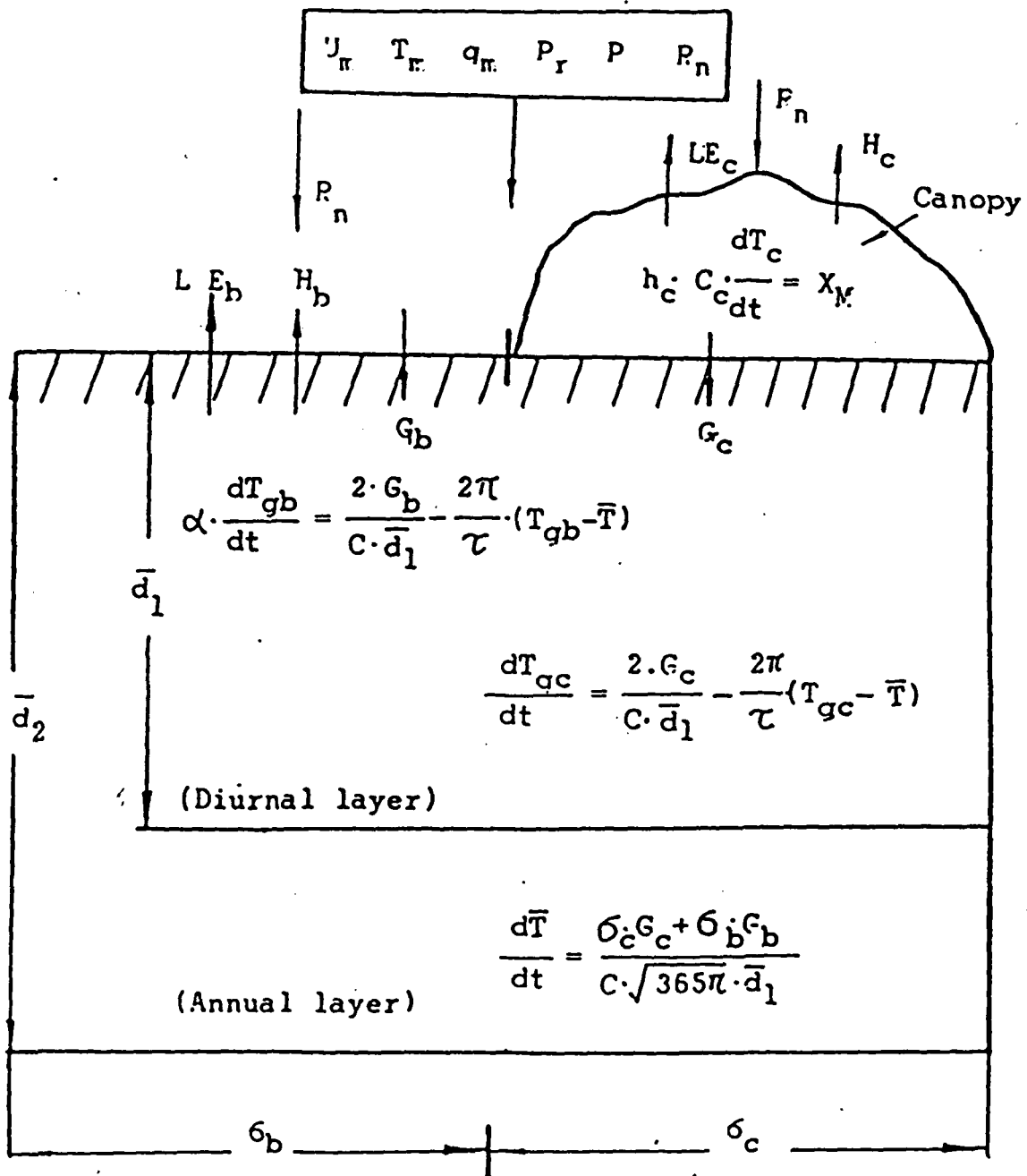
Figure 3.1-1b   Heat transport

C-2

The time-dependent variables are the soil moisture content θ_1 in the surface layer, θ_2 in the lower layer, the bare soil surface temperature T_{gb}, the vegetated ground surface temperature T_{gc}, the bulk canopy temperature T_c, and the layer average temperature $\bar{T}$ of the whole layer. Accompanying outputs are the grid average evaporation E_t and sensible heat flux H_t (note: later all variables preceded by 'grid average' are called 'grid').

In order to drive the GHM, the atmospheric variables are the temperature T_m, the wind velocity u_m, the specific humidity q_m of air (subscript m means the mean value in the PBL), precipitation P_r, air pressure P and net radiation R_n. They are generated from the GCM (Tsang and Karn, 1973; Halem etal., 1979) results.

The GHM deals with a dynamic system which, from a mathematical view point, is an initial-boundary value problem. The upper boundary conditions are obtained from coupling with the PBL, which determines evaporation and sensible heat flux in the surface layer of the PBL. The initial and lower boundary conditions should be prescribed. The formulation for the GHM is presented below section by section based on the physical phenomena.

3.1 GOVERNING EQUATION FOR SOIL MOISTURE

The saturated volumetric moisture content θ_s is defined as the volume of water per unit volume of soil when the soil is fully saturated.

The moisture content at field capacity θ_{fc} is the volumetric moisture content that a soil reaches and maintains after it has been thoroughly wetted and allowed to drain freely for a day or two.

The moisture content at permanent wilting point θ_{pwp} is the volumetric moisture content when water extraction by plants has almost ceased.

The definitions of the moisture content at field capacity and permanent wilting point are idealized and difficult to determine uniquely for different soils and different plants. In order to overcome this difficulty, the definitions used in this study are the quantitative ones given in Chapter 2. θ_{fc} is defined as θ at which the matrix potential equals to -350 H_2O-cm. θ_{pwp} is defined as θ at which the matrix potential equals to $-16,000$ H_2O-cm.

Maximum available moisture content θ_{avm} is

$$\theta_{avm} = \theta_{fc} - \theta_{pwp}$$

Available moisture content θ_{av} is

$$\theta_{av} = \theta - \theta_{pwp}$$

The fraction of available moisture content θ_{avf} is

$$\theta_{avf} = \theta_{av}/\theta_{avm}$$

The soil moisture movement in the two layers are schematically shown in Figure 3.1-1a. Without regard to the rain interception by canopy and intercell exchange, the variation of volumetric moisture content θ_1 in the surface layer for the GHM is controlled by the following components: the surface infiltration I_b (into the bare soil surface) and I_c (into the vegetated ground surface), the evaporation E_b from the bare soil, the water uptake U_1 by the roots in layer 1, the interfacial moisture flux q_{12} between layers 1 and 2 and the subsurface runoff R_{s1} when moisture content θ_1 exceeds the field capacity. Storage change of liquid water above the ground surface is neglected in the GHM. The equation for θ_1 is expressed by

$$d_1 d\theta_1/dt = (I_b - E_b/\mathcal{P}_w)\sigma_b + (I_c - U_1)\sigma_c - q_{12} - R_{s1} + I_{s1}$$

$$\sigma_c = 1 - \sigma_b \qquad (3.1.1)$$

where I_{s1} is the infiltration from melting snow and ice and is disregarded in this study.

The volumetric moisture content for the second layer θ_2 is governed by

$$d_2 d\theta_2/dt = -\sigma_c U_2 + q_{12} - q_{23} - R_{s2} + I_{s2} \qquad (3.1.2)$$

where U_2 is the water uptake by the roots in layer 2, q_{23} the interfacial moisture flux, R_{s2} the subsurface runoff from layer 2 when the moisture content in the layer exceeds the field capacity and I_{s2} is the contribution from ice melting and is also disregarded in this study.

The moisture content in the third layer below the root zone is not known. But it seems likely that the soil moisture condition in the third layer changes very slowly with time and may be expressed by

$$\theta_3 = \text{constant} + f(\mathcal{E}t) \quad (\mathcal{E} \ll 1) \tag{3.1.3}$$

However, for the short period experiments, θ_3 may be approximated by θ_{fc} for this study. Another lower boundary condition is also used as part of the sensitivity study. It is a constant flux at zero moisture gradient condition

$$q_{23} = K_{23} \quad \text{or} \quad \partial\theta/\partial z\big|_{23} = 0. \tag{3.1.4}$$

where K_{23} is defined in Eq. (3.3.4)

In Eqs. (3.1.1) and (3.1.2), the parameters d_1 and d_2 are determined based on the root zone thickness and root system distribution. For most plants, the top 10 cm below the surface has a denser root distribution and is selected as the surface layer. The deep root zone thickness depends on the vegetation type. In this study, a shallow root system and a deep root system (Hillel, 1979) have been used for the short canopy and the tall canopy, respectively. They are $d_2 = 40$ cm for the short canopy and $d_2 = 90$ cm for the tall canopy. Different values of d_2 are used in the sensitivity study.

The fluxes in Eqs. (3.1.1) and (3.1.2) are treated in the subsequent sections.

3.2 GOVERNING EQUATION FOR GROUND TEMPERATURE

Figure 3.1-1b shows the scheme for the heat transport between the air and a bare soil surface, the air and a bulk canopy layer, a bulk canopy layer and a vegetated ground surface, and in the soil. Sellers (1965) pointed out that the soil temperature has layered characteristics: a thin surface layer influenced by the diurnal temperature cycle and a deeper layer (the annual layer in Figure 3.1-1b) influenced by the annual temperature cycle. In the surface layer, the ground temperature has a high temperature gradient (Bruce et al., 1977; Kimball et al., 1976).

Bhumralkar (1975) and Blackadar (1976) have, based on the simple harmonic solution of the temperature wave, independently proposed a force-restore method to predict the soil temperature variation. According to this method, the ground surface temperature is dependent on the heat flux on the surface as well as on the restoring influence of the deeper soil layer. Deardorff (1978) compared the methods with those currently being used in the GCM model and showed that the force-restore method can provide a better prediction. Lin (1980) revised the surface temperature formulation, which assumed surface temperature to be a linearly average temperature within a thin layer of the order of 1 cm. The final rate equations for the bare soil surface temperature T_{gb} and the vegetated ground surface temperature T_{gc} in the GHM are expressed as

$$\alpha \, dT_{gb}/dt = 2G_b/(C\overline{d_1})-2\pi/\tau(T_{gb}-\overline{T}) \qquad (3.2.1a)$$

$$\alpha \, dT_{gc}/dt = 2G_c/(C\overline{d_1})-2\pi/\tau(T_{gc}-\overline{T}) \qquad (3.2.1b)$$

$$\alpha = (1+2\delta/d_1), \qquad \delta = 1 \text{ cm} \qquad (3.2.1c)$$

In Eq. (3.2.1) G_b is the heat flux into the bare soil surface, G_c is the heat flux into the vegetated ground surface, C is the heat capacity of the soil and d_1 is the damping depth of the diurnal temperature wave equal to $[\tau / (\pi C)]^{1/2}$ and $\tau = 86400$ seconds

The layer average temperature $\overline{T}$ is governed by a rate equation

$$d\overline{T}/dt = (\delta_b G_b + \delta_c G_c)/(C(365 \pi)^{1/2}\overline{d_1}) \qquad (3.2.2)$$

where the term of $(365\pi)^{1/2}\overline{d_1}$ is the penetrating depth of the annual temperature wave (Lin, 1980).

For the bulk canopy layer temperature T_c, the direct use of heat conservation principles will give

$$C_c h_c dT_c/dt = X_M \qquad (3.2.3)$$

where C_c is the volumetric heat capacity of the canopy, h_c is the height of the canopy and X_M is the increment rate of the heat storage in the bulk canopy layer of unit sectional area.

Eqs. (3.2.1)-(3.2.3) can be integrated if initial conditions are given. The determination of G_b, G_c and X_M will be discussed in the next section.

3.3 FORMULATION OF VARIOUS FLUXES OF VERTICAL MOISTURE MOVEMENT

In the previous section, there are many fluxes left to be determined. These are soil moisture fluxes q_{ij} between layers i and j, subsurface runoff R_{si}, evaporation or evapotranspiration from bare soil or canopy, water uptakes U_1 and U_2 from the root zone, infiltrations I_b and I_c, heat conductions G_b and G_c and heat storage increment rate X_M. The evaporation and evapotranspiration are related to the sensible heat fluxes H_b from the bare soil, H_c from the canopy and H_{cb} from the vegetated ground surface to the canopy layer. This section and the next section will be devoted to the formulation of these fluxes.

3.3.1 Moisture flux in soil

According to the Richards law, the moisture flux q_{ij} is expressed by

$$q_{ij} = -Dd\Theta/dz + K \qquad (3.3.1)$$

where D and K are functions of moisture content Θ. Since only average soil moisture content Θ_1 and Θ_2 are available in the GHM, q_{ij} between layers i and j is approximated by

$$\frac{1}{d_{ij}} \int_{z_i}^{z_j} q_{ij} dz = -\int_{\Theta_i}^{\Theta_j} Dd\Theta/d_{ij} + \int_{\Theta_i}^{\Theta_j} Kd\Theta/(\Theta_j - \Theta_i) \quad (3.3.2)$$

Then, the average q_{ij} is

$$q_{ij} = D_{ij}(\Theta_j - \Theta_i)/d_{ij} + K_{ij} \quad (3.3.3)$$

where $D_{ij} = 1/(\Theta_j - \Theta_i) \int_{\Theta_i}^{\Theta_j} Dd\Theta$

and $K_{ij} = 1/(\Theta_j - \Theta_i) \int_{\Theta_i}^{\Theta_j} Kd\Theta \quad (3.3.4)$

and d_{ij} is the transport distance between $\Theta = \Theta_i$ and $\Theta = \Theta_j$, depending on the layer thicknesses and the profile of soil moisture distribution in the layers. In this study, d_{ij} are approximated by

$$d_{ij} = 0.5(d_i + d_j) \quad \text{if} \quad \begin{matrix} \Theta_1 > \Theta_2 > \Theta_3 \\ \Theta_1 < \Theta_2 < \Theta_3 \end{matrix} \quad (3.3.5)$$

$$d_{ij} = 0.25(d_i + d_j) \quad \text{if} \quad \begin{matrix} \Theta_1 < \Theta_2 > \Theta_3 \\ \Theta_1 > \Theta_2 < \Theta_3 \end{matrix} \quad (3.3.6)$$

Since the relation between K, D and Θ has been approximated with straight-line segments on semi-log plots by Eq. (2.4.4)

$$K(\Theta) = a_1 \exp(a_2(\Theta - a_3)) \quad (2.4.4a)$$

$$D(\Theta) = b_1 \exp(b_2(\Theta - b_3)) \quad (2.4.4b),$$

the expression for K_{ij} and D_{ij} will depend on where Θ_i and Θ_j are located. Assuming $\Theta_i < \Theta_j$ without losing generality,

there are three possible cases shown in Figure 3.3.1 where Θ_{1b} and Θ_{2b} are the values of the moisture content at the boundary demarcation points of the segments shown under the O-term in Table 2.4.2.

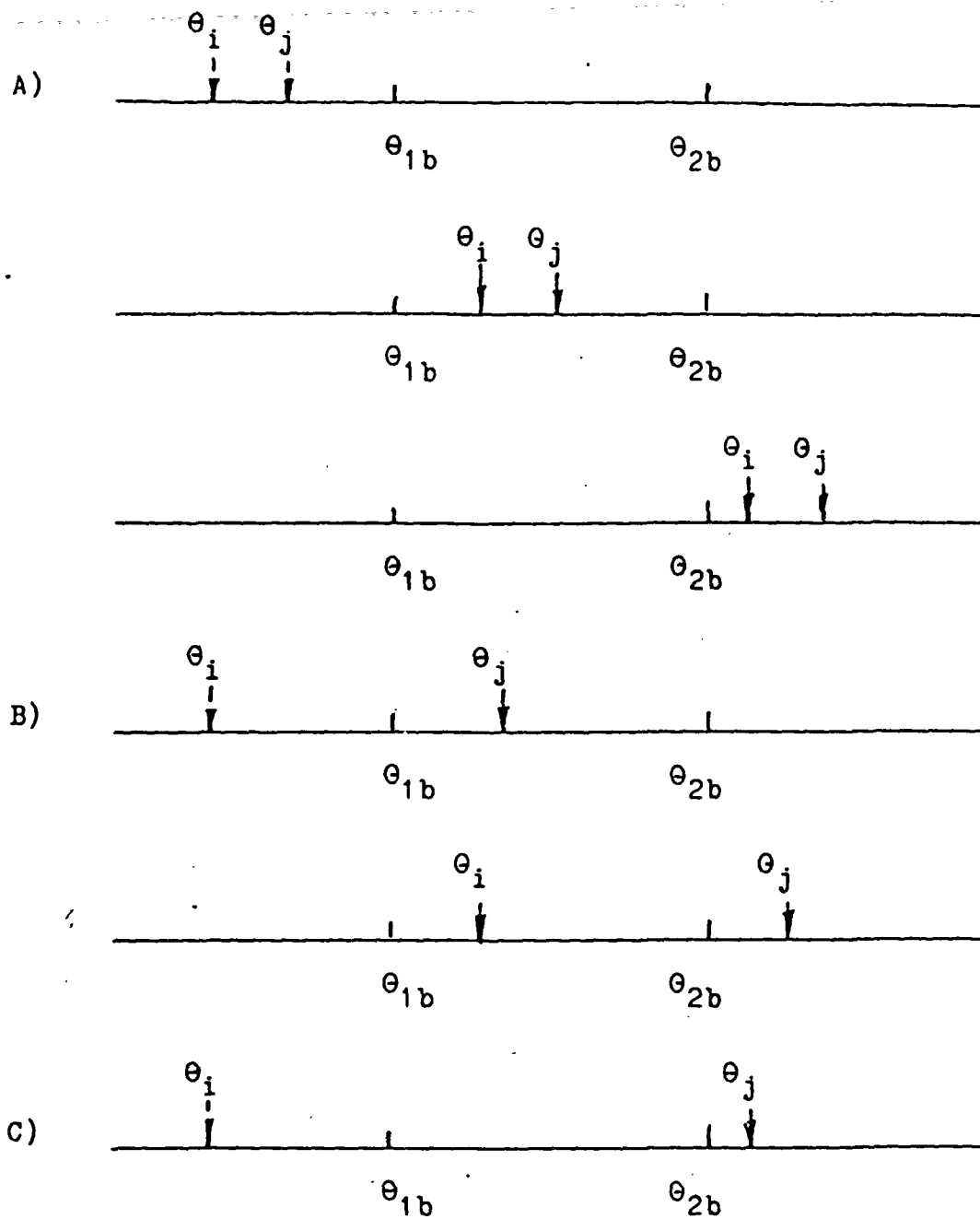If case A) is true, A_{ij} (D_{ij}, K_{ij}) is equal to

$$A_{ij} = \left[A(\Theta_i)-A(\Theta_j)\right]/\ln\left[A(\Theta_i)/A(\Theta_j)\right] \qquad (3.3.7)$$

If case B) is true and Θ_i and Θ_j are located in either side of a demarcation point Θ_{ib} (i=1,2), then

$$A_{ij} = 1/(\Theta_j-\Theta_i)\left\{\left[(A(\Theta_{ib})-A(\Theta_i)\right]/\ln\left[A(\Theta_{ib})/A(\Theta_i)\right]\right.$$
$$\left.*(\Theta_{ib}-\Theta_i)+\left[A(\Theta_j)-A(\Theta_{ib})\right]/\ln\left[A(\Theta_j)/A(\Theta_{ib})\right]\left[\Theta_j-\Theta_{ib}\right]\right\}$$
$$(3.3.8)$$

If case C) is true, Θ_i and Θ_j are separated by the demarcation points, thus

$$A_{ij} = 1/(\Theta_j)-\Theta_i)\left\{\left[(A(\Theta_{1b})-A(\Theta_i)\right]/\ln\left[A(\Theta_{1b})/A(\Theta_i)\right]*\right.$$
$$(\Theta_{1b}-\Theta_i)+\left[A(\Theta_{2b})-A(\Theta_{1b})\right]/\ln\left[A(\Theta_{2b})/A(\Theta_{1b})\right]*$$
$$\left.(\Theta_{2b}-\Theta_{1b})+\left[A(\Theta_j)-A(O_{2b})\right]/\ln\left[A(\Theta_j)/A(\Theta_{2b})\right](\Theta_j-\Theta_{2b})\right\}$$
$$(3.3.9)$$

θ_{1b}, θ_{2b} demarcation points

θ_i, θ_j moisture contents in layer i, j

Figure 3.3.1   Possible cases of volumetric moisture content

3.3.2 Infiltration at the ground surface after rainfall

Infiltration is defined as the entry of water into the soil body through the ground surface. It is an important hydrologic process because its rate determines the amount of water which accounts for surface storage and runoff after rainfall.

Given boundary and initial conditions, the rate of infiltration can be calculated with great detail by numerically solving the governing equations (Wang and Lakshminarayana, 1968; Whisler and Bouwer, 1970). However, the numerical solution is rather complex and the required soil data are also difficult to obtain. This method is not suitable for the GHM. As discussed in the introduction, several empirical methods are commonly used to model infiltration (Mein and Larson, 1973). In this study, the Green-Ampt approach is adapted for the GHM. According to their classic paper, infiltration into an initial unsaturated soil generally occurs under the combined influence of gravity potential and matrix potential. The original formulation (Green and Ampt, 1911) for infiltration rate was derived for water with a ponding surface into a deep homogeneous soil column with a initially uniform moisture distribution. It is assumed that water enters the soil creating a saturating flow zone with a sharp wetting front which separates a saturated zone from an unsaturated zone (Figure 3.3.2).
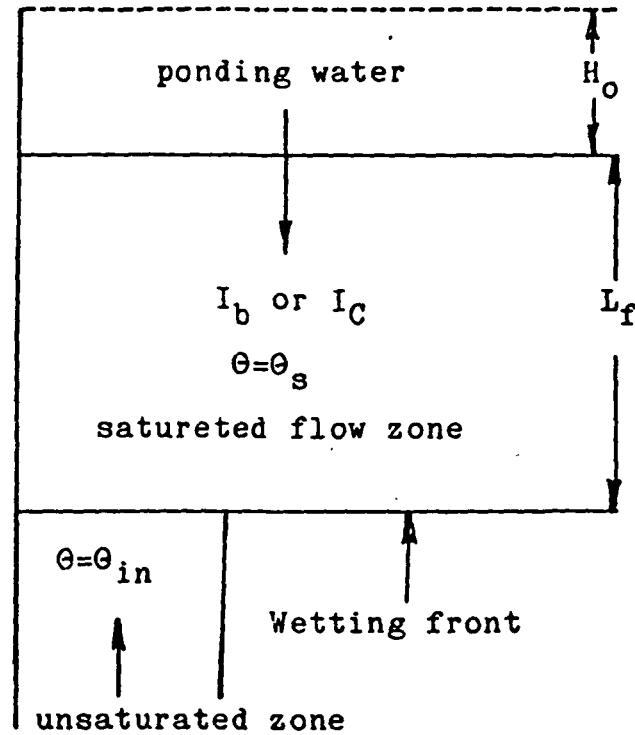
Figure 3.3.2   Infiltration

Omitting the derivation, the infiltration rate I_o (I_b or I_c) can be expressed as

$$I_o = K_s(S_f + L_f + H_o)/L_f \qquad (3.3.10)$$

where K_s is the soil hydraulic conductivity at saturation, H_o is the depth of water ponding on the surface, S_f is the effective matrix potential difference across the wetting front known as suction head and L_f is the distance from the surface to the wetting front.

In the GHM, the water ponded on the surface is ignored and thus H_o is equal to zero. The infiltration rate I_o (I_b or I_c) is determined by the following formulation:

$$I_o = Min(K_s(S_f+L_f)/L_f, \quad P_r/\rho_w) \qquad (3.3.11a)$$

L_f can be determined by

$$dL_f/dt = I_o/(\Theta_s - \Theta_j) \qquad (3.3.11b)$$

where $\Theta_j = \Theta_1$ if $L_f < d_1$ or $\Theta_j = \Theta_2$ if $L_f > d_1$.

or $\qquad L_f = \Theta$ if rain stopped or just begun. $\qquad$ (3.3.11c)

All variables in these equations are predictable except the suction head S_f. Mein and Larson (1973) suggested that the suction head can be expressed by

$$S_f = \int_{K_r(\Theta_{in})}^{1} \psi \cdot dK_r \qquad (3.3.12)$$

where $K_r = K/K_s$.

If the matrix potential and conductivity are given in terms of soil moisture, S_f can be calculated directly.

3.3.3 Surface and subsurface runoffs

Surface runoff and subsurface runoff account for the water loss from the soil as shown in Figure 3.1-1a. When rain is heavy, this loss is important for the water budget.

In the GHM, the parameterization used by Alfano (1981) is followed. In a GCM, the values of grid-average intensity of precipitation is in general smaller than the infiltration, and the ponding and evapotranspiration from the ponded water can be ignored. Thus, the surface runoff is considered as the residual of the precipitation minus the infiltration. The formula for the runoff is

$$R_o = \text{Max} \ (P_r/\rho_w - \sigma_b I_b - \sigma_c I_c, \ 0) \qquad (3.3.13)$$

For the subsurface runoff R_{si} $(i=1,2)$ a general relationship, as noted by Sellers (1965) and suggested by Arakawa and Mintz (1972), was used in this study. R_{si} can be expressed by

$$
\begin{aligned}
R_{si} Dt &= 0 & \theta_i < \theta_{fc} \ (i=1,2) \\
&= d_i(\theta_i - \theta_{fc}) r & \theta_{fc} < \theta_i < \theta_s \\
&= d_i((\theta_s - \theta_{fc}) r_m + (\theta_i - \theta_s)) & \theta_s < \theta_i
\end{aligned}
$$

$$(3.3.14)$$

where Dt is a half-hour and r is a scaling factor. Alfano (1981), by using observed data (Bruce et al., 1977), suggested that r value be calculated by

$$r = r_m((\theta_i - \theta_{fc})/(\theta_s - \theta_{fc}))^m$$

where $r_m = 0.5$ and $m = 1.0$.

3.3.4 evapotranspiration

Evapotranspiration represents the moisture loss from the land surface through evaporation from bare soil and ponded water, and transpiration of plants. It plays an important role in linking the water transport and energy transport process because latent heat flux is supplied when water evaporates. The estimation of evapotranspiration is difficult and has been studied extensively by multi-disciplinary investigators because the process involves the complex interaction of the atmosphere, plant and soil. There are many

empirical formulas that exist for estimating evapotranspi-
ration (Fritschen, 1981), among which the combination meth-
od or Monteith's formula (Monteith, 1975) has been widely
used.

One of currently-used methods is to calculate the actual
evaporation or transpiration through scaling potential eva-
poration or unstressed transpiration.

In the earlier version of GCMs, the concept of the scal-
ing factor developed by Budyko (1965) has been extensively
used, i. e.

$$\beta = E/E_p$$

In the GLAS GCM, the scaling factor depends on available
water θ_{avf} defined in Section 3.1 in the root zone of 1 m
thick. In the Lin at al. GHM, the scaling method was re-
fined. In each grid, the total evapotranspiratin is the sum
of the subgrid portions of the bare soil evaporation and
transpiration from the canopy. The bare soil scaling factor
β_b and canopy scaling factor β_c used to estimate these actu-
al fluxes from potential evaporation and the unstressed
tanspiration are adapted in this study. Potential evapora-
tion indicates the evaporation from á fully saturated soil
surface with actual ground temperature. For the direct
coupling with the PBL, the potential evaporation from bare
soil can be expressed as

$$E_p = C_T u_* \rho_a \left[q^*(T_g) - q_m \right] \tag{3.3.15}$$

where C_T is the heat transfer coefficient derived in Section 3.4.2, $q^*(T_g)$ is the saturated air specific humidity, q_m is the air specific humidity in the PBL and u_* is friction velocity. $C_T u_*$ may also be considered as the inverse of aerodynamic resistance r_v to heat transport between the ground surface and the location where q_m is defined in the PBL. The unstressed transpiration implies the transpiration from leaves when plants are under no water stress condition. The unstressed transpiration may be expressed in terms of a canopy resistance as

$$E_u = \rho_a \{q^*(T_c) - q_m\}/(r_v + r_{cm}) \qquad (3.3.16)$$

where $q^*(T_c)$ is the saturated air specific humidity, r_{cm} the unstressed canopy resistance. r_{cm} may vary diurnally in a canopy depending on the atmospheric conditions but not the soil moisture content. However, in this study, the unstressed transpiration is defined when the minimum unstressed canopy resistance is used in Eq. (3.3.16), which is a function of plant species only (from now on in the text $r_c = r_{cm}$)

Alfano (1981), using data (Bruce et al., 1977, Jackson et al., 1971 and 1975) for the actual evaoporation E from bare soil, fitted a relation between the scaling factor $_b$ and soil moisture content. The relation used in this study later is

$$\beta_b = E/E_p = (\theta_{avf}/C_6)^{C_7} \qquad (3.3.17)$$

where $C_6 = 5\theta_{avm}$ to $6.5\theta_{avm}$ and C_7 is around 3.0.

For a canopy, the actual transpiration E_c is related to the unstressed transpiration E_u (Hanks and Ashcroft, 1980) through the scaling factor by

$$\beta_c = E_c/E_u \qquad (3.3.18)$$

β_c should be estimated from the measured E_c and E_u. several relations have been proposed for it (Hanks and Ashcroft, 1980). Alfano (1981) proposed a relation for determining E_c as a function of soil moisture in the root zone by using the data given by Denmead and Shaw (1962). Since E_c is sum of the uptakes U_1 and U_2, the effective scaling factor β_c is

$$\beta_c = E_c/E_u = \rho_w U_1/E_u + \rho_w U_2/E_u$$
$$= \beta_{c1}*Rd_1 + \beta_{c2}*(1-Rd_1) \qquad (3.3.19)$$

where for layer i

$$\beta_{ci} = \rho_w U_i/E_u/R_{di} = (\theta_i - \theta_{pwp})/(\theta_t - \theta_{pwp}) \qquad \theta_{pwp} < \theta_i < \theta_t$$

or $\quad \beta_{ci} = 0 \qquad\qquad\qquad \theta_{pwp} > \theta_i$

or $\quad \beta_{ci} = 1 \qquad\qquad\qquad \theta_t < \theta_i \qquad (3.3.20)$

The threshold value θ_t depends on the soil moisture and the value of unstressed transpiration. The relation for θ_t is

$$\theta_t = \theta_{pwp} + (\theta_{fc} - \theta_{pwp})\left[C_t E_u/(\theta_{fc} - \theta_{pwp})\right]^{C_9} \qquad (3.3.21)$$

where $C_t = 2520$ sec/cm, $C_9 = 0.8$ and the dimension of E_u is cm/sec.

3.4 COUPLING WITH PBL AND DETERMINING THE INTERFACE FLUXES

3.4.1 Energy balance -- determination of heat fluxes into soil and heat storage increment in canopy

In Section 3.2, the heat fluxes into soil G_c and G_b and the heat storage increment rate X_M remain to be determined. They depend on three sub-system heat balances in the grid.

The heat flux G_b into the bare soil surface is obtained from the energy balance between the bare soil surface and the air:

$$G_b = R_{nb} - LE_b - H_b \tag{3.4.1}$$

where R_{nb} is the net radiation at the surface, LE_b the latent heat flux from the surface into the air and H_b sensible heat from the surface to the air. The R_{nb} is calculated by

$$R_{nb} = S_w(1-a_{1b}) + S_L - \sigma T_{gb}^4 \tag{3.4.2}$$

where S_w is the solar beam from air, a_{1b} the albedo of the bare soil surface, S_L the downward long wave radiation from the air and σ Stefan-Boltzmann's constant.

The heat storage increment rate in the bulk canopy layer X_M is dependent on the heat exchange between the air and the canopy layer as well as the canopy layer and the vegetated ground surface and is expressed by

$$X_M = R_{nc} - LE_c(1-C_1) - S_w EXP(-LAI*X_c)(1-a_{1c}) - H_c + H_{cb}$$
$$+ \sigma(T_{gc}^4 - T_c^4) \tag{3.4.3}$$

R_{nc} is the net radiation at the top of the canopy and is calculated

$$R_{nc} = S_w(1-a_{1c}) + S_L - 6T_c^4 \qquad (3.4.4)$$

where a_{1c} is the albedo value of the canopy.

LE_c is the total latent heat from the canopy layer, which is contributed mainly from the canopy layer itself and a small portion of which come from the vegetated ground surface, and C_1 is the ratio of the latent heat from the ground surface to the total latent heat from the canopy to the air, which is not needed in this model with the subgrid parameterization. The term $S_w EXP(-LAI*X_c)(1-a_{1c})$ represents the part of solar radiation arriving at the ground surface. H_c is the sensible heat flux from the canopy layer and H_{cb} is the sensible heat flux to the canopy layer from the vegetated ground surface. The last term on the right hand side of (3.4.3) is long wave radiation exchange between the canopy layer and the ground surface. The heat flux G_c into the vegetated ground surface under the canopy is

$$G_c = -LE_c c_1 + S_w EXP(-LAI*X_c)(1-a_{1c}) - H_{cb}$$
$$+ 6(T_c^4 - T_{gc}^4) \qquad (3.4.5)$$

In Eqs. (3.4.1), (3.4.3) and (3.4.5), the fluxes E_b, E_c, H_b, H_c and H_{cb} remain to be determined. The next subsection will discuss the estimation for the fluxes.

3.4.2   Coupling with The PBL -- fluxes of momentum, heat and moisture from interface.

The determination of turbulent fluxes across the atmosphere-land interface is the most familiar and most widely discussed aspect of the PBL parameterization problem, and in recent years promising new theories have improved the understanding (Deardorff, 1972; Randall, 1983). In the GHM, Deardorff's theory is used to estimate the fluxes. It is a kind of similarity theory, in that the fluxes across the interface are related to the bulk property of the PBL. Now the problem is posed in the following way: if the mean atmospheric field such as the wind velocity u_m, potential temperature S_m and specific humidity q_m within the PBL and the thickness of the layer h were given from GCM output, what should be the momentum, heat and moisture fluxes across the interface when the necessary conditions on the land surface have been prescribed?

Before answering this question, additional notation is needed to supplement those listed in 'NOTATION'.

Y $\log_{10}(-RI_b)-3.5$

Subscripts

a   air

av   grid averaged variables (briefly named as 'grid')

s   the interface or lower boundary of PBL $:\begin{cases} c & \text{over canopy} \\ b & \text{over bare soil} \\ av & \text{about grid average} \end{cases}$

m   mean value within PBL

N   neutral stability

v   virtual potential temperature

w   water

*   friction velocity

Superscripts

*   saturated condition.

The potential temperature S is a temperature that a parcel of air has when it moves adiabatically from the level with pressure P to the level with P=1000 mb. The virtual potential temperature T_v is approximately defined as

$$T_v = S(1.+ 0.61q) \qquad (3.4.6)$$

The kinematic vertical heat flux F is related to the kinematic sensible heat flux F_T and the kinamatic moisture flux F_w by

$$F = F_T + 0.61 S_m F_w \qquad (3.4.7)$$

Due to the effect of buoyancy, there are three states of thermal stability of the PBL: stable, unstable and neutral. The state of thermal stability of the PBL is designated by

stable,   if $(T_{vs}-T_{vm})<0$ with F<0

unstable, if $(T_{vs}-T_{vm})>0$ with F>0

neutral,   if $(T_{vs}-T_{vm})=0$ with F=0

where $T_{vs} = S_s(1.+0.61q_s)$ (3.4.8a)

$$T_{vm} = S_m(1.+0.61q_m) \qquad (3.4.8b)$$

S_s or q_s may either be S_b or q_b at the bare soil surface or S_c or q_c at the canopy layer surface, and S_s is

$$S_b = T_{gb}(1000/P)^{0.288} \tag{3.4.8c}$$

$$\text{or} \quad S_c = T_c(1000/P)^{0.288} \tag{3.4.8d}$$

The Richardson number, which is related to the exchange coefficient in these three cases, is defined as

$$RI_b = gh(T_{vm}-T_{vs})/(T_{vm}u_m^2)$$

The stable, unstable and neutral cases correspond to RI_b greater, less than or equal to zero, respectively.

According to Deardorff's work (1972), the friction coefficient C_u and heat transfer coefficient C_T for these three cases can be expressed as a function of RI_b. For the neutral case, C_{uN} and C_{TN} are given by

$$C_{uN} = (k^{-1}\ln(0.025h/z_0)+8.4)^{-1} \tag{3.4.9a}$$

$$C_{TN} = (k^{-1}R\ln(0.025h/z_0)+7.3)^{-1} \tag{3.4.9b}$$

For the stable case, the C_u and C_T are

$$C_u = C_{uN}(1-RI_b/RI_c) \tag{3.4.10a}$$

$$C_T = C_{TN}(1-RI_b/RI_c) \tag{3.4.10b}$$

where RI_c is 3.05 and RI_b should be less than $0.9RI_c$
For the unstable case, the coefficients are

$$C_u =(C_{uN}^{-1}- 0.25\exp(0.26Y-0.03Y^2))^{-1} \tag{3.4.11a}$$

$$C_T = (C_{TN}^{-1}+C_u^{-1}-C_{uN}^{-1})^{-1} \tag{3.4.11b}$$

The limiting case of free convection must be considered under the strongly unstable case. For RI_b in the vicinity

of, or exceeding, the value indicative of the commencement of free convection, C_u and C_T are not known with any accuracy. However, the main wind must be so small in this case that some inaccuracy in C_u may be tolerated. The C_u and C_T are maintained constant for R_{Ib} lying within the free convection regime. The regime can be identified by numerically testing whether C_u^{-1} and C_T^{-1} are less than 0.5 and 0.3 of their respective neutral value. For the kinematic heat flux, however, the above procedure should be further constrained with the following condition (Townsend, 1964):

$$F_{\text{free conv.}} > 0.19(T_{vs}-T_{vm})^{4/3} \qquad (3.4.12)$$

That means, when $C_u^{-1}<0.5C_{uN}^{-1}$ and $C_T^{-1}<0.3C_{TN}^{-1}$ is in free Otherwise,

$$F_{\text{free conv.}}=0.19(T_{vs}-T_{vm})^{4/3} \ (cm*\,^{\circ}K/s) \qquad (3.4.13c)$$

The kinematic vertical heat flux F can be partitioned into the kinematic sensible heat and moisture fluxes by

$$F_w=E/(\rho_a)= (q_s-q_m)/(T_{vs}-T_{vm})F \qquad (3.4.14a)$$

$$F_T=H/(\rho_a Cp)=(S_s-S_m)/(T_{vs}-T_{vm})F \qquad (3.4.14b)$$

and u_* can be obtained by

$$u_*= U_m C_u \qquad (3.4.14c)$$

Eqs. (3.4.6) through (3.4.14) are applied to the bare soil and the bulk canopy layer, respectively. Under the same mean PBL conditions, different surface conditions of either bare soil or canopy layer will correspond to different sensible heat and latent heat fluxes.

3.5 GRID AVERAGE VARIABLES

In the previous section, the calculation of the dependent variables at the different parts in a grid was described. However, in order to be consistent with a GCM, The GHM should supply the GCM with a grid average sensible heat, a grid average moisture flux, a grid average surface temperature and a grid average friction velocity (later each variable preceded with grid indicates the variable are grid-averaged.) The basic concept developed in the GHM to get the grid surface temperature T_g is such that the calculated grid friction velocity u_{*av}, grid kinematic vertical fluxes F_{av}, grid kinematic sensible heat and moisture fluxes from the ground surface, based on the grid surface temperature being calculated below and the same conditions in the PBL, are equal to the proportional summation of the corresponding values of the canopy part and bare soil part. Therefore, one has

$$u_{*av}^2 = \sigma_b u_{*b}^2 + \sigma_c u_{*c}^2 \qquad (3.5.1a)$$

$$F_{av} = \sigma_b F_b + \sigma_c F_c \qquad (3.5.1b)$$

$$F_{Tav} = \sigma_b F_{Tb} + \sigma_c F_{Tc} \qquad (3.5.1c)$$

$$F_{wav} = \sigma_b F_{wb} + \sigma_c F_{wc} \qquad (3.5.1d)$$

By using the formulas in Section 3.4, the grid ground surface temperature can be calculated inversely with given F_{av}, F_{Tav}, F_{wav}, u_{*av}^2 and the same mean PBL conditions.

Given F_{av}, the stability can be determined from

$$\text{stable} \qquad \text{if } F_{av} < 0$$

$$\text{unstable} \qquad \text{if } F_{av} > 0$$

$$\text{neutral} \qquad \text{if } F_{av} = 0$$

In each case, the grid friction coefficient may be directly calculated by

$$C_u = u_{*av}/u_m \tag{3.5.2}$$

According to Eq. (3.4.9), grid surface roughness Z_{oav} may be calculated for the neutral case as

$$\ln z_{oav} = \ln(0.025h) - k(1/C_{uN} - 8.4) \tag{3.5.3}$$

Grid average heat coefficient C_{TN} can be calculated by inserting z_{oav} from Eq. (3.5.3) into Eq. (3.4.9b). Then, using Eq. (3.4.14b) and the definition of F, the grid potential temperature at the ground surface S_{av} for the neutral case is

$$S_{av} = F_{Tav}/(u_{*av}C_{TN}) + S_m \tag{3.5.4}$$

For the stable case, an explicit solution can be obtained through mathematical treatment. First, an abbreviated notation for convenience is introduced as follows:

$$y = k^{-1} \ln(0.025h/Z_{oav}) \tag{3.5.5a}$$

$$x = (T_{vm} - T_{vav}) \tag{3.5.5b}$$

$$b = gh/(T_{vm}u_m^2) \tag{3.5.5c}$$

$$a = 7.3 - 8.4R \tag{3.5.5d}$$

From Eqs. (3.4.10a) and (3.4.9a), one has

$$C_u C_{uN}^{-1} = (1.-RI_b/RI_c) \tag{3.5.6a}$$

$$C_{uN}^{-1} = (y+8.4) \tag{3.5.6b}$$

$$C_u(y+8.4) = (1.-RI_b/RI_c) \tag{3.5.6c}$$

Also from Eqs. (3.4.10b) and (3.4.9b), one has

$$C_T C_{TN}^{-1} = (1.-RI_b/RI_c) \tag{3.5.7a}$$

$$C_{TN}^{-1} = (Ry+7.3) \tag{3.5.7b}$$

$$C_T(Ry+7.3) = (1.-RI_b/RI_c) \tag{3.5.7c}$$

Then, eliminating the variable y from Eqs. (3.5.6c) and (3.5.7c), one has

$$C_T\big(R(1.-RI_b/RI_c)/C_u +7.3 -8.4R\big)$$
$$= (1.-RI_b/RI_c) \tag{3.5.8}$$

Substituting $RI_b = bx$ and $C_T^{-1} = u_{*av}x/(-F_{av})$ into Eq. (3.5.8), one has

$$(R/C_u+a)-R/(C_u RI_c)bx = -u_{*av}x/F_{av}$$
$$+u_{*av}bx^2/(F_{av}RI_c) \tag{3.5.9}$$

After simplifying the terms, Eq. (3.5.9) becomes:

$$u_{*av}bx^2/(F_{av}RI_c) +\big(Rb/(C_u RI_c)-$$
$$u_{*av}/F_{av}\big)x -(R/C_u+a) = 0 \tag{3.5.10}$$

The above equation can be rewritten as

$$Ax^2 + Bx + C = 0 \tag{3.5.11a}$$

The solution of x is

$$x= \big[-B-(B^2-4AC)^{1/2}\big]/(2A) \tag{3.5.11b}$$

The reason for the negative sign before the square root is that x approaches to zero when F_{av} goes to zero.

The final solution should include the limitation of the stable case

$$RI_b = bx < 0.9RI_c \qquad (3.5.12)$$

If the newly calculated RI_b, based on the x from Eq. (3.5.11b), is greater than $0.9RI_c$, the solution for x should be changed to

$$x = 0.9RI_c/b \qquad (3.5.13)$$

Then,

$$C_{uN} = C_u/(1.-bx/RI_c) \qquad (3.5.14)$$

and z_{oav} can be calculated with the C_{uN} from Eq. (3.5.3) Using Eq. (3.4.14b), the grid surface potential temperature S_{av} becomes

$$S_{av} = S_m - F_{Tav}/F_{*av}x$$

and $\qquad T_g = S_{av}(P/1000.)^{0.288} \qquad (3.5.15)$

For the unstable case, the explicit solution can not be obtained. However, it is possible to seek an equation for x which is easy to iterate and fast to converge. Again, using abbreviation

$$Y = Y(x) = \log_{10}(-RI_b) - 3.5 \qquad (3.5.16a)$$

$$X = X(x) = \exp(0.26Y - 0.03Y^2) \qquad (3.5.16b)$$

From Eqs. (3.4.11a,b), one has

$$C_u^{-1} = C_{uN}^{-1} - 25X \qquad (3.5.17a)$$

$$C_T^{-1} = C_{TN}^{-1} - 25X \qquad (3.5.17b)$$

From Eqs. (3.4.9a,b), one has

$$C_{uN}^{-1} = y + 8.4 \qquad (3.5.18a)$$

$$C_{TN}^{-1} = Ry + 7.3 \qquad (3.5.18b)$$

Substituting Eqs. (3.5.18a,b) into Eqs. (3.5.17a,b) and eliminating y, one has

$$-u_{*av}x/F_{av}=-25(1-R)X+8.4(1-R)-1.1+C_u^{-1}R \qquad (3.5.19a)$$

or $\qquad \Delta T = F(\Delta T) \qquad (3.5.19b)$

where $\Delta T= -x$ and $F(-x)$ is equal to the right-hand-side of Eq. (3.5.19a) divided by u_{*av}/F_{av}. Eq. (3.5.19b) is nonlinear and can only be solved by an iteration method.

Examining Eq. (3.5.16a), it can be shown that Y will increase with increasing ΔT. Also, $\log_{10}(-RI_b)$ is always less than 3.5 and thus Y is always negative. X will increase with increasing Y because

$$dX/dY= \exp(0.26Y-0.03Y^2)(0.26-0.06Y)>0$$

Since

$$dF/d(\Delta T) = -25(1-R)dX/dYdY/d(\Delta T)$$

and

$$dY/d(\Delta T) = -b/RI_b >0$$

$dF/d(\Delta T)<0$ and thus $F(\Delta T)$ decreases with increasing T. Under the unstable state, ΔT is greater than zero. So, $F(\Delta T)$ is greater than zero at $\Delta T=0$. Figure 3.5.1a shows the scheme for the curves of the left-hand-side and right-hand-side in Eq. (3.5.19b)
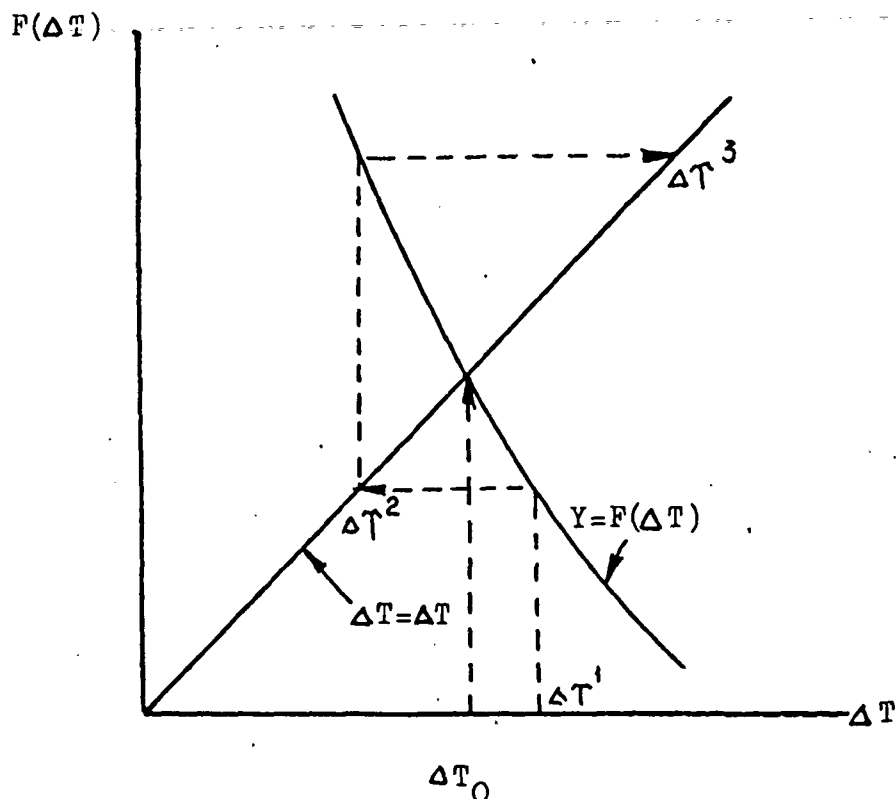
Figure 3.5-1a Iteration scheme

If a simple and direct iteration is used, choose $\Delta T^{n+1} = F(\Delta T^n)$ $(n=1,2,3,4\ldots\ldots)$ and the equation may not converge to the true solution ΔT_0 or may converge to it slowly (see Figure 3.5-1a). In this study, $\Delta T^{n+1} = 0.5$ $(\Delta T^n + F(\Delta T^n))$ $(n=1,2,3\ldots\ldots)$ was chosen and the iteration did converge to the real solution more rapidly (see Figure 3.5-1b).

After the solution ΔT_0 is obtained, S_{av} and Z_{oav} can be solved as in the stable case. Then, grid surface temperature T_g can be calculated from Eq. (3.5.15).
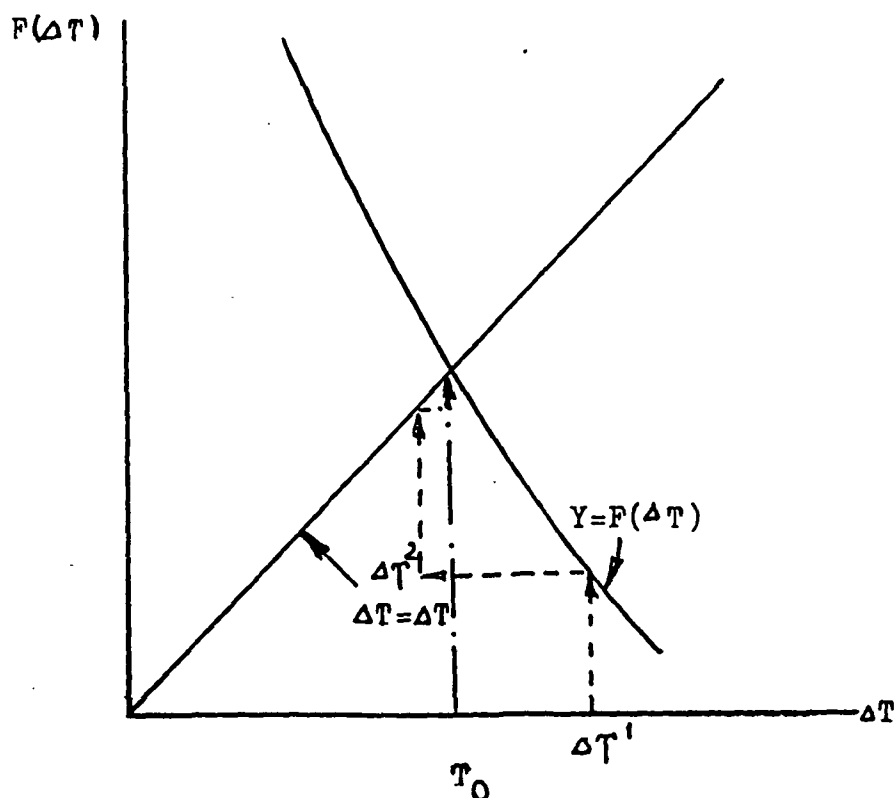
Fig 3.5-1.b Iteration scheme

3.6 SPECIFICATION OF CONDITIONS AT LOWER BOUNDARY OF THE PBL

If the lower boundary of the PBL is located in the neighborhood above the roughness height of bare soil or canopy, the values of atmospheric conditions at this boundary may not be the same as they would be at the physical surface of the bare soil or canopy. In general, one may assume the air temperature at the lower boundary equal to the temperature of the bare soil surface or canopy. However,

this assumption may not be true for the specification of the specific humidity. This section will be devoted to formulation of the specific humidity.

It is very difficult to directly determine the air specific humidity q_s in the neighborhood above land surface. One of the currently-used approaches is to relate the q_s with $q(T_s)^*$ by the scaling factor.

In terms of resistances, the potential evaporation E_{pb} and the actual evaporation E_b from the bare soil can be expressed by

$$E_{pb} = \rho_a(q_b^* - q_m)/r_v \qquad (3.6.1a)$$

$$E_b = \rho_a(q_b - q_m)/r_v \qquad (3.6.1b)$$

where r_v is the air resistance for the evaporation from the bare soil. The air specific humidity at the lower boundary of the PBL q_b can be estimated from Eq. (3.6.1) using the scaling factor derived in Eq. (3.3.17)

$$q_b = \beta_b q_b^* + (1 - \beta_b)q_m \qquad \text{if } q_b^* > q_m$$

$$\text{or} \qquad q_b = q_b^* \qquad\qquad\qquad \text{if } q_b^* < q_m \qquad (3.6.2)$$

For a canopy, the maximum unstressed transpiration E_u, according to its definition, is equal to

$$E_u = \rho_a(q_c^* - q_m)/(r_v + r_c) \qquad (3.6.3a)$$

$$E_c = \rho_a(q_c - q_m)/r_v \qquad (3.6.3b)$$

where r_v is the air resistance above canopy and r_c is the minimum unstressed canopy resistance. Defining

$$f_c = (1 + r_c/r_v)^{-1} \qquad (3.6.4)$$

and using the same derivation and assumption for q_b over bare soil, one has

$$q_c = f_c \, \beta_c q_c^* + (1 - f_c \, \beta_c) q_m \qquad \text{if } q_c^* > q_m$$

$$\text{or} \qquad q_c = q_c^* \qquad\qquad\qquad \text{if } q_c^* < q_m \qquad (3.6.5)$$

In Eqs. (3.6.1) and (3.6.3), r_v depends on the air specific humidity and temperature near the land surface. Strictly speaking, Eqs. (3.6.1) and (3.6.3) should be solved iteratively through the PBL. However, in this study, r_v is calculated assuming the air specific humidity near the land surface is under saturated conditions at the land surface temperature.

Chapter IV

COMPUTATIONAL SCHEME

4.1 METHOD FOR SOLVING SOIL MOISTURE AND TEMPERATURE RATE EQUATIONS

In the GHM, a system of six basic differential equations should be solved simultaneously grid by grid. Since the six time-dependent variables can be classified into two basic types: fast variation (T_{gb} and T_c) and slow variation ($\bar{T}$, T_{gc}, Θ_1 and Θ_2), a backward implicit finite difference method and an explicit finite difference method are applied to the equations with fast variation and those with slow change, respectively.

The explicit approach is straight forward and discussed here briefly. For example, if one has nonlinear equations for an unknown vector A_j ($j=1,2\ldots,m$):

$$dA_j/dt = F_j(A_1, \ldots, A_m), \qquad j= 1,\ldots,m \qquad (4.1.1)$$

The basic formula for solving the nonlinear system with the explicit finite difference scheme is

$$A_j^{n+1} = A_j^n + Dt F_j(A_1^n, A_2^n,\ldots,A_m^n) \qquad (4.1.2)$$

where n indicates the nth time step and Dt is the time interval, 1800 seconds used in this study.

For the backward implicit finite difference, the dynamic system defined by (4.1.1) can be expressed by

$$(A_j^{n+1}-A_j^n)/Dt = F_j(A^n) + \sum_{k=1}^{m} dF_j^n/dA_k(A_k^{n+1}-A_k^n)$$
$$(j=1,2,\ldots m) \quad (4.1.3)$$

In the GHM, a simpler scheme is used , that is the second term in the right-hand-side of Eq. (4.1.3) involves only the fast variable.

4.2 IMPLICIT SCHEME FOR BARE SOIL SURFACE TEMPERATURE

The governing equation for bare soil surface temperature is

$$dT_{gb}/dt = \left[2G_b/(C\bar{d}_1)-2\pi/\tau(T_{gb}-\bar{T})\right]/\alpha = F, \quad (3.2.1)$$

Thus, the backward implicit scheme with an expansion term of T_{gb} will produce

$$(T_{gb}^{n+1}-T_{gb}^n)/Dt=2G_b^n/(\alpha C\bar{d}_1) -2\pi/(\tau\alpha)(T_{gb}^n-$$
$$\bar{T}^n)+2/(\alpha C\bar{d}_1)dG_b^n/dT_{gb} (T_{gb}^{n+1}-T_{gb}^n)$$
$$-2\pi/(\tau\alpha)(T_{gb}^{n+1}-T_{gb}^n) \qquad (4.2.2a)$$

Then, $T_{gb}^{n+1} = T_{gb}^n+F^n(\ldots)/(1/Dt-dF/dT_{gb}^n)$ (4.2.2b)

where $dF/dT_{gb}^n = 2/(\alpha C\bar{d}_1)dG_b/dT_{gb}^n-2\pi/(\tau\alpha)$ (4.2.2c)

Since

$$G_b= R_{nb}-LE_b-H_b$$

$$R_{nb}=S_w(1-a_{1b})+S_L-\sigma T_{gb}^4$$

so,

$$dG_b/dT_{gb} = dR_{nb}/dT_{gb} -LdE_b/dT_{gb}- dH_b/dT_{gb}$$
$$(4.2.3)$$

and

$$dR_{nb}/dT_{gb} = -4\,\sigma T_{gb}^{3} \qquad\qquad (4.2.4)$$

Since

$$H_b = \rho_a Cp C_{Tb} u_{*b}(S_b - S_m)$$

$$LE_b = \rho_a L C_{Tb} u_{*b}(q_b - q_m)$$

and $\qquad u_{*b} = C_{ub} u_m \qquad\qquad (4.2.5)$

thus,

$$dH_b/dT_{gb} = \rho_a Cp u_m \cdot C_{ub} C_{Tb} dS_b/dT_{gb} + (S_b - S_m)$$

$$*(C_{ub} dC_{Tb}/dT_{gb} + C_{Tb} dC_{ub}/dT_{gb}). \qquad (4.2.6a)$$

and $\qquad LdE_b/dT_{gb} = \rho_a L u_m \cdot C_{ub} C_{Tb} dq_b/dT_{gb} + (q_b - q_m)$

$$*(C_{ub} dC_{Tb}/dT_{gb} + C_{Tb} dC_{ub}/dT_{gb}). \qquad (4.2.6b)$$

dq_b/dT_{gb}, dS_b/dT_{gb}, dC_{Tb}/dT_{gb} and dC_{ub}/dT_{gb} are derived one by one as follows.

Since $S_b = T_{gb}(1000/P)^{0.288}$,

thus, $\qquad dS_b/dT_{gb} = (1000/P)^{0.288} \qquad\qquad (4.2.7)$

Since $\qquad q_b = \beta_b q_b^* + (1 - \beta_b)q_m \qquad$ if $q_b^* < q_m$

or $\qquad q_b = q_b^* \qquad\qquad$ if $q_b^* < q_m \qquad (4.2.8)$,

thus,

$$dq_b/dT_{gb} = \beta_b dq_b^*/dT_{gb} = 5418\,\beta_b q_b^*/T_{gb}^{2}$$

$$\text{if } q_b^* > q_m$$

or $\qquad dq_b/dT_{gb} = 0 \qquad\qquad$ if $q_b^* < q_m \qquad (4.2.9)$

where $d\beta_b/dT_{gb} = 0$ because β_b is only a function of θ_i.

dC_{Tb}/dT_{gb} and dC_{ub}/dT_{gb} depend on the stability condition. For the neutral case,

$$dC_{Tb}/dT_{gb} = dC_{ub}/dT_{gb} = 0 \qquad\qquad (4.2.10)$$

For the stable case, C_{ub} and C_{Tb} are given by Eq. (3.4.10). So,

$$dC_{ub}/dT_{gb} = -C_{uN}/RI_c dRI_b/dT_{gb}$$

or $\qquad$ =0 $\quad$ if $\quad RI_b=0.9RI_c$ $\hfill$ (4.2.11a)

$$dC_{Tb}/dT_{gb}=-C_{TN}/RI_c\,dRI_b/dT_{gb}$$

or $\qquad$ =0 $\quad$ if $\quad RI_b=0.9RI_c$ $\hfill$ (4.2.11b)

where $\quad dRI_b/dT_{gb}= -dT_{vb}/dT_{gb}\,hg/(T_{vm}u_m^2)$ $\hfill$ (4.2.12)

and $\quad dT_{vb}/dT_{gb}= 0.61dq_b/dT_{gb}S_b +dS_b/dT_{gb}(1.+0.61q_b)$

$$\hfill (4.2.13)$$

For the unstable case, there are two subcases: the normal case and the free convection. Under the normal case, the equations for dC_{ub}/dT_{gb} and dC_{Tb}/dT_{gb} are :

$$dC_{ub}/dT_{gb} = C_{ub}^2(25X(Y)(0.26-0.06Y)(dRI_b/dT_{gb})/$$
$$(RI_b\ln10) \hfill (4.2.14)$$

and $\quad dC_{Tb}/dT_{gb} = (C_{Tb}/C_{ub})^2dC_{ub}/dT_{gb}$ $\hfill$ (4.2.15)

Under the free convection, there are also another two subcases:

1), If $C_{Tb}^{-1}=0.5C_{TN}^{-1}$, then

$$dC_{Tb}/dT_{gb} = 0 \hfill (4.2.16)$$

Similarly, if $C_{ub}^{-1}=0.3C_{uN}^{-1}$, then

$$dC_{ub}/dT_{gb} = 0 \hfill (4.2.17)$$

2) if $C_{Tb}=0.19(T_{vb}-T_{vm})^{1/3}/u_{*b}$, then

$$dC_{Tb}/dT_{gb}=0.19(T_{vb}-T_{vm})^{-2/3}/(3u_{*b})dT_{vb}/dT_{gb}$$

$$\hfill (4.2.18)$$

4.3 IMPLICIT SCHEME FOR CANOPY TEMPERATURE

The equation for T_c is

$$C_c h_c dT_c/dt = X_M \qquad (3.2.3)$$

The backward implicit scheme with the expansion terms of T_c and T_{gc} for the canopy temperature is

$$C_c h_c (T_c^{n+1} - T_c^n)/Dt = X_M^n + dX_M/dT_{gc}(T_{gc}^{n+1} - T_{gc}^n)$$
$$+ dX_M/dT_c(T_c^{n+1} - T_c^n)$$

So,

$$T_c^{n+1} = T_c^n + (X_M^n + dX_M/dT_{gc}^n(T_{gc}^{n+1} -$$
$$T_{gc}^n))/(h_c Cc/Dt - dX_M/dT_c^n) \qquad (4.2.20)$$

where

$$dX_M/dT_{gc} = 4 \sigma T_{gc}^3 + dH_{cb}/dT_{gc} \qquad (4.2.21)$$

The H_{cb} can be approximately estimated by (Monteith, 1975)

$$H_{cb} = \rho_a Cp(T_{gc} - T_c)/r_{cb} \qquad (4.2.22)$$

where r_{cb} is the air resistance for sensible heat between the canopy and the vegetated ground surface, and is approximated by

$$r_{cb} = 1/(C_D u_{cb}) \qquad (4.2.23)$$

where C_D is the average drag coefficient inside the canopy and u_{cb} is the mean wind velocity inside the canopy.

The drag coefficient and the average wind velocity in the canopy are both approximated by (Monteith, 1975)

$$C_D = 0.2(0.37/\ln(h_c/Z_{oc}))^2 \qquad (4.2.24)$$

$$u_{cb} = 0.4u_{top} \qquad (4.2.25)$$

where u_{top} is the velocity at the top of canopy and equal to

$$u_{top} = u_{*c}/0.371n(0.3h_c/Z_{oc}) \qquad (4.2.26)$$

In regard to dX_M/dT_c, it is represented by

$$dX_M/dT_c = -L(1-C_1)dE_c/dT_c - dH_c/dT_c + dH_{cb}/dT_c - 8\,6\,T_c{}^3$$

$$(4.2.27)$$

dE_c/dT_c and dH_c/dT_c has exactly the same expressions as dE_b/dT_{gb} and dH_b/dT_{gb} provided that the quantities E_b, H_b, T_{gb}, C_{Tb}, C_{ub}, u_{*b}, S_b, q_b, dq_b/dT_{gb}, dS_b/dT_{gb}, dC_{Tb}/dT_{gb}, dC_{ub}/dT_{gb}, dC_{uN}/dT_{gb}, dC_{TN}/dT_{gb}, dRI_b/dT_{gb}, dT_{vb}/dT_{gb}, $dq_b{}^*/dT_{gb}$, β_b, F_{Tb} and F_{wb} are successively replaced by E_c, H_c, T_c, C_{Tc}, C_{uc}, u_{*c}, S_c, q_c, dq_c/dT_c, dS_c/dT_c, dC_{Tc}/dT_c, dC_{uc}/dT_c, dC_{uN}/dT_c, dC_{TN}/dT_c, dRI_b/dT_c, dT_{vc}/dT_c, $dq_c{}^*/dT_c$, $f_c\,\beta_c$, F_{Tc} and F_{wc}, and $d(f_c\,\beta_c)/dT_c$ is assumed to be zero.

Chapter V

RESULT AND DISCUSSION

5.1 SIMULATION AND SENSITIVITY STUDIES

Simulation and sensitivity studies of the GHM have been conducted in a non-interactive mode. Atmospheric conditions are generated by the NASA/GLAS GCM (Halem et al., 1979). This version of the GCM has a resident GHM which has been used by Mintz and Sarafini (1982) to study the global climatic soil moisture distribution. The output land surface data of a global simulation run for 45 days between July 10 to August 25, 1975 were used to drive the GHM. Eight regions across the North America continent were selected for the simulation and sensitivity studies (see Figure 5.1). The emphasis is placed on the response of the GHM to the atmospheric forcing in a relatively short time period under a variety of climatic and land surface conditions. It is obvious that there are no feedback effects in this non-interactive mode. However, the interactively simulated hydrologic results of the resident GHM are available for this study. The basic properties for these regions are listed in Table 5.1.1.

Atmospheric conditions provided by the GCM were given in the neighborhood of the land surface. Alfano (1981) applied these surface data at the anemometer height to drive the GHM in his study. In this study, the surface data were converted to the mean conditions in the PBL using the Deardorrf (1972) formulation. The detailed derivation to obtain the mean conditions is discussed in Appendix.

Since the parameterization of albedo in the GHM is different from that of the GCM, the absorbed net radiation in the GHM is different from that provided by the GCM and should be adjusted prior to running the model. The adjustment was discussed by Alfano (1981) and will be described briefly in Appendix.

For evaluating the performance of the GHM, the results of grid surface temperature, grid available moisture fraction in the root zone, grid sensible and latent heat fluxes obtained from this model are compared with the corresponding results furnished by the GCM.

The analysis of the results of the sensitivity study are presented in terms of the daily averaged soil moistures, temperatures, and grid latent heat and sensible heat fluxes.
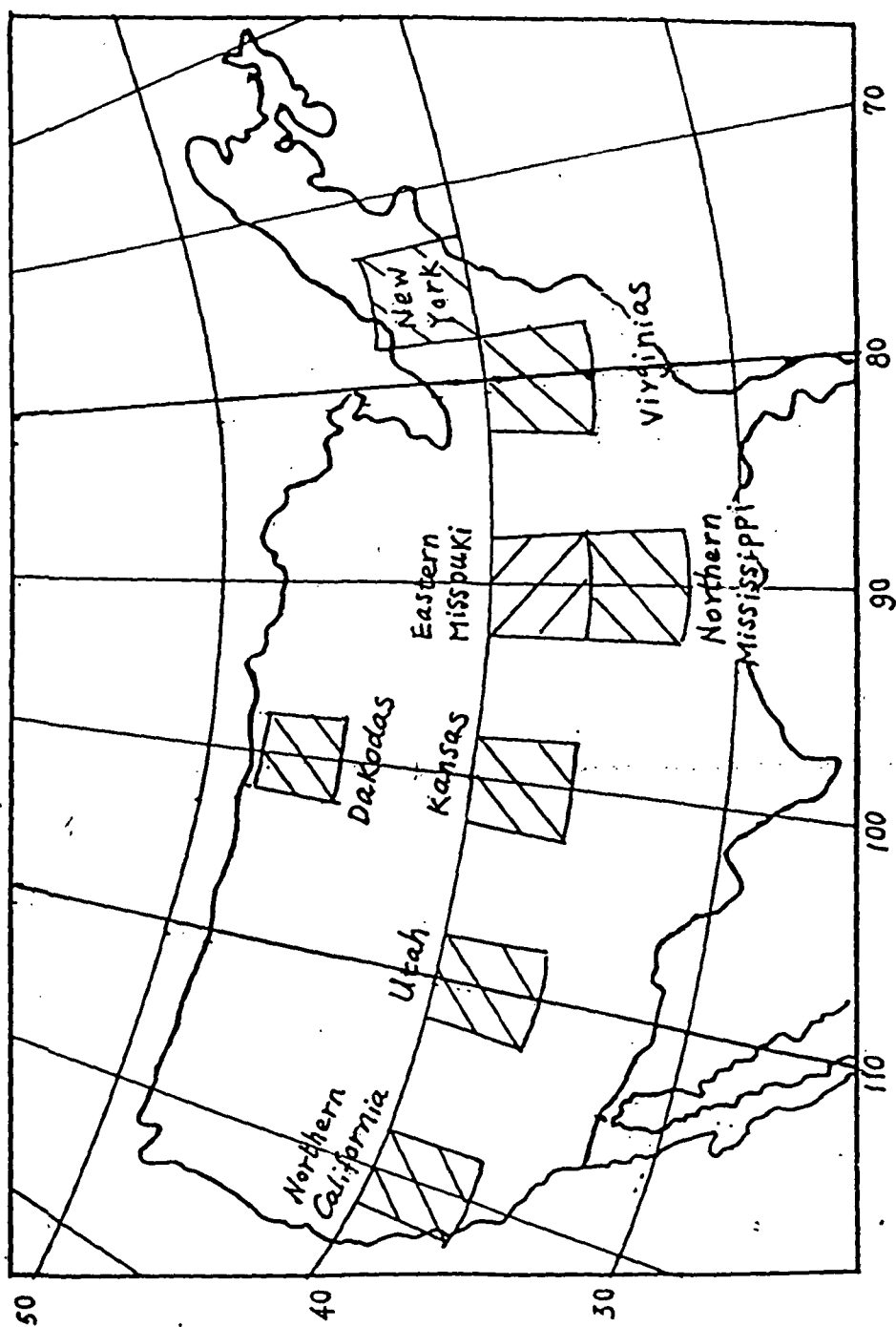
Figure 5.1 Eight regions across the North America continent

I	J	Θ_s	Θ_{fc}	Θ_{pwp}	Vegetation type	Soil type	Bare soil density
32	19	.475	.320	.185	seasonal forest(7)	silty clay loam (E)	25
33	13	.465	.162	.061	wood land (3)	sandy loam (B)	25
33	15	.465	.162	.061	desert (6)	sandy loam (B)	75
33	17	.503	.270	.098	grass land (5)	loam (D)	50
33	19	.394	.220	.100	seasonal forest(7)	loamy sand (C)	25
33	21	.394	.220	.100	seasonal forest(7)	loamy sand (C)	25
34	22	.394	.220	.100	seasonal forest(7)	loamy sand (C)	25
35	17	.503	.270	.098	grass land (5)	loam (D)	50

Table 5.1.1   Properties of the regions investigated

5.2 COMPARISON BETWEEN THE RESULTS OF THE GHM AND THE GCM

The resident hydrologic model in the GCM (Mintz and Sarafini, 1982) differs from the GHM in many respects. The difference between these two models will be explained to aid in understanding the subsequent comparisons.

5.2.1 Difference between the GHM and the hydrologic model in the GCM

In Chapters 2 and 3, the formulation of the GHM have been described in detail. The most important differences between the GHM and the GCM's resident hydrologic model are the implementation of features in the GHM: characterization of soil and vegetation, subgrid parameterization of vegetation density and formulation of moisture and heat movements in the soil layers.

In the resident hydrologic model in the GCM, all grids on the land surface are considered to be identical, consisting of a uniform soil layer with the same maximum available soil moisture, hydraulic and thermal properties. The effects of canopy are not considered and albedo is prescribed for each grid. For the moisture movement, the water budget in the GCM in entire root zone is calculated in terms of precipitation, evaporation, runout and change of available moisture content. Only the available moisture fraction Θ_{avfs} in the root zone is predicted. The evapora-

tion is parameterized by using potential evaporation and a scaling factor which is a function of the available moisture fraction. For the heat transport, ground temperature in the GCM accounts for average temperature within a bulk layer equal to the penetration of the diurnal temperature wave. Its change is only forced by surface air conditions.

5.2.2 Comparing the simulation results

The eight regions shown in Figure 5.1 are Northern Mississippi (J=32, I=19), Northern California (J=33, I=13), Utah (J=33, I=15), Kansas (J=33, I=17), Eastern Missouri (J=33, I=19), Virginias (J=33, I=21), New York (J=34, I=22) and Dakotas (J=35, I=17). The experiment period is from July 11 to August 25 in 1975. The following analysis is based on comparing the daily average results from the GHM under the normal conditions with those from the GCM. The parameters of the normal case are listed below:

J	I	Location	Albedo	$\sigma_b\%$	r_c	d_2	R_{d1}
32	19	Northern Mississippi	Formula	25	75	90	.25
33	13	Northern California	Formula	25	75	90	.25
33	15	Utah	Formula	75	100	40	.50
33	17	Kansas	Formula	50	100	40	.50
33	19	Eastern Missouri	Formula	25	75	90	.25
33	21	Virginias	Formula	25	75	90	.25
34	22	New York	Formula	25	75	90	.25
35	17	Dakotas	Formula	50	100	40	.50

d_1 = 10 cm for all grids

Normal conditions for eight regions

Figures 5.2-1 through 5.2-8 summarize the results of comparisons, where the curves with 'square' represent the results from the GHM, The curves with 'plus' represent the results from the GCM. In the temperature plots, the curves with 'asterisk' mean the air surface temperature from the GCM. The quantities with subscript 'd' indicate the daily average value. In figure 5.2-1c through 5.2-8c, it is evident that the grid surface temperatures from these two models follow a similar trend. However, the GHM predicts larger diurnal variation than the GCM does.

In the forest regions with relatively moist soil ($J=32$ and $I=19$, Northern Mississippi; $J=33$ and $I=19$, Eastern Mis-

souri; J=33 and I=21, Virginias; J=34 and I=22, New York),
the daily averaged grid surface temperatures T_{gd} from the
GHM and the daily averaged ground surface temperature T_{gsd}
from the GCM are in phase and agree to each other reason-
ably well (see Figures 5.2-1c, 5.2-5c, 5.2-6c, 5.2-7c). The
maximum difference T_{gsmax} between T_{gd} and T_{gsd} for the four
regions ranges from 1.7 to 3.0 ^{O}K and its average T_{gsb} over
45 days ranges from 0.78 to 1.3 ^{O}K. The daily averaged
surface air temperature T_{ad} is also shown in the figures
which is nearly equal to both of these temperatures. From
Table 5.2.1 the maximum difference T_{gamax} between T_{ad} and
T_{gd} varies from 1.4 to 2.9 ^{O}K and its average T_{gab} over 45
days from 0.56 to 0.87 ^{O}K for the GHM; the maximum differ-
ence T_{samax} between T_{ad} and T_{gsd} varies from 1.8 to 3.1 ^{O}K
and its average T_{sab} over 45 days from 0.69 to 1.02 ^{O}K for
the GCM.

There is one region (J=33 and I=13, Northern California)
with tall canopy but relatively dry soil. During the first
20 days, the daily averaged grid surface temperature T_{gd}
from the GHM is relatively close to the daily averaged
ground surface temperature T_{gsd} from the GCM in both magni-
tude and trend (see Figure 5.2-2c). After 20 days, how-
ever, the soil is dried out and evapotranspiration becomes
very small. Under this situation, the moderating function
of latent heat becomes weakened and albedo plays a more im-
portant role in determining the surface cover temperature.

Since the albedo in the GHM is larger than that in the GCM, the daily averaged grid surface temperature predicted by the GHM becomes much smaller than the daily averaged grid surface temperature given by the GCM. From Figure 5.2-2c, the temperature difference increases and eventually goes up to 6.3 $^{\circ}$K. From Table 5.2.1, the averaged temperature difference T_{gsb} between these two temperatures over 45 days is 2.1 $^{\circ}$K. These two daily averaged grid surface temperatures from these two models are both higher than the daily averaged air temperature. But the difference between T_{gd} from the GHM and T_{ad} of the air is smaller than that between T_{gsd} from the GCM and T_{ad}. From Table 5.2.1, the averaged temperature difference T_{gab} between T_{gd} and T_{ad} over 45 days is 1.43 $^{\circ}$K, which is lower than the corresponding difference T_{sab} between T_{gsd} and T_{ad}, 3.13 $^{\circ}$K.

For the grids with 50% covered by short canopy (J=33 and I=17, Kansas; J=35 and I=17, Dakotas), the daily averaged grid surface temperature from the GHM T_{gd} and from the GCM T_{gsd} agree reasonably well in trend and in magnitude (see Table 5.2.1 and Figures 5.2-4c and 5.2-8c). From Table 5.2.1, the absolute temperature differences T_{gsb} between these two temperatures averaged over 45 days are 1.72 and 1.18 $^{\circ}$K, respectively. The daily averaged surface air temperature T_{ad} shown in the figures is also nearly equal to both of these temperatures. From Table 5.2.1, the absolute differences T_{gab} between T_{gd} and T_{ad} averaged over 45

days are 1.46 and 0.84 ^{O}K; the absolute differences T_{sab} between T_{gsd} and T_{ad} averaged over 45 days are 0.88 and 0.77 ^{O}K

There is one short canopy region (J=33, I=15, Utah) but with 75% covered by bare soil where the difference between T_{gd} and T_{gsd} is less than 3 ^{O}K on most days. But the larger difference between temperatures T_{gd} and T_{gsd} occurs on some days. The maximum difference T_{gsmax} between T_{gd} and T_{gsd} is 6.8 ^{O}K and its average T_{gsb} over 45 days is 2.90 ^{O}K (see Figure 5.2-3c). The large difference of these two temperatures on some days can be explained by the following reasons. This grid is 75% covered by bare soil. The grid average surface temperature is more dependent on the bare soil surface temperature variation. There are heavy rainfalls on these days when the larger grid surface temperature difference occurs. The rainfall will increase the moisture content of the surface layer in the GHM and thus increase the evaporation from bare soil greatly. On the other hand, the rainfall does not significantly increase the moisture content of the entire root zone in the GCM and the evaporation in the GCM is affected by the heavy rainfall to a smaller degree. Since the bare soil temperature in the GHM only accounts for a thin surface layer, the large increase of evaporation on these days will depress the surface temperature increment. Thus, larger grid temperature difference between T_{gd} and T_{gsd} occurs.

I	J	T_{gsmax}	T_{gamax}	T_{samax}	T_{gsb}	T_{gab}	T_{sab}
19	32	2.4	2.9	1.8	1.08	0.87	0.78
13	33	6.3	2.8	6.2	2.09	1.43	3.13
15	33	6.8	6.6	2.8	2.90	2.20	1.07
17	33	4.0	4.2	2.9	1.72	1.46	0.88
19	33	1.7	1.4	2.0	0.78	0.56	0.69
21	33	2.4	1.5	2.0	1.19	0.57	0.85
22	34	3.0	2.6	3.1	1.30	0.72	1.02
17	35	3.5	2.2	2.4	1.18	0.84	0.77

Table 5.2.1 Maximum and averaged temperature differences between the GCM, the GHM and air surface condition (^{o}K)

Since the parameterization of soil moisture in these two models are quite different, a comparison can only be made by introducing a grid available soil moisture fraction in the root zone as follows:

$$\bar{\Theta}_{av} = (\Theta_1 {*} d_1 + \Theta_2 {*} d_2)/(d_1 + d_2) - \Theta_{pwp}$$

$$\Theta_{avf} = \bar{\Theta}_{av}/\Theta_{avm} \qquad (5.1.1),$$

which is shown in Figures 5.2-1b to 5.2-8b. The soil moistures from the GHM show a more sensitive response to rainfall, which correlate with the rainfall events as shown in Figure 5.2-1a to 5.2-8a. The soil moisture from the GCM has an overall monotonically decreasing trend during the period of simulation. The difference in magnitudes of the soil moisture near the end of the simulation period are difficult to assess because the characterization of soil and vegetation type varies from cell to cell as compared with a uniform maximum available soil moisture and field capacity prescribed in the GCM. The results of the two-layer parameterization can not be examined by using grid available soil moisture fraction as defined in Eq. (5.1.1). However, the effects on the ground surface temperature indirectly through evapotranspiration and albedo have been demonstrated in the above discussion. For example, in the dry and the sparsely vegetated regions such as Northern California (J=33, I=13) and Utah (J=33, I=15), the grid surface temperatures of the GHM are lower than those of the GCM. The effects of the soil layers on evapotranspiration will be discussed as follows.

The daily averaged grid evapotranspirations from the GHM and the GCM follow similar trend. However, the magnitude from the GHM in general is less than that from the GCM in most regions (see Figures 5.2.-1d,5.2-2d, 5.2-4d through 5.2-8d). Only one region with more bare soil cover (Utah) is exceptional (see Figure 5.2-3d). The averaged ratios of evapotranspiration E_{td} from the GHM to evaporation E_{sd} from the GCM over 45 days are equal to 0.78 (Northern Mississippi), 0.25 (Northern California) 1.15 (Utah), 0.87 (Kansas), 0.73 (Eastern Missouri), 0.71 (Virginias), 0.70 (New York) and 0.82 (Dakotas). These ratios indicate that, in most regions, the evapotranspiration from the GHM is reduced by 10% to 30% of those from the GCM. The only grid with the ratio greater than unity is located in southern Utah and northern Arizona. In this region, the land surface is characterized by 75% bare soil or a sparsely vegetated surface. It appears that the rainfall events in the simulation period kept the soil moisture in the GHM larger than that in the GCM as seen in Figures 5.2-3a and b, and thus enhanced the evapotranspiration.

The sensible heat flux of the GHM shown in Figures 5.2-1e to 5.2-8e varies with a larger amplitude than those of the GCM, which can be explained by the reduction of latent heat flux as discussed above. In general, the sensible heat flux is the result of the complex energy balance of the land surface.

5.3   SENSITIVITY STUDIES

A series of sensitivity study have been conducted for three sets of initial conditions, two lower boundary conditions and a number of physical parameters including vegetation density, albedo, canopy resistance, root density distribution and root zone thickness. The results of daily averaged soil moisture, temperature and fluxes are presented in Figures 5.3-1 through 5.3-5 for 45 days and for two regions. These are New York (J=34, I=22) with $\sigma_c = 0.75$, tall canopy and more water supplied by precipitation and and Dakodas (J=35, I=17) with $\sigma_c = 0.50$, short canopy and relatively dry climate. The maximum difference and averaged difference in the 45 days period of daily averaged soil moisture, temperature and fluxes are summarized in Table 5.3-2 for all eight regions selected for this study. Abbreviated notation and symbols are given at the beginning of the table.

5.3.1   Sensitivity to initial condition

Two sets of initial conditions have been chosen as variations to the normal case for the eight regions. They are the wet condition as specified by both the soil moisture θ_1 and θ_2 at the field capacity and the dry condition by the soil moistures at the permanent wilting point. The normal initial conditions were obtained from the GCM run output

from July 10 to August 25 , 1975. Comparison is made between two extreme cases. In the figures, the square symbol indicates the results with the wet initial condition and the triangle symbol indicates the results with the dry initial condition.

No matter where a grid cell is, the effect from different initial soil moisture content in the surface layer only lasts approximately one week (see Figure 5.3-1a). After a week, the soil moistures in the surface layer starting from quite different initial values tend to approach to each other and are subsequently determined mainly by the atmospheric conditions. The reason is that the surface layer is thin and the initial difference of the available water containing in this layer between these two extreme cases is not enough to sustain the different evapotranspiration from the surface layer for a long period

On the other hand, the difference in daily averaged soil moisture content in the lower layer θ_{2d} was reduced gradually throughout the experiment period but remains at the end of the period for all regions (see Figure 5.3-1b). For the regions with sparsely vegetated cover and shallow root system such as Utah (J=33, I=15), Kansas (J=33, I=17) amd Dakotas (J=35, I=17), the water uptake function from the lower layer is weak and the initial difference in θ_2 is more difficult to be eliminated. For the regions with

dense vegetation and deep root system, the reduction was more substantial. This behavior implies that an influence of initial moisture conditions in Θ_2 is more significant and lasting than in Θ_1. In fact, grid evapotranspiration (Figure 5.3-1f), grid averaged sensible heat flux (Figure 5.3-1g) and layer average temperature (Figure 5.3-1e) also exhibit a large difference for the whole experiment period.

The effect of the initial soil moisture conditions on bare soil surface temperature only occurs during the first week (see Figure 5.3-1c), which is consistent with the trend of soil moisture in the surface layer (see Figure 5.3-1a)

Table 5.3.2 Summary of sensitivity experiment results

d_2	thickness of the second layer
σ_c	vegetation fraction
r_c	canopy resistance (sec/m)
R_{d1}	root density distribution
Lower B.C	lower boundary condition in layer 3
LEM	max $(60L|\dot{E}_{td}(1)-E_{td}(2)|)$ (ly/min)
LEB	aver $(60L|E_{td}(1)-E_{td}(2)|)$ over 45 days (ly/min)
HSM	max $(60|H_{td}(1)-H_{td}(2)|)$ (ly/min)
HSB	aver $(60|H_{td}(1)-H_{td}(2)|)$ over 45 days (ly/min)
TBARM	max $(|T_d(1)-T_d(2)|)$ $^\circ K$
TBARB	aver $(|T_d(1)-T_d(2)|)$ over 45 days $^\circ K$
TCM	max $(|T_{cd}(1)-T_{cd}(2)|)$ $^\circ K$
TCB	aver $(|T_{cd}(1)-T_{cd}(2)|)$ over 45 days $^\circ K$
TGBM	max $(|T_{gbd}(1)-T_{gbd}(2)|)$ $^\circ K$
TGBB	aver $(|T_{gbd}(1)-T_{gbd}(2)|)$ over 45 days $^\circ K$
VMC1M	max $(|\theta_{1d}(1)-\theta_{1d}(2)|)$
VMC1B	aver $(|\theta_{1d}(1)-\theta_{1d}(2)|)$ over 45 days
VMC2M	max $(|\theta_{2d}(1)-\theta_{2d}(2)|)$
VMC2B	aver $(|\theta_{2d}(1)-\theta_{2d}(2)|)$ over 45 days

(X) indicates the extreme conditions.

aver means average.

(a) Values of VMC1M

I	J	6_c	Albedo	r_c	d_2	R_{d1}	Lower B.C.
19	32	0.0827	0.0190	0.0218	0.0135	0.0323	0.0045
13	33	0.0236	0.0059	0.0061	0.0003	0.0094	0.0006
15	33	0.0777	0.0213	0.0061	0.0009	0.0041	0.0034
17	33	0.0726	0.0223	0.0213	0.0018	0.0134	0.0064
19	33	0.0902	0.0171	0.0156	0.0096	0.0313	0.0022
21	33	0.0838	0.0157	0.0175	0.0076	0.0311	0.0023
22	34	0.0883	0.0134	0.0126	0.0061	0.0170	0.0016
17	35	0.0804	0.0186	0.0185	0.0027	0.0121	0.0028

(b) Values of VMC1B

I	J	6_c	Albedo	r_c	d_2	R_{d1}	Lower B.C.
19	32	0.0419	0.0062	0.0089	0.0039	0.0127	0.0020
13	33	0.0051	0.0010	0.0017	0.0001	0.0034	0.0001
15	33	0.0273	0.0076	0.0021	0.0002	0.0017	0.0007
17	33	0.0293	0.0079	0.0098	0.0007	0.0062	0.0013
19	33	0.0503	0.0059	0.0072	0.0020	0.0112	0.0006
21	33	0.0451	0.0062	0.0073	0.0021	0.0128	0.0008
22	34	0.0505	0.0050	0.0057	0.0019	0.0091	0.0005
17	35	0.0451	0.0104	0.0110	0.0010	0.0061	0.0010

(c) values of VMC2M

I	J	σ_c	Albedo	r_c	d_2	R_{d1}	Lower B.C.
19	32	0.1005	0.0094	0.0494	0.0265	0.0262	0.0265
13	33	0.0290	0.0004	0.0063	0.0091	0.0045	0.0003
15	33	0.0346	0.0021	0.0065	0.0075	0.0093	0.0032
17	33	0.1220	0.0137	0.0520	0.0245	0.0313	0.0663
19	33	0.1071	0.0065	0.0517	0.0477	0.0286	0.0050
21	33	0.0995	0.0077	0.0439	0.0423	0.0259	0.0062
22	34	0.1002	0.0081	0.0449	0.0435	0.0260	0.0050
17	35	0.0805	0.0130	0.0425	0.0210	0.0210	0.0695

(d) Values of VMC2B

I	J	σ_c	Albedo	r_c	d_2	R_{d1}	Lower B.C.
19	32	0.0621	0.0056	0.0286	0.0157	0.0152	0.0130
13	33	0.0248	0.0002	0.0025	0.0027	0.0025	0.0001
15	33	0.0281	0.0015	0.0047	0.0053	0.0066	0.0023
17	33	0.0607	0.0068	0.0274	0.0133	0.0152	0.0395
19	33	0.0696	0.0043	0.0313	0.0276	0.0179	0.0024
21	33	0.0566	0.0043	0.0237	0.0311	0.0140	0.0025
22	34	0.0553	0.0044	0.0237	0.0282	0.0140	0.0020
17	35	0.0464	0.0070	0.0261	0.0089	0.0130	0.0350

(e) Values of TGBM ($^\circ$K)

I	J	σ_c(*)	Albedo	r_c	d_2	R_{d1}	Lower B.C.
19	32	5.7000	1.9001	1.1001	0.5999	1.5999	0.2002
13	33	4.7000	2.9001	0.8000	0.1001	1.6001	0.6001
15	33	5.3999	4.5000	0.7000	0.2000	0.5000	0.8999
17	33	3.5000	2.2000·	1.0000	0.1001	0.7002	0.5000
19	33	4.5000	1.8999	1.4001	0.3000	2.0000	0.2000
21	33	4.3000	1.7000	1.1001	0.5000	1.6001	0.2002
22	34	4.5000	2.2000	1.3000	0.6001	1.6001	0.2000
17	35	2.5000	2.2000	0.7000	0.1001	0.5000	0.3000

(f) Values of TGBB ($^\circ$K)

I	J	σ_c(*)	Albedo	r_c	d_2	R_{d1}	Lower B.C.
19	32	1.6689	0.6067	0.2600	0.0889	0.3733	0.0578
13	33	2.5778	1.6400	0.1356	0.0111	0.2134	0.2378
15	33	1.8711	1.5667	0.1556	0.0244	0.1467	0.2111
17	33	1.4778	0.9000	0.2889	0.0245	0.2178	0.1378
19	33	1.7088	0.6200	0.2578	0.0511	0.4733	0.0356
21	33	1.2800	0.5200	0.2244	0.0422	0.3444	0.0400
22	34	1.6822	0.6378	0.2022	0.0733	0.2756	0.0489
17	35	1.0778	0.8956	0.2533	0.0222	0.1800	0.0956

(*) under σ_c term means the given values indicate the difference of grid surface temperature between afforestation and desertification cases.

(g) Values of TCM (°K)

I	J	6_c	Albedo	r_c	d_2	R_{d1}	Lower B.C.
19	32		0.8000	1.5999	0.1001	0.3000	0.3999
13	33		0.6001	0.5000	0.3000	0.6001	0.1001
15	33		2.3000	2.3000	1.2000	1.5999	0.6001
17	33		1.0000	2.7000	0.0000	0.8000	0.8999
19	33		0.5000	0.8000	0.6001	0.5000	0.2002
21	33		0.4001	1.2002	0.6001	0.2000	0.1001
22	34		0.5000	0.7000	0.7000	0.4001	0.1001
17	35		0.7000	2.1001	0.0000	0.3000	0.3000

(h) Values of TCB (°K)

I	J	6_c	Albedo	r_c	d_2	R_{d1}	Lower B.C.
19	32		0.2778	0.6356	0.0044	0.0289	0.0689
13	33		0.4045	0.0844	0.0889	0.0689	0.0422
15	33		0.9778	0.8578	0.2511	0.3222	0.2000
17	33		0.5156	1.5111	0.0000	0.0689	0.1578
19	33		0.2956	0.4800	0.2244	0.0800	0.0222
21	33		0.2356	0.4533	0.1155	0.0178	0.0089
22	34		0.2533	0.4133	0.1111	0.0356	0.0111
17	35		0.4733	1.1844	0.0000	0.0200	0.0333

(i) Values of TBARM (°K)

I	J	σ_c	Albedo	r_c	d_2	R_{d1}	Lower B.C.
19	32	1.9001	0.5000	0.6001	0.1001	0.2002	0.2002
13	33	3.3000	1.1001	0.1001	0.2002	0.1001	0.5000
15	33	5.1001	2.0000	0.1001	0.1001	0.1001	0.5000
17	33	5.3000	1.4001	0.8000	0.1001	0.3000	0.3999
19	33	0.8000	0.5000	0.5000	0.4001	0.3000	0.1001
21	33	0.8999	0.4001	0.5000	0.3000	0.2002	0.1001
22	34	0.8000	0.6001	0.4001	0.3000	0.2002	0.1001
17	35	6.3000	1.4001	0.6001	0.1001	0.2002	0.3000

(j) Values of TBARB (°K)

I	J	σ_c	Albedo	r_c	d_2	R_{d1}	Lower B.C.
19	32	0.9089	0.3622	0.3844	0.0156	0.1400	0.0222
13	33	2.3511	0.7089	0.0356	0.0844	0.0311	0.2467
15	33	3.7533	1.2556	0.0622	0.0222	0.0489	0.2000
17	33	4.0222	0.8644	0.4733	0.0067	0.1222	0.1022
19	33	0.3956	0.3667	0.3067	0.1444	0.1511	0.0156
21	33	0.2533	0.2933	0.2933	0.0489	0.1178	0.0111
22	34	0.2955	0.3311	0.2956	0.0667	0.0822	0.0244
17	35	4.4977	0.8978	0.3933	0.0067	0.1089	0.0822

(k) Values of LEM (ly/min)

I	J	σ_c	Albedo	r_c	d_2	R_{d1}	Lower B.C.
19	32	0.2481	0.0336	0.1146	0.0145	0.0492	0.0394
13	33	0.1516	0.0143	0.0612	0.0491	0.0220	0.0026
15	33	0.2088	0.0676	0.0237	0.0084	0.0125	0.0131
17	33	0.2716	0.0515	0.0991	0.0043	0.0349	0.0325
19	33	0.2450	0.0342	0.1072	0.0864	0.0561	0.0203
21	33	0.1766	0.0372	0.1159	0.1225	0.0378	0.0062
22	34	0.2447	0.0347	0.1102	0.0725	0.0530	0.0032
17	35	0.2320	0.0536	0.0873	0.0037	0.0207	0.0076

(l) Values of LEB (ly/min)

I	J	σ_c	Albedo	r_c	d_2	R_{d1}	Lower B.C.
19	32	0.0721	0.0171	0.0622	0.0023	0.0109	0.0079
13	33	0.0314	0.0027	0.0109	0.0116	0.0066	0.0007
15	33	0.0648	0.0207	0.0074	0.0031	0.0045	0.0025
17	33	0.0813	0.0181	0.0390	0.0009	0.0094	0.0060
19	33	0.0817	0.0135	0.0552	0.0278	0.0164	0.0034
21	33	0.0510	0.0144	0.0471	0.0152	0.0087	0.0010
22	34	0.0675	0.0151	0.0479	0.0167	0.0091	0.0006
17	35	0.0732	0.0171	0.0351	0.0008	0.0071	0.0016

(m) Values of HSM (ly/min)

I	J	σ_c	Albedo	r_c	d_2	R_{d1}	Lower B.C.
19	32	0.1492	0.0993	0.1051	0.0070	0.0402	0.0352
13	33	0.1476	0.1106	0.0500	0.0431	0.0191	0.0148
15	33	0.1400	0.1049	0.0176	0.0059	0.0079	0.0270
17	33	0.1726	0.0809	0.0679	0.0026	0.0255	0.0308
19	33	0.1965	0.1110	0.0965	0.0759	0.0526	0.0168
21	33	0.1122	0.0882	0.1011	0.1051	0.0332	0.0124
22	34	0.0955	0.1097	0.1016	0.0656	0.0447	0.0119
17	35	0.1104	0.0830	0.0654	0.0018	0.0160	0.0154

(n) Values of HSB (ly/min)

I	J	σ_c	Albedo	r_c	d_2	R_{d1}	Lower B.C.
19	32	0.0459	0.0411	0.0570	0.0012	0.0075	0.0069
13	33	0.0914	0.0892	0.0096	0.0102	0.0056	0.0077
15	33	0.0330	0.0335	0.0054	0.0016	0.0025	0.0057
17	33	0.0474	0.0309	0.0317	0.0005	0.0059	0.0059
19	33	0.0572	0.0509	0.0518	0.0246	0.0140	0.0034
21	33	0.0323	0.0355	0.0439	0.0131	0.0058	0.0010
22	34	0.0420	0.0454	0.0446	0.0146	0.0067	0.0013
17	35	0.0398	0.0355	0.0305	0.0004	0.0045	0.0023

5.3.2   Sensitivity to vegetation density

The large scale subgrid parameterization of vegetation density is expressed in terms of vegetation fraction or bare soil fraction which varies seasonally and spatially with latitude.

Two extreme cases of land surface cover have been investigated in addition to the normal case. One represents desertification with vegetation fraction $\sigma_c=0$ and the other afforestation with $\sigma_c=1$.   In Figure 5.3-2, the square symbol represents the result of afforestation and the triangle symbol represents the result of desertification. The normal case is represented by a solid line.   It is evident that the density of land surface cover have significant effects on all soil moistures, temperatures and fluxes.

The vegetation density exerts the most important influence on evapotranspiration and soil moisture as shown in Figures 5.3-2a, b and f and Tables 5.3-2(a), (b), (c), (d), (k) and (1).   The overall evapotranspiration for the case of afforestation in the New York region (J=34, I=22) is almost the same as the normal case, while for the desertification case it is reduced by an average of 0.0675 ly/min or approximately 40 to 50% (Figure 5.3-2f). However, the variation in the magnitude of evaporation, as modulated by precipitation events, is substantially reduced by afforestation. The maximum difference between these two cases can

be as large as 0.2447 ly/min (Table 5.3-2(k)) because of the difference in water uptake patterns. Evaporation from the bare soil is practically cut off when the surface layer becomes dry, while the vegetated cover can continue to transpire by uptaking water from the root zone. The difference in water uptake patterns leads to very different soil moisture profiles in the two soil layers for these two extreme cases as shown in Figures 5.3-2a and b. The results are similar for the rest of the regions as indicated in Tables 5.3-2(k), (l) except the Northern California region where the level of soil moisture is low during this period (see Figure 5.2-2b). As a result, the maximum difference of the evapotranspiration in Northern California is 30% less and the average difference is 55% less than those of the New York region. The difference in soil moisture exhibits the same trend as listed in Tables 5.3-2(a) and(b).

Canopy cover has quite different thermal properties from bare soil. Moreover, plants take up additional water from the lower layer, which consumes latent heat. Therefore, the energy balance in these two extreme cases must be very different. It results in a great change in the sensible heat flux, heat flux into the soil, layer-average temperature and grid surface temperature. Figure 5.3-2g shows the difference in sensible heat. In Tables 5.3-2(m) and (n), the maximum differences of daily averaged sensible heat in 45 days HSM vary from 0.086 to 0.20 ly/min and the averaged

differences of daily averaged sensible heat over 45 days
HSB vary from 0.032 to 0.091 ly/min. Figure 5.3-2e shows
the difference in layer-average temperature. From Tables
5.3-2(i) and (j), the maximum difference of daily averaged
layer- average temperature in 45 days TBARM varies from 0.8
to 5.3 ^{o}K and its average over 45 days TBARB varies from is
0.25 to 4.5 ^{o}K for all regions. Figure 5.3-2c shows the
difference in the grid surface temperatures for these two
cases. In Tables 5.3-2(e) and (f) TGBM ranges from 2.5 to
5.7 ^{o}K and TGBB from 1.1 to 2.6 ^{o}K (note TGBM or TGBB here
describes maximum difference or averaged difference over 45
days of daily averaged grid surface temperatures between
two cases instead of bare soil surface temperature). The
above values indicate that the afforestation reduces aver-
age surface temperature about 2°K and the maximum differ-
ence in daily averaged surface temperature can be two to
three times the above values. It should be noted that the
subgrid change of vegetation density affects all the param-
eters and hence outputs because the canopy implies differ-
ent root system, canopy resistance, albedo and so on when
compared with the bare soil. In this sense, an accurate
estimation of σ_c is very important in a GHM.

5.3.3 Sensitivity to canopy resistance

In this study, two selections of minimum canopy resistance are added to the normal case. The values of minimum canopy resistance can depend on the species and physiological conditions of plants and can vary greatly. Table 5.3.3 only lists the values that are used for this study.

Canopy resistance controls transpiration through leaves and thus governs water uptake from root zone. From the results of sensitivity study, it is found that the change in the canopy resistance primarily affects the transpiration and soil moisture in the lower layer. The following discussion is based on comparison of the results with the two extreme values of canopy resistance.

Canopy resistance has only a small effect on soil moisture content in the surface layer as shown Figure 5.3-3a. In Tables 5.3-2(a) and (b), VMC1M varies from 0.006 to 0.02 and VMC1B from 0.0017 to 0.011. These are small differences.

The moisture content in the lower layers is influenced more which tends to increase with time during the experiment period. Figure 5.3-3b gives a typical trend for the eight regions with tall canopy or short canopy. In Tables 5.3-2(c) and (d) VMC2M varies from 0.006 to 0.052 and VMC2B from 0.00257 to 0.031.

The effect on the temperatures is generally weak. The temperature of the bare soil portion in a grid is affected indirectly and shows little difference between the two different canopy resistances (see Figure 5.3-3c). On the other hand, the canopy temperature is directly affected by different latent heat flux. However, the difference in the temperature is not significant because the heat capacity of canopy is greater than that of the thin soil surface layer, especially for tall canopies. Figure 5.3-3d shows the typical change of canopy temperature in all regions with tall canopy and short canopy. From Tables 5.3-2(g) and (h), TCM varies from 0.50 to 2.70 $^\circ$K and TCB from 0.084 to 1.51 $^\circ$K. The layer-average temperature has less than 1 $^\circ$K difference during the whole operation period, which only slightly increases. It is not clear whether larger difference will occur after a longer period experiment. In Tables 5.3-2(i) and (j), TBARM varies from 0.1 to 0.8 $^\circ$K and TBARB from 0.036 to 0.47 $^\circ$K.

The evapotranspiration is sensitive to the variation of the canopy resistance. Figure 5.3-3f demonstrates the significant difference in evapotranspiration. Sensible heat always acts to compensate the latent heat in the energy balance and a bigger difference also occurs (see Figure 5.3-3g). These results are typical for the regions for both tall canopy and short canopy. In Table 5.3-2(f), EVM varies from 0.024 to 0.12 ly/min and EVB from 0.007 to

0.062 ly/min. From Tables 5.3-2(m) and (n) HSM varies from 0.018 to 0.10 ly/min and HSB from 0.005 to 0.057 ly/min.

symbols in Fig.		solid curves (normal)	square	triangle
I	J	r_c (s/m)	r_c (s/m)	r_c (s/m)
19	32	75	100	200
13	33	75	100	200
15	33	100	50	200
17	33	100	50	200
19	33	75	100	200
21	33	75	100	200
22	34	75	100	200
17	35	100	50	200

Table 5.3.3   Different selection of r_c

5.3.4   Sensitivity to albedo

In the GHM, the albedo varies according to the formulation given in Section 2.6.   The albedo affects the energy balance on the land surface.   In this study, albedo was varied by increasing the normal value by 15% and decreasing it by 5%.   The results shown in Figure 5.3-4 and Table 5.3-2 indicate that the sensible heat fluxes change in all regions. The difference between the two extreme cases can reach the order of o.1 ly/min.   HSM varies   from 0.083 to 0.11 ly/min and HSB from 0.031 to 0.089 ly/min.

The associated changes in temperatures are as follows. First, the bare soil surface temperature has been affected to several degrees.   In some regions with low level of soil moisture, where the evaporation can not compensate the variation of sensible heat, the bare soil surface temperature differences can become large, e.g. the Utah region (I=15, J=33) as listed in Table 5.3-4(e).   In Tables 5.3-2(e) and (f), TGBM varies from 1.7 to 4.5 ^{o}K and TGBB from 0.60 to 1.60 ^{o}K.   Second, the effect on the layer-average soil temperature increases with time as shown in Figure 5.3-4e. In Tables 5.3-2(i) and (j), TBARM varies from 0.4 to 2.0 ^{o}K and TBARB from 0.29 to 1.26 ^{o}K.   For canopy temperature, the difference between the two cases is smaller than for bare soil surface temperature because of the larger heat capacity of the canopy (see Figure 5.3-4d).   In Tables

5.3-2 (g) and (h), TCM varies from 0.4 to 2.5 $^{\circ}$K and TCB from 0.24 to 0.98 $^{\circ}$K.

Since albedo only influences the absorbed solar radiation, the latent heat is only indirectly affected through the energy balance. The difference in latent heat is about one third of the difference in sensible heat. Figure 5.3-4f shows the typical results of the eight regions for grid averaged latent heat flux. Since evapotranspiration is affected weakly, the moisture contents in both layers would be influenced weakly too. Figure 5.3-4a and b show the typical change in θ_{1d} and θ_{2d}. In Table 5.3-2(a), VMC1M varies from 0.006 to 0.022 and VMC1B from 0.005 to 0.0104. In Table 5.3-2(b), VMC2M varies from 0.0004 to 0.014 and VMC2B from 0.0002 to 0.007.

5.3.5 Sensitivity to root density distribution, root zone thickness and lower boundary condition

The remain sensitivity studies were conducted for the distribution of root density, thickness of root zone and boundary condition at the bottom of root zone. Since the influence of these parameters are in general small, the results are combined for comparison with the normal case (see Figures 5.3-5a to g). However, the maximum differences and the average differences in 45 days for all regions are summarized in Tables 5.3-2(a) to (n).

Root density is a parameter describing the relative root distribution in the two layers. It partitions transpiration into two uptakes, one from the surface layer of 10 cm and the other from the lower layer. For tall forest, most of the roots are located in the lower layer and the root density fraction in the surface layer R_{d1} for the normal case is designed to be equal to 0.25. For short plants or crops, a large part of the roots gathers in a shallow surface layer and R_{d1} for the normal case is designed to be equal to 0.5. However, this distribution also changes with region and season. In this study, R_{d1}=0.5 for tall canopy regions and R_{d1}=0.75 for short canopy regions are used as a variation of the normal case.

As a result of the root density distribution, the water uptake for transpiration is partitioned, which has a direct influence on the amount of available soil moisture stored in the two layers or the root zone. However, the mean soil moisture contents in these two layers also depend on the thicknesses of these layers. In this study, the surface layer is fixed at 10 cm in thickness. In the normal case, the thickness of the lower layer is taken as 40 cm for short canopy and 90 cm for tall canopy. For the sensitivity study, 90 cm for short canopy and 40 cm for tall canopy were used.

At the bottom of root zone, there are normally two kinds of boundary condition that are used in modeling the soil moisture transport: constant soil moisture content and zero soil moisture content gradient. In this study the condition of constant soil moisture content at the field capacity is used for the normal case and the condition of zero gradient is used as a variation.

As seen in Figure 5.3-5, significant changes occur only in the soil moisture content in the lower layer, latent and sensible heat fluxes for both tall and short canopy. In the figures, the canopy type in a region can be found in Table 5.1.1.

In Figure 5.3-5b, the soil moisture in the lower layer becomes smaller as the root density fraction is decreased because of the reduction in water uptake. However, the tendency for the thickness of the lower layer is difficult to assess due to the fact that the soil moisture depends not only on the uptake but also on the change of the interfacial fluxes. The soil moisture also becomes small in the second layer for the zero gradient condition because an upward interfacial flux is not possible in this case.

In Figure 5.3-5f and g, the effects on the latent and sensible fluxes are small and more for the tall canopy than for the short canopy.

5.3.6 Summary of the sensitivity study

The above analysis has shown that different parameters have different effects on the water transport and heat transfer. For example, canopy resistance produces a strong influence on evapotranspiration and soil moisture content but has a weaker effect on the temperatures. Conversely, albedo shows a greater effect on the energy balance and temperature but has a small influence on evapotranspiration and soil moisture content. The vegetation density has strong effects both on the water transport and heat transfer and changes temperatures and moisture contents. But, the parameters such as d_2, R_{d1} and the lower boundary condition only exert minor influences on the land surface processes. The sensitivity of the parameters selected for this study are summarized in Table 5.3.4 in the order of their significant changes as listed in Table 5.3-2. The importance of a parameter is indicated by a number. For example, r_c has the most important effect on all variables listed in the first column while albedo has the least effect on θ_2.

	6_c	r_c	Albedo	R_{d1}	d_2	Lower B. C.
E_t	1	2	3	3	3	3
H_t	1	3	2	4	4	4
O_1	1	2	2	2	3	4
O_2	1	2	4	3	3	4
T_{gb}	1	3	2	3	4	4
T_c	1	2	2	3	3	3
$\overline{T}$	1	3	2	4	4	4

d_2 : thickness of second layer

6_c : vegetation fraction

r_c : canopy resistance

R_{d1} : root density distribution

Lower B. C. : lower boundary condition

Table 5.3.4 Classification of importance of parameters
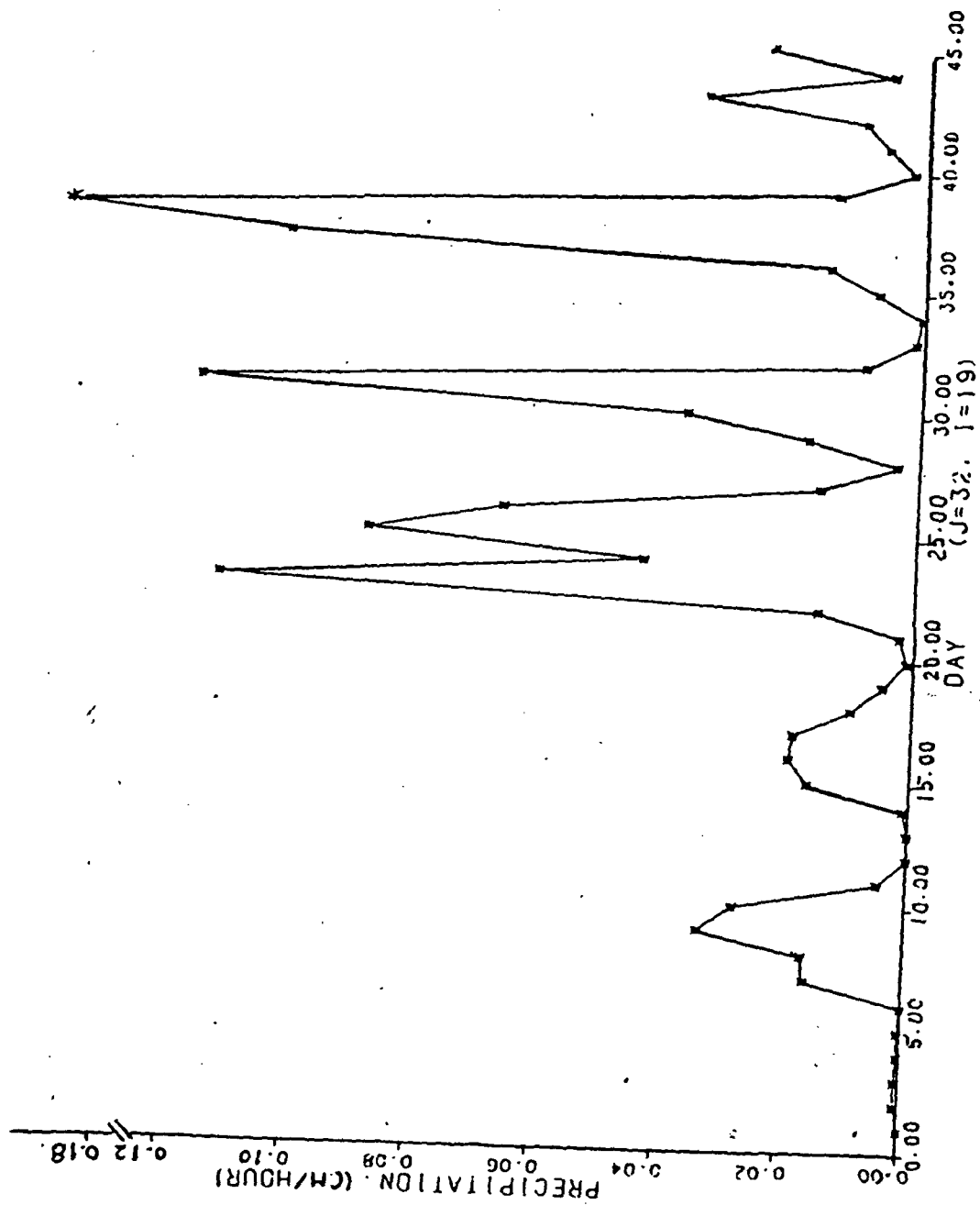
Figure 5.2-1a Precipitation
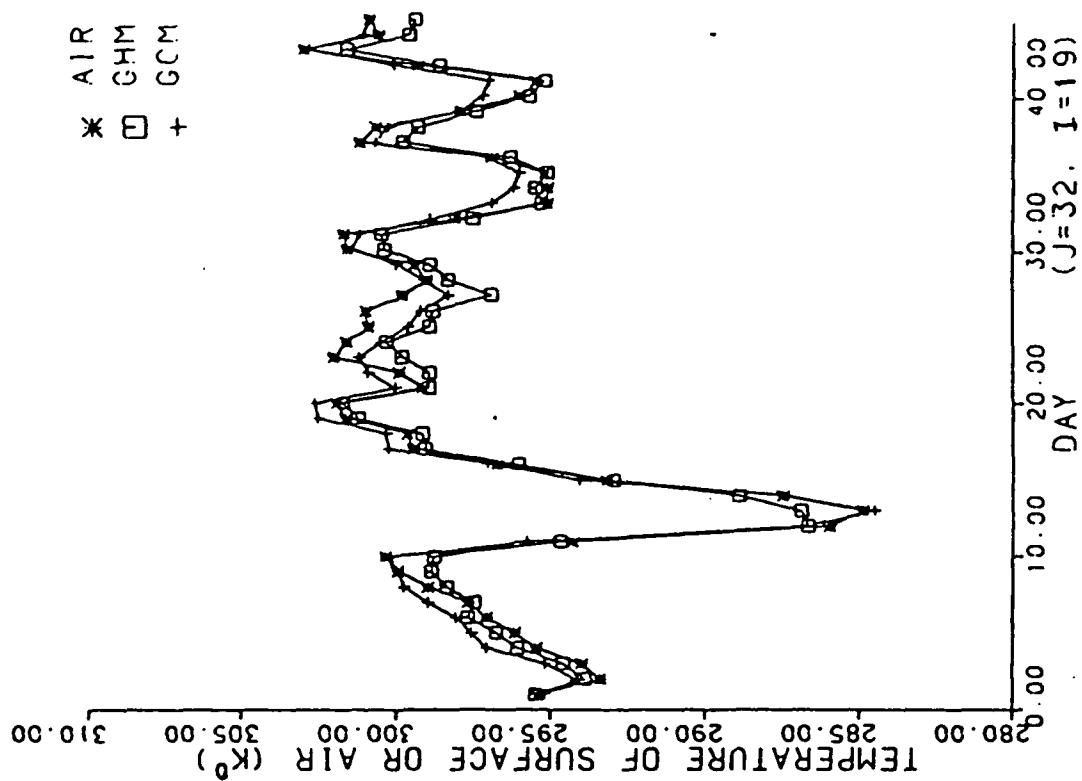
Figure 5.2-1c Comparison of grid surface temperature
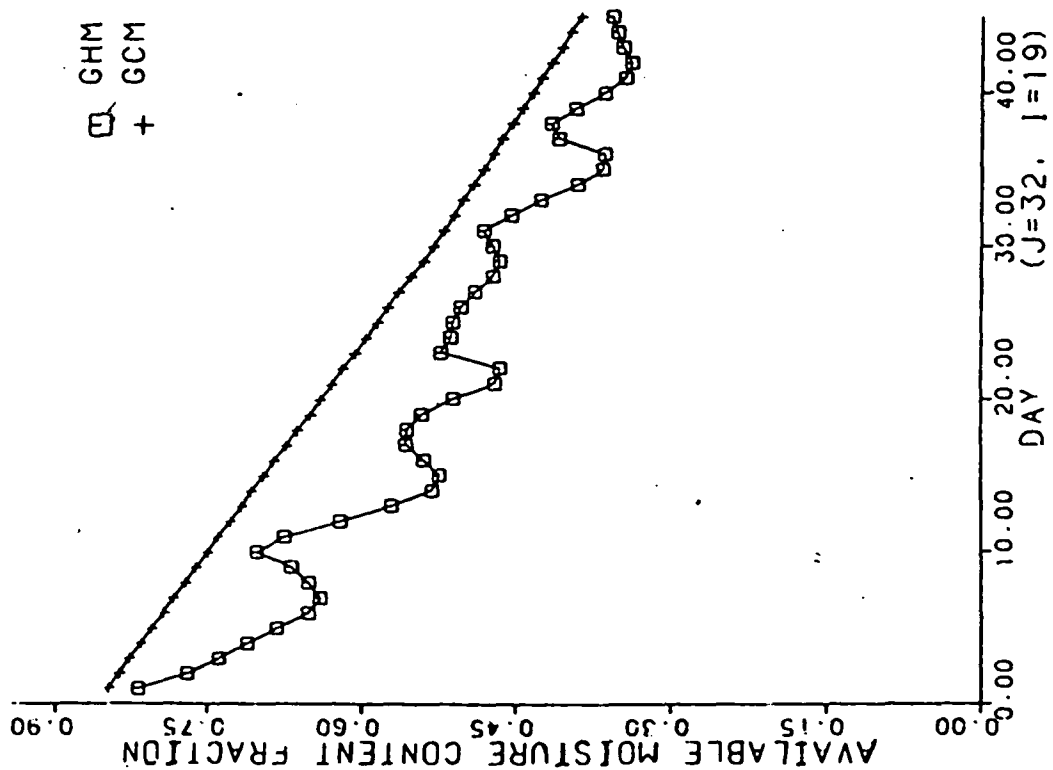
Figure 5.2-1b Comparison of available moisture content fraction

150
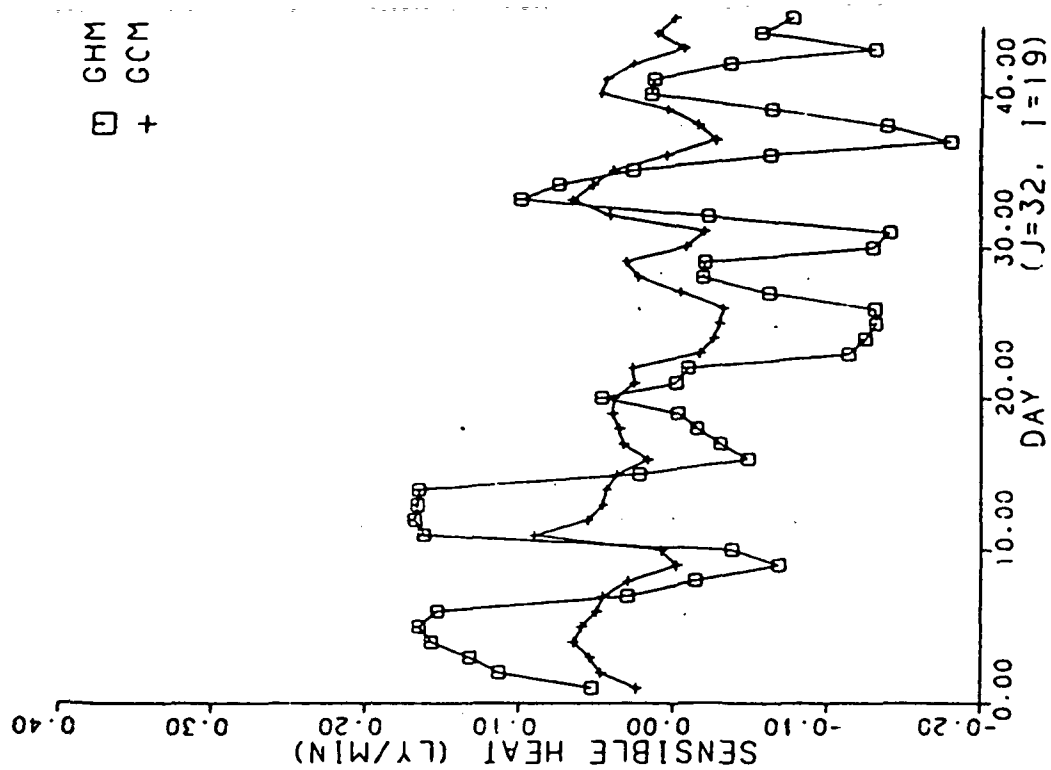
Figure 5.2-1e Comparison of sensible heat
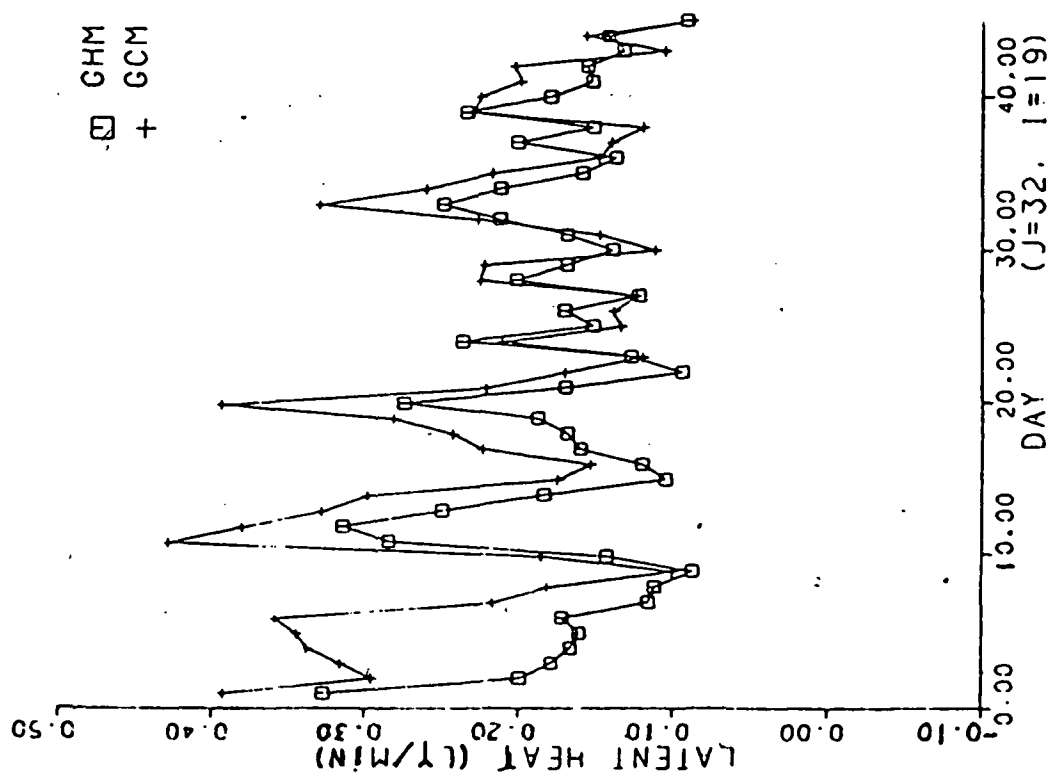
Figure 5.2-1d Comparison of latent heat
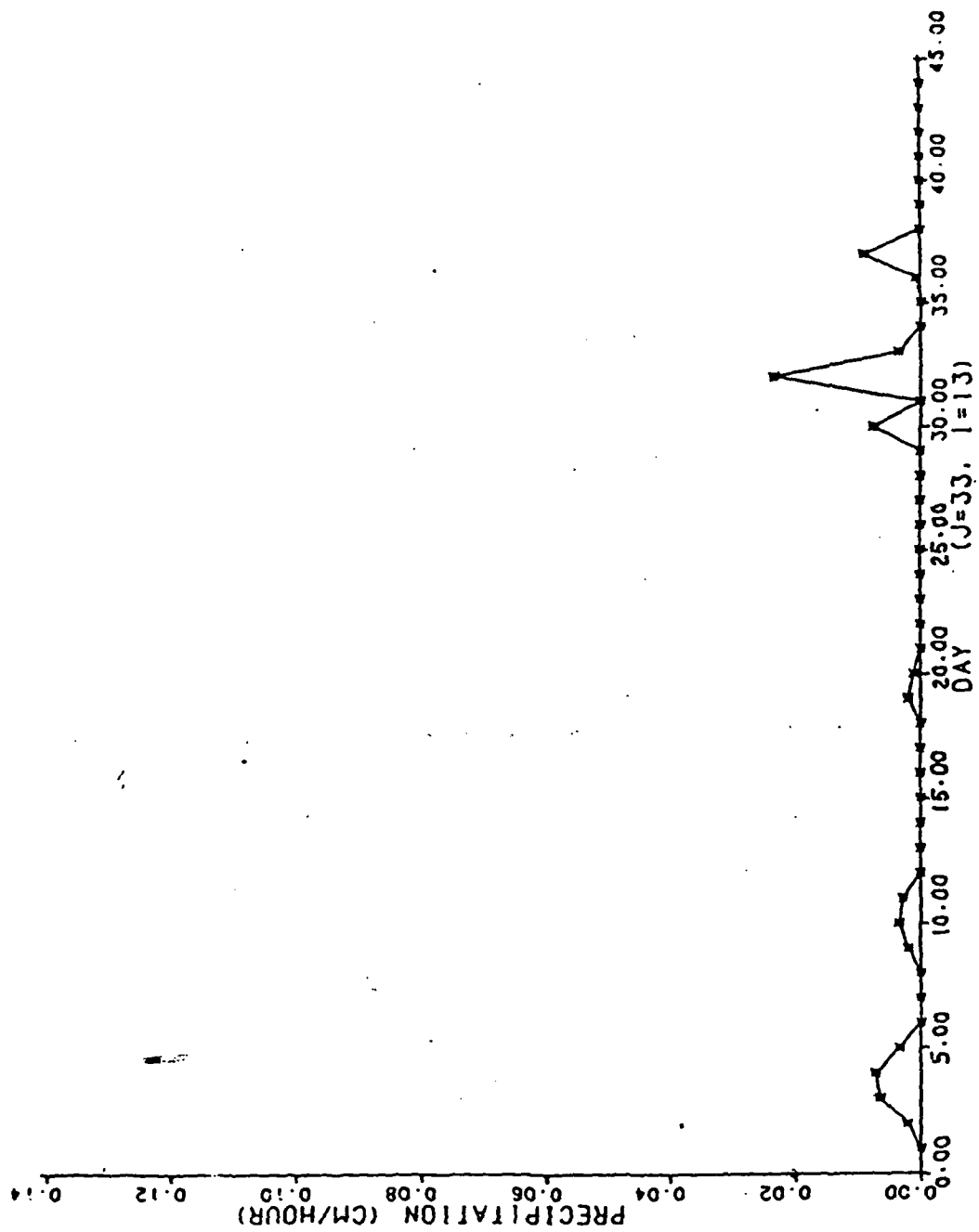
Figure 5.2-2a Precipitation

AiR
GHM
GCM

✳
⊟
+

40.00
30.00
(J=33, I=13)
20.00
DAY
10.00
0.00
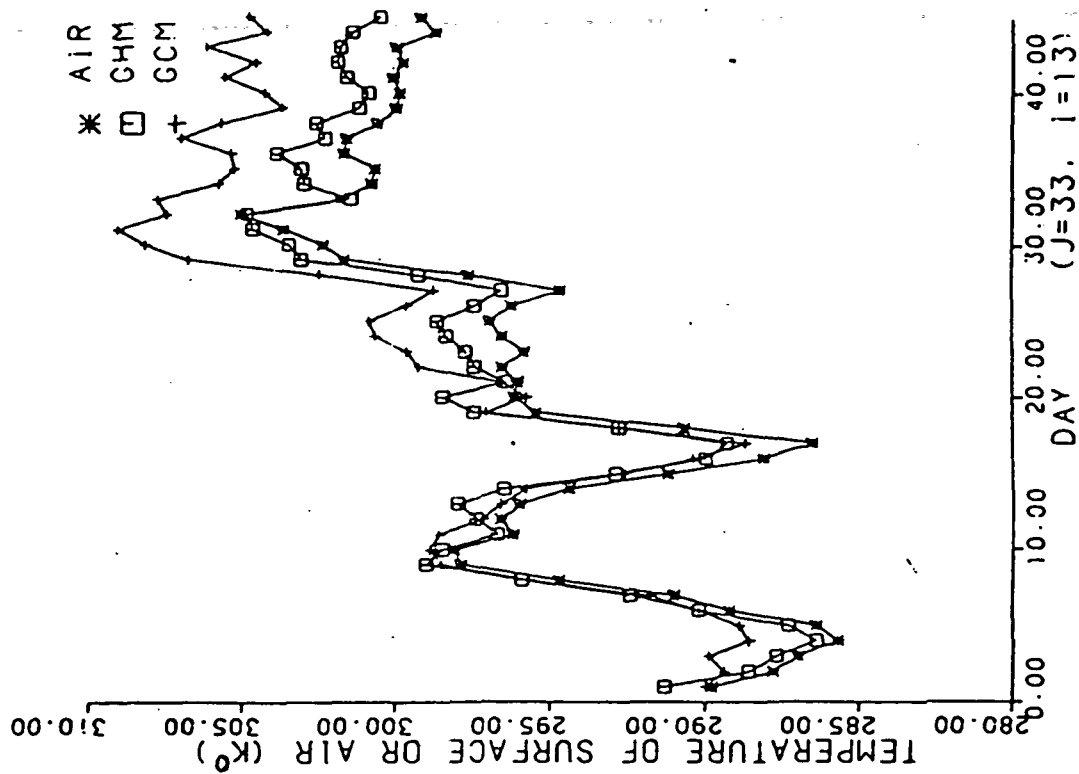
Figure 5.2-2c Comparison of grid
surface temperature

310.00 305.00 300.00 295.00 290.00 285.00 280.00
TEMPERATURE OF SURFACE OR AIR (K°)

GHM
GCM

⊟
+

40.00
30.00
(J=33, I=13)
20.00
DAY
10.00
0.00
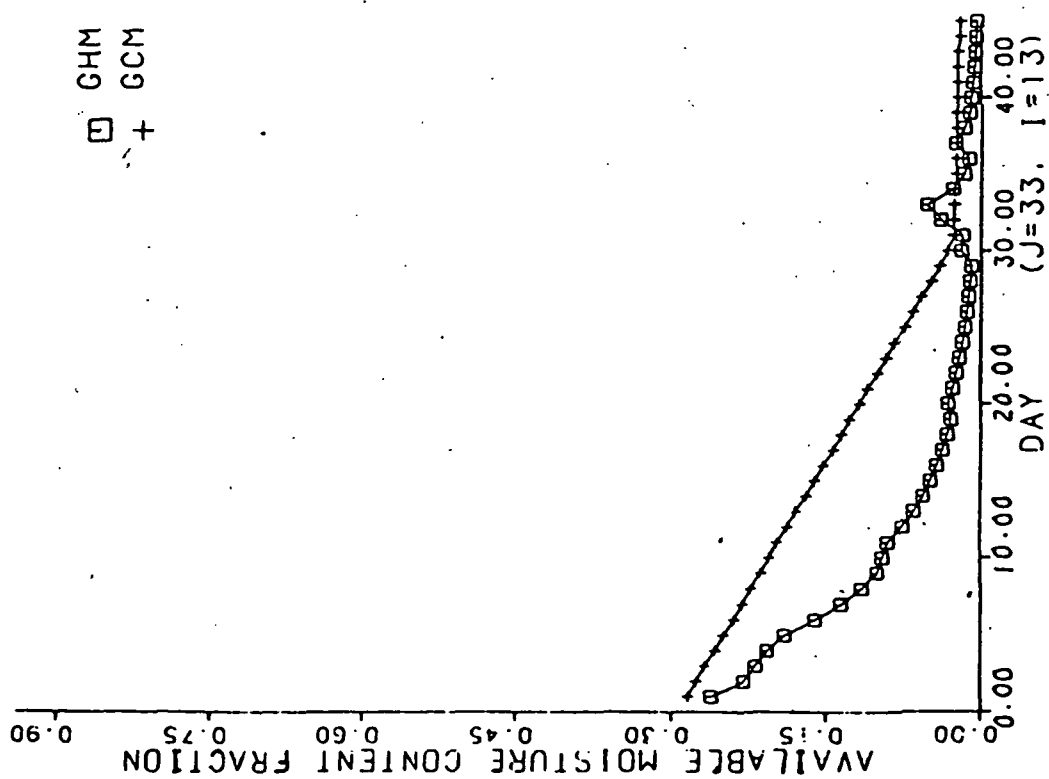
Figure 5.2-2b Comparison of available
moisture content fraction

0.90 0.75 0.60 0.45 0.30 0.15 0.0
AVAILABLE MOISTURE CONTENT FRACTION

153
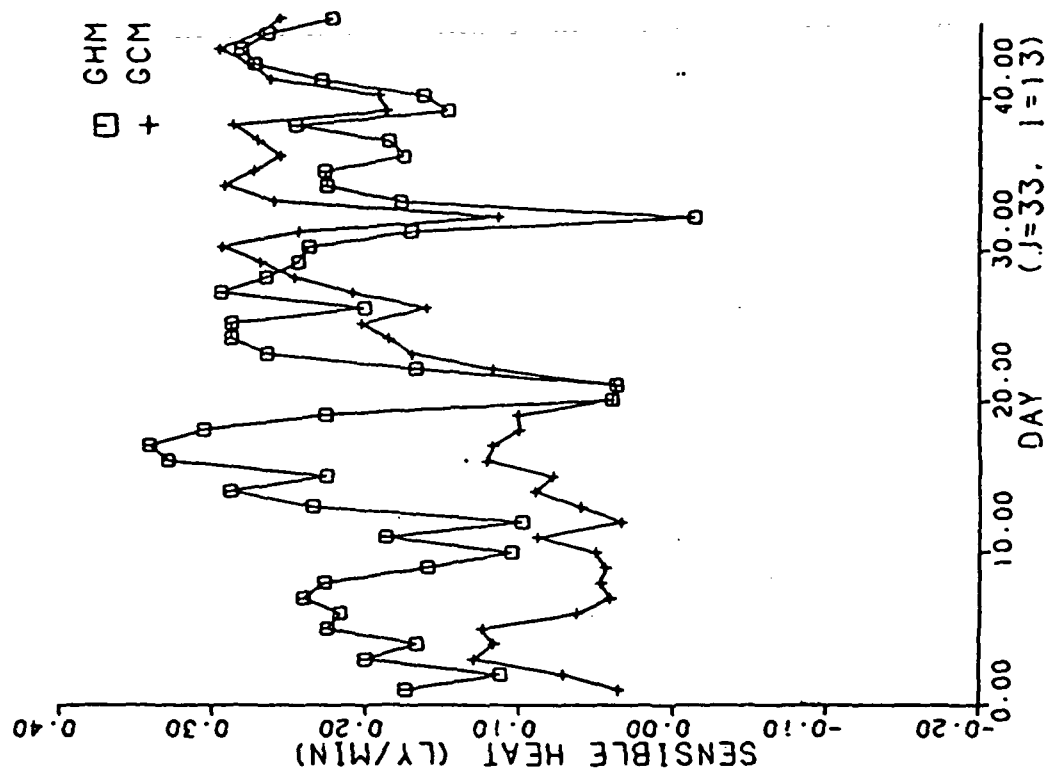
Figure 5.2-2e Comparison of sensible heat
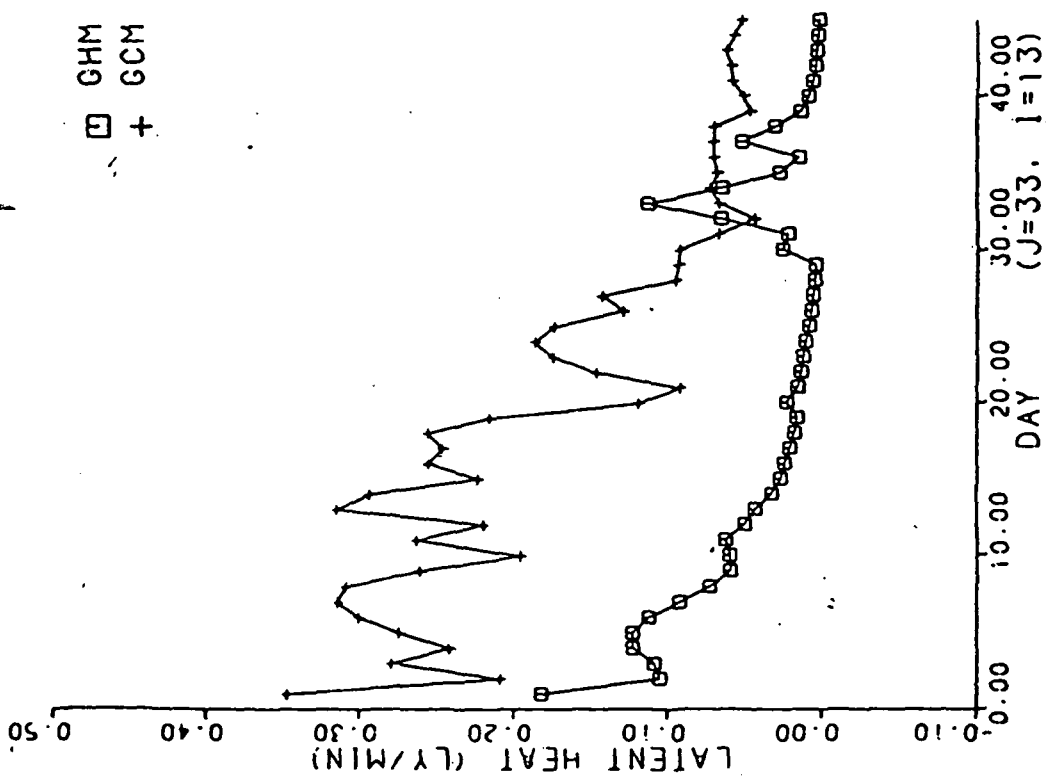
Figure 5.2-2d Comparison of latent heat
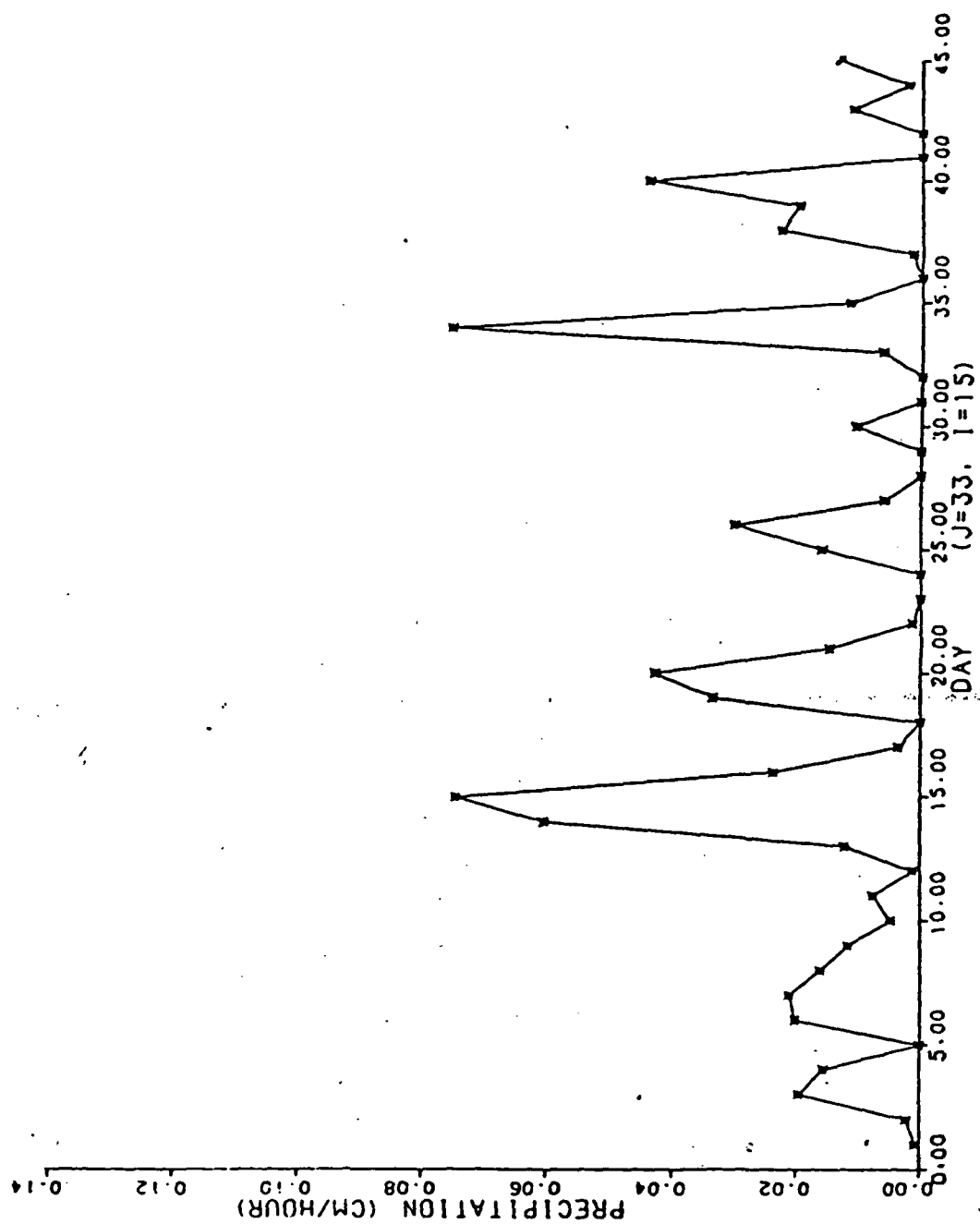
Figure 5.2-3a Precipitation
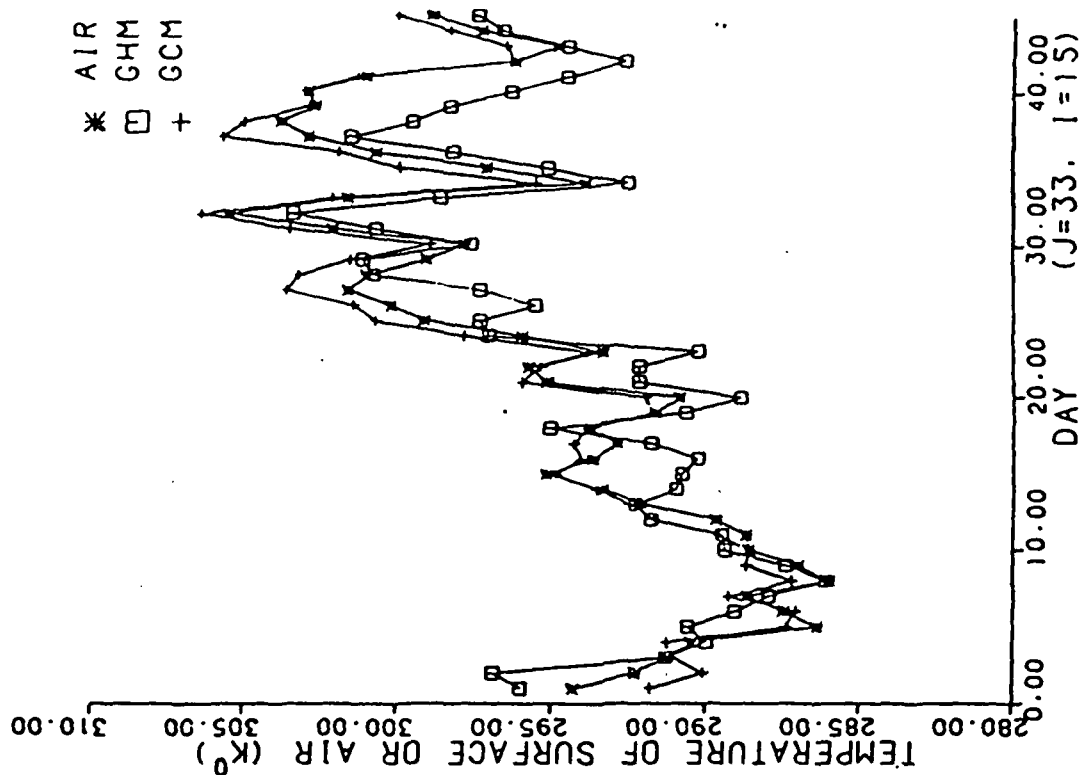
Figure 5.2-3c Comparison of grid surface temperature
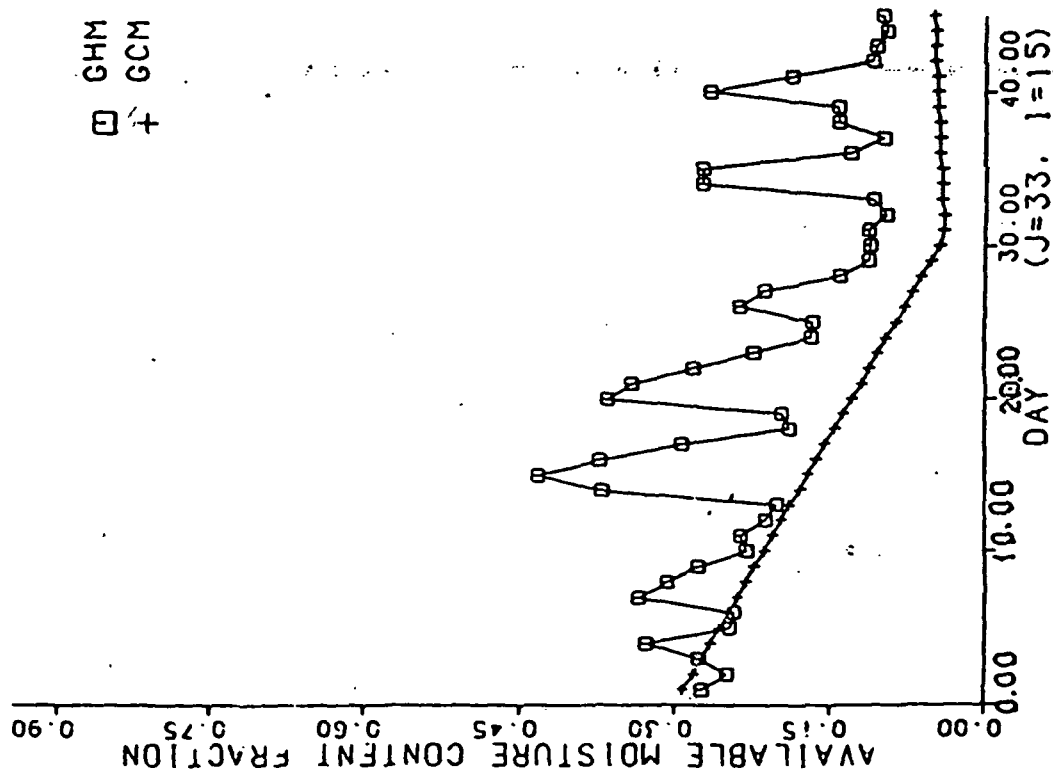
Figure 5.2-3b Comparison of available moisture content fraction
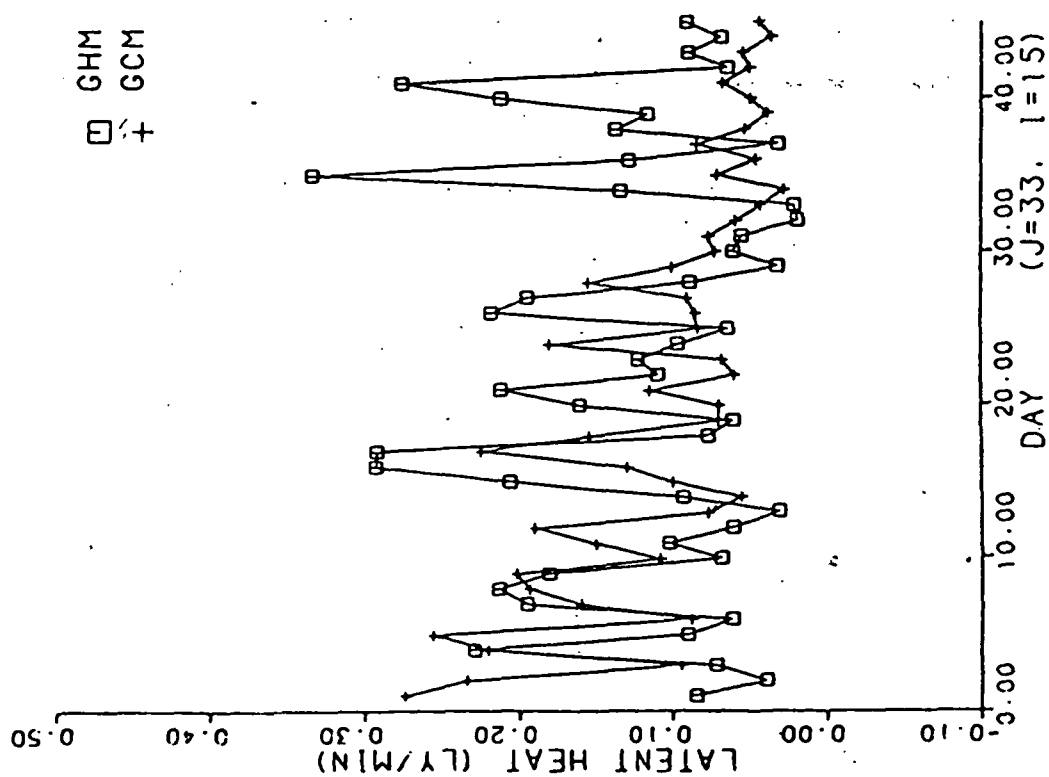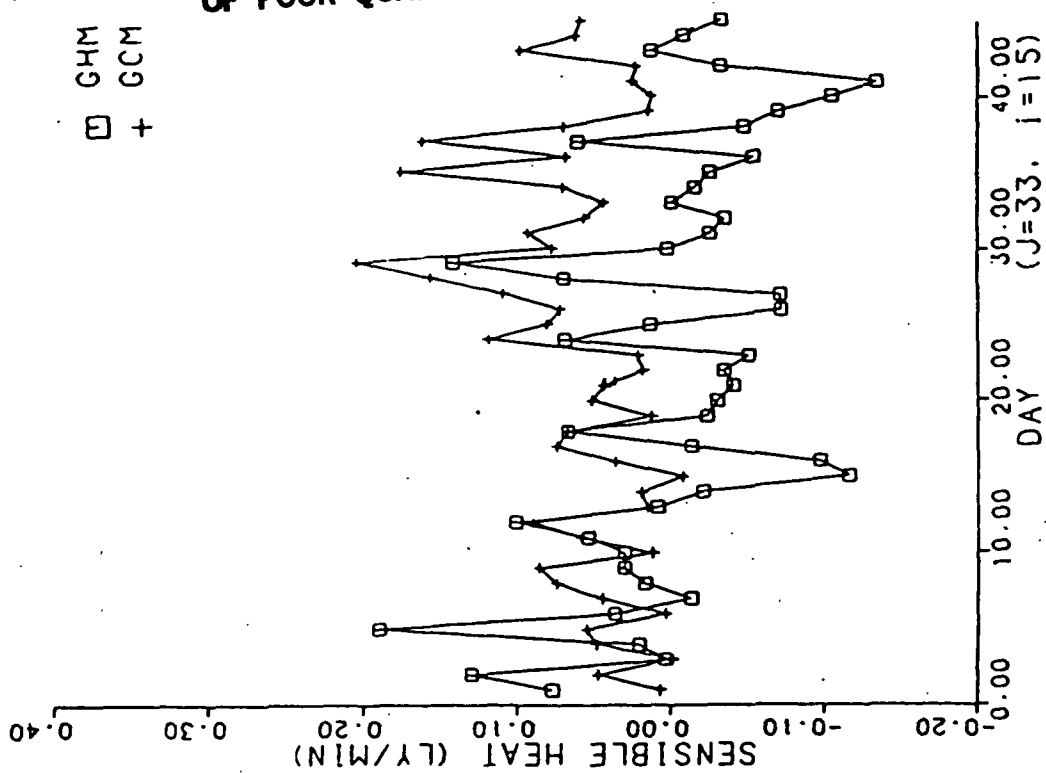
Figure 5.2-3e Comparison of sensible heat

Figure 5.2-3d Comparison of latent heat
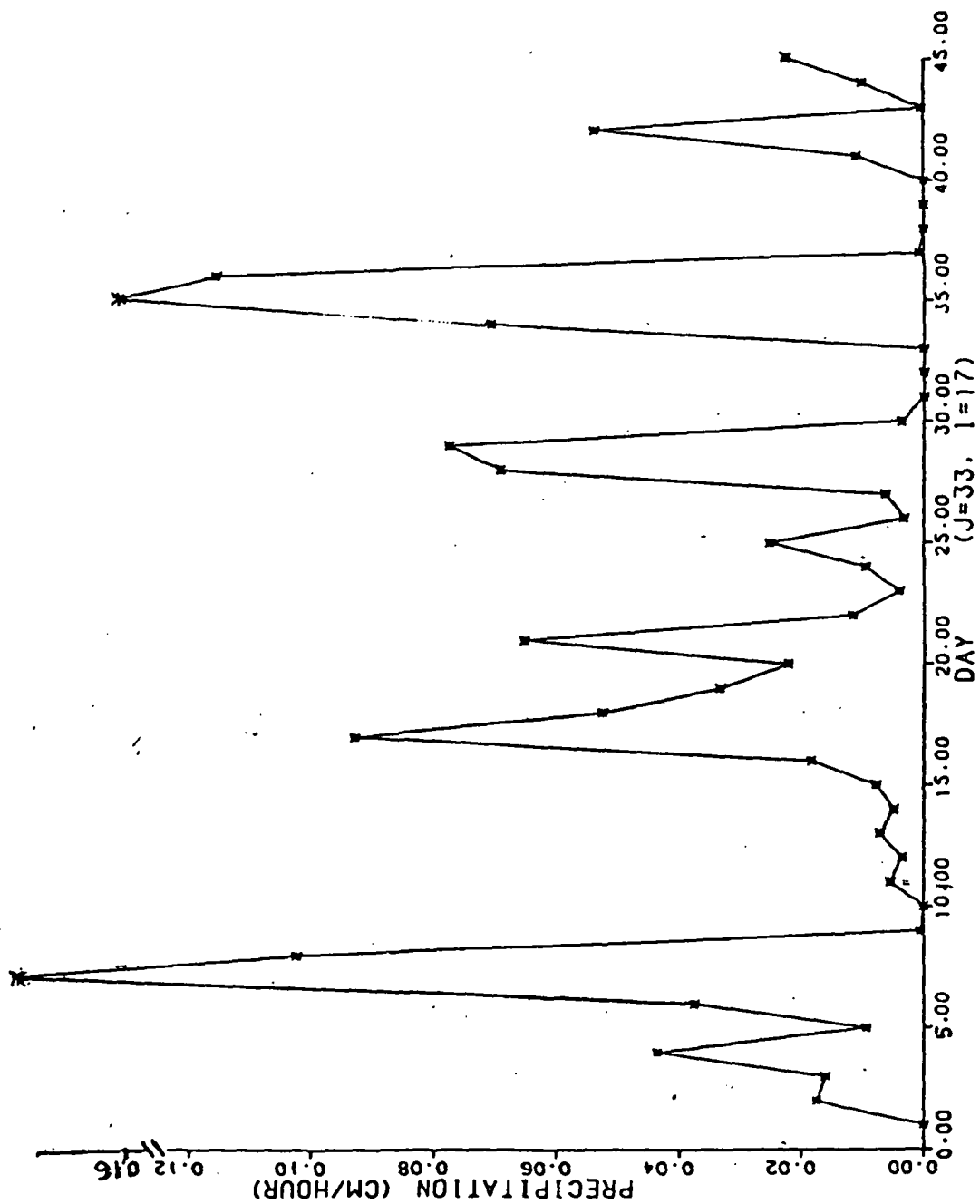
Figure 5.2-4a Precipitation

Figure 5.2-4c Comparison of grid surface temperature

TEMPERATURE OF SURFACE OR AIR (K°)

* AIR
□ GHM
+ GCM

Figure 5.2-4b Comparison of available moisture content fraction

AVAILABLE MOISTURE CONTENT FRACTION

□ GHM
+ GCM
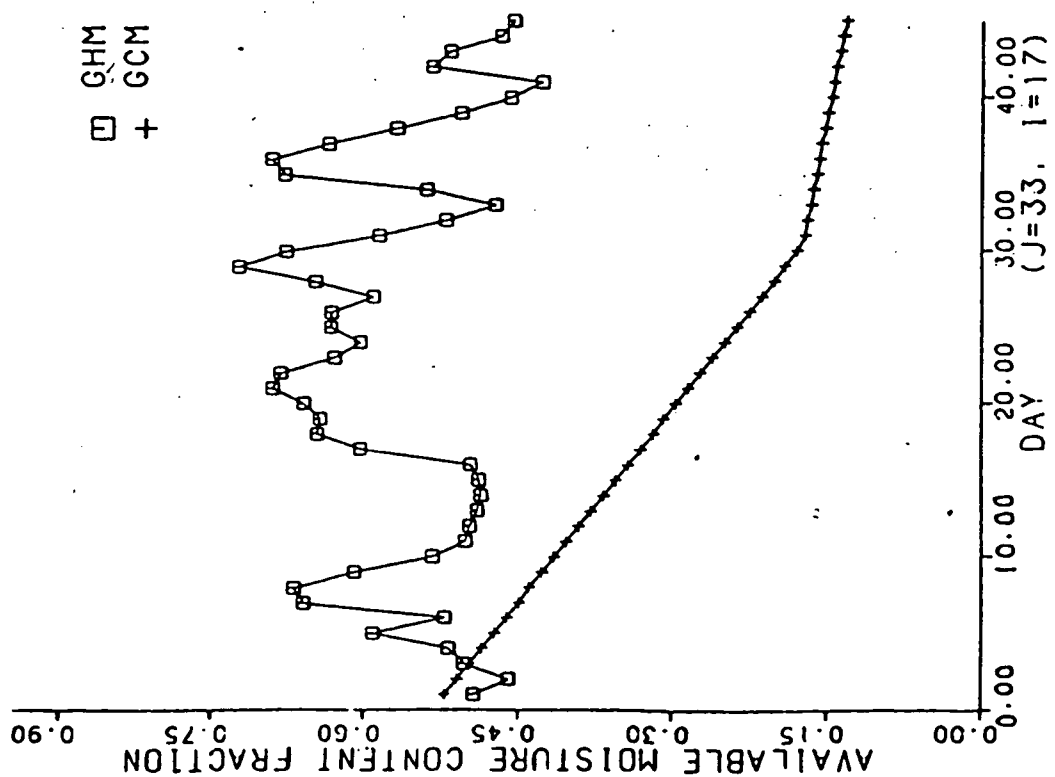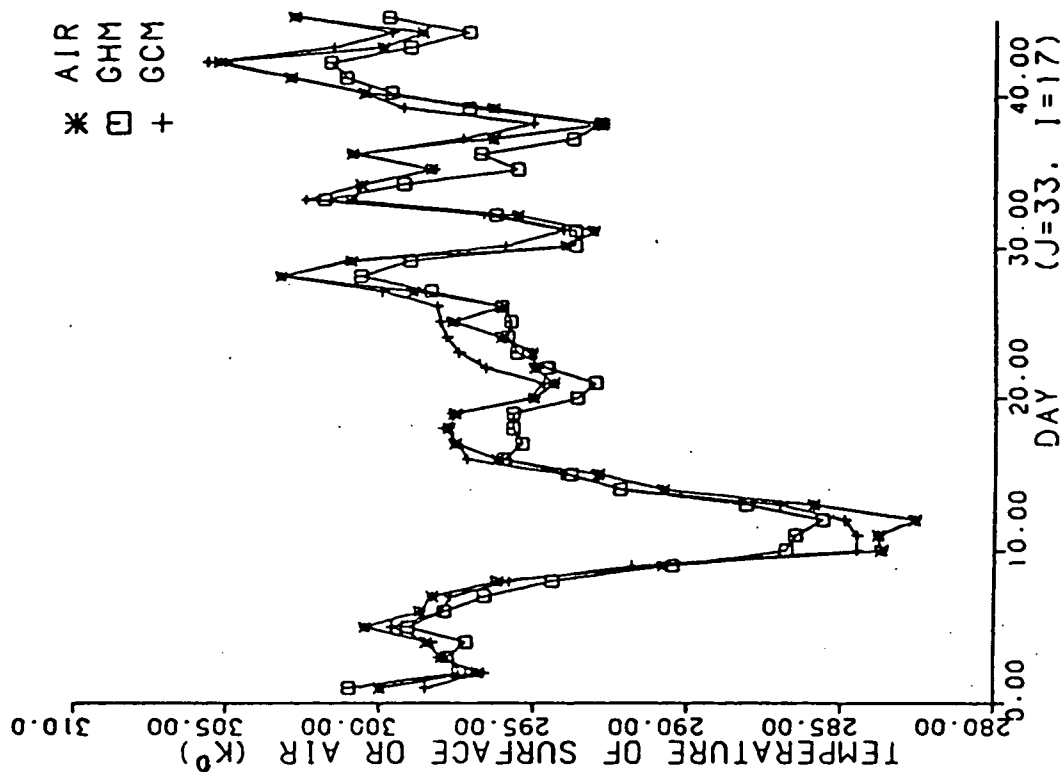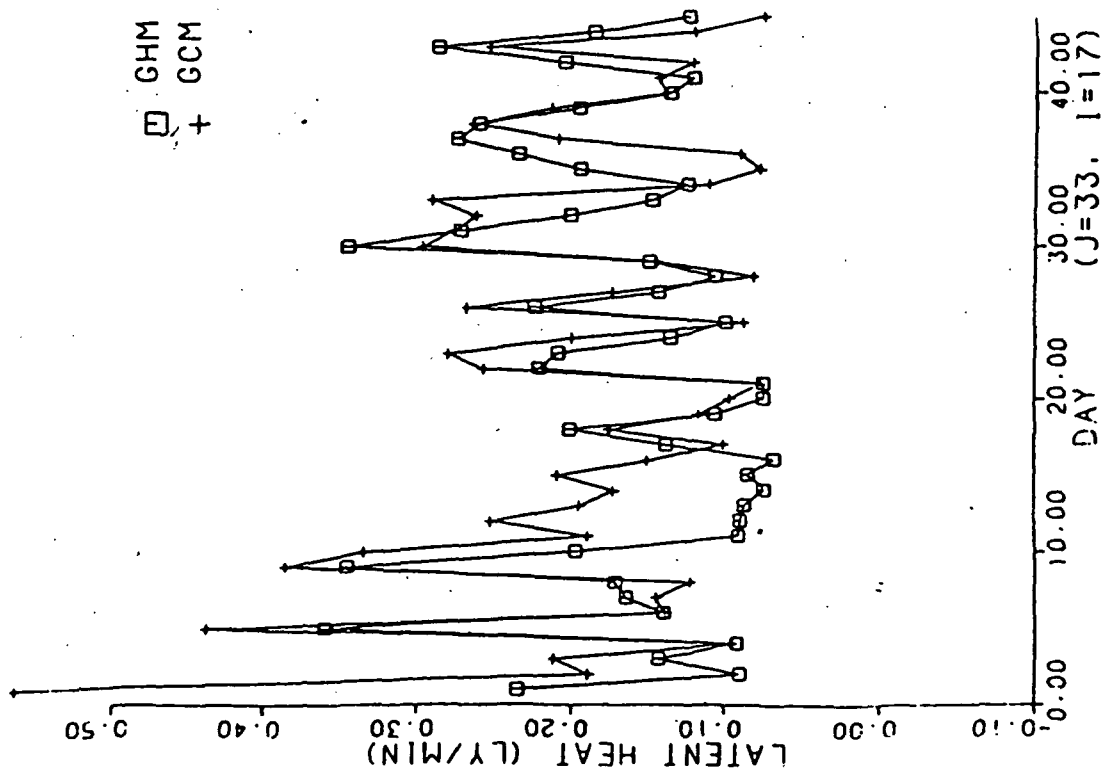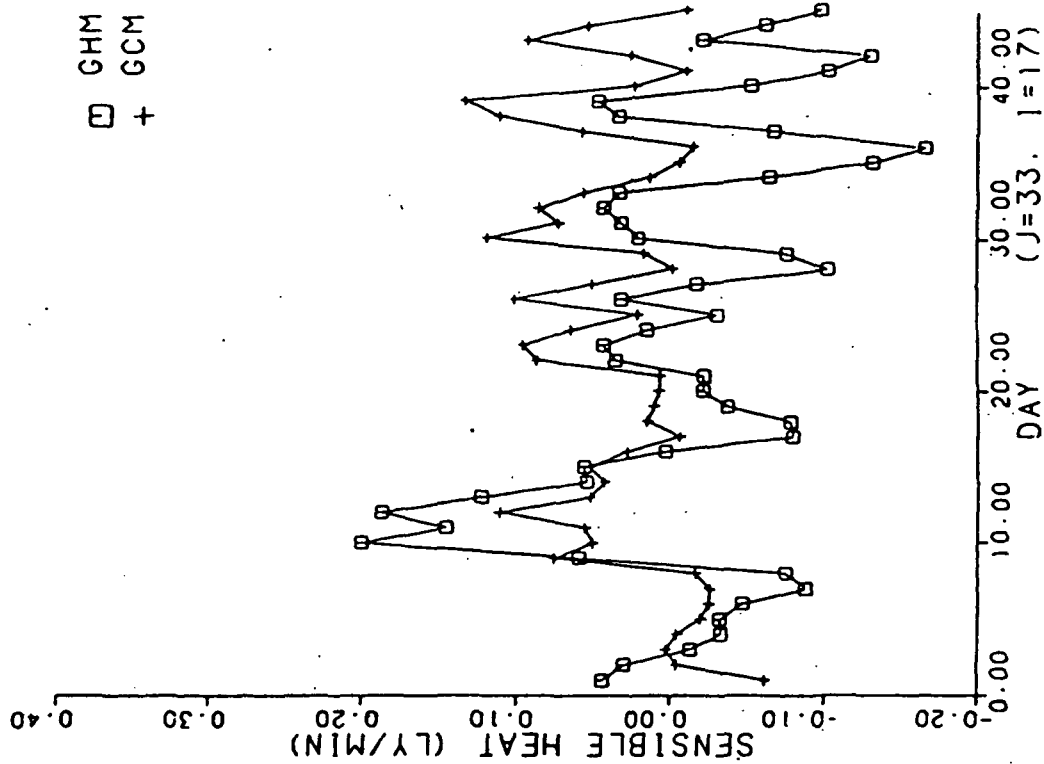
Figure 5.2-4e Comparison of sensible heat

Figure 5.2-4d Comparison of latent heat
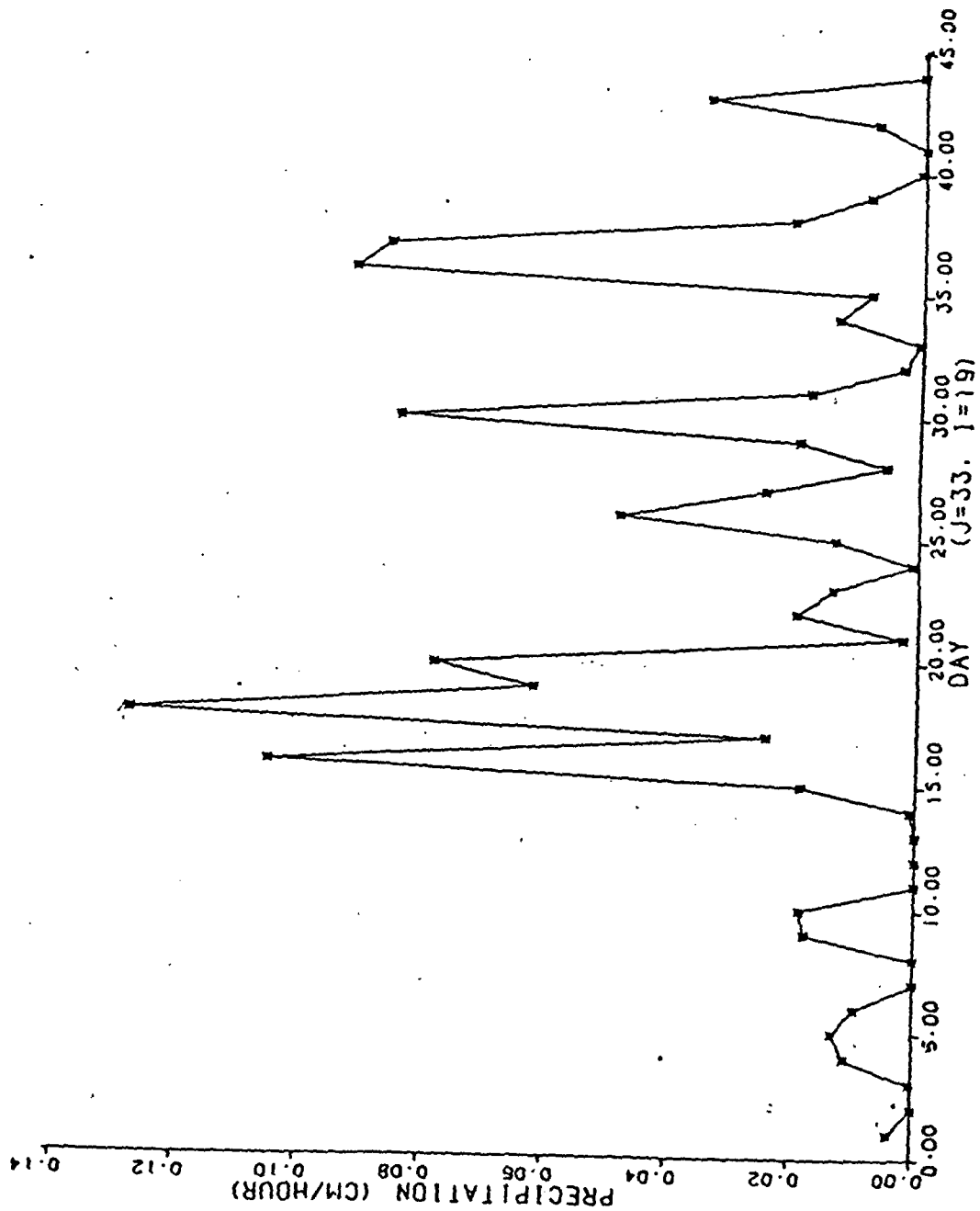
Figure 5.2-5a Precipitation

Figure 5.2-5c Comparison of grid
surface temperature

Figure 5.2-5b Comparison of available
moisture content fraction
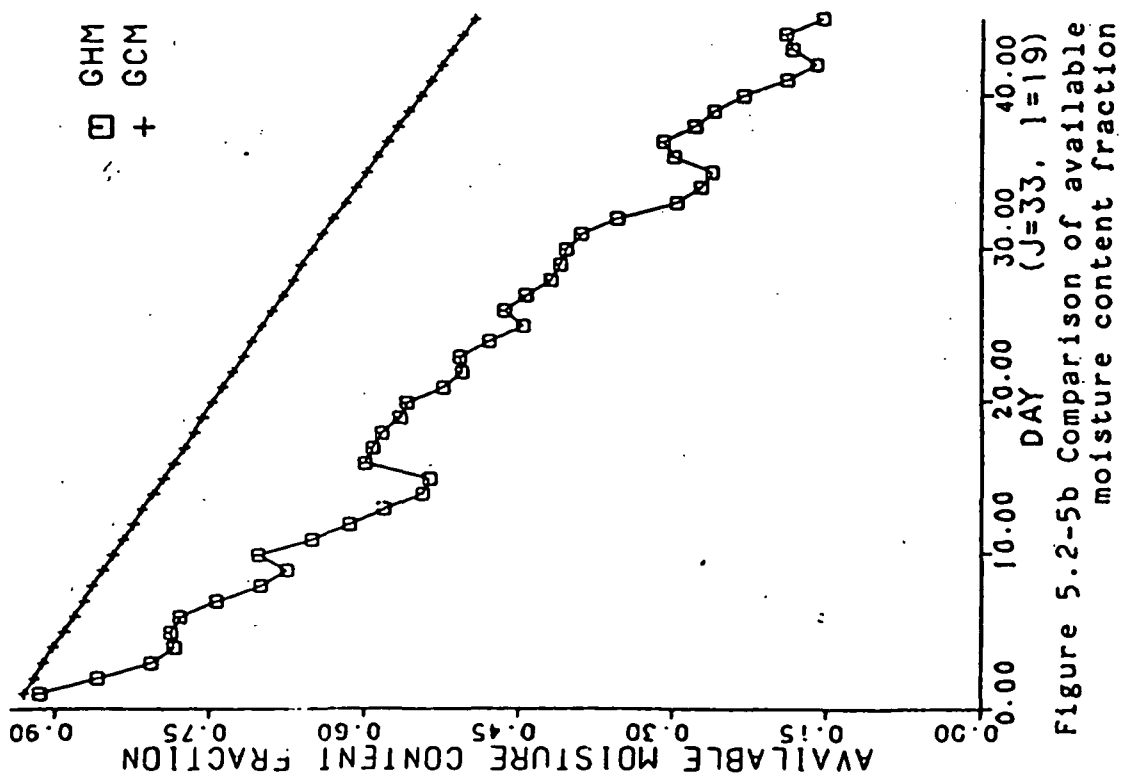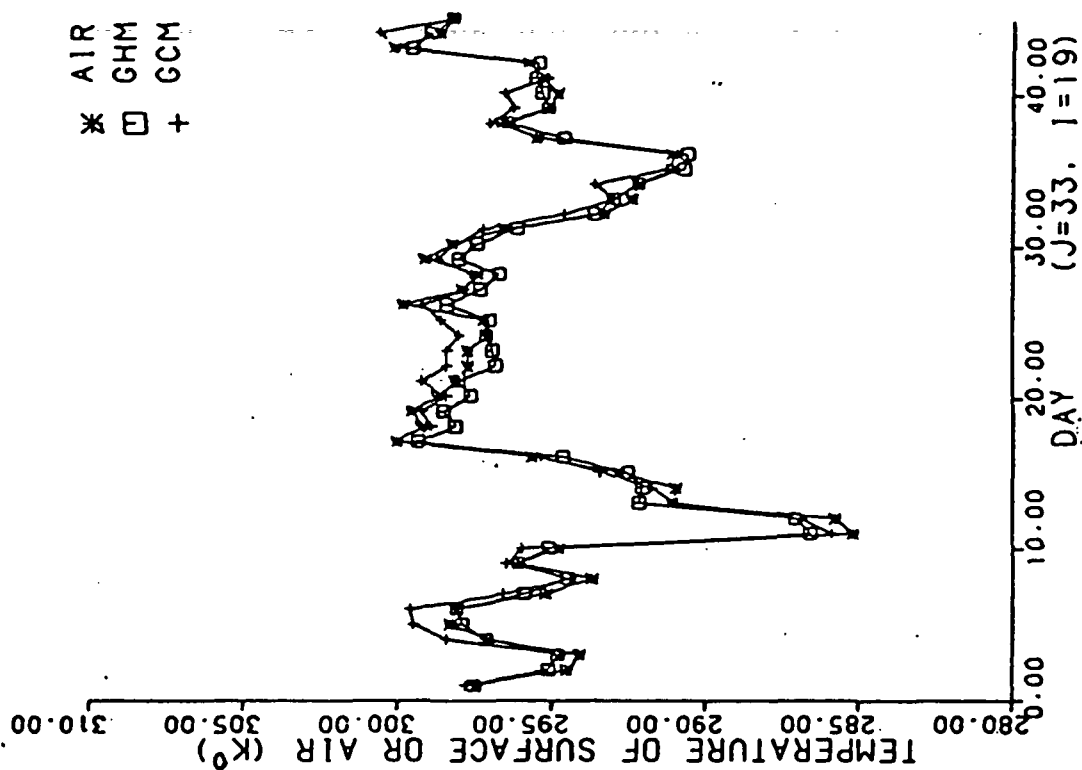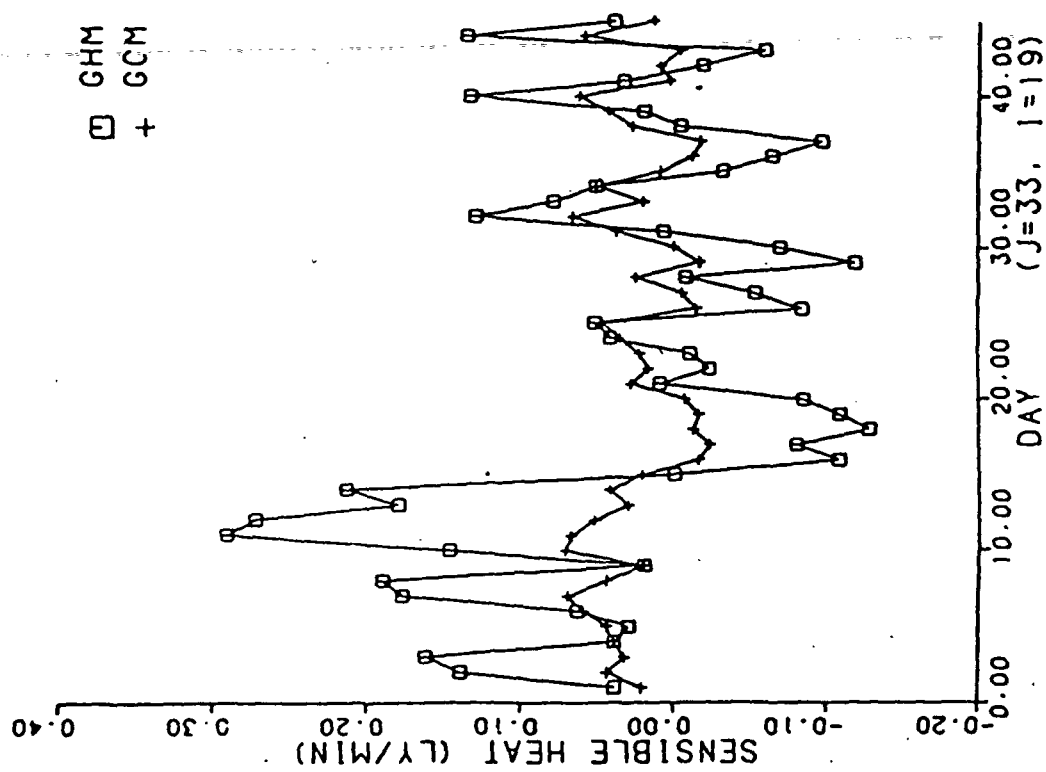
Figure 5.2-5e Comparison of sensible heat
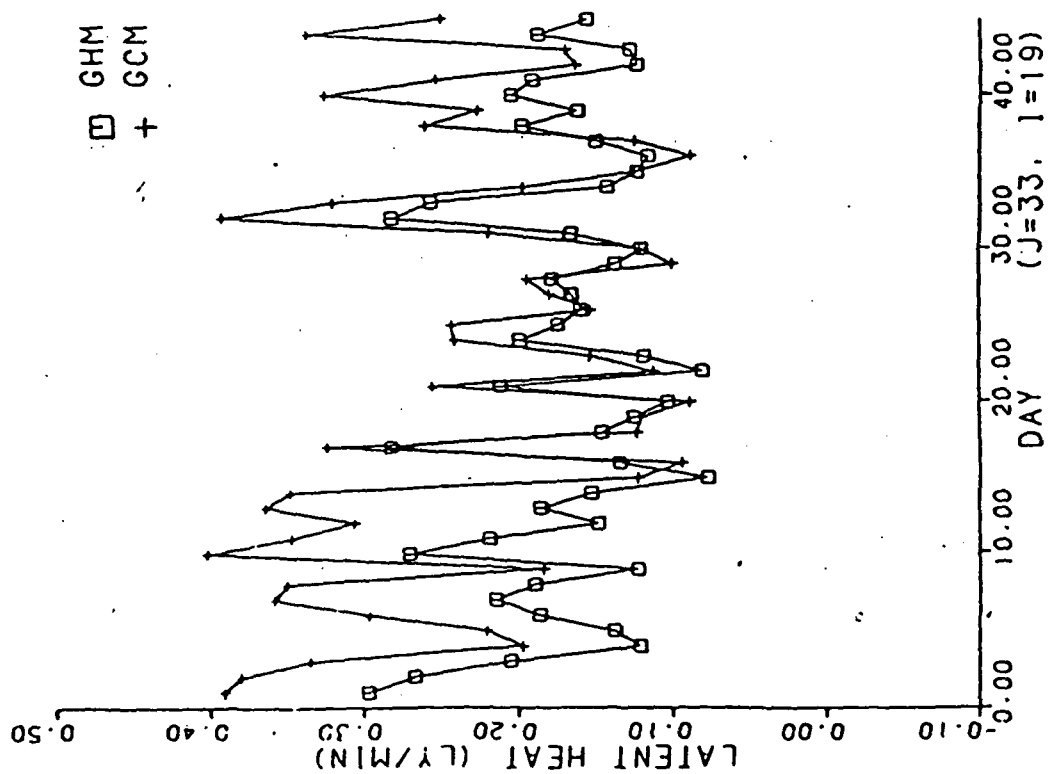
Figure 5.2-5d Comparison of latent heat
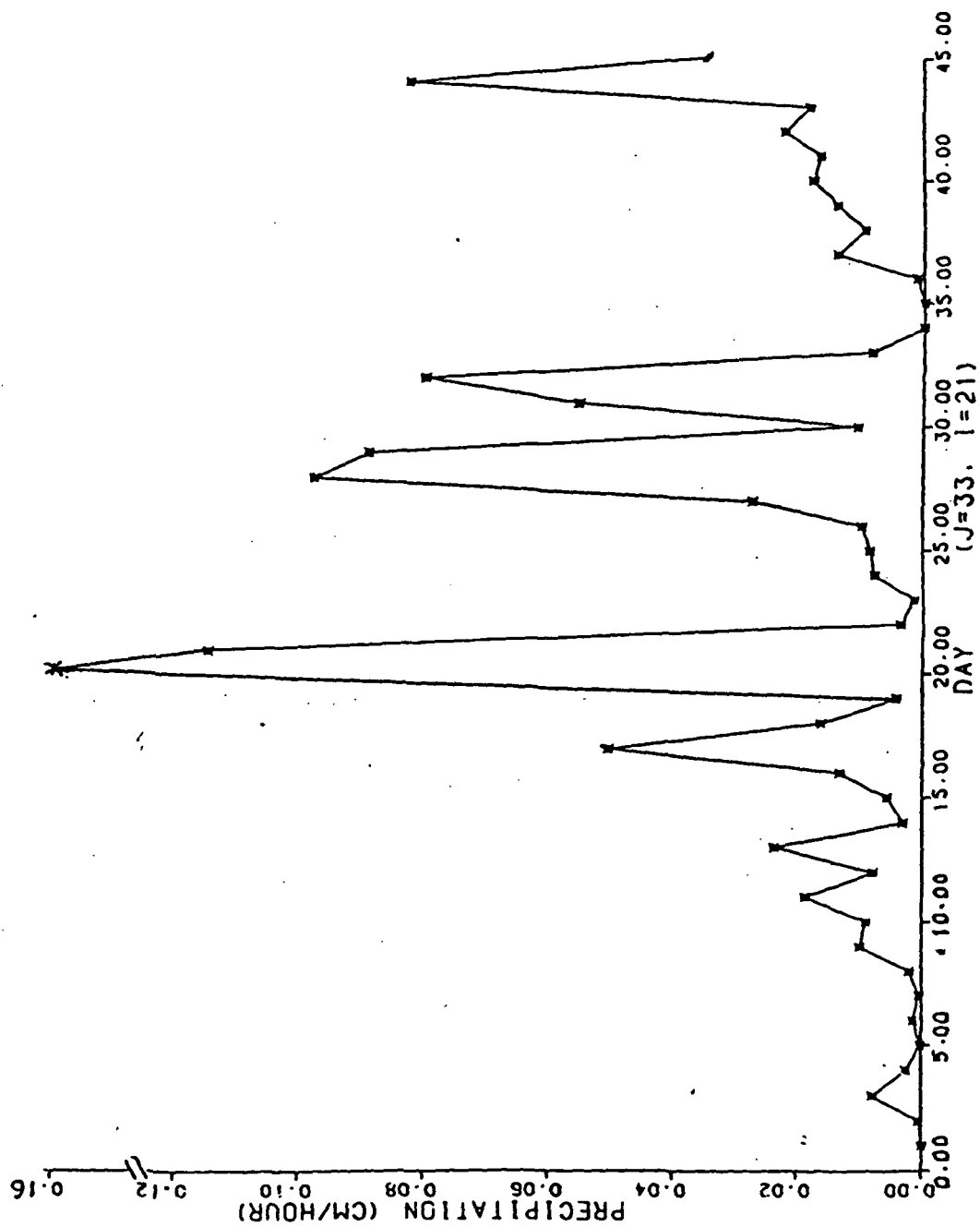
Figure 5.2-6a Precipitation
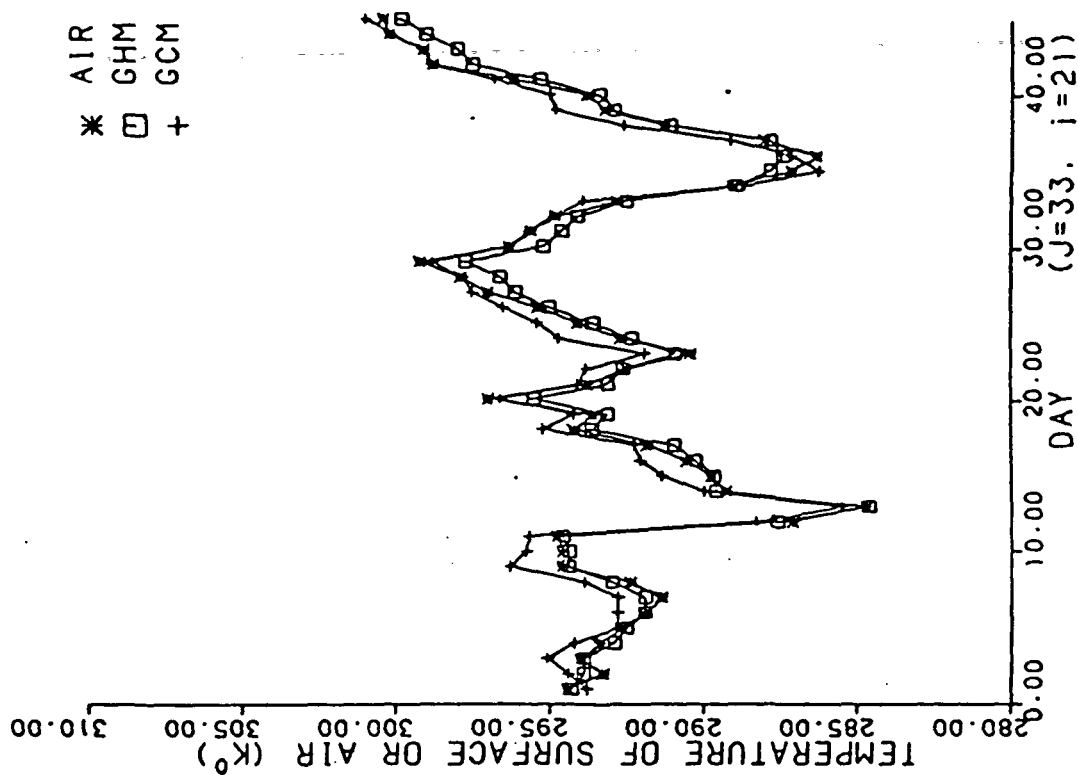
Figure 5.2-6c Comparison of grid surface temperature
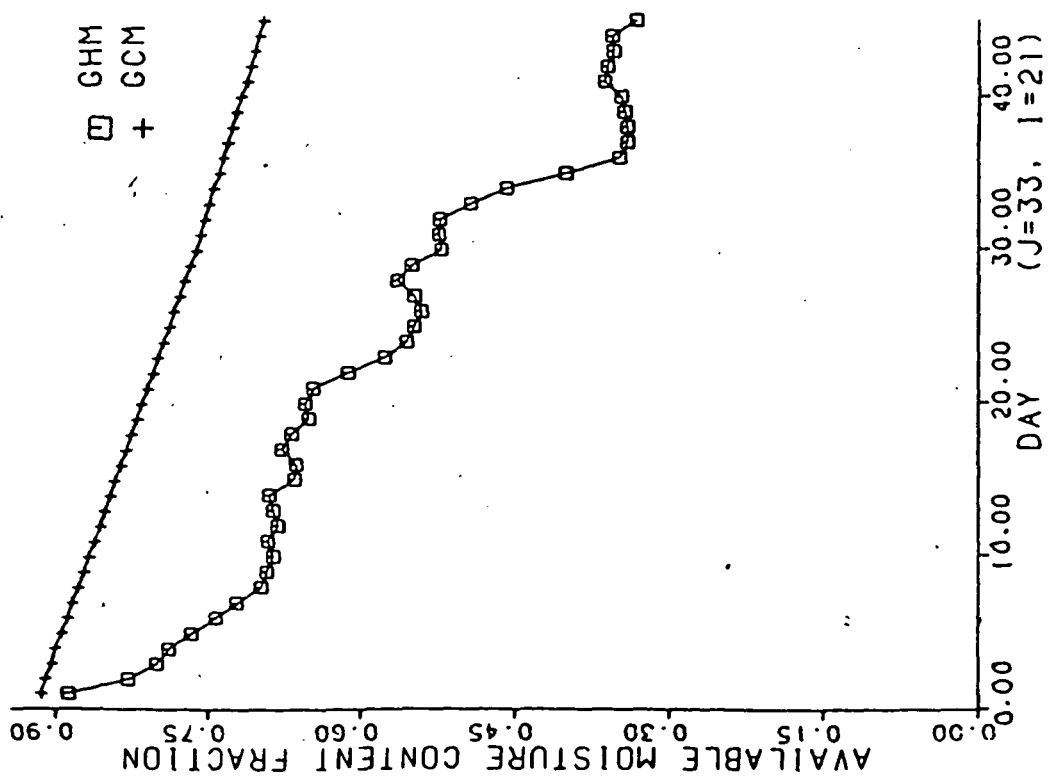
Figure 5.2-6b Comparison of available moisture content fraction

Figure 5.2-6e Comparison of sensible heat

Figure 5.2-6d Comparison of latent heat
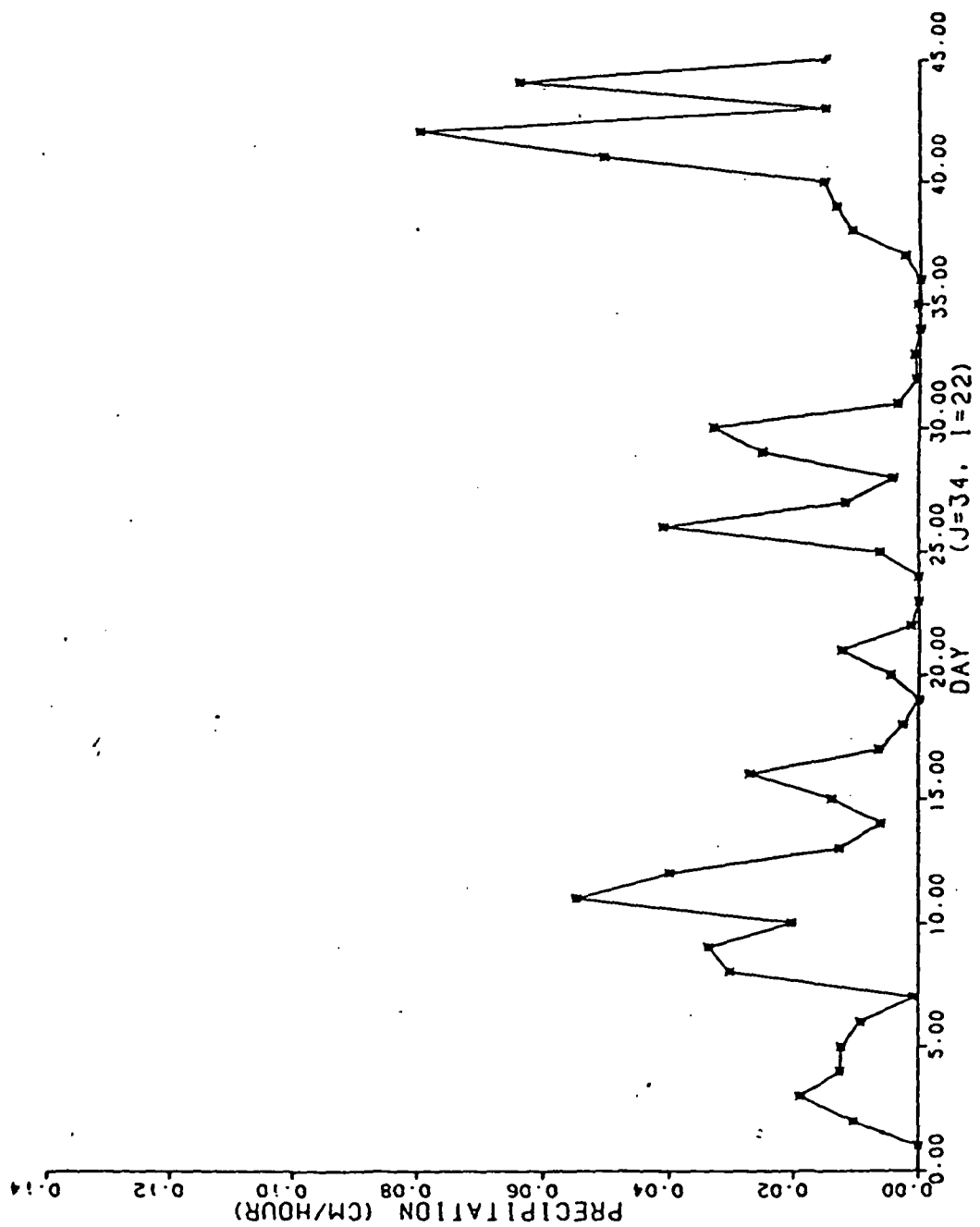
Figure 5.2-7a Precipitation

167

Figure 5.2-7c Comparison of grid
surface temperature

Figure 5.2-7b Comparison of available
moisture content fraction

Figure 5.2-7e Comparison of sensible heat
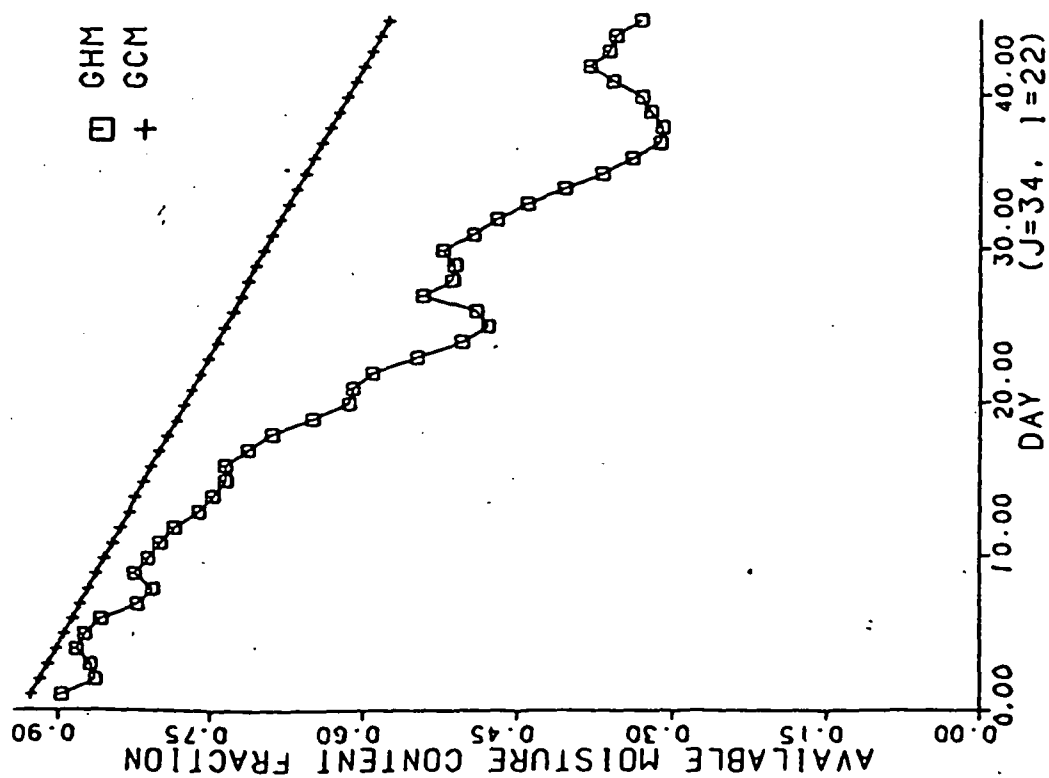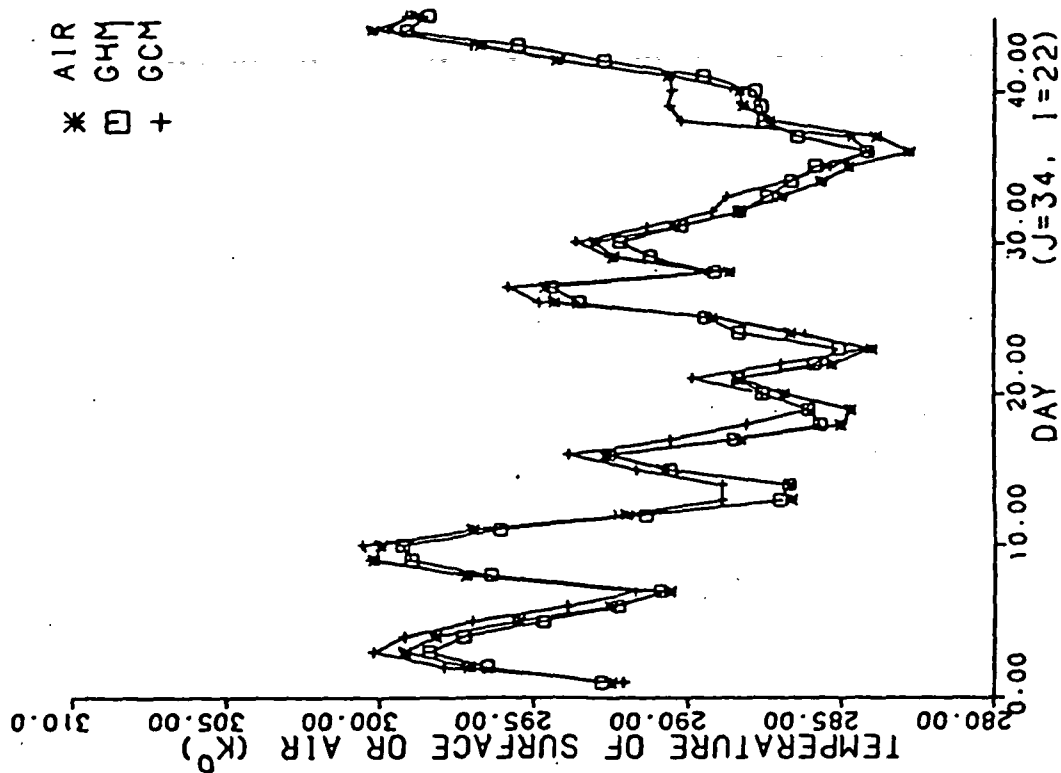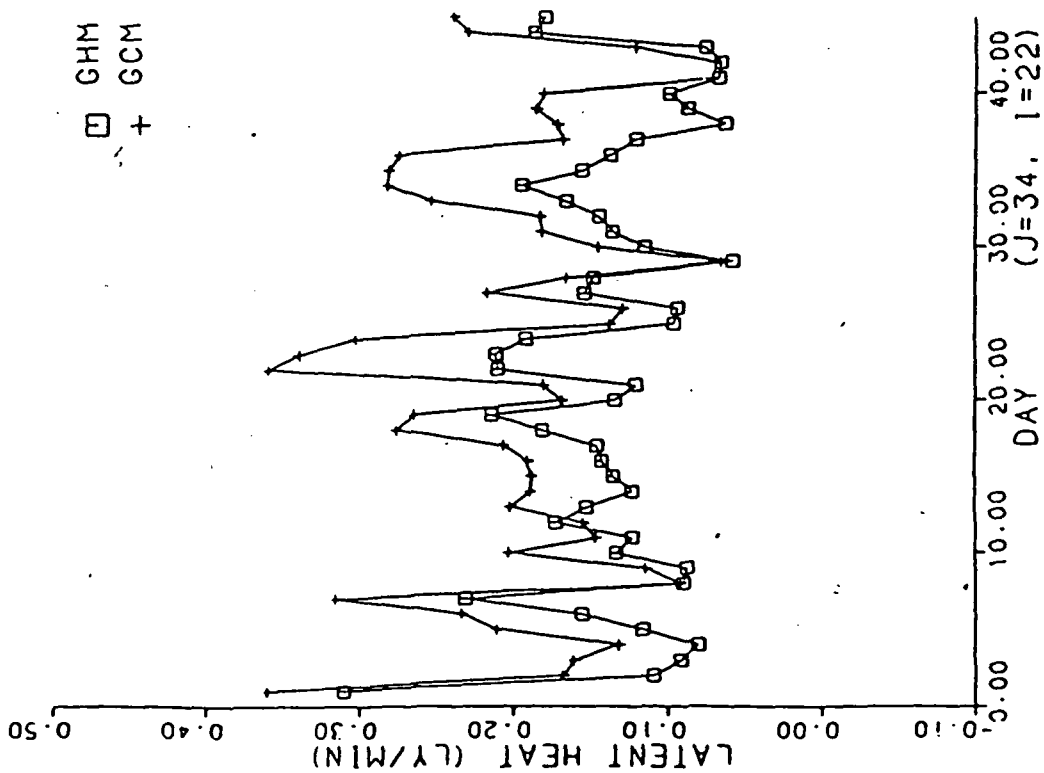
Figure 5.2-7d Comparison of latent heat
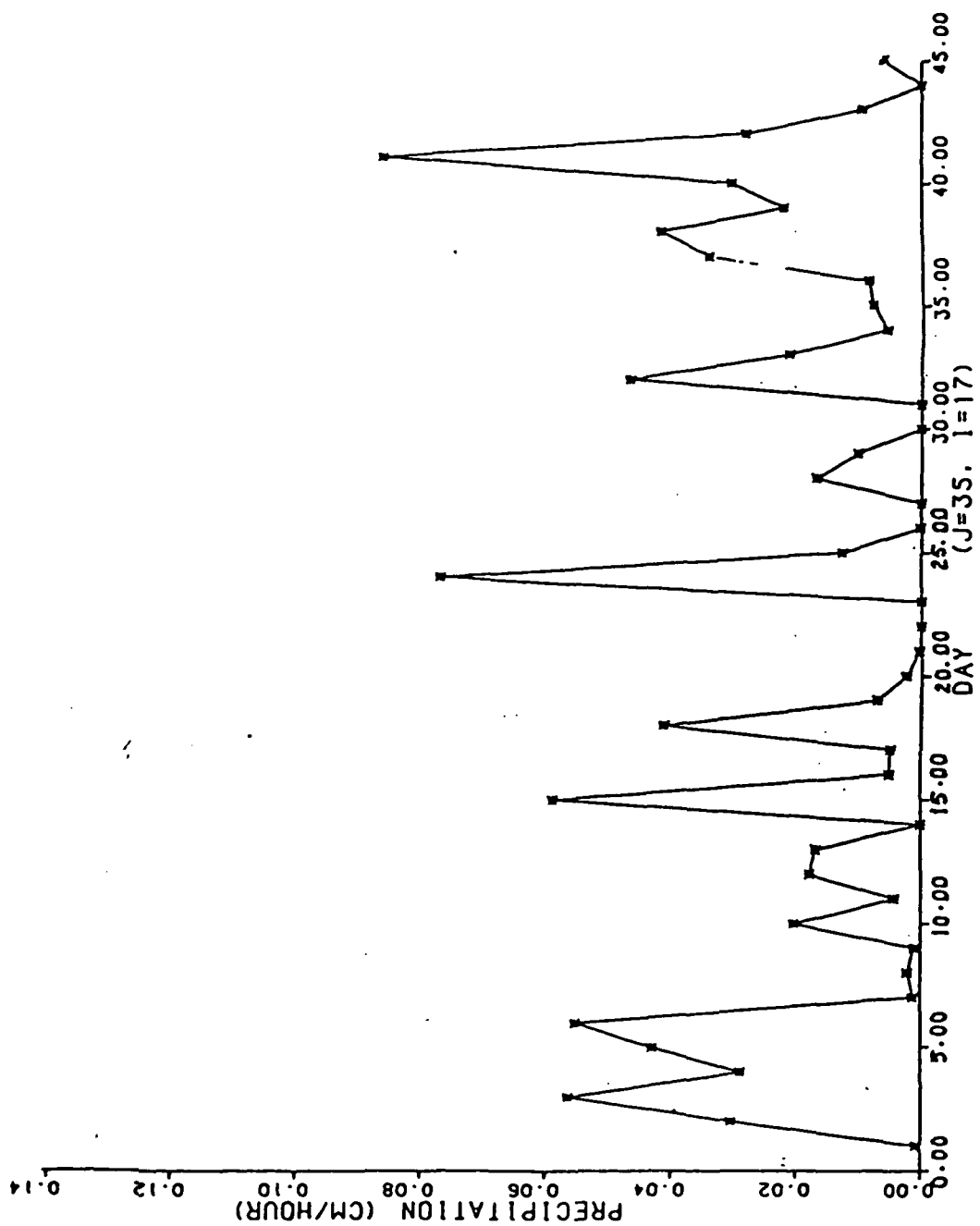
Figure 5.2-8a Precipitation
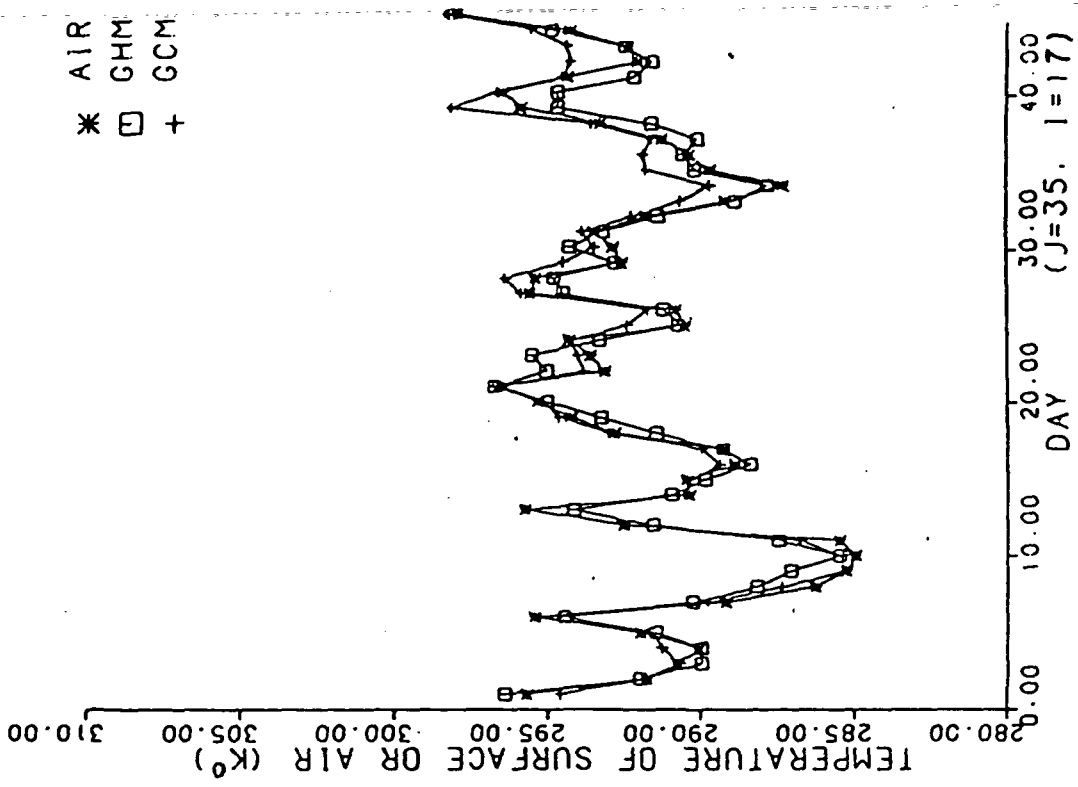
Figure 5.2-8c Comparison of grid surface temperature
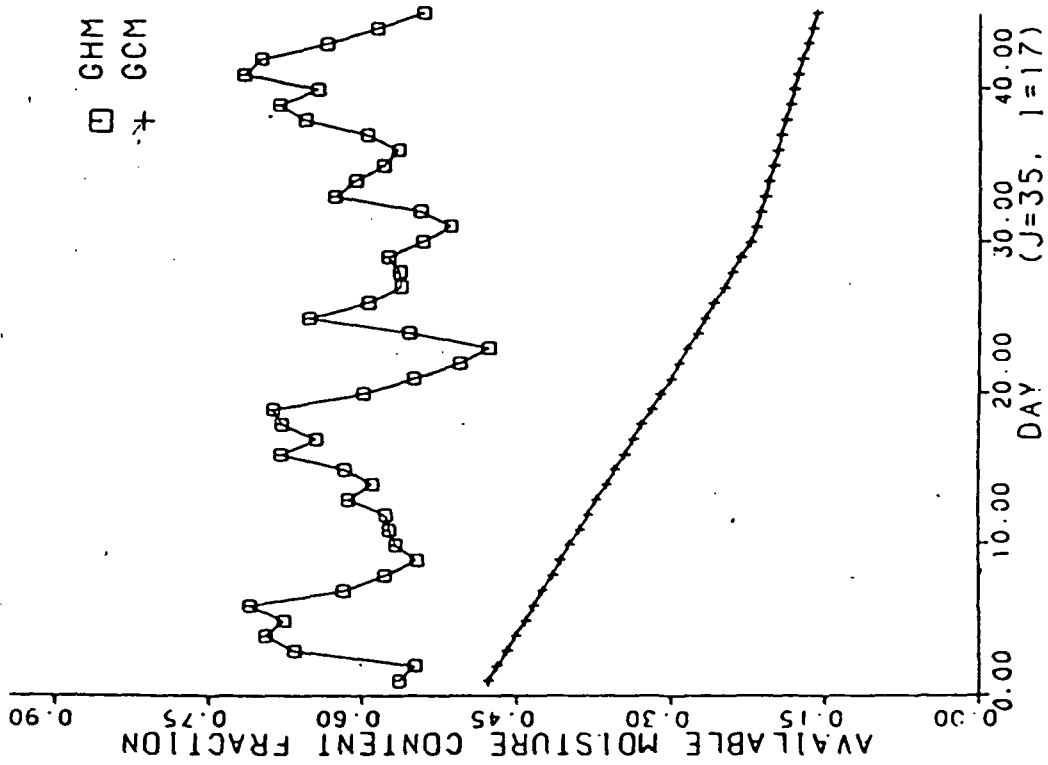
Figure 5.2-8b Comparison of available moisture content fraction

C-3

Figure 5.2-8e Comparison of sensible heat

Figure 5.2-8d Comparison of latent heat
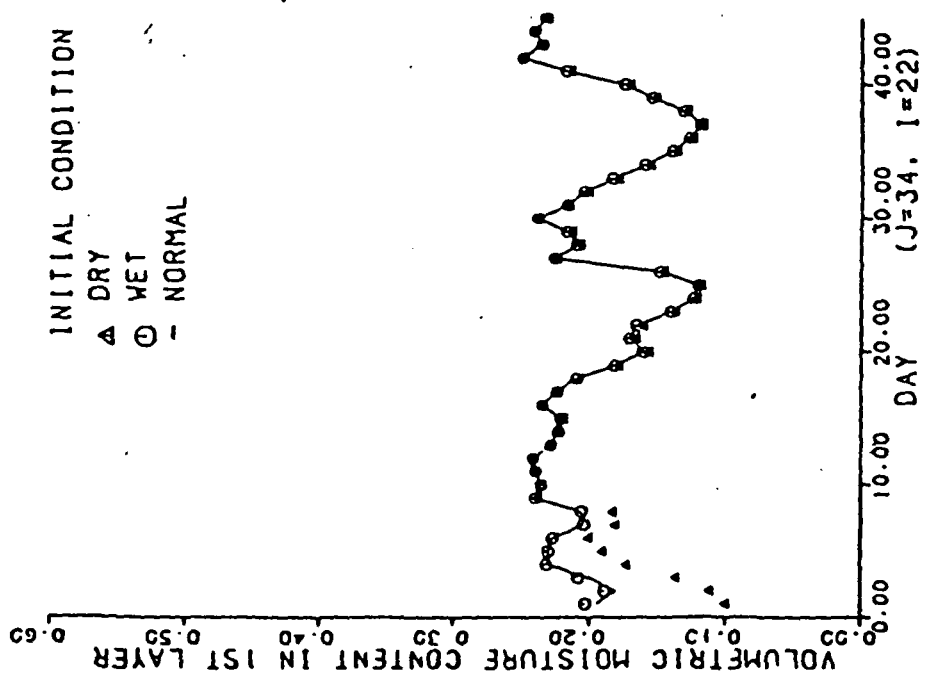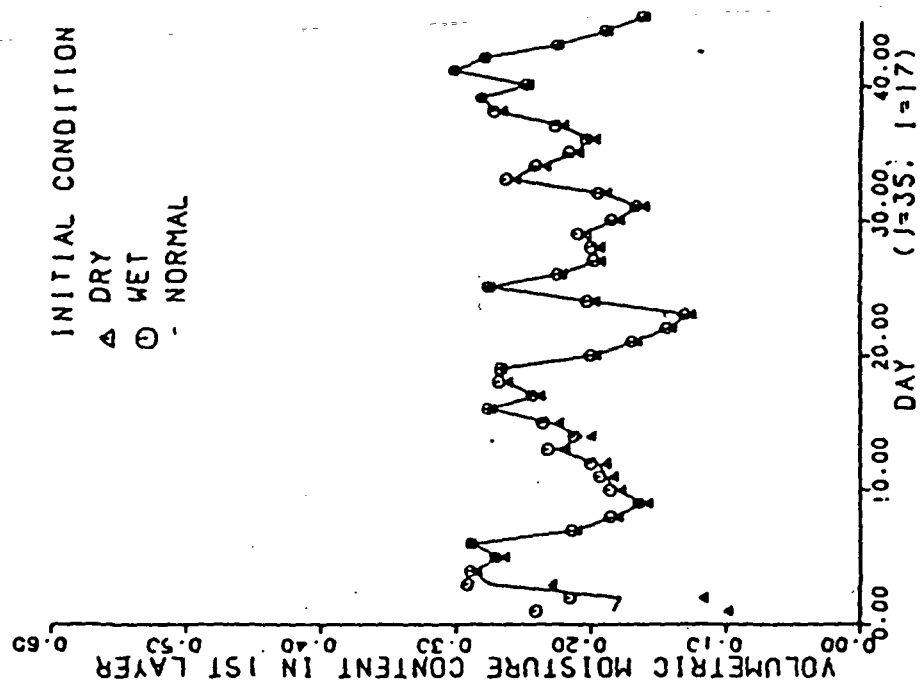
Figure 5.3-1a   Sensitivity to initial condition
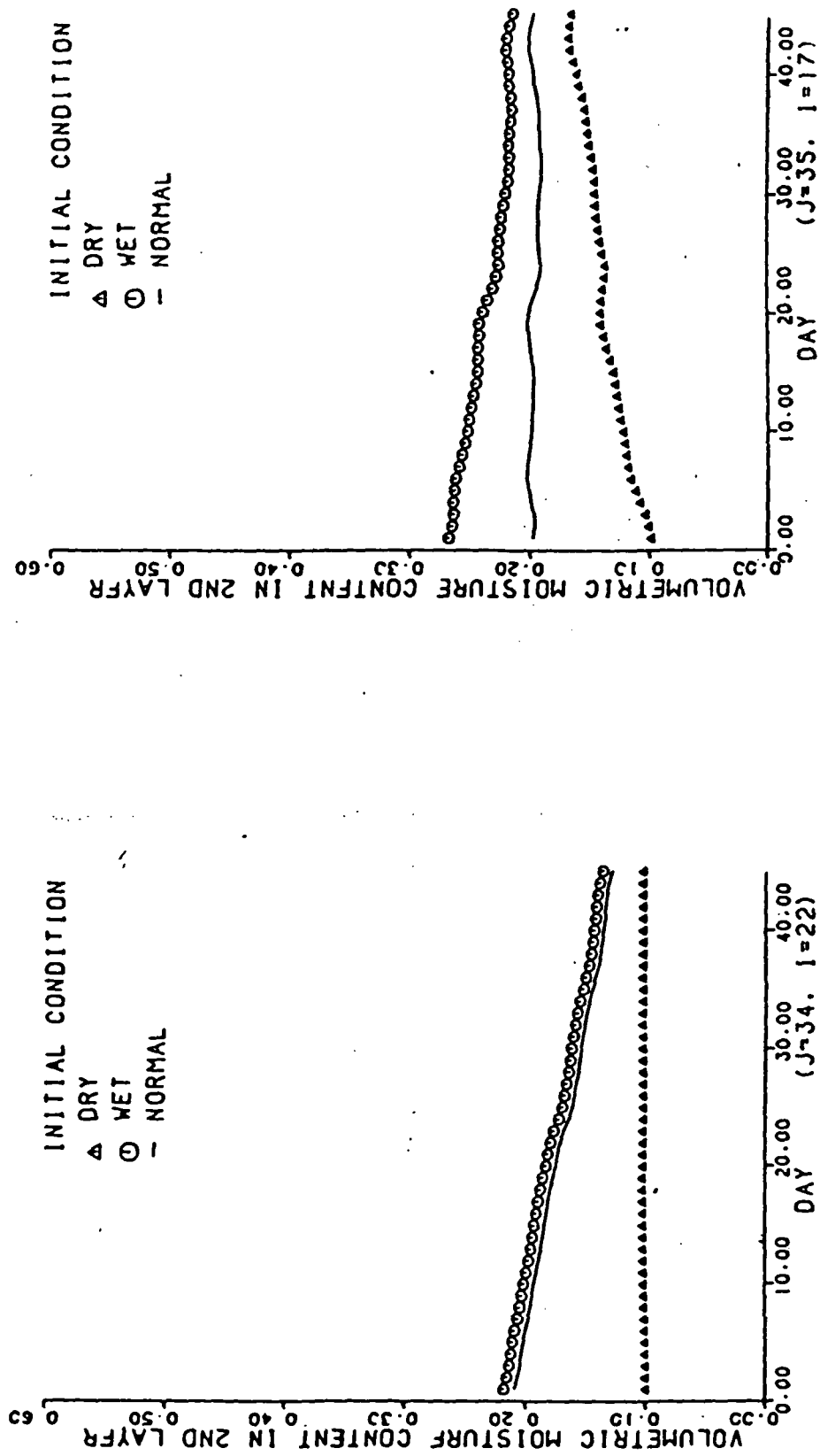
Figure 5.3-1b Sensitivity to initial condition
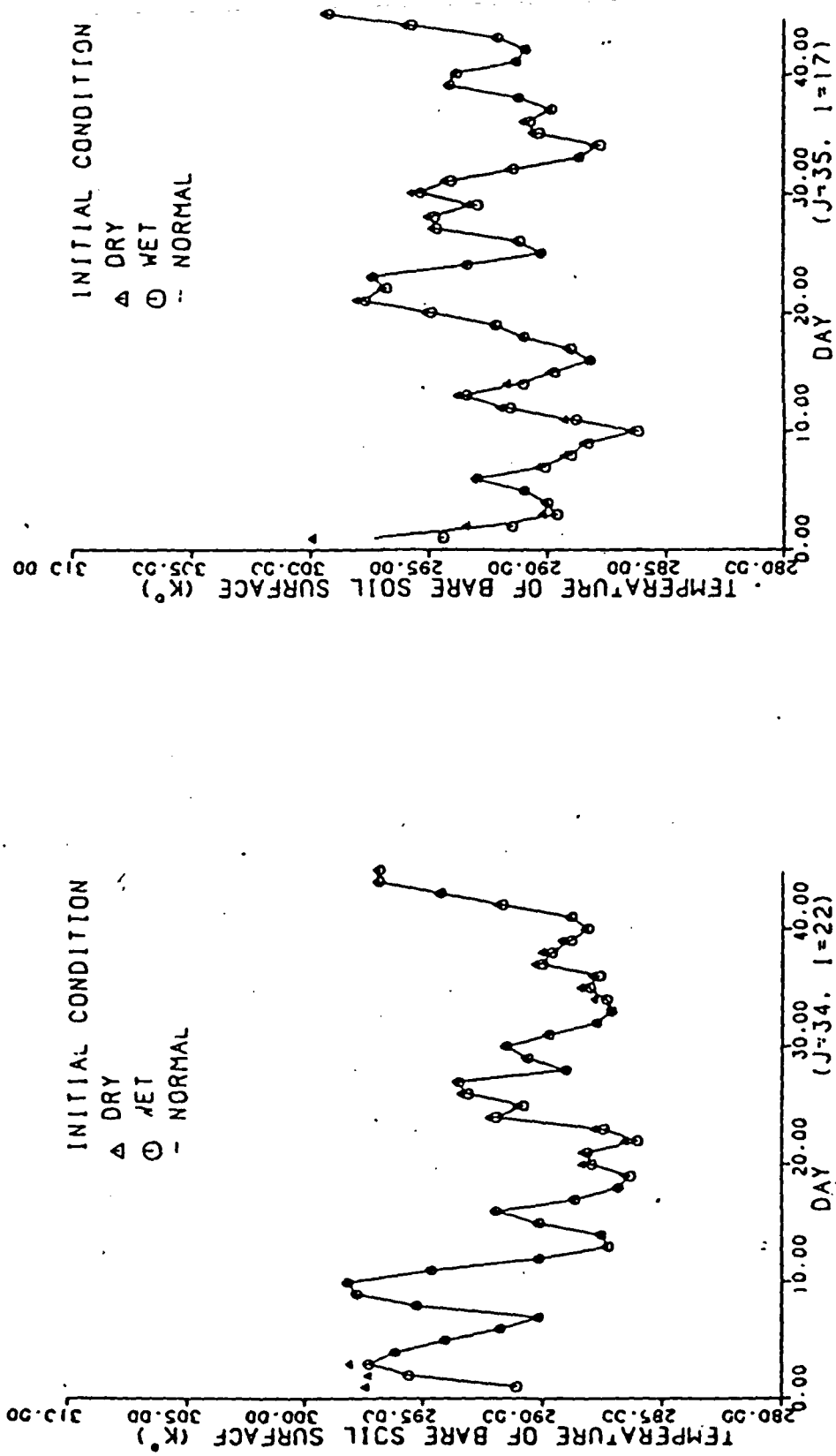
Figure 5.3-1c Sensitivity to initial condition
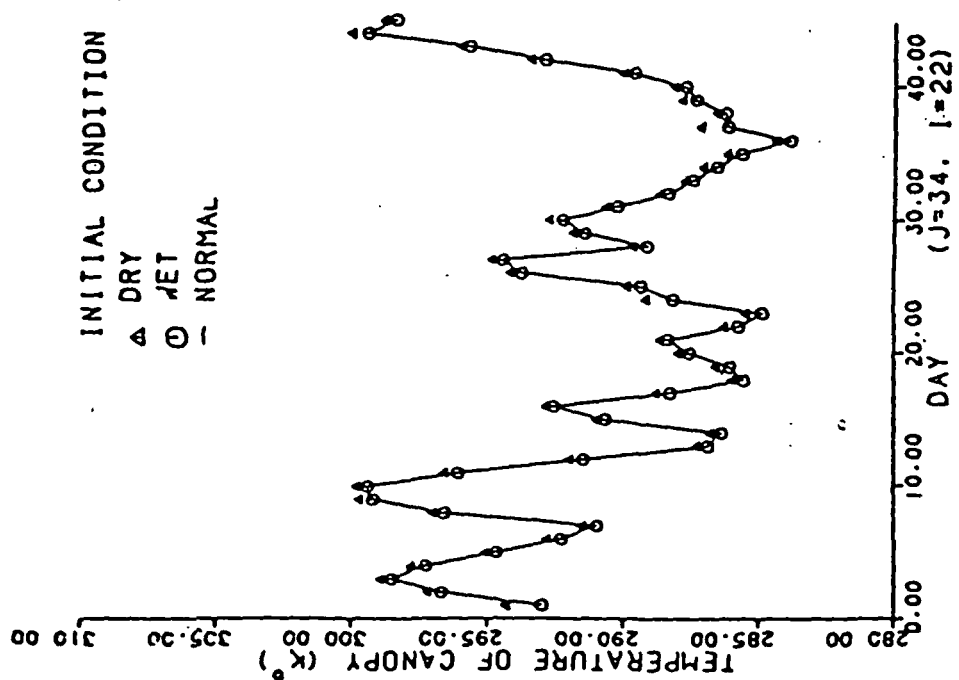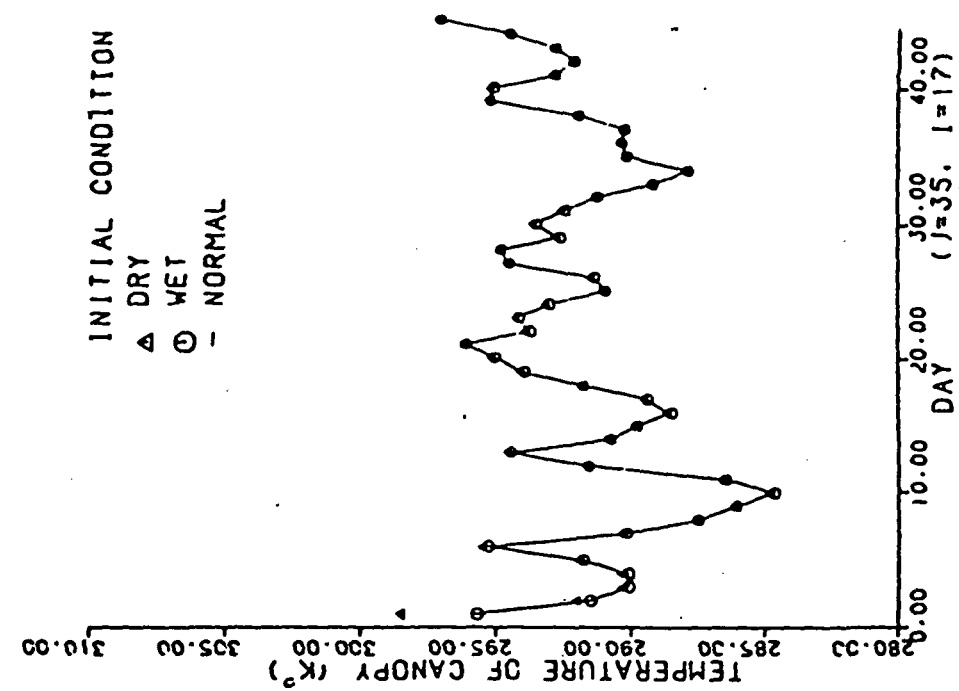
Figure 5.3-1d   Sensitivity to initial condition
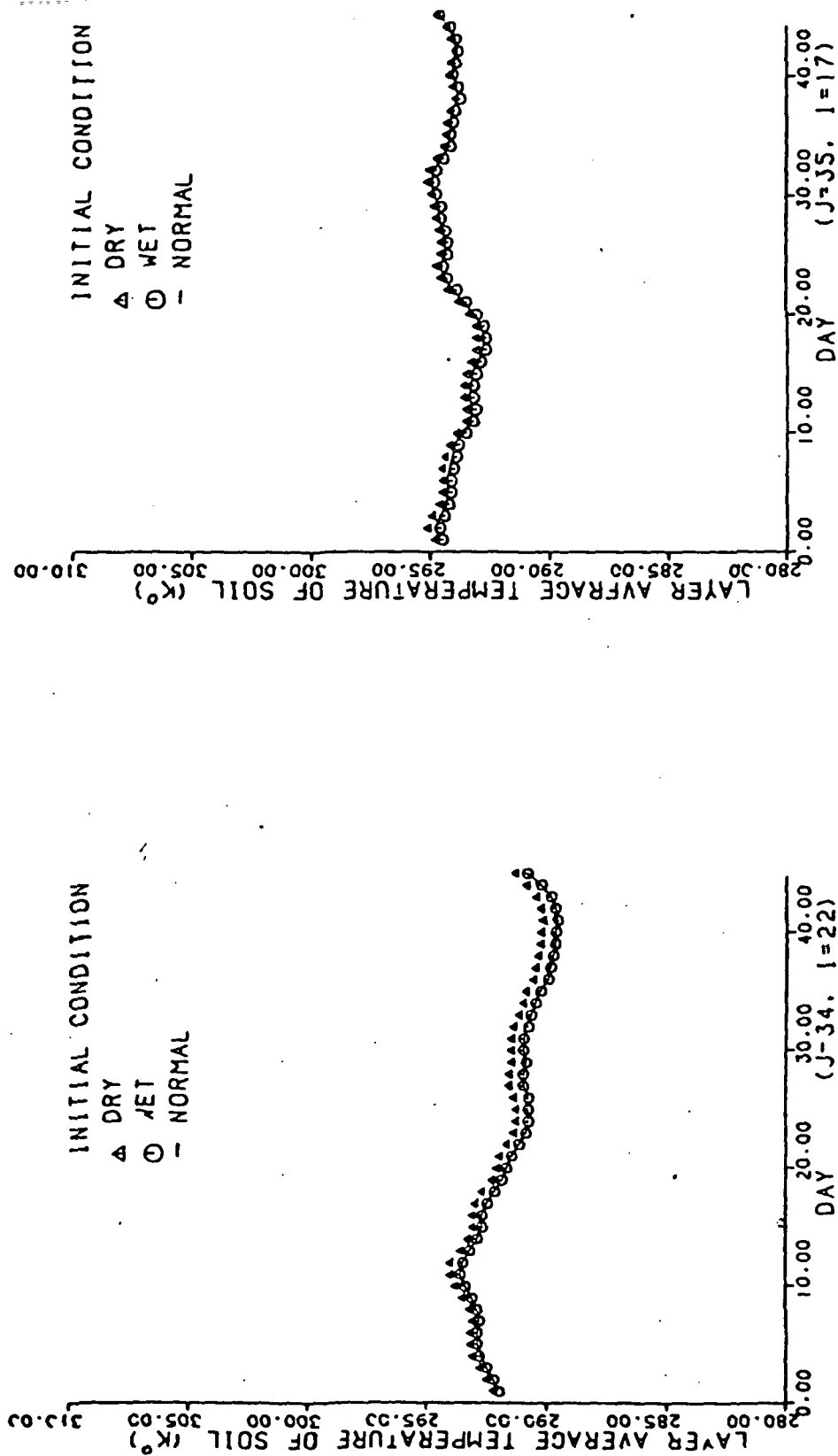
Figure 5.3-1e   Sensitivity to initial condition
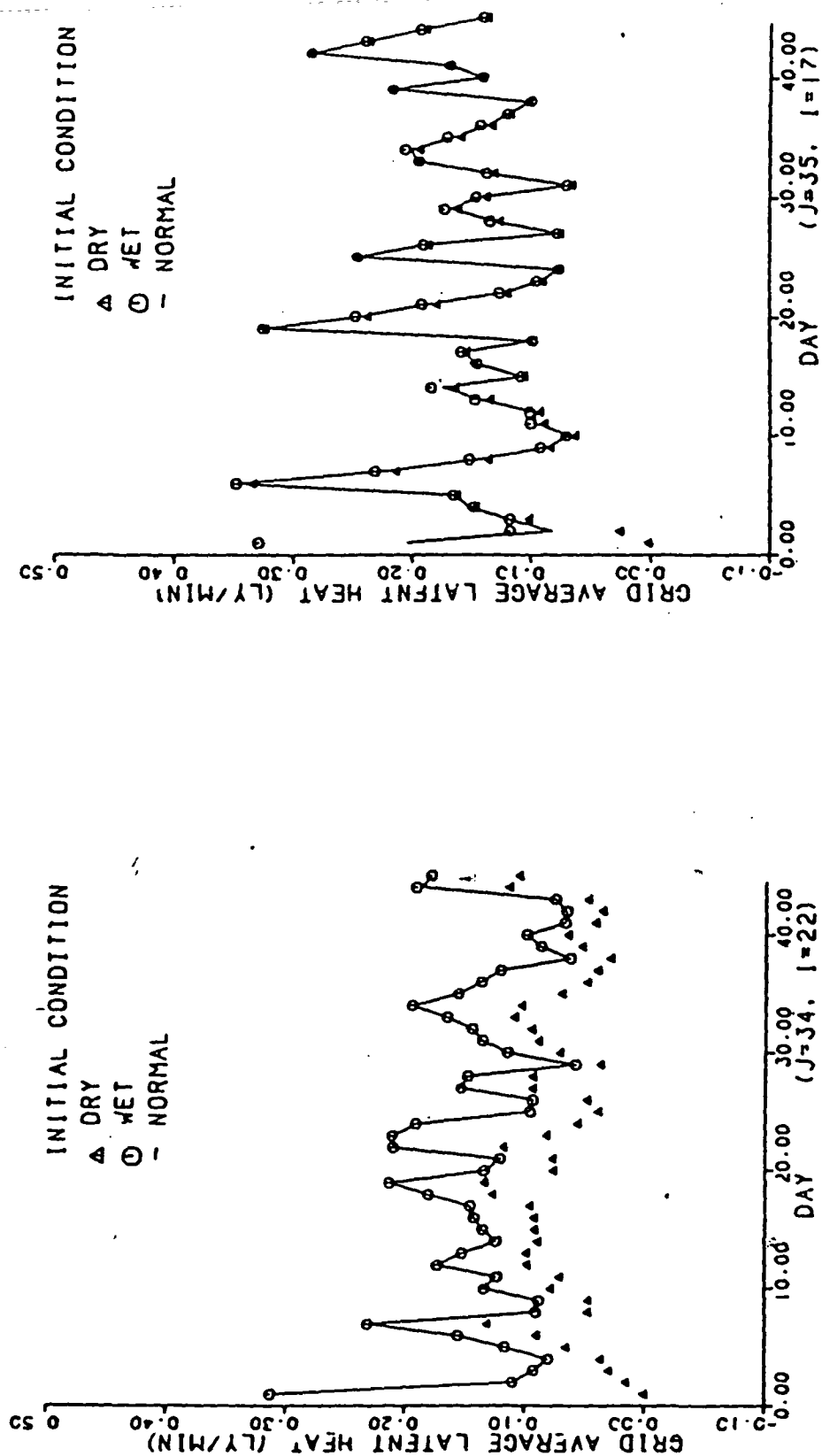
Figure 5.3-1f Sensitivity to initial condition
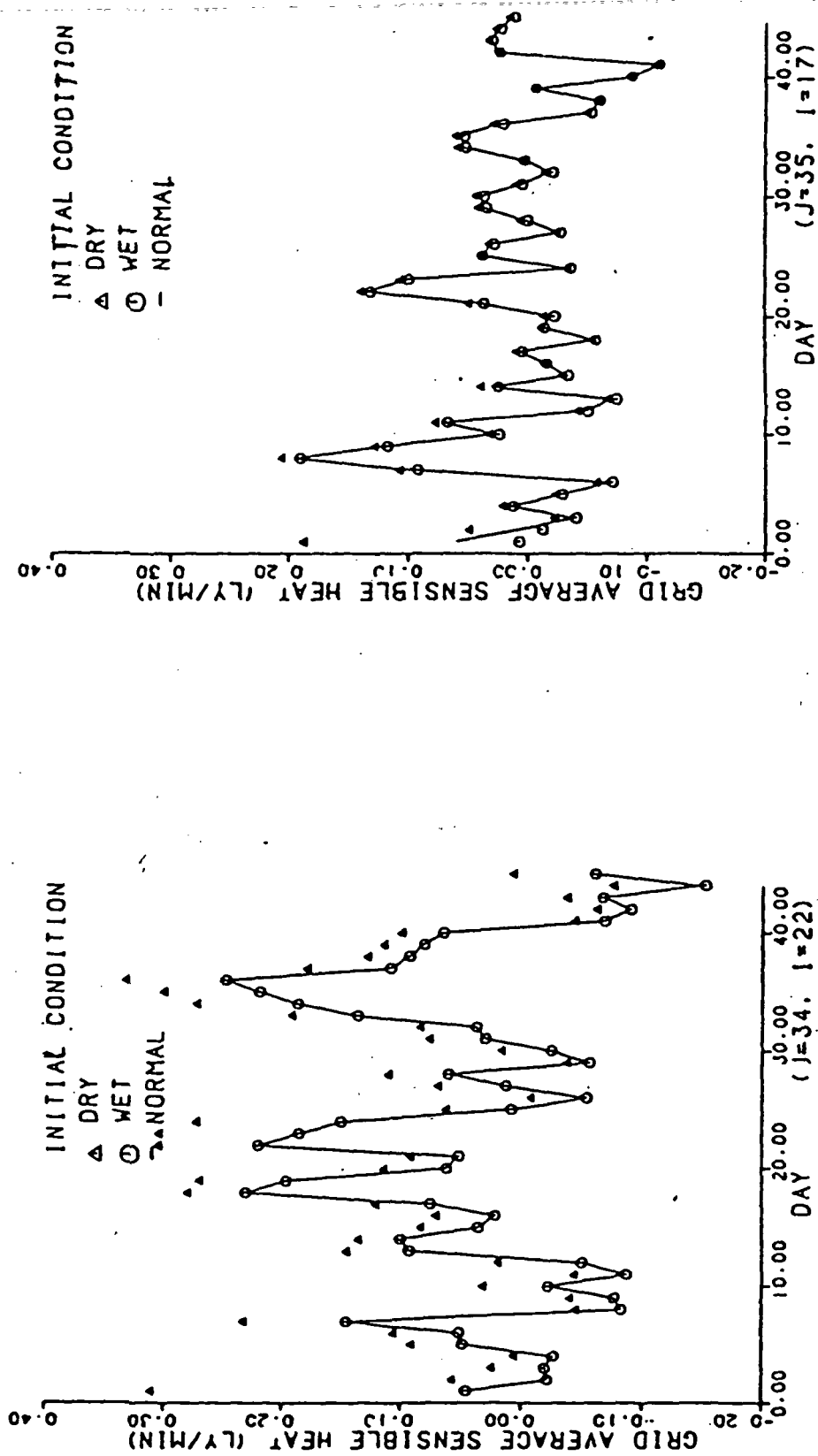
Figure 5.3-1g   Sensitivity to initial condition
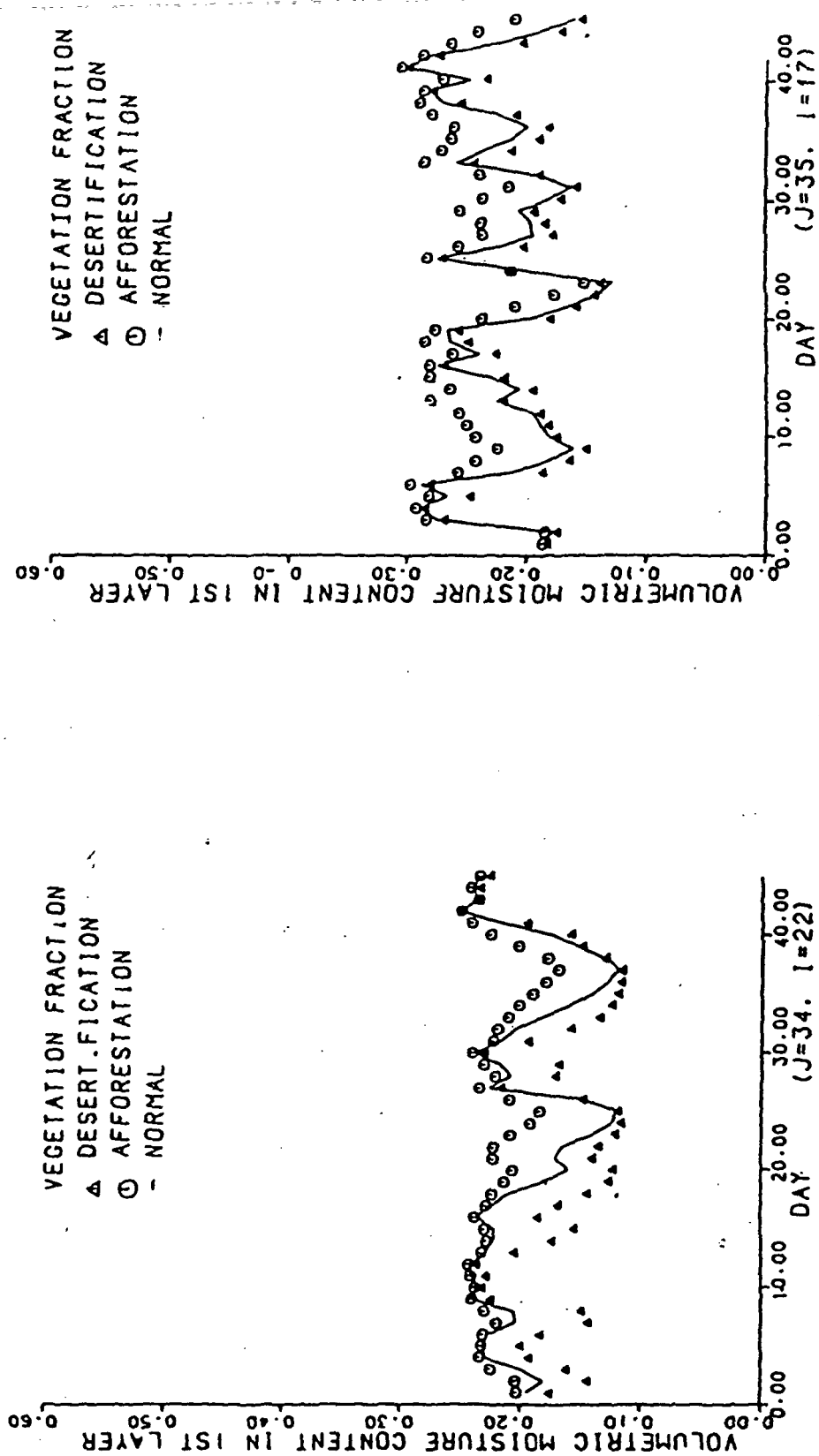
Figure 5.3-2a   Sensitivity to vegetation fraction
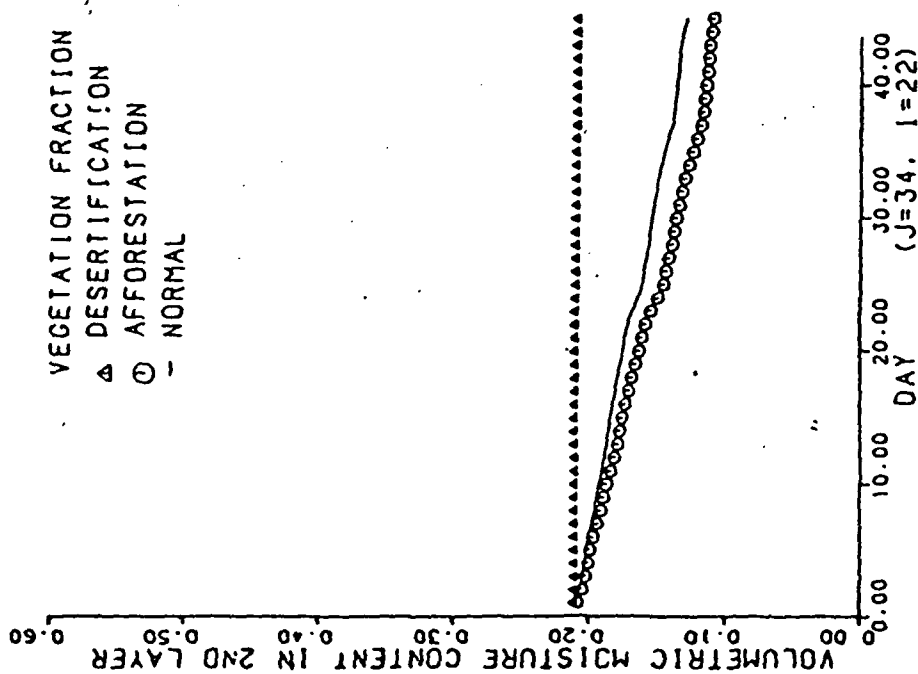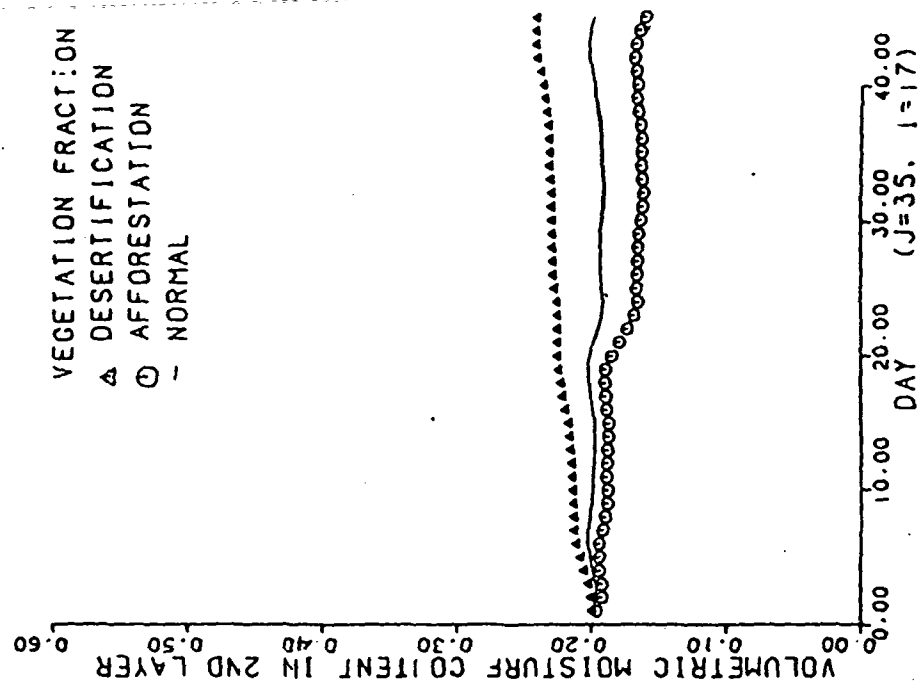
Figure 5.3-2b Sensitivity to vegetation fraction
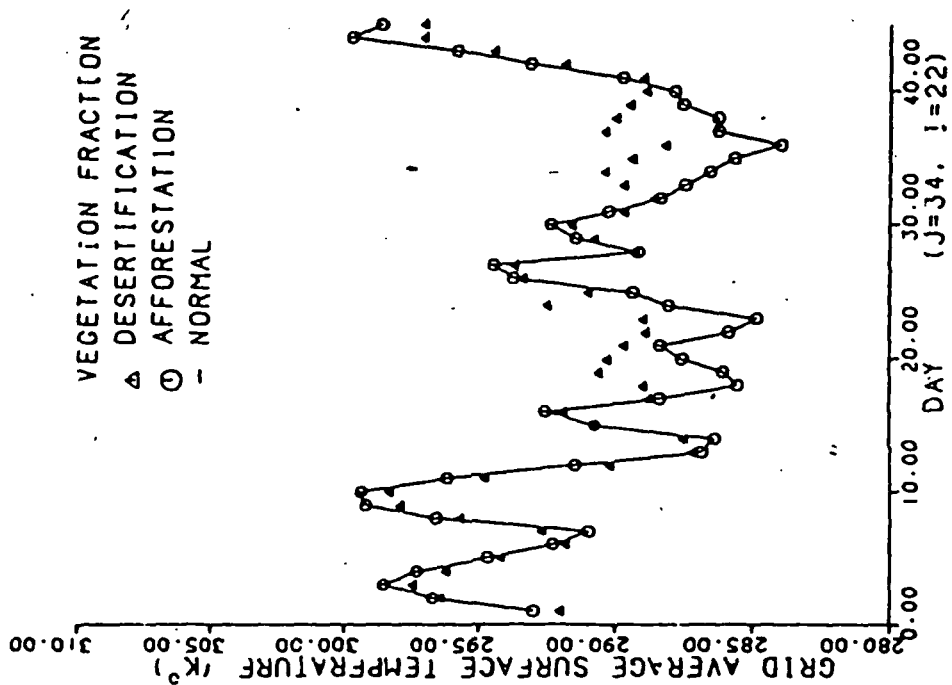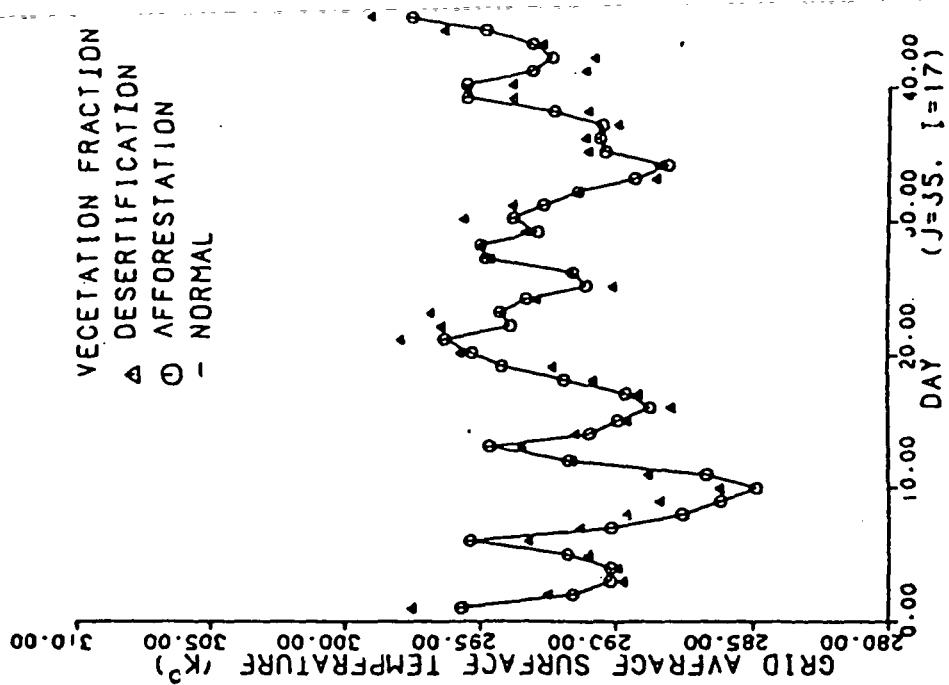
Figure 5.3-2c Sensitivity to vegetation fraction
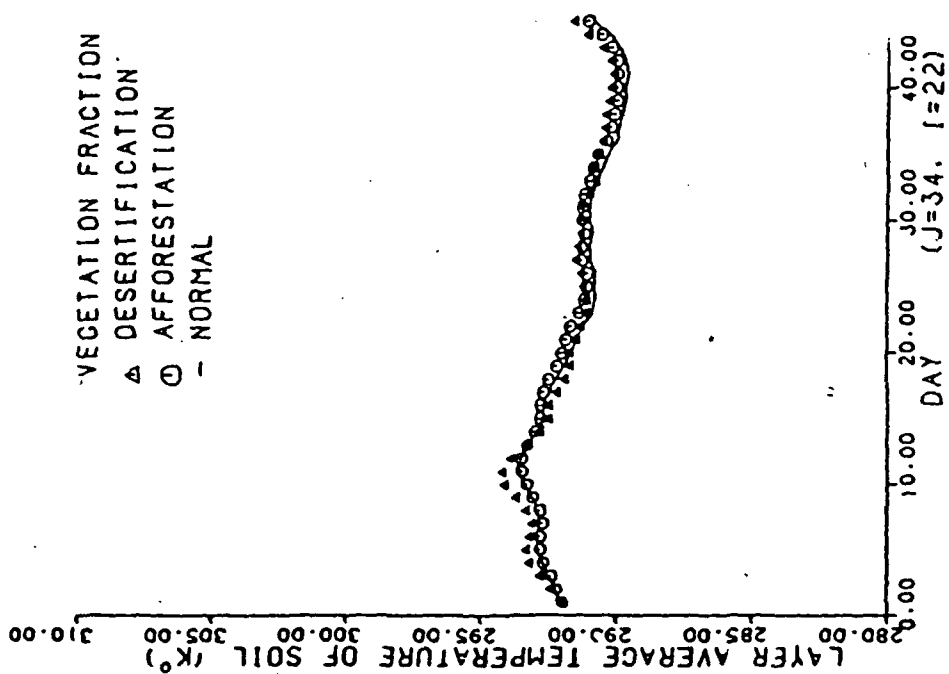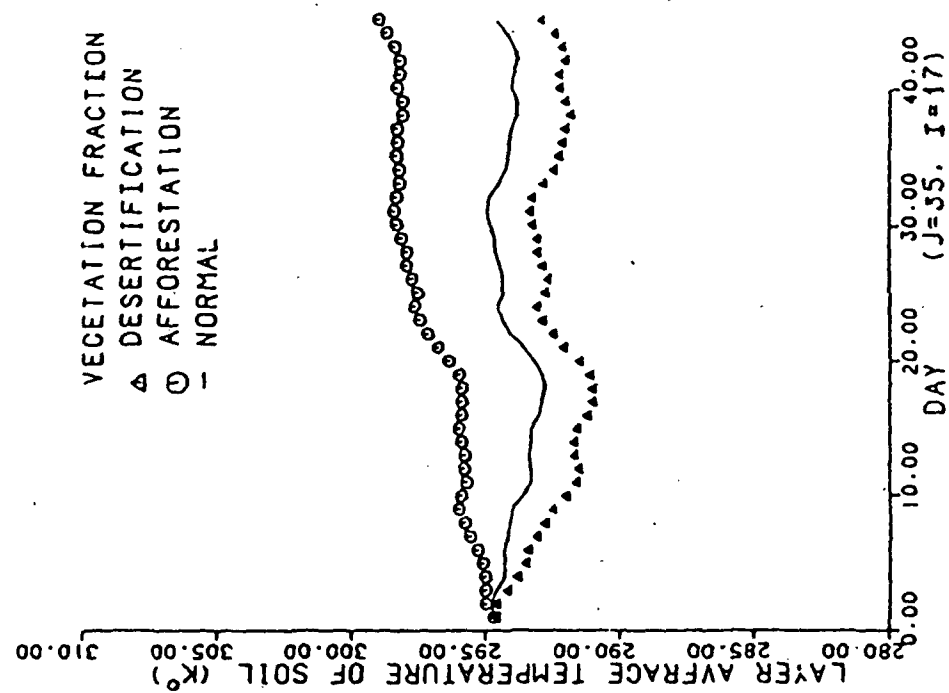
Figure 5.3-2e Sensitivity to vegetation fraction
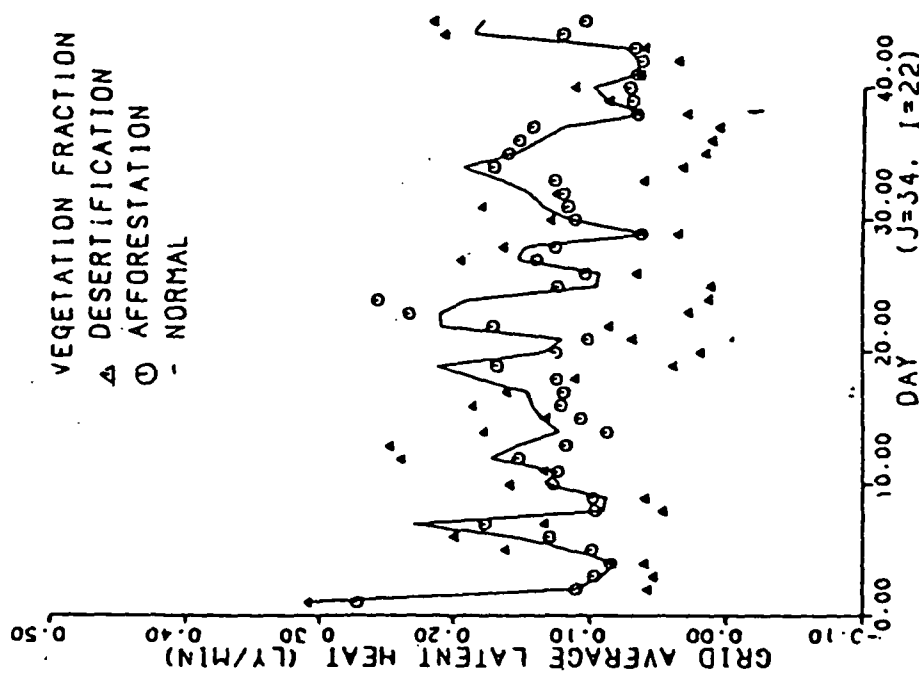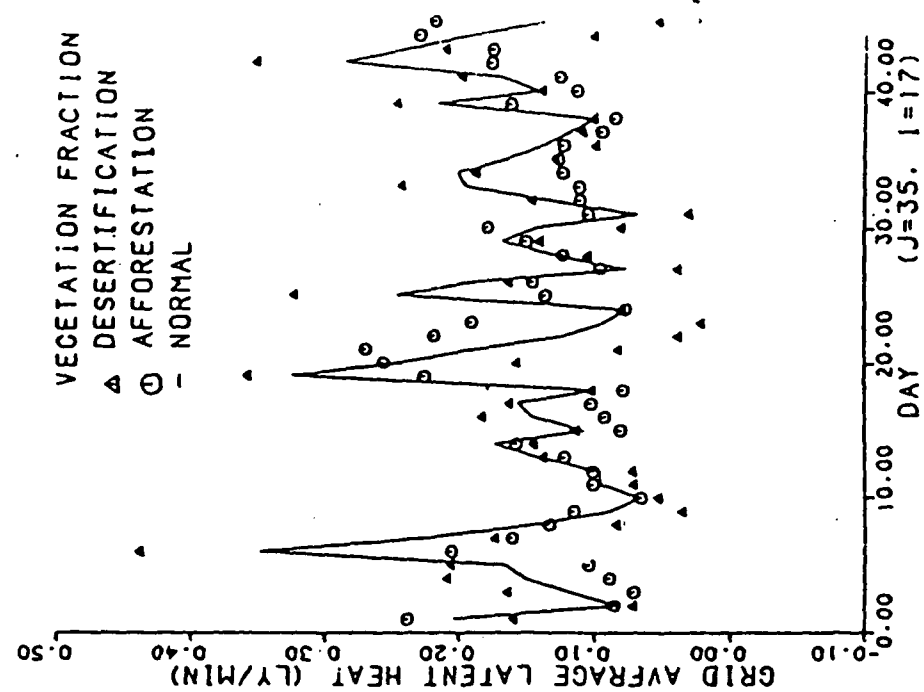
Figure 5.3-2f Sensitivity to vegetation fraction
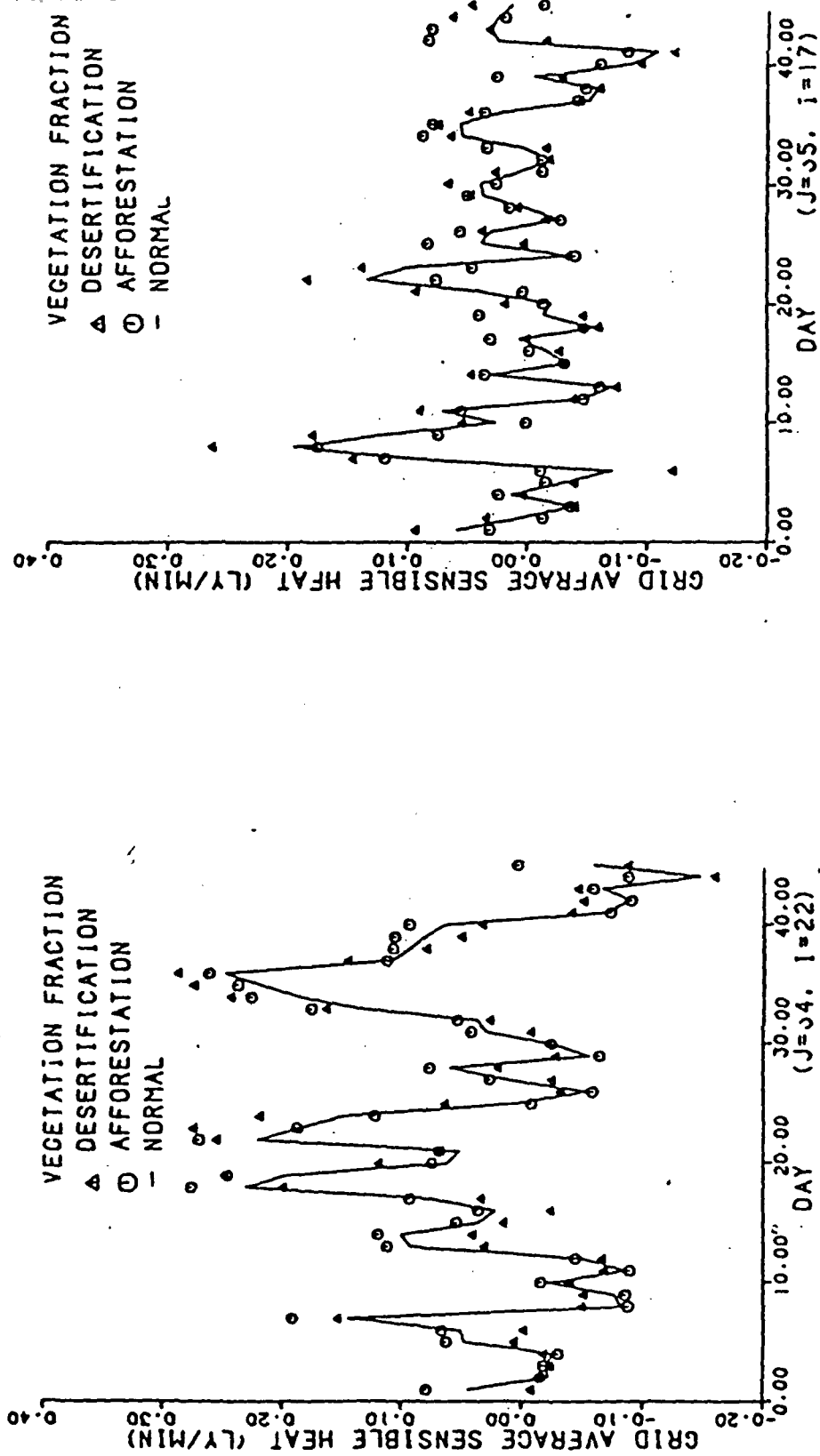
Figure 5.3-2g Sensitivity to vegetation fraction

185
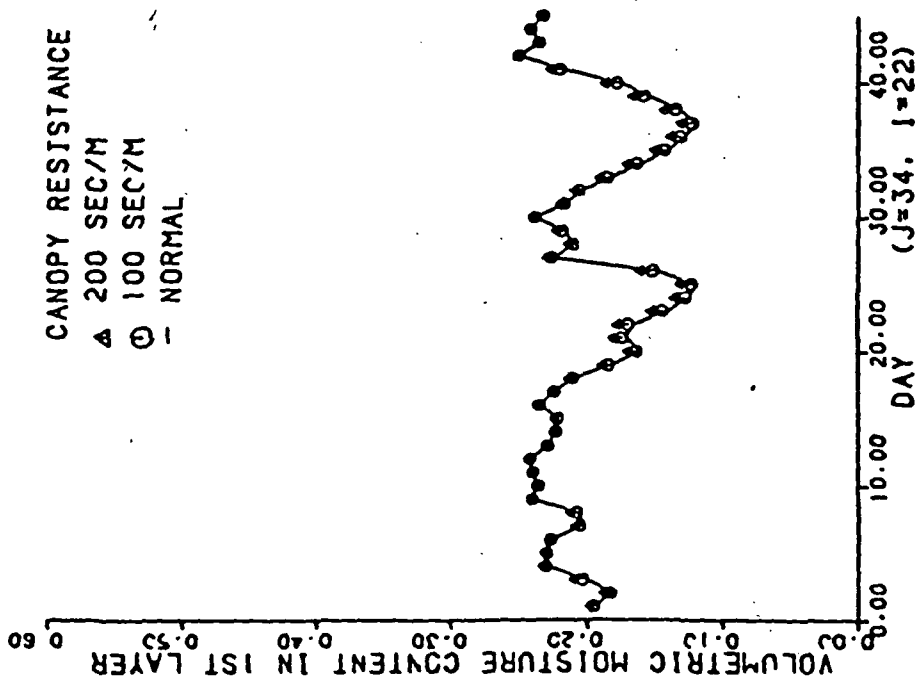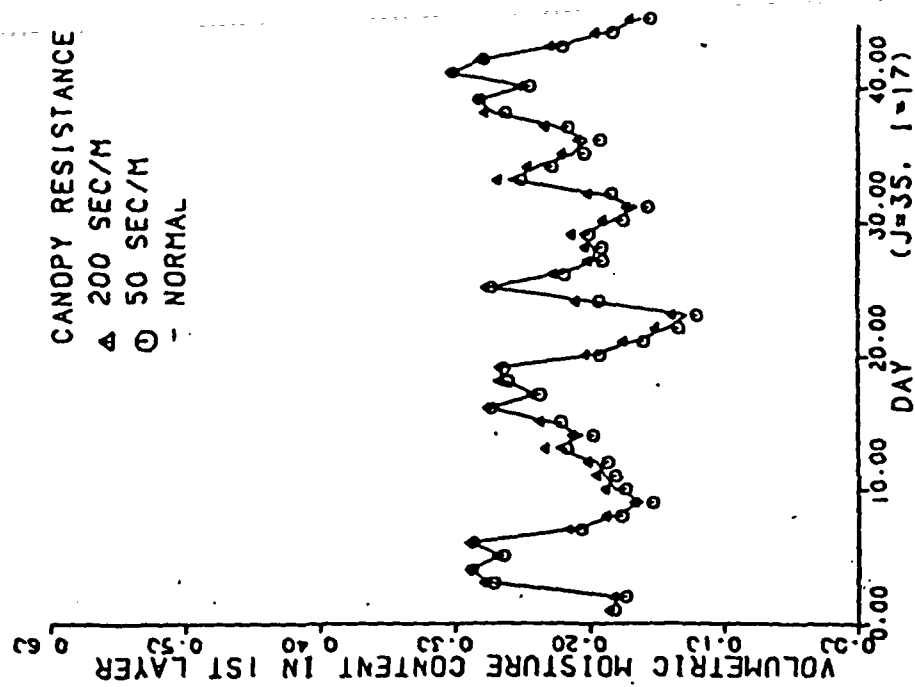
Figure 5.3-3a Sensitivity to canopy resistance
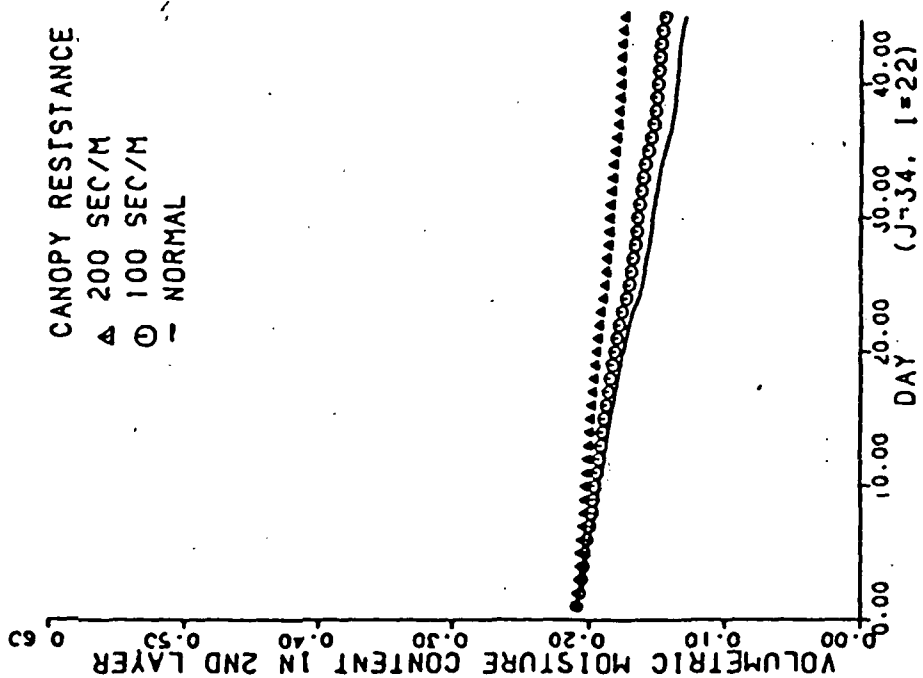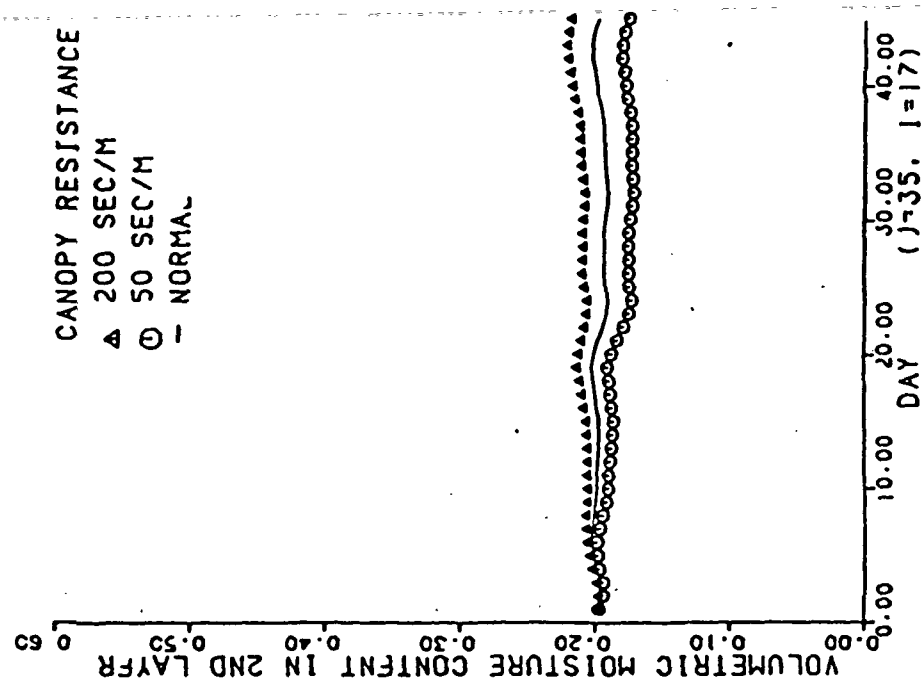
Figure 5.3-3b Sensitivity to canopy resistance
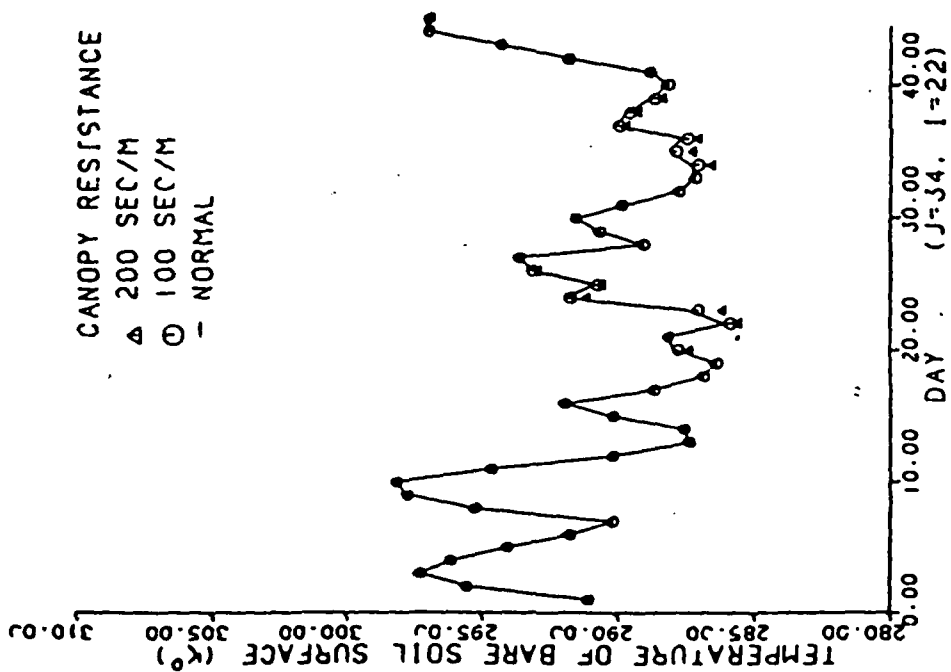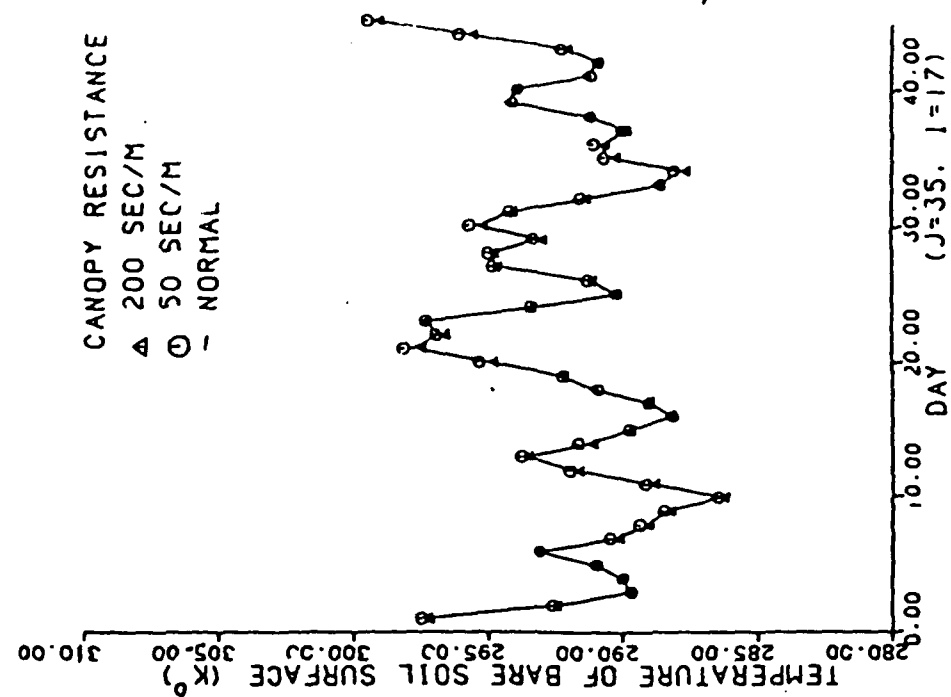
Figure 5.3-3c Sensitivity to canopy resistance
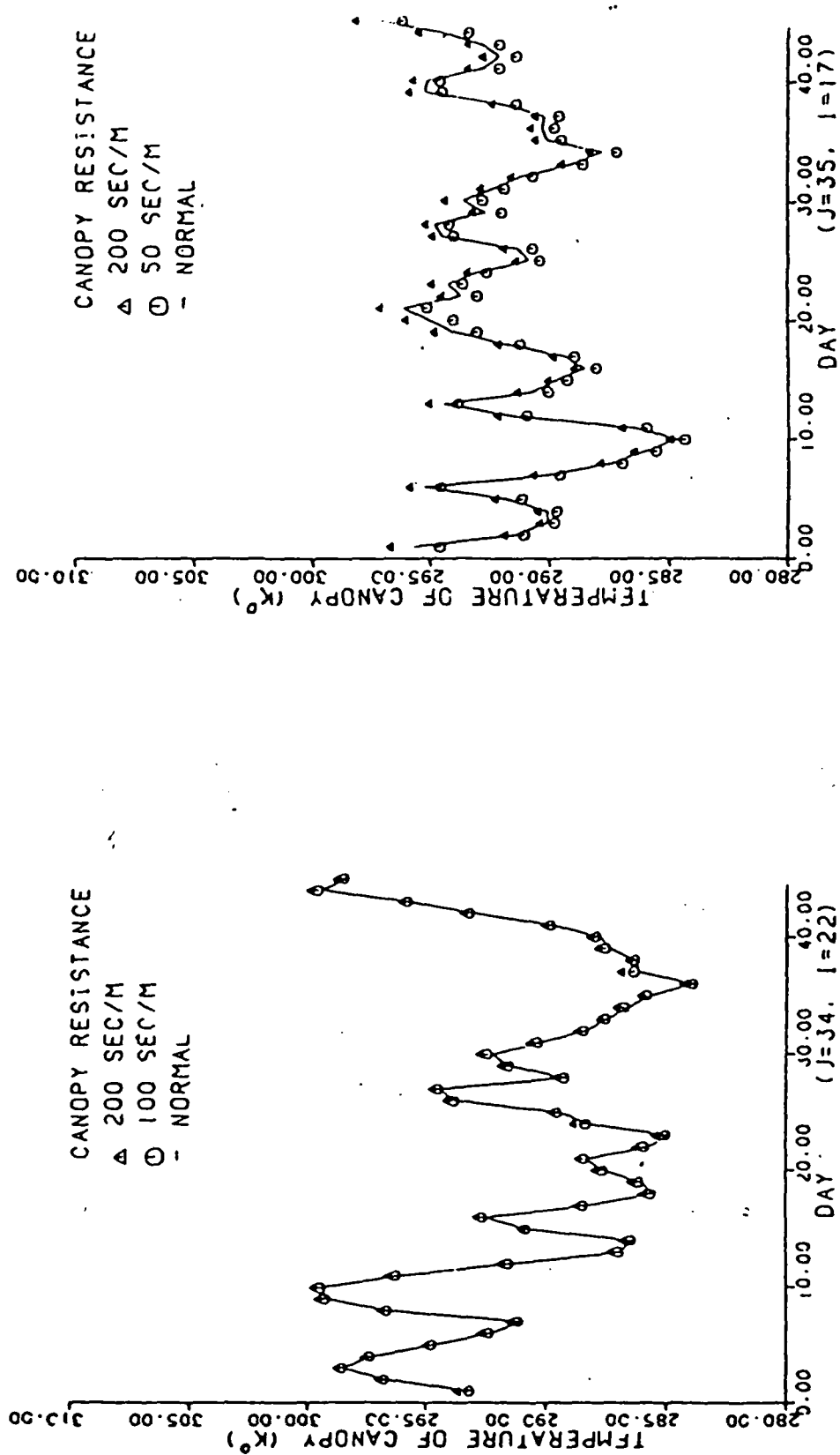
Figure 5.3-3d Sensitivity to canopy resistance
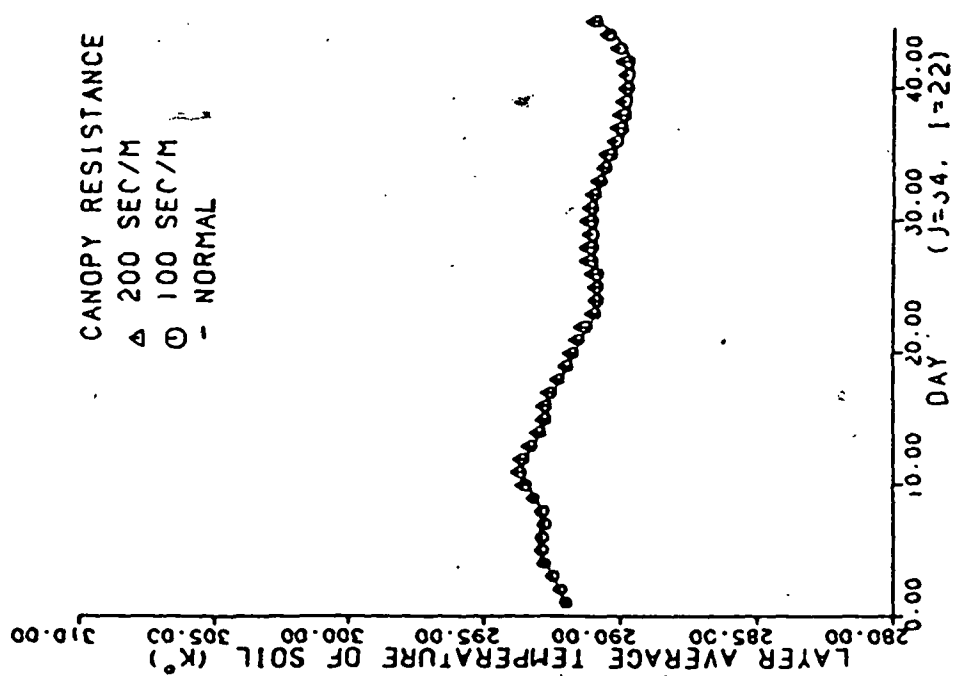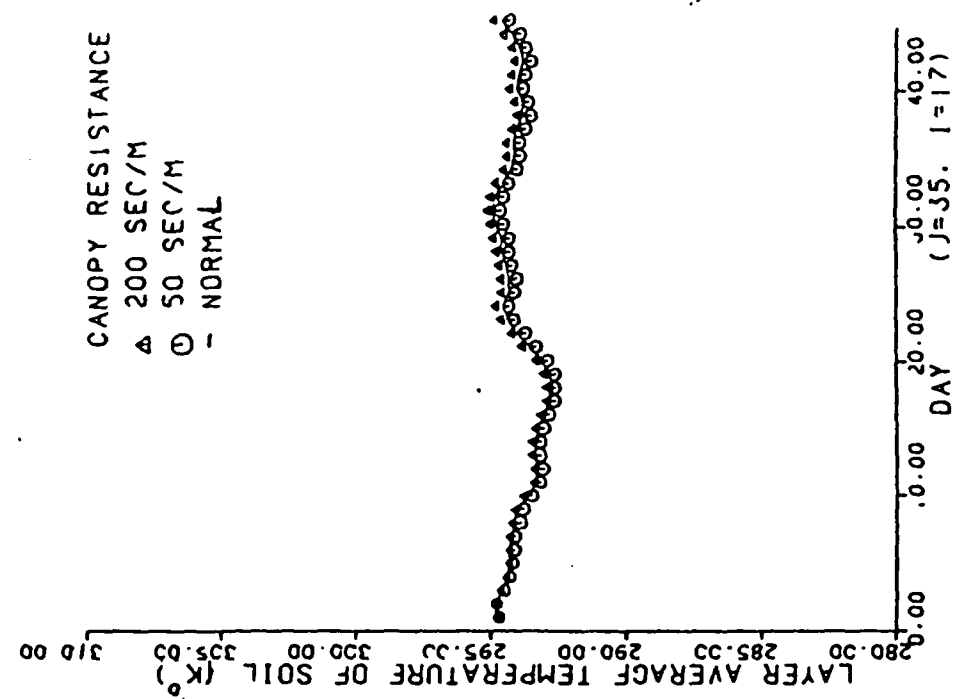
Figure 5.3-3e   Sensitivity to canopy resistance
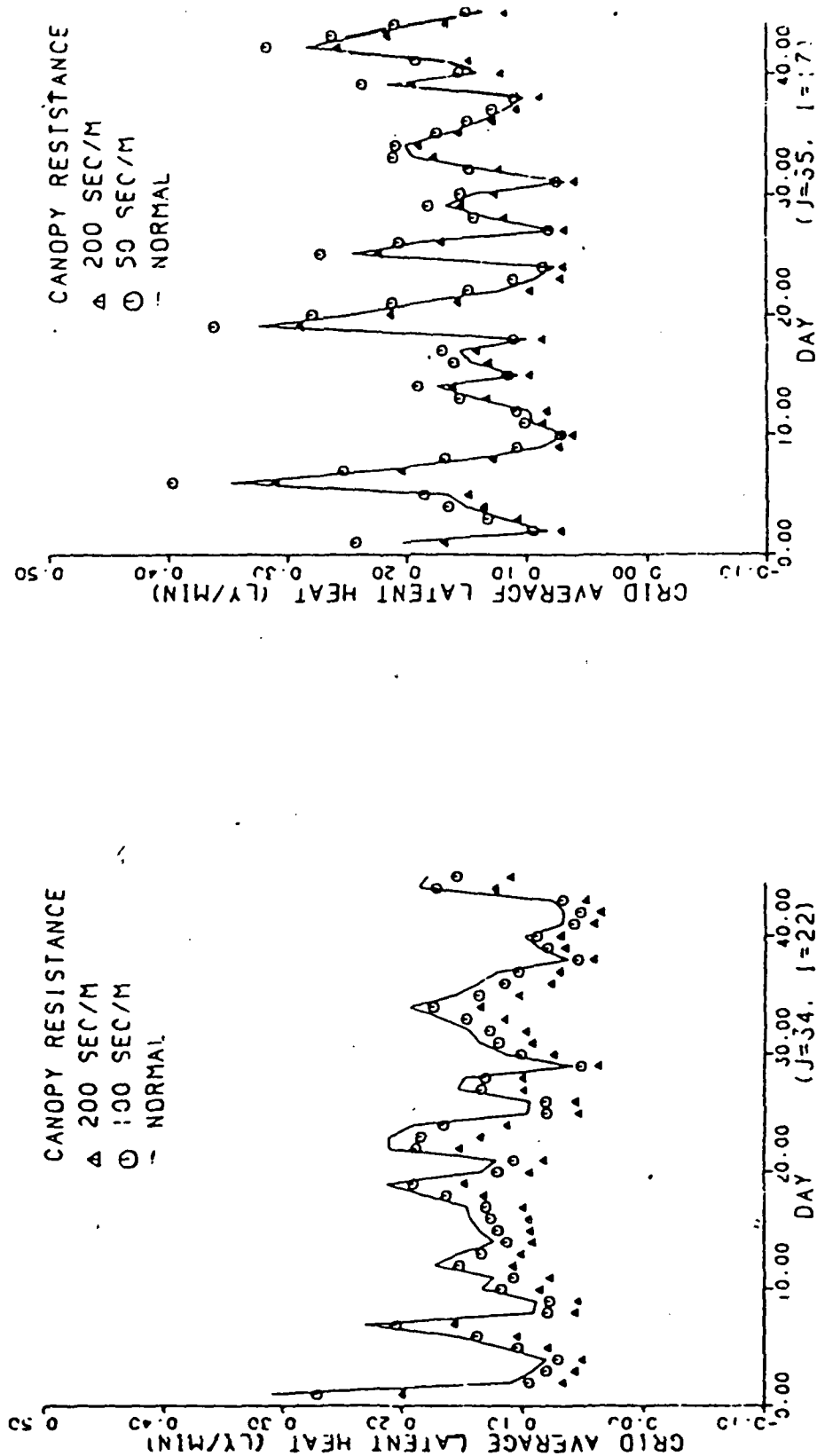
Figure 5.3-3f Sensitivity to canopy resistance
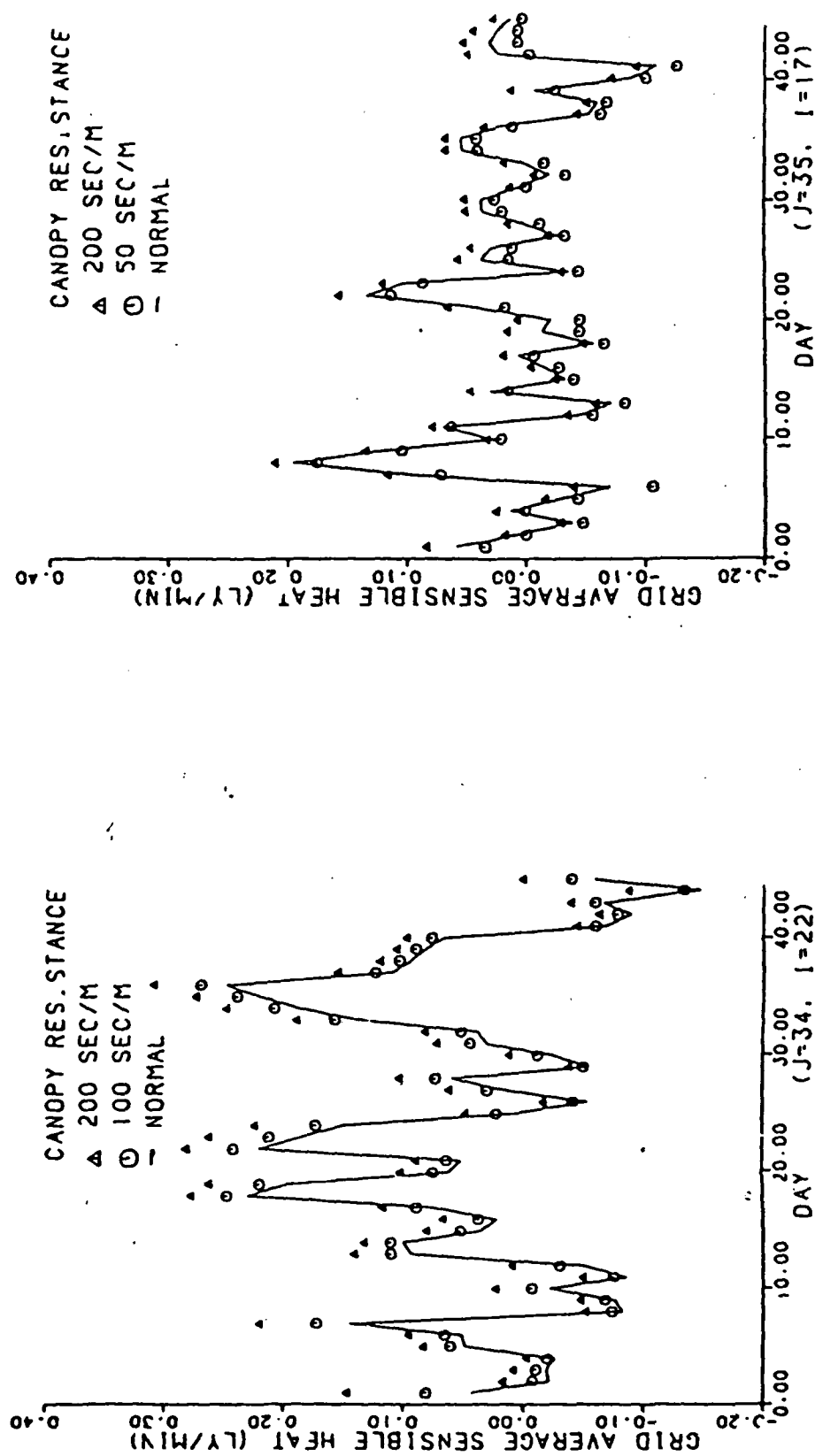
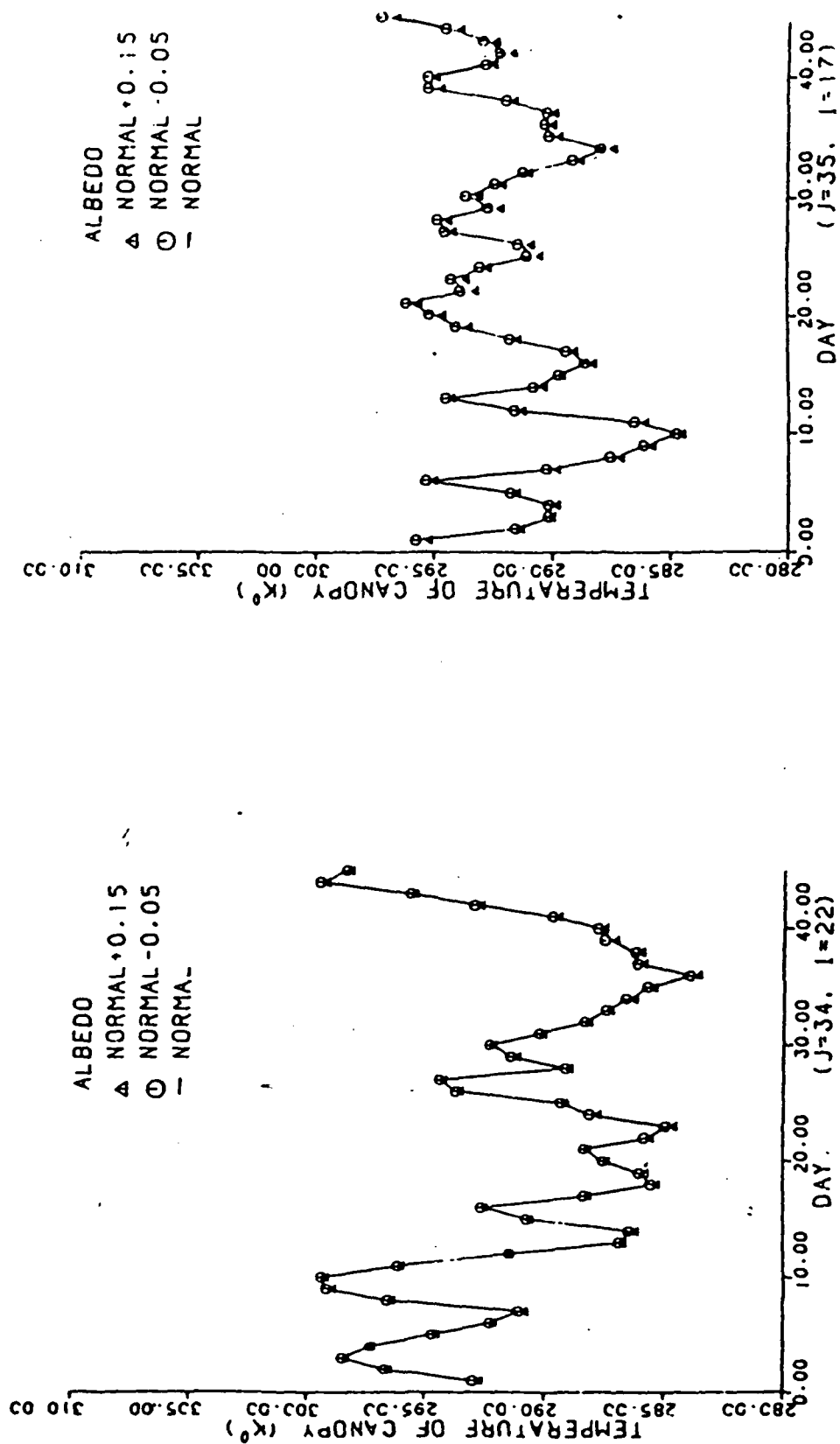Figure 5.3-3g   Sensitivity to canopy resistance
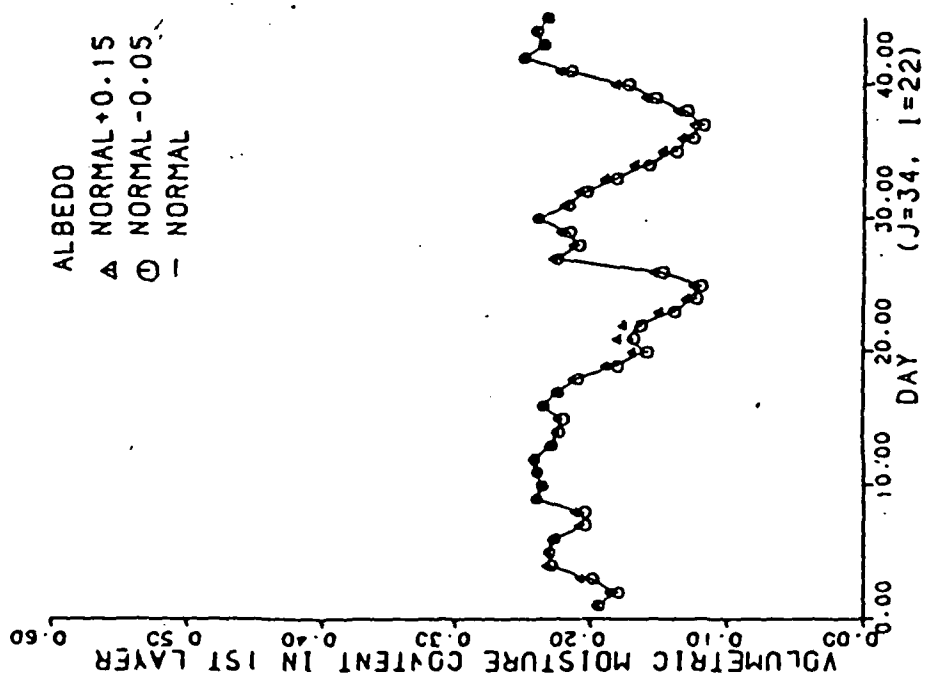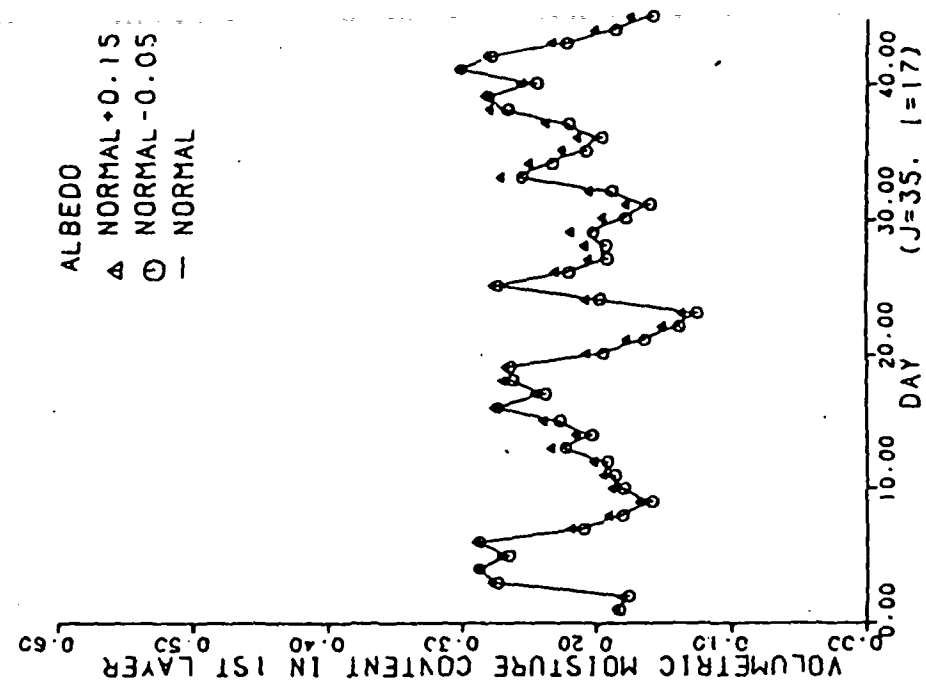
Figure 5.3-4a Sensitivity to albedo
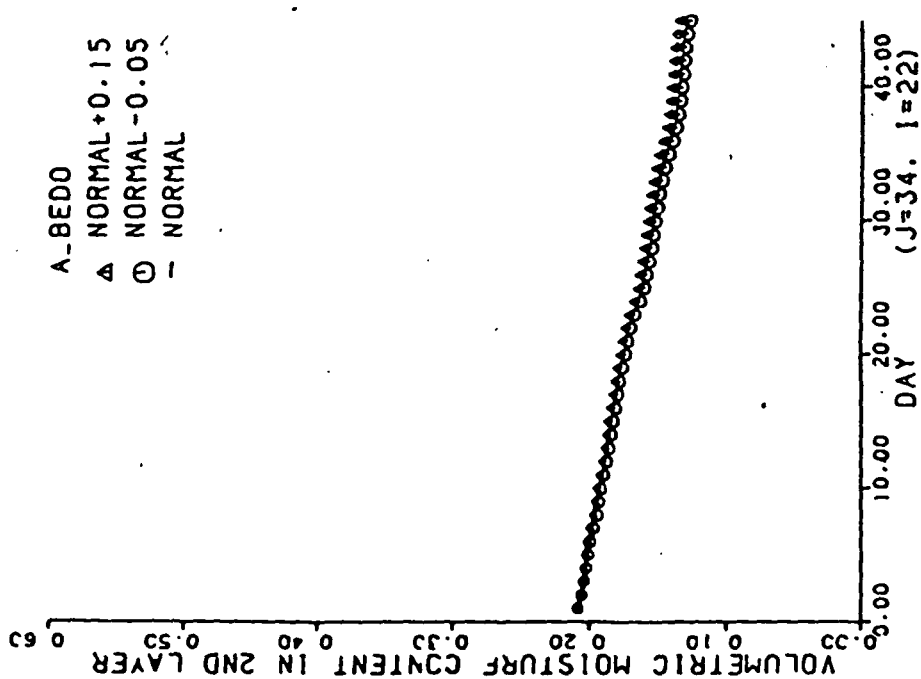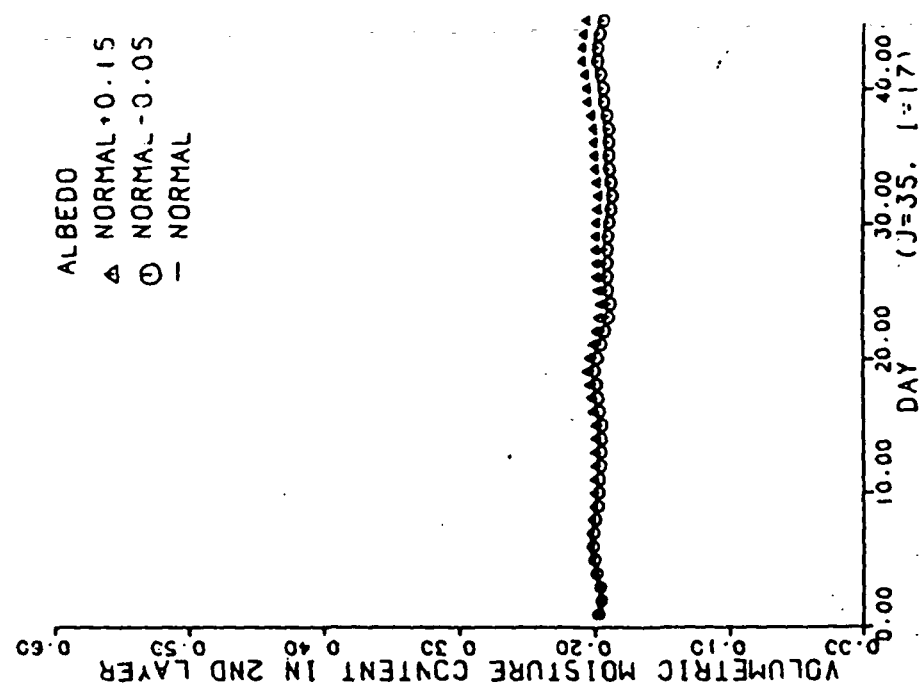
Figure 5.3-4b Sensitivity to albedo
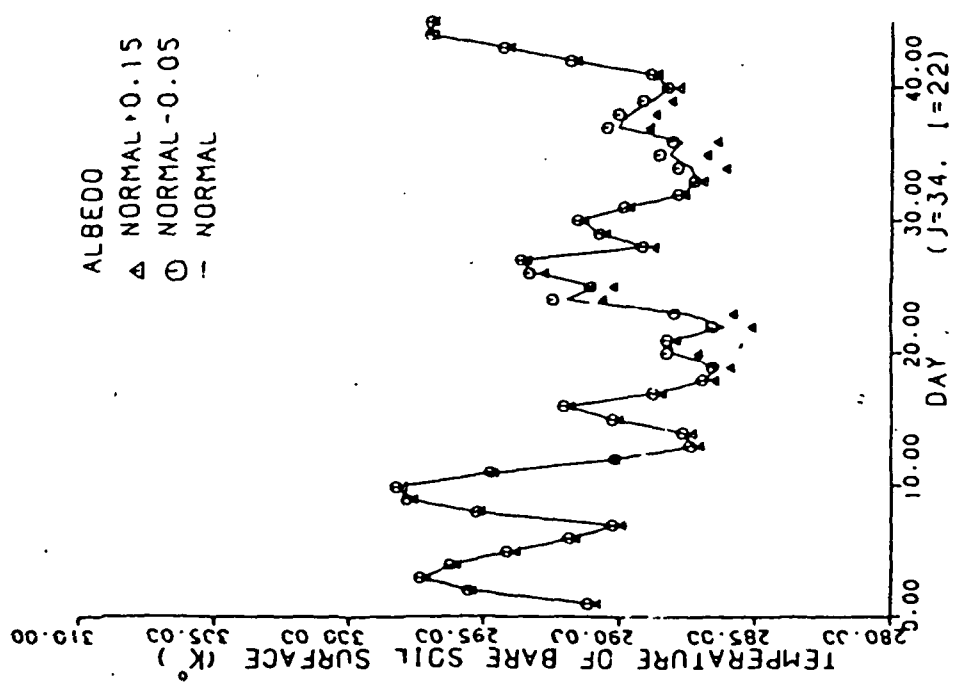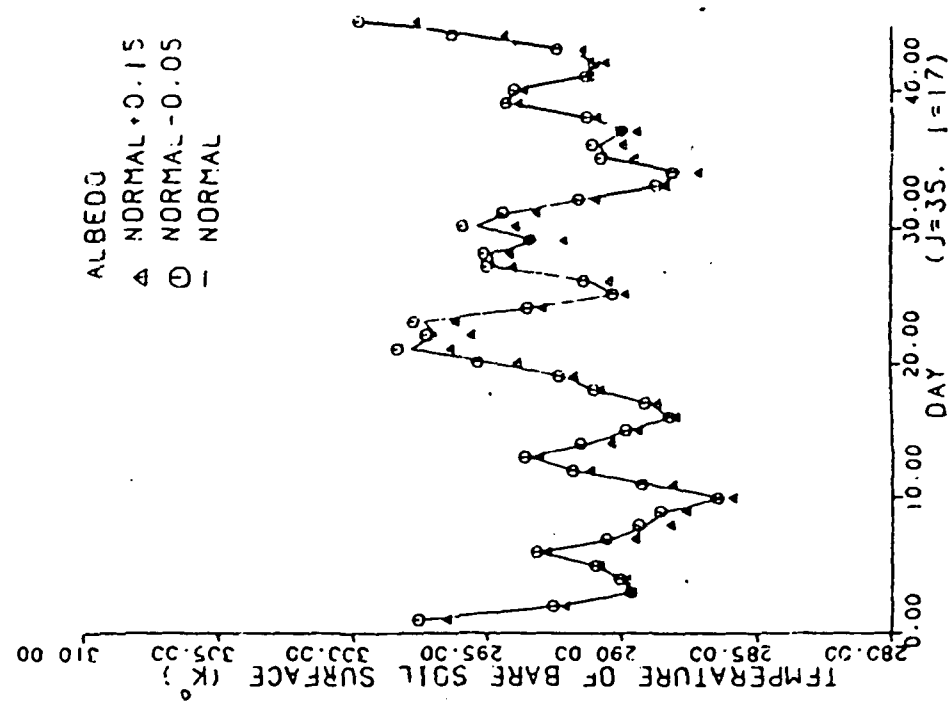
Figure 5.3-4c Sensitivity to albedo
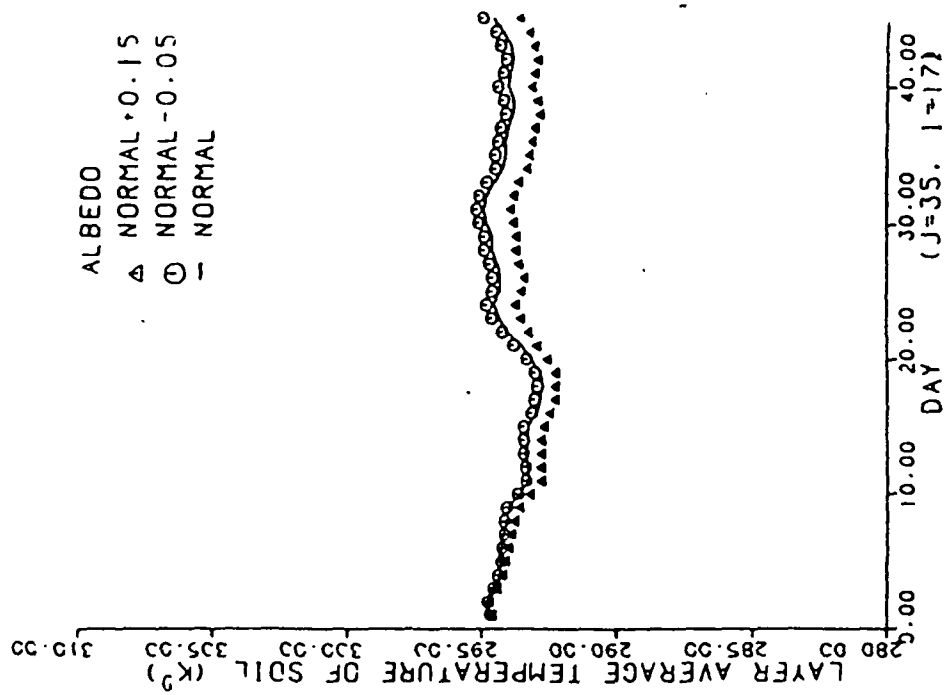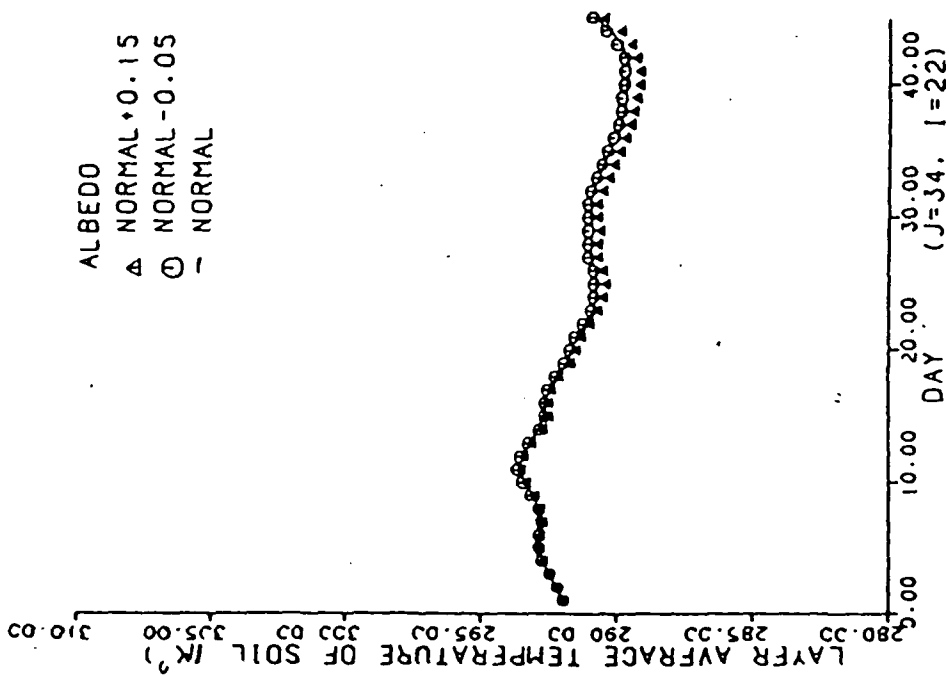
Figure 5.3-4d   Sensitivity to albedo
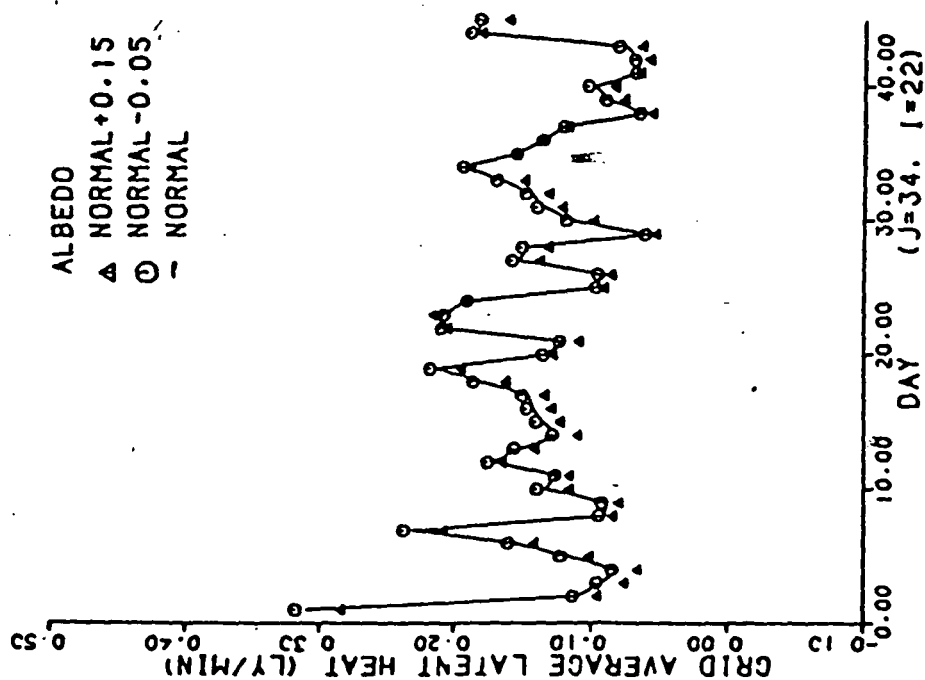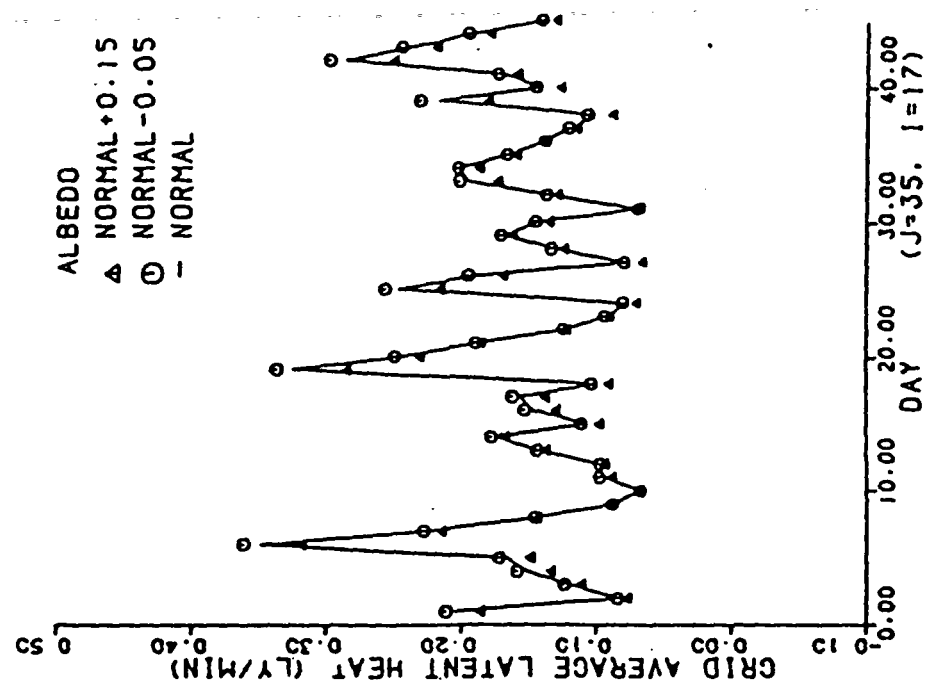
Figure 5.3-4e Sensitivity to albedo
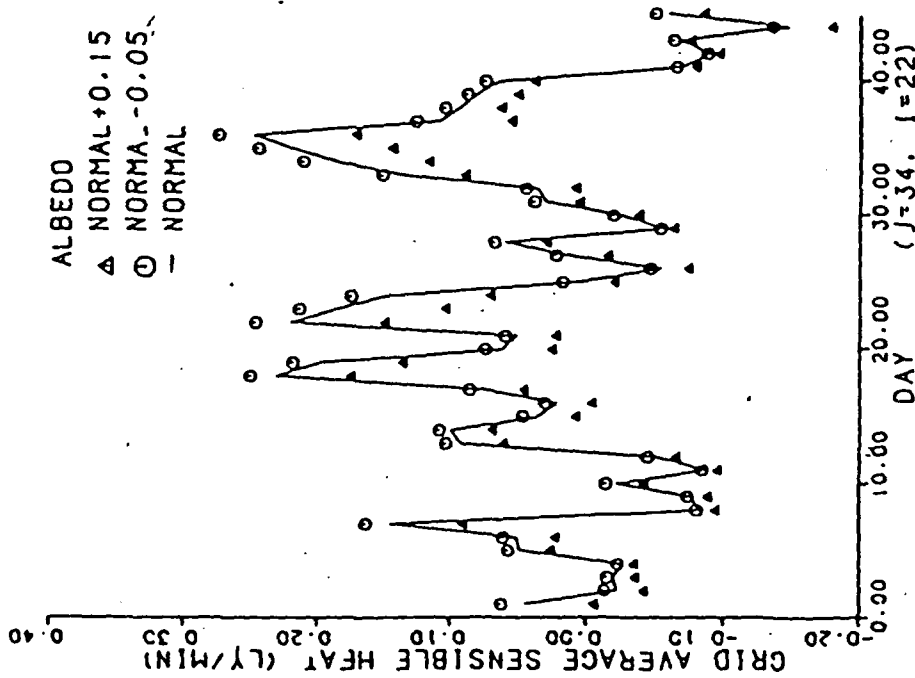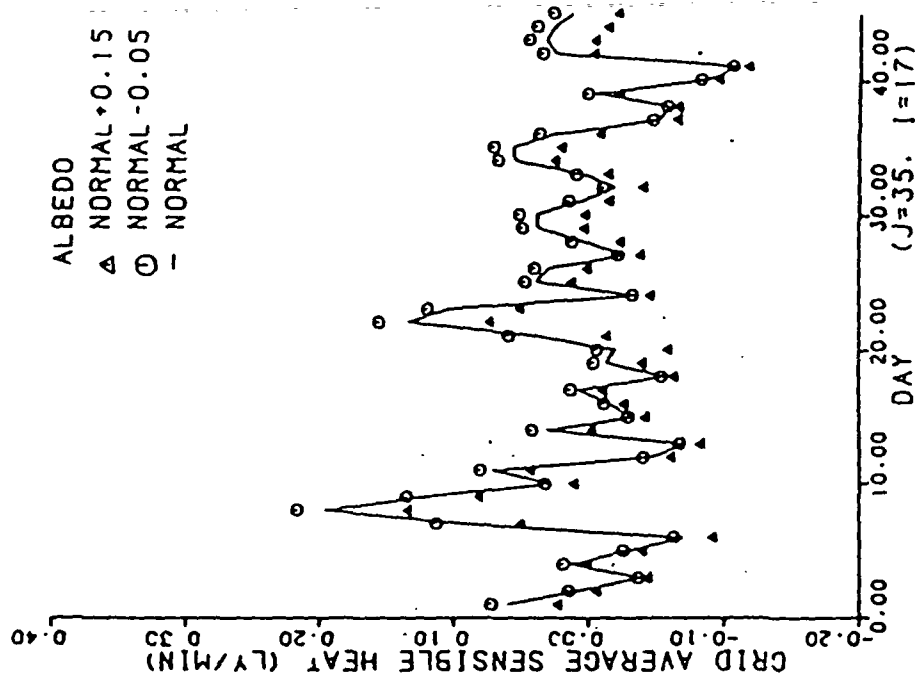
Figure 5.3-4f Sensitivity to albedo

Figure 5.3-4g   Sensitivity to albedo

Figure 5.3-5a Sensitivity to lower boundary condition,
root density distribution and root zone thickness

Figure 5.3-5b Sensitivity to lower boundary condition,
root density distribution and root zone thickness

Figure 5.3-5c Sensitivity to lower boundary condition,
root density distribution and root zone thickness

Figure 5.3-5d Sensitivity to lower boundary condition, root density distribution and root zone thickness
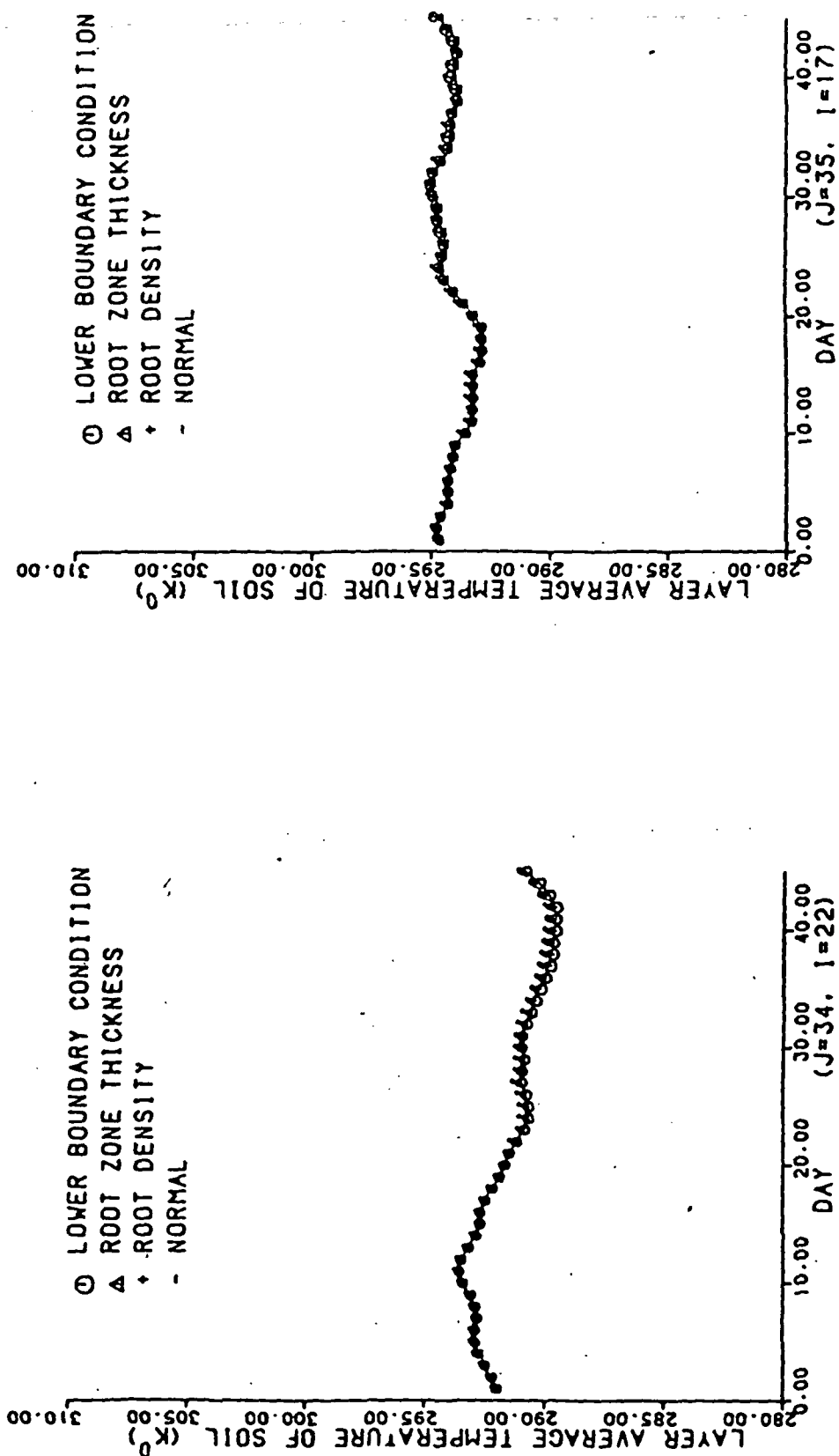
Figure 5.3-5e Sensitivity to lower boundary condition,
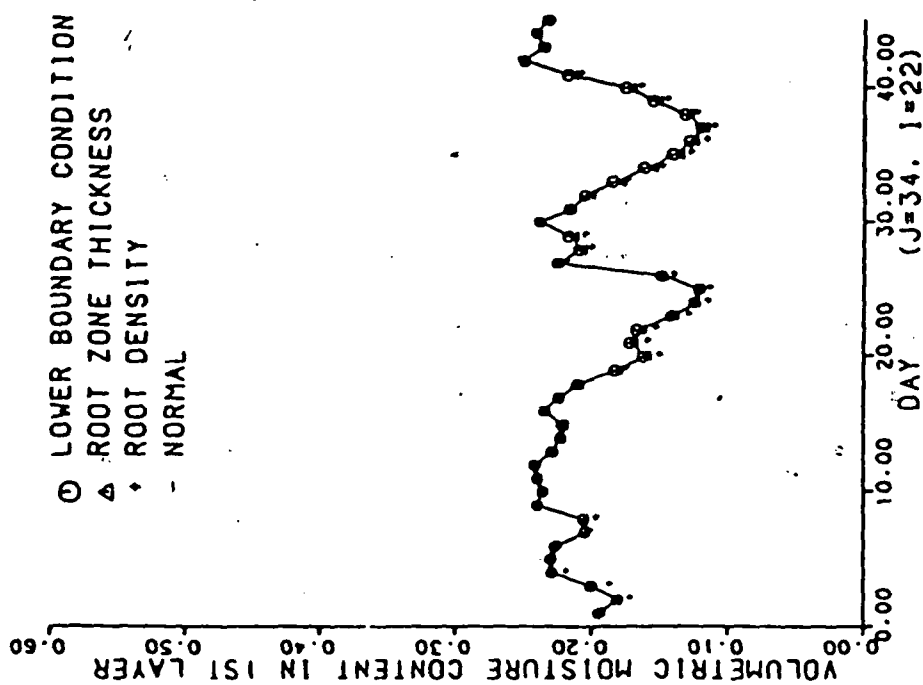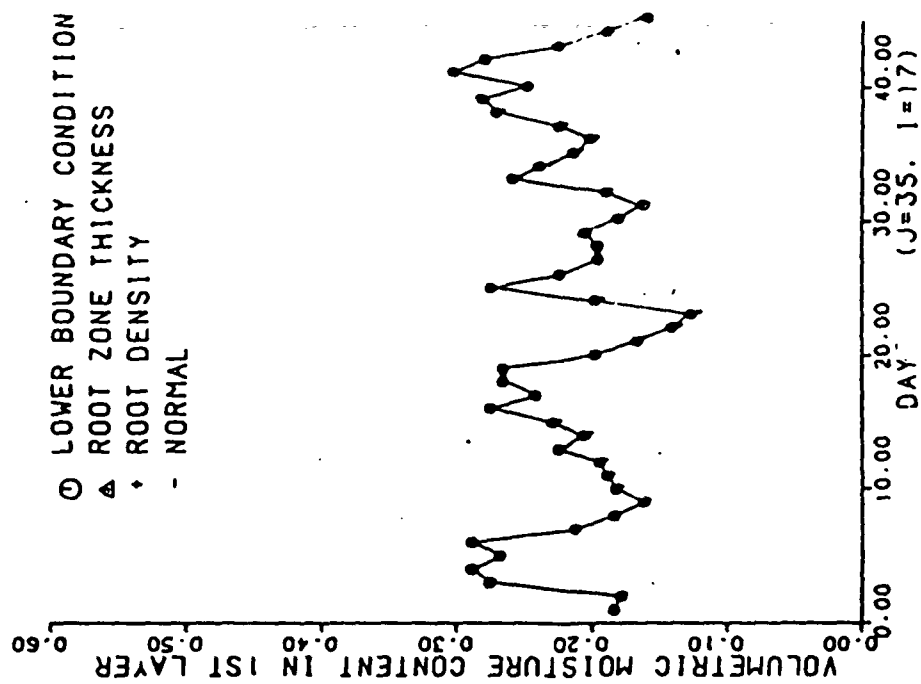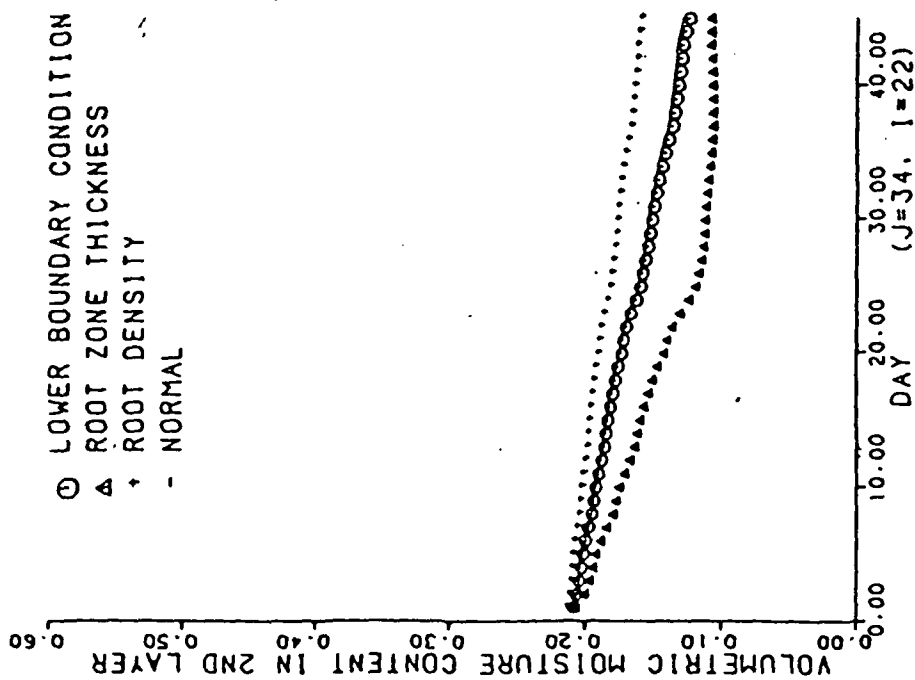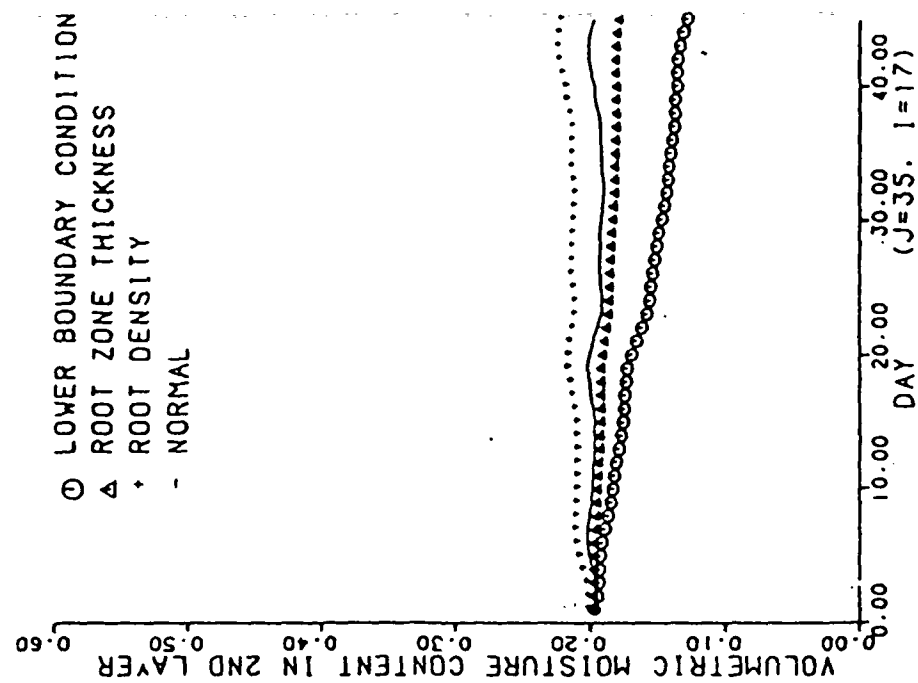root density distribution and root zone thickness
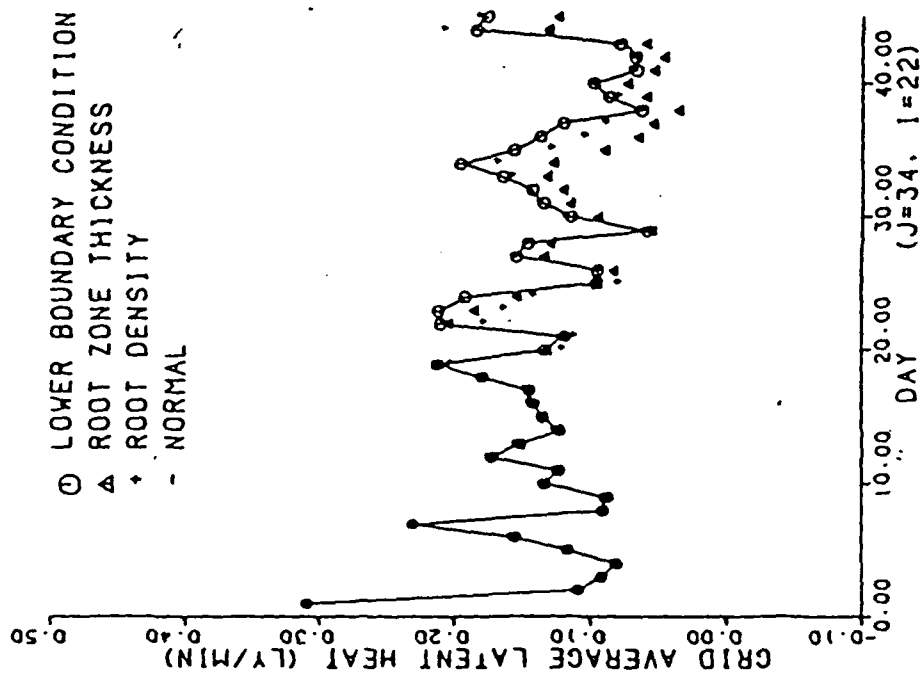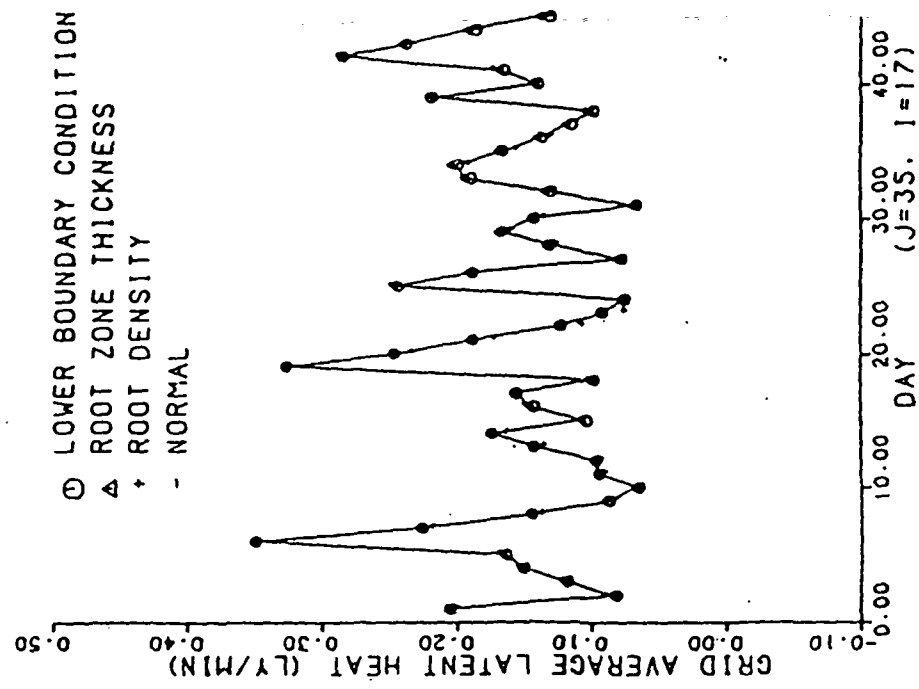
Figure 5.3-5f Sensitivity to lower boundary condition,
root density distribution and root zone thickness
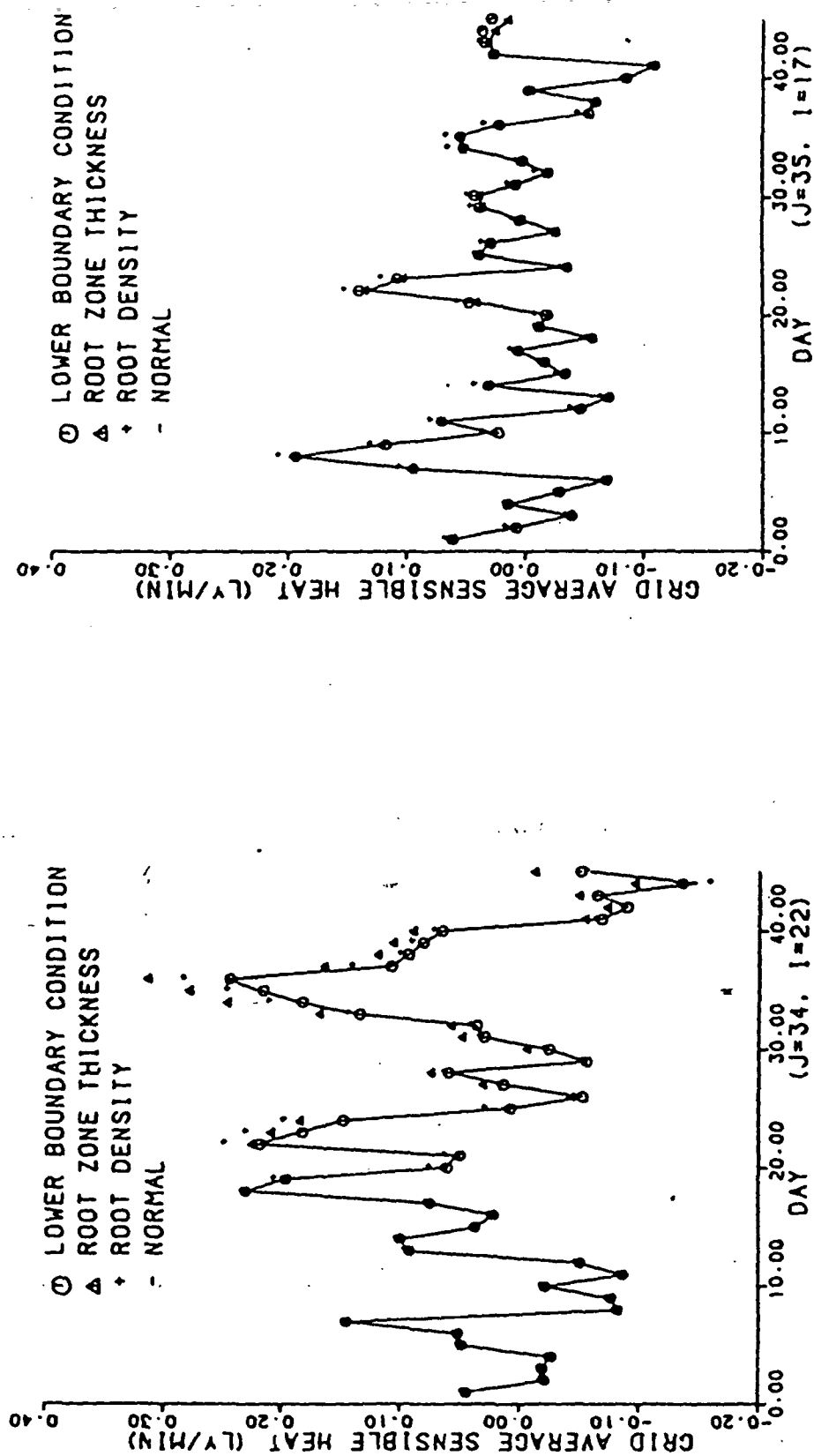
Figure 5.3-5g Sensitivity to lower boundary condition,
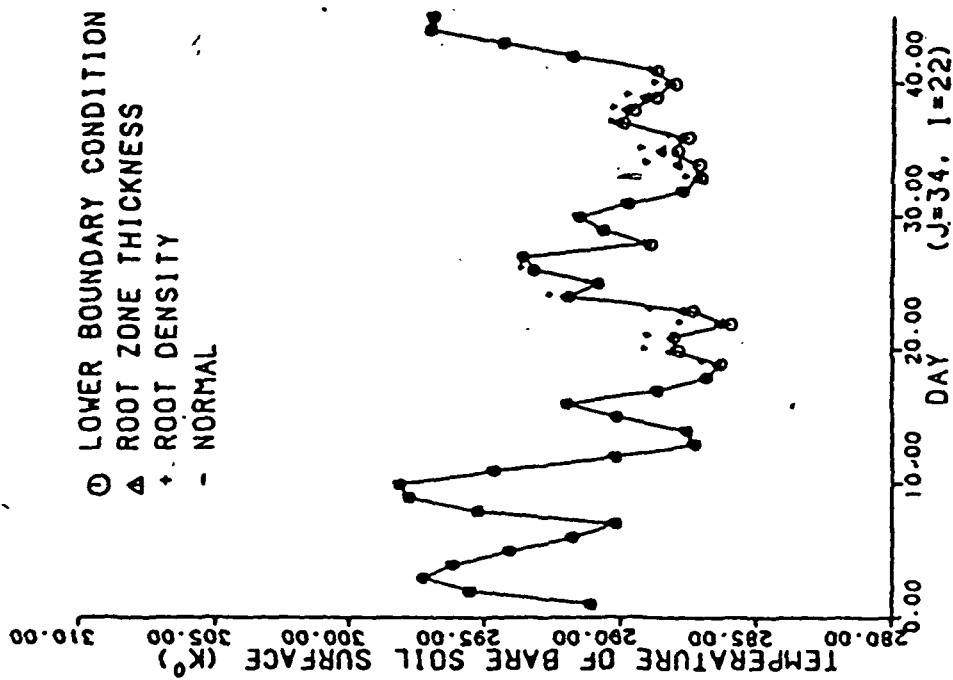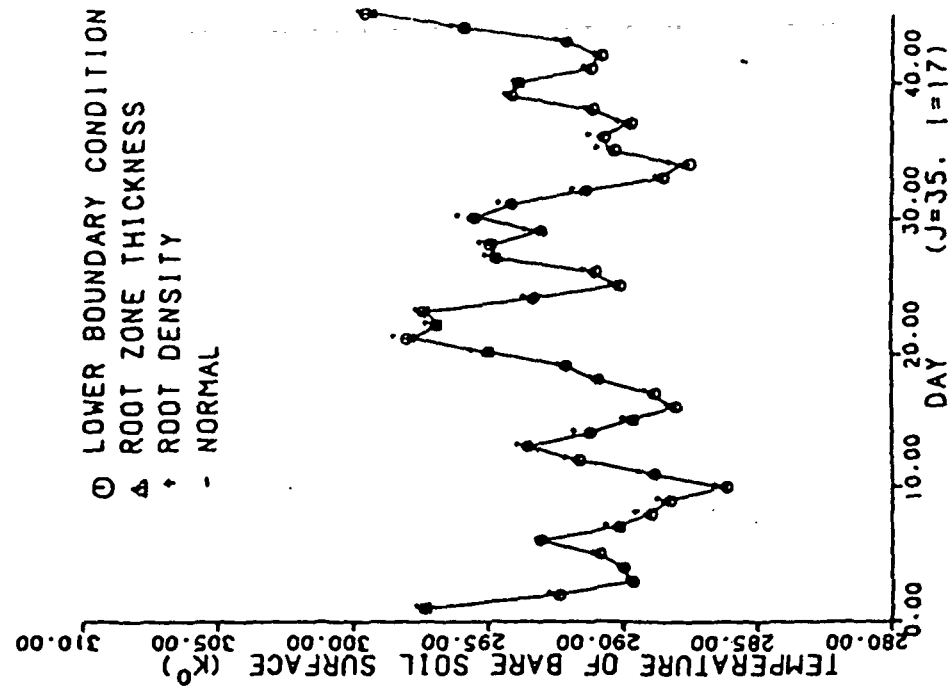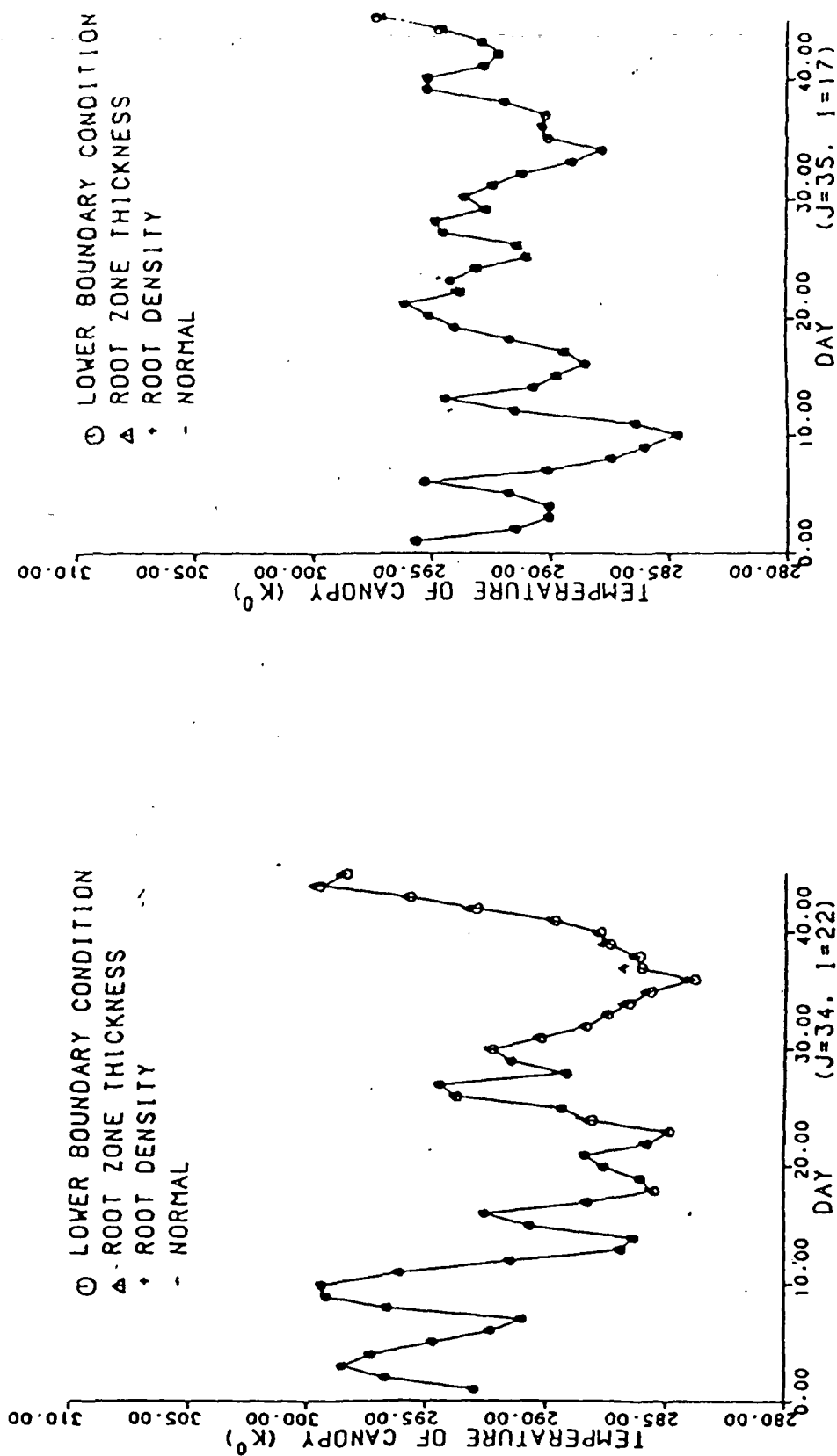root density distribution and root zone thickness

Chapter VI

CONCLUSION AND FUTURE STUDY

6.1 CONCLUSION

This study is a continuation in the development of a large-scale ground hydrologic model at the University of Connecticut for use in the NASA-GLAS atmospheric general circulation model (Lin et al., 1978). The major refinements of the GHM, which include addition of a canopy layer in the subgrid parameterization of vegetation density and coupling of the GHM with the Deardorff (1972) version of planetary boundary layer parameterization, have realistically enhanced the hydrologic feature in the GHM and improved the estimate of momentum, heat and moisture exchange at the atmosphere-land interface. From the 45-day simulation study and the comparison with the resident GHM in the GCM, the following conclusions are made:

1) The actual evapotranspiration predicted by the GHM is in general reduced by 10% to 30% from this given by the GCM. The resident GHM in the GCM is known to overestimate the actual evapotranspiration by the 'bucket' model.

2) The soil moistures in the two layers of root zone in the GHM are more sensitive to the precipitation events than that from the resident GHM. The variation of soil moisture appears to correlate with the precipitation events. The soil moisture in the resident GHM is constantly reduced throughout the experiment period, which might be caused by the overestimate of evaporation.

3) The results of soil moisture, temperature and fluxes from the GHM represent cell to cell variation as a result of the more realistic characterization of land surface cover in the model.

4) The GHM is a two-layer model for soil moisture and heat transports. Soil moisture and temperature in the surface layer are more sensitive to the diurnal forcing of the atmosphère, while the lower layer provides an adequate storage of soil moisture and heat for seasonal changes.

5) By coupling with the PBL in the GCM, the GHM provides a more reasonable exchange mechanism in the atmospheric boundary layer. For such a large horizontal scale, it is not conceivable that the atmospheric conditions are uniform over the whole grid at the 'anemometer height'.

The sensitivity study of the selected parameters provides the following conclusions:

1) The effect of initial moisture condition in the surface layer lasts in the order of five days even under the extreme conditions of the field capacity and the permanent wilting point. However, the difference in the soil moisture content in the lower layer which comprises most of the root zone persists for all 45 days in the experiment period. Therefore, it is extremely important for a short-term numerical experiment that the initial volume of root zone soil moisture be accurately estimated. Even for a longer experiment,such as seasonal or annual, it is likely that the initial noises in the root zone soil moisture are difficult to eliminate because such a long term (over 45 days) is required.

2) The relative importance of the parameters investigated in this study is summarized in Table 5.3-4. It indicates that the subgrid parameterization of vegetation density is the most significant parameter and the root density distribution, root zone thickness and lower boundary condition have minor effects on the response of the GHM.

3) The vegetation density exerts influence on all soil moistures, temperatures and fluxes. However, the most important influence is on evapotranspiration and soil moisture. Afforestaion tends to increase evapotranspiration to a more extent for a sparsely vegetated wet region than a dry region.

6.2   FUTURE STUDY

1)   Field data is required for evaluating the model performance as well as the isolated processes parameterized in the model. In addition, the sensitivity study has shown the importance of accurate initial soil moisture condition in the root zone. Therefore, it is desirable to collect large-scale data sets for soil moisture and ground temperature globally and regionally.

2)   This study was conducted in a non-interactive mode. The GHM should replace the resident GHM in a GCM to conduct the simulation and sensitivity studies interactively.

3)   This study was limited to a time period of 45 days due to the limited availability of GCM-generated atmospheric data.   It is desirable to extend it to seasonal and interannual experiments.

4) Only eight isolated grids in the North America continent were selected for this study. Future numerical experiments should be extended globally or to include contiguous grids in large regions with different climatic conditions.

Appendix A

1. Deriving mean values in the PBL from 'surface data'.

From the earlier version of the GLAS GCM (Tsang and Karn, 1973), the 'surface data', u_a, T_a and q_a, and interfacial fluxes such as evaporation E, sensible heat flux H and friction velocity u_* among others are available. With Deardorff's parameterization (1972), one can calculate the mean values of u_m, T_m and q_m within the PBL by using the surface data that are the standard output of a GCM run.

According to the definition given in chapter 3,

$$F_w = E/\rho_a \qquad (A.1.1)$$

$$F_T = H/(\rho_a Cp) \qquad (A.1.2)$$

and $\qquad F = F_T + 0.61 S_m F_w \qquad (A.1.3)$

As a first approximation, the S_m can be approximated by

$$S_a = T_a (1000/P)^{.288} \qquad (A.1.4)$$

Three stability cases can be determined from the magnitude of F, i.e.

Unstable, if $F>0$ $\qquad$ (A.1.5)

Stable, if $F<0$ $\qquad$ (A.1.6)

Neutral, if $F=0$ $\qquad$ (A.1.7)

If $F = 0$, the neutral case occurs and the relation between the mean atmospheric conditions in the PBL and the surface data is given by

$$(u_m-u_a)/u_* = 8.4 \tag{A.1.8}$$

and $\quad (S_{vm}-S_{va})u_*/F = 7.3 \tag{A.1.9}$

from which, u_m and S_{vm} can be solved explicitly.

If $F < 0$, the stable case occurs and the equations are

$$(u_m-u_a)/u_* = 8.4+.6h/L_m \tag{A.1.10}$$

$$(S_{vm}-S_{va})u_*/F = 7.3+.6h/L_m \tag{A.1.11}$$

and

$$L_m = u_*^3 S_{vm}/(kgF) \tag{A.1.12}$$

from which, u_m, S_{vm} and L_m can be solved expliciltly.

If $F > 0$, the unstable case occur and equations are

$$(u_m-u_a)/u_* = 8.4(1.-50h/L_m)^{-.16} \tag{A.1.13}$$

$$(S_{vm}-S_{va})u_*/F = 7.3(1.-5.8h/L_m)^{-.47} \tag{A.1.14}$$

and $\quad L_m = u_*^3 S_{vm}/(kgF) \tag{A.1.12}$

from which, u_m, S_{vm} and L_m must be solved numerically.

After having the solution u_m, S_{vm} and L_m, the S_m and q_m can be calculated by the following relations:

$$(S_m-S_a)/F_T = (S_{vm}-S_{va})/F \tag{A.1.15}$$

and $\quad (q_m-q_a)/F_w = (S_{vm}-S_{va})/F \tag{A.1.16}$

2. Adjustment of net radiation:

The net radiation from the GCM must be adjusted for the GHM to use under the noninteractive mode in order to account for the difference in the subgrid parameterization of albedo between the value furnished by GCM and the value calculated by the GHM formulation. From the GCM, one has

$$R_n^* = S_w^* + R_L - 6T_{gs}^4 \qquad \qquad \text{(A.2.1)}$$

where S_w^* is the absorbed solar radiation in the GCM, R_L is the downward long wave radiation and T_{gs} is the ground surface temperature provided by the GCM. The downward solar radiation S_w can be calculated from

$$S_w = S_w^* / (1-a_1^*) \qquad \qquad \text{(A.2.2)}$$

where a_1^* is the surface albedo given in the GCM. The net radiation R_n in the GHM is given by

$$R_n = S_w(1-a_1) + R_L - 6T_{co}^4 \qquad \qquad \text{(A.2.3)}$$

where T_{co} is either bare soil surface temperature or canopy temperature from the GHM and a_1 is the GHM albedo given in Section 2.6.

BIBLIOGRAPHY

Alfano, J. A., A Two-Layer Ground Hydrology Model Inte-
      ractive With an Atmospheric General Circulation
      Model, Ph. D. Dissertation. Department of Civil
      Engineering, the University of Connecticut, 1981.

Arakawa, A. and Y. Mintz, The UCLA Atmospheric General
      Circulation Model, Unpublished Notes Distributed
      at UCLA Workshop, March 25 to April 4, 1974.

Bhumralkar, C. M., Numerical Experiments on the
      Computation of Ground Surface Temperature in an
      Atmospheric General Circulation Model, J. Appl
      Meteorol., 14: 1246-1258, 1975.

Blackadar, A. K., Modeling the Nocturnal Boundary
      Layer, In Proc. of the Third Symposium on
      Atmospheric Turbulence, Diffusion and Air
      Quality, PP. 46-49, American Meteorol. Society,
      Boston, MA, 1976.

Bridges, E. M., World Soil. 2nd Ed., Cambridge Univer-
      sity Press, New York, 1978.

Bruce, R. R., A. W. Thomas, L .A. Harper and H.R.
      Leonard, Diurnal Soil Water Regime in the Tilled
      Plow Layer of a Warm Humid Climate, Am. J. Soil
      Sci. Society, 41: 455-460, 1977. Detailed Magnetic
      Tape Data Supplied by L. A. Harper for the
      Period 1900 hrs. June 15, 1973-24 hrs.,
      June 22, 1973.

Brutsaert, W., Evaporation into the Atmosphere:Theory,
      History and Application, D. Reidel Publ. Co.,
      Dordrecht and Boston, 1981.

Buckman, H. O. and N. C. Brady, The Nature and Proper-
      ties of Soils, 6th ed. The Macmillan Co.,
      New York, 1960.

Childs, E. C., An Introduction to the Physical Basis
      of Soil and Water Phenomena, John Wiley, New York,
      1969.

Collinson, A.S., Introduction to World Vegetation,
      George Allen & Unirin, London, England, 1977.

Carson, D. J., Current Parameterizations of Land-Surface Processes in Atmospheric General Circulation Models, A Paper Presented at the JSC Study Conference on Land Surface Processes in Atmospheric General Circulation Models, Greenbelt, USA, 5-10 Jan., 1981.

Corby, G. A., A. Gilchrist and P. R. Rowntree, United Kingdom Meteorological office Five-Level General Circulation Model, Methods in Computational Physics, 17, 67-110, Academic Press, New York, 1977.

Chow, V. T., ed., Handbook of Applied Hydrology, McGraw-Hill Co., New York, 1964.

Deardorff, J. W., Parameterization of the Planetary Boundary Layer for Use in General Circulation Model, Mon. Wea. Rev., 100: 93-100, 1972.

Deardorff, J. W., Efficient Prediction of Ground Surface Temperature and Moisture, with Inclusion of a Layer of Vegetation, J.G.R., 83(C4): 1889-1903, 1978.

Denmead, O.T.and R.H. Shaw, Availability of Soil Water to Plants as Affected by Soil Moisture Content and Meteorological Conditions, Agron. J., 54:385-439, 1962.

Eagleson, P. S., Dynamic Hydo-thermal balance at Macroscale, A Paper Presented at the JSC Study Conference on Land Surface Processes in Atmospheric General Circulation Models, Grennebelt, USA, 5 -10 Jan., 1981.

Eyre, S. R., Vegetation and Soil: A World Picture, 2nd ed., Edward Arnold Ltd. 25 Hill Street, London, 1968.

Federer, C. A., Spatial Variation of Net Radiation, Albedo, Surface Temperature of Forests N. H., J. Appl. Meteorol., 7: 789-795, Oct., 1968.

Federer, C. A., A Soil-Plant-Atmosphere Model for Transpiration and Availability of Soil Water, Water Resour. Res., 15 (3): 555-562, 1977.

Fritschen, L. J., The Vertical Fluxes of Heat and Moisture at a Vegetated Land Surface, A Paper Presented at the JSC Study Conference on Land Surface Processes in Atmospheric General Circulation Models, Grennebelt, USA, 5 -10 Jan., 1981.

Gates, W. L. and M. E. Schlesinger, Numerical Simulation of the January and July Global Climate with a Two-Level Atmospheric Model, J. Atmos. Sci., 34: 36-76, 1977.

Green, R. E. and G. A. Ampt, Studies on Soil physics, 1, The Flow of Air and Water through Soils, J. Agr. Sci., 4: 1-24, 1911.

Haan, C. T., H. P. Johnson and D. L. Brakensiek, Hydrological Modeling of Small Watersheds, The American Society of Agricultural Engineers, Michigan, 1982.

Halem, M., J. Shukla, Y. Mintz, M. L. Wu, R. Godball, G. Herman and Y. Sud, Comparisons of Observed Seasonal Climate Features With a Winter and Summer Numerical Simulation Produced With the GLAS General Circulation Model, Report of the JOC Study Conference on Climate Models, GARP NO. 22, Vol. I, pp. 207-253, 1979.

Hanks, R, J. and G. L. Ashcroft, Applied Soil Physics, Springer-Verlag, New York, 1980.

Heinrich, W., Vegetation of the Earth, 2nd ed, Springer-Verlag New York Inc., New York, 1979.

Hillel, D., Soil and Water: Physical Principles and Processes, Academic Press, New York, 1971.

Hillel, D., Computer Simulation of Soil Water Dynamics. A Compendium of Recent Work, International Development Research Center, Ottowa, Canada (Fig.5.3, P. 169), 1977.

Holtan, H. N., A Concept for Infiltration Estimates in Watershed Engineering, Agricultural Research Service, U. S. Department of Agriculture, ARS 41-51, October, 1961.

Horton, R. E., An Approach Toward a Physical Interpretation of of Infiltration Capacity, Proc. Soil Sci. Soc. Am., 5, 399-417, 1940.

Huggins, L. F., and E. J. Monke, The Mathematical Simulation of the Hydrology of Small Watersheds, Tech. Rep. 1, 130 pp., Water Resour. Res. Center, Purdue Univ., Lafayette Ind. 1966.

Huttel, Cl., Root Distribution and Biomass in Three Ivory Coast Rain Forests Plots, Ecol. Stud., 11, 123-130, 1975.

Idso S. B., R. D. Jackson, R. J. Reginato, B. A.
    Kimball and F. S. Nakayama, The Dependence of
    Bare Soil Albedo on Soil Water Content, J.
    Appl. Meteorol., 14 (1): 109 -113, Feb, 1975.

Jackson, R. D., Unpublished Bare Soil Field Data,
    March 2, 1971-March 12, 1971. U. S. Water
    Conservation Lab, Phoenix, AZ, 1971.

Jackson, R. D., Diurnal Changes in Soil-Water Content
    During Drying, pp. 37-55, in Field Soil Water Re-
    gimes, by R. R. Bruce (ed.), Soil Sci. Soc. Amer.,
    Special Pub. 5, 1973.

Jackson, R. D., B. A. Kimball, R. J. Reginato, S. B.
    Idso and S. A. Nakayama, Heat and Water Transfer
    in a Natural Soil Environment, pp. 67-76, in Heat
    and Mass Transfer in the Biosphere, Part 1, Trans-
    fer Processes in the Plant Environment, Scripta
    Book Pub. Co., Washington, D.C., 1975.

Jury, W., Simulation Transport of Heat and Moisture
    Through a Medium Sand, Ph.D. Thesis, University of
    Wisconsin, 1973.

Kimball, B. A., R. D. Jackson, R. J. Reginato,
    F. S.Nakayama and S. B. Idso, Comparison of
    Field-Measured and Calculated Soil-Heat Fluxes,
    Soil. Sci. Soc. Am. J., 40, 1825, 1976.

Kondratyev, K. Ya., The Shortwave Albedo and The
    Surface Emissivity, A Paper Presented at the
    JSC Study Conference on Land Surface Processes in
    Atmospheric General Circulation Models,
    Grennebelt, USA, 5 -10 Jan., 1981.

Korner, Ch., Maximum Leaf Diffusive Conductance in
    Vascular Plants, Photosynthetica, 13 (1): 45-62,
    1979.

Landsberg, J. J. and C. V. Cutting (ed.), Environmental
    Effects on Crop Physiology, Academic Press, New
    York, 1975.

Lee, L., U.S. Photo Mosaic, General Electric Company,
    Herzel Place, Beltsville, MD, 20705, 1977.

Lee, L., Private Communication, General Electric Com-
    pany, Herzel Place, Beltsville, MD 20705,1980.

Lin, J. D., J. Alfano and P. Bock, A Documentation of
    a Ground Hydrology Parameterization Used in the
    GISS Atmospheric General Circulation Model, Tech.
    Rept., University of Connecticut, 1978.

Lin, J. D., On the Force-Restore Method for Prediction of Ground surface Temperature, J. of Geophysical Research, 85: 3251-3254, June 1980.

Manabe,S., J. Smagorinsky and R. F. Strickler, Simulated Climatology of a General Circulation Model With a Hydrologic Cycle, Mon. Wea. Rev.,93: 769-798, 1965.

Manabe, S. Climate and Ocean Circulation, I The Atmospheric Circulation and Hydrology of the Earth's Surface, Mon. Wea. Rev., 97: 739-774, 1969.

Mein, R. G. and C. L. Larson, Modeling Infiltration during a Steady Rain, Water Resour. Res., 9(2): 384-394, 1973.

Mellor, G. L., and T. Yamada, A Hierarchy of Turbulence Closure Models for Planetary Boundary Layers, J. Atmos. Sci., 31: 1791-1806, 1974.

Miller, E., Plant Physiology, McGraw-Hill Company, INC, New York, 1938.

Mintz, Y., P. J. Sellers and C. J. Willmont, On the Design of an Interactive Biosphere for the GLAS General Circulation Model, NASA Tech. Memo. 84973, Goddard Space Flight Center, Greenbelt Maryland 20771, 1983.

Mintz, Y. and Y. Sarafini, Monthly Normal Global Fields of Soil Moisture and Land-Surface Evapotranspiration, Unpublished Report, Laboratory for Atmospheric Sciences, NASA/Goddard Space Flight Center, Greenbelt, MD 20771, 1982.

Mintz, Y., The Sensitivity of Numerically Simulated climates to Land Surface Conditions, A Paper Presented at the JSC Study Conference on Land Surface Processes in Atmospheric General Circulation Models, Grennbelt, USA, 5-10 Jan., 1981.

Molz, F. J., J. M. Davidson and E. W. Tollner, Unsaturated-Zone Water, Reviews of Geophysics and Space physics, 17(6):1221-1239, 1979.

Money, D. C., Climate, Soils and Vegetation, University Tutorial Press Ltd., London, England, 1976.

Monteith, J. L., Vegetation and the Atmosphere, Vol.I, Principles and Vol. II, Case Studies, New York: Principles, Academic Press, 1975.

Nielsen, D. R. and J. W. Biggar, Measuring Capillary Conductivity, Soil Sci., 92 192-193, 1961.

Nielsen, D. R., J. W. Biggar and K. T. Erh, Spatial Variability of Field Measured Soil-Water Properties, Hilgardia, 42: 215-259, 1973.

Nielsen, D. R., J. W. Davidson, J. W. Biggar and R. J. Miller, Water Movement Through Panoche Clay Loam Soil, Hilgardia, 35: 491-506, 1964.

Peele, W. T., The Physical World (MAP #02683), National Geographic Society, Washington, D.C., 1975.

Perrier, A., Land Surface Processes: Vegetation, A Paper Presented at the JSC Study Conference on Land Surface Processes in Atmospheric General Circulation Models, Grennbelt, USA, 5-10 Jan., 1981

Philip, J. R., Evaporation and Moisture and Heat Fields in the Soil, J. of Meteorol., 14 (4): 354-366, 1957.

Philip, J. R. and D. A. DeVries, Moisture Movement in Porous Materials Under Temperature Gradients, Trans. Amer. Geophys. Union, 38: 222-228, 1957.

Posey, J. W. and P. F. Clapp, Global Distribution of Normal Surface Albedo, Geofisica Intl., 4: 33-48, 1964.

Randall. D. A., Performance of the PBL Parameterization in the GLAS and UCLA Models, Goddard Laboratory for Atmospheric Sciences, NASA/Goddard Space Centeer, Greenbelt, MD, 20771, 1983.

Richards, L. A., Capillary Conduction of Liquids through Porous Mediums, Physics 1, pp. 318-333, 1931

Rijtema, P. E., Soil Moisture Forecasting; Rep. No 513, Institute for land and water managemrnt research, Wageningen, The Netherlands, 1970.

Rosema, A., A Mathematical Model for Simulation of the Thermal Behavior of the Bare Soil, Based on the Heat and Moisture Transfer, Niwars-Publication No. 11, 3 Kanaalweg, 1975.

Rosenberg, N. J., Microclimate: The Biological Environment, John Wiley & Sons, New York, 1974.

Sellers, W. D., Physical Climatelogy, University of Chicago Press, Chicago, 1965.

Shukla, J. and Y. Mintz, Influence of Land-surface Evapotranspiration on the Earth's Climate, Sci., 215: 1498-1501, 1982.

Somerville, R. C. J., P. H. Stone, M. Halem, J. E. Hansen, J. S. Hogan, L. M. Druyan, G. Russell, A. A. Lacia, W. J. Quirk and J. Tennenbaum, The GISS Model of the Global Atmosphere, J. Atmos. Sci., 31:84-117, 1974.

Strahler, A. N., The Earth Sciences, Harper & Row, Illinois, 1971.

Strahler, A. N. and A. H. Strahler, Modern Physical Geography, John Wiley & Sons, new, York, 1978.

Townsend, A. A, Natural Convection in Water Over on Ice Surface, Quarterly Journal of the Royal Meteorological Society, London, England, 90 (385): 248-259, 1964.

Tsang, L. C. and R. Karn, A Documentation of the GISS Nine-Level Atmospheric General Circulation Model, Computer Sciences Corporation, 1973.

Waggoner, P. E. and N. C. Turner, Transpiration and Its Control by Stomata in a Pine Forest, Bulletin of the Connecticut Agricultural Experiment Station, New Haven, 1971.

Wang,F. C., and V. Lakshminarayana, Mathematical Simulation of Water Movement Through Unsaturated Non-homogeneous Soils, Soil Sci. Soc. Amer. Proc., 32 (3): 329-334, 1968.

Washington, W. M. and D. L. Williamson, A Description of the NCAR Global Circulation Models. Methods in Computational Physics, 17:111-172, 1977.

Washington, W. M., R. Dickinson, V. Ramanathan, T. Mayer, D. Williamson, G. Williamson,and R. Wolski, Preliminary Atmospheric Simulation With the Third Generation NCAR General Circulation Model: January and July, Report of the JOC Study Conference on Climate Models, GARP Publ. Series, No.22, 95-138, 1979.

Whisler, F.D., and H. Bouwer, Comparison of Methods for
Calculating Vertical Drainage and infiltration in
Soils, J. Hydrol, 10(1): 1-19, 1970.

Wood, T. E., Biological and Chemical Control of Phosphorus Cycling in a Northern Hardwood Forest, Ph.
D. Dissertation, Yale University, New Haven, 1980.